3 September 2010 | $10

Science

AAAS

CONTENTS continued >>

page 1140

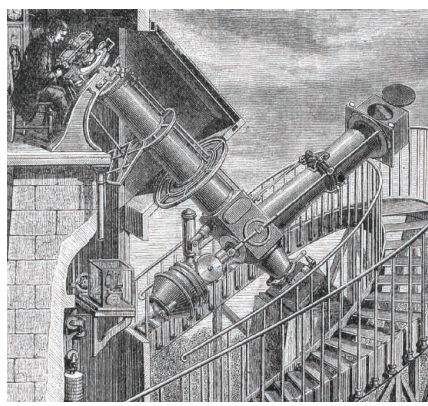

page 1150

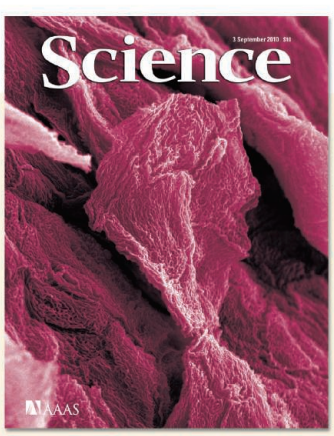

COVER

False-colored scanning electron micrograph showing the shedding of superficial cells in the urogenital tract of a female mouse (magnification ~3000×). Exfoliation of epithelial cells inhibits microbial colonization of the mucosa. On page 1197, Muenzner *et al*. report how specialized pathogens suppress this host defense to successfully establish a firm foothold in their host.

Image: Jochen Hentschel and Christof R. Hauck/Lehrstuhl Zellbiologie, Universität Konstanz, Germany

DEPARTMENTS

Published by AAAS

BREVIA

RESEARCH ARTICLES

REPORTS

CONTENTS continued >>

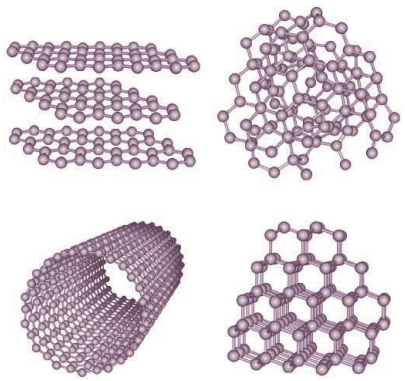

pages 1159 & 1180

page 1185

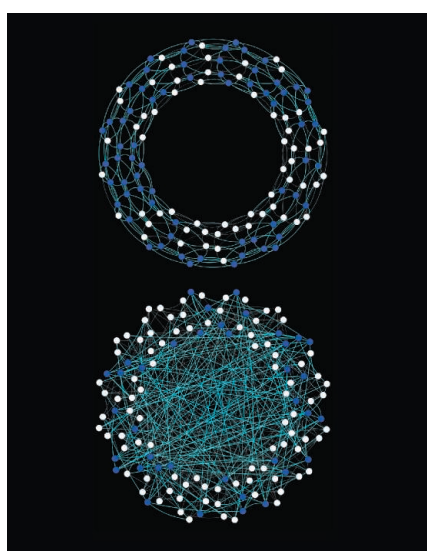

page 1194

SCIENCEONLINE

SCIENCEXPRESS
www.sciencexpress.org

Piezo1 and Piezo2 Are Essential Components of Distinct Mechanically Activated Cation Channels
B. Coste et al.
Cation channel genes encode for a transducer molecule that converts mechanical stimuli into cell signaling.
10.1126/science.1193270

A Critical Role for LTA_4H in Limiting Chronic Pulmonary Neutrophilic Inflammation
R. J. Snelgrove et al.
Cigarette smoke promotes lung inflammation by hindering an enzyme that degrades an immune cell chemoattractant.
10.1126/science.1190594

The Genetic and Molecular Basis for Sunscreen Biosynthesis in Cyanobacteria
E. P. Balskus and C. T. Walsh
A gene cluster encodes a four-enzyme pathway that uses an unusual mechanism to synthesize small-molecule sunscreens.
10.1126/science.1193637

Observing Supernova 1987A with the Refurbished Hubble Space Telescope
K. France et al.
Images of the remnants of a stellar explosion reveal details of fast astrophysical shock waves.
10.1126/science.1192134

A New Mixing Diagnostic and Gulf Oil Spill Movement
I. Mezić et al.
An ocean model can account for the trajectory and fragmentation of the recent Gulf of Mexico oil spill.
10.1126/science.1194607

SCIENCENOW
www.sciencenow.org
Highlights From Our Daily News Coverage

Quantum Physicists Dream Up Smallest Possible Refrigerator
One or two quantum particles are enough to approach absolute zero.

The First Feast?
Researchers find evidence for the earliest symbolic meal 12,000 years ago in Israel.

'Hunting for Conservation' Backfires
Overeager trophy hunters may be the biggest threat to African lions.

SCIENCESIGNALING
www.sciencesignaling.org
The Signal Transduction Knowledge Environment

EDITORIAL GUIDE: Focus Issue—Systems Analysis of Protein Phosphorylation
N. R. Gough and J. F. Foley
Kinases and phosphatases are stars in the signaling universe.

RESEARCH RESOURCE: Comprehensive Expression Profiles of Genes for Protein Tyrosine Phosphatases in Immune Cells
Y. Arimura and J. Yagi
Gene expression analysis suggests that protein tyrosine phosphatases exhibit immune cell–specific expression profiles.

RESEARCH RESOURCE: Collection and Motif-Based Prediction of Phosphorylation Sites in Human Viruses
D. Schwartz and G. M. Church
A database of known phosphorylation sites on viral proteins also enables the prediction of other potential sites.

PROTOCOL: Targeting the Reversibly Oxidized Protein Tyrosine Phosphatase Superfamily
B. Boivin et al.
Mildly acidic pH and degassed buffers are the keys to successfully identifying redox-sensitive tyrosine phosphatases.

NETWATCH: Viral Post-Translational Modification Database (virPTM)
Browse a collection of demonstrated and predicted phosphorylation sites in proteins of viruses that infect humans; in Protein Databases.

NETWATCH: PHOSIDA Posttranslational Modification Database
Browse and search a database of phosphorylation, acetylation, and N-glycosylation sites determined by mass spectrometry; in Protein Databases.

SCIENCECAREERS
www.sciencecareers.org/career_magazine
Free Career Resources for Scientists

Taken for Granted: The New California Postdoc Contract
B. Benderly
After lengthy talks and some strategic arm-twisting, the University of California comes to terms with its postdoc union.

In Person: How Our Adventures Led to Careers in Science
K. Jardine and A. Jardine
Science and outdoor activities form a positive feedback loop for scientists Kolby and Angela Jardine.

***Science* Careers Blog**
Science *Careers Staff*
Find advice, opinions, news, funding opportunities, and links to other career-related resources.

SCIENCETRANSLATIONAL MEDICINE
www.sciencetranslationalmedicine.org
Integrating Medicine and Science

PERSPECTIVE: Molecular Profiling—Moving Away from Tumor Philately
J. S. Reis-Filho et al.
Cutting-edge technologies that deliver diverse molecular data may dramatically alter breast cancer characterization and treatment.

PERSPECTIVE: Translational Medicine and the Value of Biomarker Qualification
F. M. Goodsaid and D. L. Mendrick
The U.S. Food and Drug Administration's new process for biomarker qualification developed from a need for better biomarkers of renal injury.

RESEARCH ARTICLE: Platelet CD154 Potentiates Interferon-α Secretion by Plasmacytoid Dendritic Cells in Systemic Lupus Erythematosus
P. Duffau et al.
In the autoimmune disease lupus, platelets activated by self-antigens contribute to pathology by triggering the secretion of interferon from immune cells.

RESEARCH ARTICLE: Overlap and Effective Size of the Human $CD8^+$ T Cell Receptor Repertoire
H. S. Robins et al.
The adaptive immune system is far less diverse, and the interpersonal overlap of T-cell receptor repertoires is thousands of times larger, than expected.

SCIENCEPODCAST
www.sciencemag.org/multimedia/podcast
Free Weekly Show
Download the 3 September *Science* Podcast to hear about how social network structure affects the spread of behavior, challenging the mammoth-killer impact hypothesis, your letters to *Science*, and more.

SCIENCEINSIDER
news.sciencemag.org/scienceinsider
Science Policy News and Analysis

SCIENCE (ISSN 0036-8075) is published weekly on Friday, except the last week in December, by the American Association for the Advancement of Science, 1200 New York Avenue, NW, Washington, DC 20005. Periodicals Mail postage (publication No. 484460) paid at Washington, DC, and additional mailing offices. Domestic individual membership and subscription (51 issues): $146 ($74 allocated to subscription). Domestic institutional subscription (51 issues): $910; Foreign postage extra: Mexico, Caribbean (surface mail) $55; other countries (air assist delivery) $85. First class, airmail, student, and emeritus rates on request. Canadian rates with GST available upon request, GST #1254 88122. Publications Mail Agreement Number 1069624. **Printed in the U.S.A.**

Change of address: Allow 4 weeks, giving old and new addresses and 8-digit account number. **Postmaster:** Send change of address to AAAS, P.O. Box 96178, Washington, DC 20090–6178. **Single-copy sales:** $10.00 current issue, $15.00 back issue prepaid includes surface postage; bulk rates on request. *Science* is indexed in the *Reader's Guide to Periodical Literature* and in several specialized indexes.

AAAS
ADVANCING SCIENCE, SERVING SOCIETY

Published by AAAS

China's Research Culture

Yigong Shi is a professor and dean of the School of Life Sciences at Tsinghua University, Beijing, China. E-mail: shi-lab@tsinghua.edu.cn.

Yi Rao is a professor and dean of the School of Life Sciences at Peking University, Beijing, China. E-mail: yrao@pku.edu.cn.

GOVERNMENT RESEARCH FUNDS IN CHINA HAVE BEEN GROWING AT AN ANNUAL RATE OF MORE than 20%, exceeding even the expectations of China's most enthusiastic scientists. In theory, this could allow China to make truly outstanding progress in science and research, complementing the nation's economic success. In reality, however, rampant problems in research funding—some attributable to the system and others cultural—are slowing down China's potential pace of innovation.

Although scientific merit may still be the key to the success of smaller research grants, such as those from China's National Natural Science Foundation, it is much less relevant for the megaproject grants from various government funding agencies, which range from tens to hundreds of millions of Chinese yuan (7 yuan equals approximately 1 U.S. dollar). For the latter, the key is the application guidelines that are issued each year to specify research areas and projects. Their ostensible purpose is to outline "national needs." But the guidelines are often so narrowly described that they leave little doubt that the "needs" are anything but national; instead, the intended recipients are obvious. Committees appointed by bureaucrats in the funding agencies determine these annual guidelines. For obvious reasons, the chairs of the committees often listen to and usually cooperate with the bureaucrats. "Expert opinions" simply reflect a mutual understanding between a very small group of bureaucrats and their favorite scientists. This top-down approach stifles innovation and makes clear to everyone that the connections with bureaucrats and a few powerful scientists are paramount, dictating the entire process of guideline preparation. To obtain major grants in China, it is an open secret that doing good research is not as important as schmoozing with powerful bureaucrats and their favorite experts.

This problematic funding system is frequently ridiculed by the majority of Chinese researchers. And yet it is also, paradoxically, accepted by most of them. Some believe that there is no choice but to accept these conventions. This culture even permeates the minds of those who are new returnees from abroad; they quickly adapt to the local environment and perpetuate the unhealthy culture. A significant proportion of researchers in China spend too much time on building connections and not enough time attending seminars, discussing science, doing research, or training students (instead, using them as laborers in their laboratories). Most are too busy to be found in their own institutions. Some become part of the problem: They use connections to judge grant applicants and undervalue scientific merit.

There is no need to spell out the ethical code for scientific research and grants management, as most of the power brokers in Chinese research were educated in industrialized countries. But overhauling the system will be no easy task. Those favored by the existing system resist meaningful reform. Some who oppose the unhealthy culture choose to be silent for fear of losing future grant opportunities. Others who want change take the attitude of "wait and see," rather than risk a losing battle.

Despite the roadblocks, those shaping science policy and those working at the bench clearly recognize the problems with China's current research culture: It wastes resources, corrupts the spirit, and stymies innovation. The time for China to build a healthy research culture is now, riding the momentum of increasing funding and a growing strong will to break away from damaging conventions. A simple but important start would be to distribute all of the new funds based on merit, without regard to connections. Over time, this new culture could and should become the major pillar of a system that nurtures, rather than squanders, the innovative potential of China.

– Yigong Shi and Yi Rao

10.1126/science.1196916

Published by AAAS

www.sciencemag.org

Science

1200 New York Avenue, NW
Washington, DC 20005
Editorial: 202-326-6550, FAX 202-289-7562
News: 202-326-6581, FAX 202-371-9227
Bateman House, 82-88 Hills Road
Cambridge, UK CB2 1LQ
+44 (0) 1223 326500, FAX +44 (0) 1223 326501

Subscription Services For change of address, missing issues, new orders and renewals, and payment questions: 866-434-AAAS (2227) or 202-326-6417, FAX 202-842-1065. Mailing addresses: AAAS, P.O. Box 96178, Washington, DC 20090-6178 or AAAS Member Services, 1200 New York Avenue, NW, Washington, DC 20005

Institutional Site Licenses please call 202-326-6755 for any questions or information

Reprints: Author Inquiries 800-635-7181
Commercial Inquiries 803-359-4578

Permissions 202-326-7074, FAX 202-682-0816

Member Benefits AAAS/Barnes&Noble.com bookstore www.aaas.org/bn; AAAS Online Store www.apisource.com/aaas/ code MKB6; AAAS Travels: Betchart Expeditions 800-252-4910; Apple Store www.apple.com/eppstore/aaas; Bank of America MasterCard 1-800-833-6262 priority code FAA3YU; Cold Spring Harbor Laboratory Press Publications www.cshlpress.com/affiliates/aaas.htm; GEICO Auto Insurance www.geico.com/landingpage/go51.htm?logo=17624; Hertz 800-654-2200 CDP#343457; Office Depot https://bsd.officedepot.com/portalLogin.do; Seabury & Smith Life Insurance 800-424-9883; Subaru VIP Program 202-326-6417; VIP Moving Services www.vipmayflower.com/domestic/index.html; Other Benefits: AAAS Member Services 202-326-6417 or www.aaasmember.org.

science_editors@aaas.org	(for general editorial queries)
science_letters@aaas.org	(for queries about letters)
science_reviews@aaas.org	(for returning manuscript reviews)
science_bookrevs@aaas.org	(for book review queries)

Published by the American Association for the Advancement of Science (AAAS), *Science* serves its readers as a forum for the presentation and discussion of important issues related to the advancement of science, including the presentation of minority or conflicting points of view, rather than by publishing only material on which a consensus has been reached. Accordingly, all articles published in *Science*—including editorials, news and comment, and book reviews—are signed and reflect the individual views of the authors and not official points of view adopted by AAAS or the institutions with which the authors are affiliated.

AAAS was founded in 1848 and incorporated in 1874. Its mission is to advance science, engineering, and innovation throughout the world for the benefit of all people. The goals of the association are to: enhance communication among scientists, engineers, and the public; promote and defend the integrity of science and its use; strengthen support for the science and technology enterprise; provide a voice for science on societal issues; promote the responsible use of science in public policy; strengthen and diversify the science and technology workforce; foster education in science and technology for everyone; increase public engagement with science and technology; and advance international cooperation in science.

Information for Authors
See pages 352 and 353 of the 15 January 2010 issue or access www.sciencemag.org/about/authors

EDITOR-IN-CHIEF **Bruce Alberts**
EXECUTIVE EDITOR **Monica M. Bradford**
NEWS EDITOR **Colin Norman**
MANAGING EDITOR, RESEARCH JOURNALS **Katrina L. Kelner**
DEPUTY EDITORS **R. Brooks Hanson, Barbara R. Jasny, Andrew M. Sugden**

Editorial senior editors/commentary Lisa D. Chong, Brad Wible; **senior editors** Gilbert J. Chin, Pamela J. Hines, Paula A. Kiberstis (Boston), Marc S. Lavine (Toronto), Beverly A. Purnell, L. Bryan Ray, Guy Riddihough, H. Jesse Smith, Phillip D. Szuromi (Tennessee), Valda Vinson, Jake S. Yeston; **associate editors** Kristen L. Mueller, Jelena Stajic, Nicholas S. Wigginton, Laura M. Zahn; **research associate** Alexis Wynne Mogul; **book review editor** Sherman J. Suter; **associate letters editor** Jennifer Sills; **editorial manager** Cara Tate; **senior copy editors** Jeffrey E. Cook, Cynthia Howe, Harry Jach, Lauren Kmec, Barbara P. Ordway, Trista Wagoner; **copy editor** Chris Filiatreau; **editorial coordinators** Carolyn Kyle, Beverly Shields; **publications assistants** Ramatoulaye Diop, Joi S. Granger, Emily Guise, Jeffrey Hearn, Michael Hicks, Lisa Johnson, Scott Miller, Jerry Richardson, Jennifer A. Seibert, Brian White, Anita Wynn; **editorial assistants** Emily C. Horton, Patricia M. Moore, Miriam Weinberg; **executive assistant** Alison Crawford; **administrative support** Maryrose Madrid; **editorial fellow** Melissa R. McCartney

Editorial director, web and new media Stewart Wills; **senior web editor** Tara S. Marathe; **web editor** Robert Frederick; **web development manager** Martyn Green; **web developer** Andrew Whitesell; **intern** Sophia Cai

News deputy news editors Robert Coontz, David Grimm, Eliot Marshall, Jeffrey Mervis, Leslie Roberts; **contributing editors** Elizabeth Culotta, Polly Shulman; **news writers** Yudhijit Bhattacharjee, Adrian Cho, Jennifer Couzin, Jocelyn Kaiser, Richard A. Kerr, Eli Kintisch, Greg Miller, Elizabeth Pennisi, Lauren Schenkman, Robert F. Service (Pacific NW), Erik Stokstad (Online); **web developer** Daniel Berger; **intern** Kristen Minogue; **contributing correspondents** Jon Cohen (San Diego, CA), Daniel Ferber, Ann Gibbons, Sam Kean, Robert Koenig, Andrew Lawler, Mitch Leslie, Charles C. Mann, Virginia Morell, Gary Taubes; **copy editors** Linda B. Felaco, Melvin Gatling, Melissa Raimondi; **administrative support** Scherraine Mack; **bureaus** San Diego, CA: 760-942-3252, FAX 760-942-4979; Pacific Northwest: 503-963-1940

Production director James Landry; **senior manager** Wendy K. Shank; **assistant manager** Rebecca Doshi; **senior specialists** Steve Forrester, Chris Redwood, Anthony Rosen; **Preflight director** David M. Tompkins; **manager** Marcus Spiegler; **specialist** Jason Hillman

Art director Yael Fitzpatrick; **associate art director** Laura Creveling; **senior illustrators** Chris Bickel, Katharine Sutliff; **illustrator** Yana Hammond; **senior art associates** Holly Bishop, Preston Huey, Nayomi Kevitiyagala; **art associates** Kay Engman, Matthew Twombly; **photo editor** Leslie Blizard

***Science* International**

Europe (science@science-int.co.uk) **editorial: international managing editor** Andrew M. Sugden; **senior editor/commentary** Julia Fahrenkamp-Uppenbrink; **senior editors** Caroline Ash, Stella M. Hurtley, Ian S. Osborne, Peter Stern; **associate editor** Maria Cruz; **locum editor** Helen Pickersgill; **editorial support** Rachel Roberts, Alice Whaley; **administrative support** John Cannell, Janet Clements, Louise Hartwell; **news: europe news editor** John Travis; **deputy news editor** Daniel Clery; **contributing correspondents** Michael Balter (Paris), John Bohannon (Vienna), Martin Enserink (Amsterdam and Paris), Gretchen Vogel (Berlin); **intern** Sarah Reed

Latin America contributing correspondent Antonio Regalado

Asia Japan Office: Asca Corporation, Tomoko Furusawa, Rustic Bldg. 7F, 77 Tenjin-cho, Shinjuku-ku, Tokyo 162-0808, Japan; +81 3 6802 4616, FAX +81 3 6802 4615, inquiry@sciencemag.jp; **asia news editor** Richard Stone (Beijing: rstone@aaas.org); **contributing correspondents** Dennis Normile [Japan: +81 (0) 3 3391 0630, FAX +81 (0) 3 5936 3531; dnormile@gol.com]; Hao Xin [China: cindyhao@gmail.com]; Pallava Bagla [South Asia: +91 (0) 11 2271 2896; pbagla@vsnl.com]

EXECUTIVE PUBLISHER **Alan I. Leshner**
PUBLISHER **Beth Rosner**

Fulfillment Systems and Operations (membership@aaas.org); **director** Waylon Butler; **customer service supervisor** Pat Butler; **specialists** Latoya Casteel, LaVonda Crawford, Vicki Linton, April Marshall; **data entry supervisor** Cynthia Johnson; **specialists** Shirlene Hall, Tarrika Hill, William Jones

Business Operations and Administration director Deborah Rivera-Wienhold; **business systems and financial analysis director** Randy Yi; **manager, business analysis** Eric Knott; **manager, business operations** Jessica Tierney; **financial analysts** Priti Pamnani, Celeste Troxler; **rights and permissions: administrator** Emilie David; **associate** Elizabeth Sandler; **marketing director** Ian King; **marketing managers** Allison Pritchard, Alison Chandler, Julianne Wielga; **marketing associates** Aimee Aponte, Mary Ellen Crowley, Wendy Wise; **senior marketing executive** Jennifer Reeves; **director, site licensing** Tom Ryan; **director, corporate relations** Eileen Bernadette Moran; **publisher relations, eresources specialist** Kiki Forsythe; **senior publisher relations specialist** Catherine Holland; **publisher relations, east coast** Phillip Smith; **publisher relations, west coast** Philip Tsolakidis; **fulfillment supervisor** Iquo Edim; **fulfillment coordinator** Carrie MacDonald; **marketing manager** Christina Schlecht; **marketing associate** Laura Tutino; **electronic media: manager** Lizabeth Harman; **project manager** Trista Snyder; **assistant manager** Lisa Stanford; **senior production specialists** Ryan Atkins, Christopher Coleman, **computer specialist** Walter Jones, Kai Zhang; **production specialists** Angela Forest, Nichele Johnston, Kimberly Oster; **director, web and new media** Will Collins

advertising director, worldwide ad sales Bill Moran
commercial editor Sean Sanders: 202-326-6430
assistant commercial editor Tianna Hicklin 202-326-6463
project director, outreach Brianna Blaser

Product (science_advertising@aaas.org); **midwest** Rick Bongiovanni: 330-405-7080, FAX 330-405-7081; **east coast/e. canada** Laurie Faraday: 508-747-9395, FAX 617-507-8189; **west coast/w. canada** Lynne Stickrod: 415-931-9782, FAX 415-520-6940; **uk/europe/asia** Roger Goncalves: TEL/FAX +41 43 243 1358; **japan** ASCA Corporation, Nanako Ide +81 (0) 3 6802 4616, FAX +81 (0) 3 6802 4615; ads@sciencemag.jp; **senior traffic associate** Deiandra Simms

worldwide associate director of *Science* Careers Tracy Holmes: +44 (0) 1223 326525, FAX +44 (0) 1223 326532

Classified (advertise@sciencecareers.org); **u.s.: midwest/west coast/south central/canada** Tina Burks: 202-326-6577; **east coast/industry** Elizabeth Early: 202-326-6578; **advertising operations manager** Kate Panganiban **sales coordinators** Rohan Edmonson, Shirley Young; **europe/row sales:** Susanne Kharraz, Dan Pennington, Alex Palmer; **sales assistant** Lisa Patterson; **japan** ASCA Corporation, Jie Chin +81 (0) 3 6802 4616, FAX +81 (0) 3 6802 4615; careerads@sciencemag.jp; **advertising support manager** Karen Foote: 202-326-6740; **advertising production operations manager** Deborah Tompkins; **senior production specialist/graphic designer** Amy Hardcastle; **production specialist** Yuse Lajiminmuhip; **senior traffic associate** Christine Hall

A rap on the knuckles for IPCC
1135

China scopes out Antarctica
1136

EMBRYONIC STEM CELLS

Controversial Ruling Throws U.S. Research Into a Tailspin

A U.S. judge's surprise decision last week to block government funding of human embryonic stem cell (hESC) research has left scientists across the country confused, upset, and angry. Some, those on the intramural staff of the National Institutes of Health (NIH) near Washington, D.C., got orders this week to stop all hESC work immediately. At universities from California to Massachusetts, independent researchers funded by NIH were trying to understand what the ruling means for their own labs. On Monday, NIH issued a notice indicating that no more money will be released for hESC studies—all pending proposals and renewals are on hold—but investigators who received grant awards before 23 August can continue to spend the funds. That interpretation could, however, be open to challenge.

Scrambling to save projects in mid-experiment, at least one lab chief shifted hESC work from U.S.-funded to privately backed facilities. Most can't afford that luxury. Another called together junior colleagues to let them know that their work would have to stop soon, barring a reprieve, and that some might have to be let go. Still others hoped that a legal appeal—filed by the U.S. Justice Department as *Science* went to press—would bring a stay of execution. In a blunt statement last week, NIH Director Francis Collins summed up the turmoil by saying, "This decision has just poured sand into that engine of discovery."

The crisis erupted on 23 August, when Chief Judge Royce Lamberth of the U.S. District Court for the District of Columbia issued a preliminary injunction requested by two researchers who claim that federal funding for hESC research is illegal. The injunction cites a ban on support for research in which human "embryos are destroyed," adopted initially by the U.S. Congress in 1996 and known as the Dickey-Wicker Amendment. The judge said the government must set aside NIH's 2009 Guidelines for Human Stem Cell Research—the Obama Administration document that lays out NIH's rules for working with the cells—and halt the hESC funding it allowed (*Science*, 10 July 2009, p. 131).

The Administration has asked the courts to lift the injunction until an appeal can be heard. Legal experts say that even if granted, relief could be temporary because a higher court could affirm Lamberth's ruling later. The judicial process could take months.

Most observers agree that action by Congress will be needed to ensure federal funding of hESC research in the long run. Indeed, stem cell research champions hope to persuade Congress to override the Dickey-Wicker Amendment for research on hESCs soon after members return to Washington on 13 September. However, the prospects for action on such a hot-button issue in an election year are hard to predict.

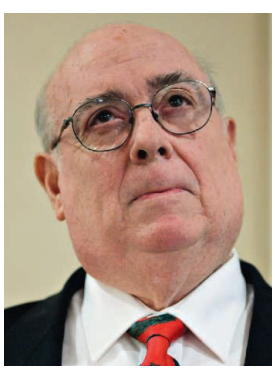

"If one step or 'piece of research' ... results in the destruction of an embryo, the entire project is precluded from receiving federal funding."

—JUDGE ROYCE LAMBERTH, U.S. DISTRICT COURT FOR THE DISTRICT OF COLUMBIA

At the heart of Judge Lamberth's ruling is the question of whether the Dickey-Wicker rule prohibits federal funding for research on hESCs that have already been derived. Both the George W. Bush Administration and the Obama Administration agreed that the amendment bars federal funds for deriving hESCs because embryos are destroyed in the process. But Bush announced on 9 August 2001 that work on cell lines derived before that date would be permitted, and Obama's executive order, issued on 9 March 2009, extended the permission to many other hESCs (*Science*, 13 March 2009, p. 1412). Judge Lamberth ruled, however, that the distinction between deriving hESCs and using them is invalid: "If one step or 'piece of research' … results in the destruction of an embryo, the entire project is precluded from receiving federal funding."

Experts do not agree on the strength of Lamberth's legal arguments. Some say the challenge was to be expected. Louis Guenin, a lecturer in ethics in science at Harvard Medical School in Boston who has written extensively on the ethics of embryo research and hESCs, supports federal funding for hESCs but believes the judge is correct that funding for hESC work is incompatible with current law. Guenin warned shortly after Obama's election that an executive order like the one Obama issued would be vulnerable to legal challenge. If Congress wants to avoid future problems, Guenin and others say, it must remove the prohibition against embryo research or pass a law that says the government can fund hESC work.

But others think the ruling was a bad decision. Professor Hank Greely of Stanford Law School in Palo Alto, California, argues that Dickey-Wicker is unclear on whether it allows for research on hESC lines. And in cases in which a law is ambiguous, the courts must defer to the interpretation of the executive branch, he says. Three successive presidential administrations have found that Dickey-Wicker allows for hESC research, Greely points out. "We've got 11 years of consistent interpretation by the federal government. That's pretty powerful," he says.

Robert Charrow, a former Health and Human Services Department attorney now at the Greenberg Traurig firm in Washington, D.C., says the case should never have gone this far. He thinks the courts "erred" in recognizing that the plaintiffs—James Sherley and Theresa Deisher—had standing to sue the government. These two researchers work with adult stem cells but avoid hESCs for moral reasons. In their suit they claimed that as competitors for NIH grants, they would be injured by policies that allowed others to win funding for hESC studies, a type of research they consider illegal. That claim of harm gained them

CREDIT: J. SCOTT APPLEWHITE/AP PHOTO

Published by AAAS

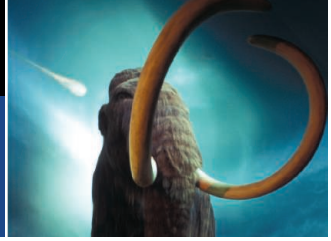

The rise and fall of a killer theory

1140

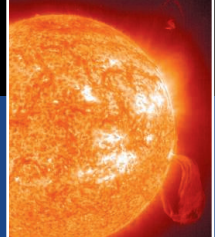

Hot dispute over the sun's makeup

1144

access to court and yielded an injunction.

In the confusion surrounding the legal issues, one thing seems clear: For researchers working with the cells, the world has changed. That wasn't immediately apparent from Lamberth's ruling, which said that halting federal support "would not seriously harm ESC researchers because the injunction would simply preserve the status quo." Stem cell researchers beg to differ.

Raising funds to replace frozen NIH grants is no easy prospect, says Margaret Goodell, a stem cell scientist at Baylor College of Medicine in Houston, Texas. Goodell says she received her annual grant renewal notice a few days before the injunction was issued, so she is assuming for now that she can continue work. But had the notice been delayed by a few days, she says, she might have had to lay off as many as 20 people in her lab who are supported by the grant.

For Amander Clark, a developmental biologist at the University of California, Los Angeles, the situation is more acute. Her $1.9 million grant application has been tabled—meaning it's out of competition indefinitely—and a 5-year $1.7 million grant funded under the Bush Administration rules, due for renewal in January, is at risk. "As a new PI [principal investigator] just getting my lab off the ground, I am devastated. I am worried about my tenure, I am worried about my graduate students, and I am worried about my postdocs." The situation has hit young investigators particularly hard, she says: "We do not have the track record yet to easily or quickly secure funds from nonfederal sources."

Research results soon become stale. Clark says she may write papers quickly so the preliminary data aren't lost, even though the grant is only 1.5 years old. For now, Clark says, the grant under review is in limbo. Although only one-third of the project involves hESCs, NIH has told her that she can't revise it to remove the hESC component. Submitting a new grant from scratch would take at least a year from review to receiving funding, she says.

C. Anthony Blau, a hematologist at the University of Washington, Seattle, says the ruling has made him rethink two grant applications he is about to turn in. Both were supposed to involve hESCs, but he is now revising his plans. "It's a very promising approach that is just going to be blocked at this point," he says.

GRANTS AT RISK

Number	Funding
50 grant proposals awaiting peer review	Not available
12 proposals through initial peer review, awaiting council review	$15 million to $20 million
24 grants up for annual renewal in September	$54 million
199 grants up for annual renewal in 2011	$131 million

Frozen. September grant renewals and review of new grants for hESC studies are on hold; more grants could be at risk next year. UCLA's Amander Clark could lose her funding in February.

Stay of execution?

Evidence on promising treatments delayed and the disruption of research plays a role in the government's request for a stay of the preliminary injunction. Federal lawyers argue that the potential harm to the careers of Sherley and Deisher is outweighed by the harm to taxpayers whose research investments are being wasted and to patients who are potentially being deprived of new treatments.

"I think there's a very good chance that this [injunction] will be stayed" while the appeals court reviews Lamberth's ruling, Greely says. If so, he adds, the case could be heard by early 2011 and a decision issued by spring. But if the appeals court upholds the injunction, he expects the government to request an expedited appeal, which could take less time.

"This decision has just poured sand into that engine of discovery."

—FRANCIS COLLINS, DIRECTOR, NIH

Meanwhile, stem cell research supporters are hoping Congress will take quick action to reverse the research ban when members return from recess in mid-September. Representative Diana DeGette (D–CO) plans to push for passage of a bill she co-sponsored with Michael Castle (R–DE) that would codify Obama's executive order. A similar bill passed Congress twice but was vetoed by Bush.

The bill in previous forms would not end the Dickey-Wicker problem. That is likely to persist unless Congress votes to eliminate the amendment or modify it to allow for hESC research. "We will find a way to fix this," a House Democratic aide says. On the Senate side, Tom Harkin (D–IA) announced that, as chair of the appropriations subcommittee that approves NIH's budget, he will hold a hearing on 16 September to look at ways to modify the Dickey-Wicker rider.

Although some observers expected that lawmakers would steer clear of the divisive stem cell issue before the November midterm elections, they may not be able to avoid it. Even so, with House of Representatives and Senate Democratic leadership so far silent on the issue, it's unclear how far their efforts will get in the 3 weeks before Congress breaks again. The turmoil in Washington over Lamberth's ruling could leave stem cell researchers in limbo for many more months.

–JOCELYN KAISER AND GRETCHEN VOGEL

Published by AAAS

CLIMATE CHANGE

Panel Faults IPCC Leadership But Praises Its Conclusions

The world's most authoritative climate science body has performed well enough so far, says a new independent review of the Intergovernmental Panel on Climate Change (IPCC). But the report, from a panel convened by a coalition of national science academies, says the increased public scrutiny IPCC is facing and the growing importance of its work means that it must do better than that.

"Overall, IPCC's assessment process has been a success and served society well," says Harold Shapiro, president emeritus of Princeton University and head of the review carried out by the InterAcademy Council (IAC). But "it's not as agile and responsive as it needs to be," the report says.

Repair man. Shapiro says critics have put "dents" in IPCC's reputation.

The review comes at a trying time for IPCC. It has produced four major assessment reports on the world's changing climate since it was established by the United Nations in 1988, each involving thousands of scientists and running for thousands of pages. And it was awarded the Nobel Peace Prize in 2007. But the disclosure late last year of e-mails from climate scientists being dismissive of critics' arguments and requests for data, and the discovery of errors in its 2007 report related to Himalayan glaciers (*Science*, 13 November 2009, p. 924) and sea-level rise, have put "dents" in its reputation, says Shapiro. The group's response has exacerbated the problem, say a number of IPCC's scientific supporters. "After 20 years, there's room for improvement," says economist Richard Richels, a longtime IPCC contributor.

Reports by the U.S. National Academies and scores of individual papers in recent months have confirmed the bottom line of the IPCC assessments: The world is warming due to release of greenhouse gases from human activities, and the emerging consequences are severe. But the 113-page report, requested by IPCC and the United Nations, identified plenty of areas needing work. It called for a stronger leadership structure, including adding the positions of executive director and an executive board, and term limits for top panel officials. It also recommends tighter review procedures, along with a clear conflict-of-interest policy, greater attention to viewpoints outside the scientific mainstream, and improved handling of outsider comments.

The report notes that IPCC lacks procedures to deal with any errors, and it asserts that its current structure is poorly designed to deal with the public consequences of those mistakes. In the case of the infamous error on the Himalayan glaciers—the IPCC report said that the mountains would be ice-free by 2035—IPCC Chair Rajendra Pachauri said a report contrary to that assertion was "voodoo science." Months later, however, IPCC reversed itself and issued a statement of regret. That "very poor" response was one example of why IPCC needs stronger leadership, Shapiro told *Science*.

In 2007, Pachauri created an executive team comprised of top officials and scientists from each of IPCC's three working groups to make its leadership more cohesive. Shapiro called the change "a good idea that failed." The report said a formalized executive board and executive director, reporting to the chair, would be better suited to respond to day-to-day issues. Although the report called for a 6-year term limit for the chair and other top positions, Pachauri, in his ninth year on the job, showed no signs of willingness to hand over the reins today. (Shapiro said his group was not asked to provide advice on whether Pachauri should remain.)

The report said that increasingly varied and complex studies of climate science have taxed the limited resources of the IPCC staff and hundreds of volunteer reviewers. To help ease the onslaught, the report suggested that existing review editors—who oversee each chapter's multistep review process—rank the importance of the comments they do receive and that they urge chapter authors to respond to public comments.

IPCC critic and respected climate skeptic John Christy of the University of Alabama, Huntsville, called that a "welcome" recommendation. Several comments had pointed out the 2035 error to no avail, for example, although Shapiro said he didn't know if more forceful oversight would have prevented authors from ignoring them.

The IAC report scolds IPCC's Working Group 2, which deals with the effects of climate change, for being imprecise. The report criticized the working group's "high confidence" in the assertion that adapting to sea-level rise "could amount to 5%-10%" of gross domestic product despite the fact that it was based on only "a small number of unpublished studies." It calls for a more rigorous emphasis on explaining uncertainty.

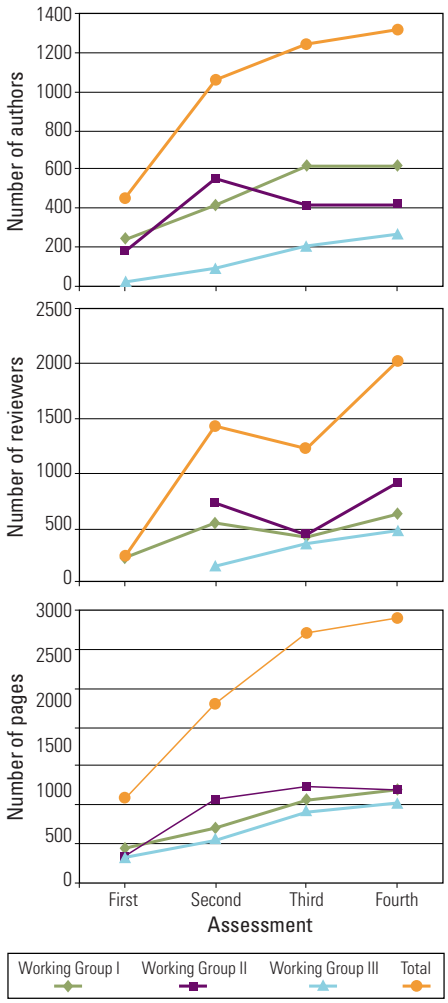

A growing burden. Each successive assessment has needed more reviewers and authors to monitor more research findings.

In a press conference, Pachauri said repeatedly that he was open to nearly every suggestion but that IPCC would "have to discuss" many of them before implementing any new policies. Any fundamental changes to the panel's leadership structure would need to be adopted by IPCC's sponsoring governments at their yearly meeting in October in Busan, South Korea.

Shapiro hopes that the chair and his colleagues will respond. He says it's important to the world that the "thousands of scientists working somehow together to deliver important information on the state of the climate … succeed." **–ELI KINTISCH**

CREDITS (LEFT TO RIGHT): PRINCETON UNIVERSITY; (SOURCE) COMMITTEE TO REVIEW THE IPCC, INTERACADEMY COUNCIL

Published by AAAS

ANTARCTICA

In Ground-Based Astronomy's Final Frontier, China Aims for New Heights

XI'AN, CHINA—No place on Earth rivals the Antarctic Plateau for stargazing. The air is thin and bone-dry; dust is minimal. As observatories go, the higher the better—and at 4093 meters above sea level, it doesn't get any higher on the East Antarctic icecap than Dome A. Last year, Chinese researchers opened Kunlun Station near Dome A. Now they intend to find out if a superior vantage point translates into superior astronomy. At a workshop here last month, astronomers unveiled plans to build two major telescopes at Dome A during the Chinese government's next 5-year plan, to start in 2011.

The 2.5-meter Kunlun Dark Universe Telescope, or KDUST, would survey the optical and near-infrared bands for planets beyond our solar system and plumb the mysteries of dark matter and dark energy. However, "one instrument would be lonely," says astronomer Yang Ji, director of Nanjing's Purple Mountain Observatory, which is developing a companion: a 5-meter terahertz (THz) telescope to observe 200- to 350-micrometer wavelengths. This "underexplored frequency window" is acutely sensitive to gas clouds—ideal for probing, for example, star and planet formation, says Qizhou Zhang, an astrophysicist at the Harvard-Smithsonian Center for Astrophysics in Cambridge, Massachusetts, and a member of the group that initiated the THz telescope project. Outside experts are impressed. "It's a very ambitious and exciting program," says John Storey, an astronomer at the University of New South Wales (UNSW) in Sydney, Australia.

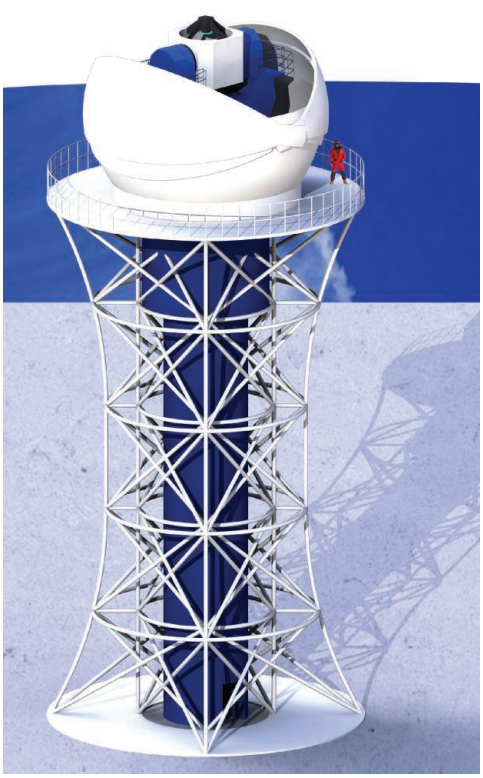

Steady gaze. KDUST would sit above Dome A's thin layer of turbulent air.

The Chinese Academy of Sciences has requested 1 billion yuan ($150 million) for the telescopes and support platform—one of several science megafacilities that the country's powerful National Development and Reform Commission is weighing for the 12th 5-year plan. A decision is expected around year's end.

The two telescopes would be a major expansion of China's formidable Antarctic buildup. During the 2007–08 International Polar Year, China erected Kunlun Station, teamed with the United States and others to study the Gamburtsev Mountains—the origin of the East Antarctic ice sheet—and with Australia began testing observing conditions at Dome A. To pave the way for expansion, China last year built an ice runway at Kunlun; until now, all materials and people have been brought in by arduous traverses.

China is not making a leap into the unknown. Antarctic astronomy first made headlines in 1998, when BOOMERANG, a U.S. National Science Foundation (NSF)–sponsored balloon experiment, mapped the cosmic microwave background and found that the universe is flat. As an encore, a 10-meter telescope at the U.S. Amundsen-Scott South Pole Station brought online in 2007 has begun microwave background studies. "South Pole shows it is possible to build major astronomical facilities in Antarctica," says Storey.

Plenty more is in the works. The coming austral summer at the South Pole should see completion of IceCube, the biggest neutrino observatory in the world. Then next year, the NSF-funded South Pole Ultraviolet Pathfinder will lay the groundwork for mapping the cosmic web, the universe's scaffolding of dark matter. Also next year, U.S.-led teams plan to field two experiments—the Stratospheric Terahertz Observatory balloon to be launched from McMurdo Station, and the High Elevation Antarctic Terahertz telescope, a 0.5-meter instrument to be installed at Ridge A in East Antarctica. And a six-nation consortium has proposed a 2.5-meter optical-infrared telescope for Dome C, where the French-Italian Concordia station has conducted extensive site testing.

The numerous efforts underscore the fabulous observing conditions on the plateau. Frigid temperatures make for a low infrared background, and aerosol concentrations are 1/50 of those at temperate sites. Water vapor is a bane for submillimeter and THz observations. Compared with one of the best sites in temperate latitudes—Mauna Kea in Hawaii—"Dome A is a factor of 10 drier," says Storey. "That's a staggering advantage."

Indeed, the view from Dome A may be unbeatable. "This is a totally different ballgame from other astronomical sites," says UNSW's Michael Ashley. In January 2008, Chinese astronomers deployed PLATO, a suite of site-characterization instruments, at Dome A. It confirmed not only that Dome A surpasses other plateau outposts, says Ashley, but also that "sometimes the view rivals Hubble." And the boundary layer of turbulent air at Dome A is only about 14 meters thick, compared with 200 meters at the South Pole, making it far cheaper to perch telescopes above Dome A.

Chinese astronomers won't have to wait for a decision on the megaproject proposal to start ramping up at Dome A. Funding is set for installation next year of the Antarctic Schmidt Telescopes, a trio of 50-centimeter telescopes that should detect at least one Earth-sized extrasolar planet per year and supernova explosions within half an hour after they become visible, says Lifan Wang, an astronomer at Texas A&M University in College Station and director of the Chinese Center for Antarctic Astronomy. "This will help us study explosion mechanisms," he says.

Meanwhile, plans are in full swing for KDUST, designed by the Nanjing Institute of Astronomical Optics and Technology, and the 5-meter THz telescope. The latter has a hard act to follow: Europe's year-old Herschel Space Observatory, which "has opened up a new field for terahertz astronomy," Zhang says. But Herschel has a 3-year design life, and "it's very difficult to get time on it," he says. "The 5-meter at Dome A will continue discovery that Herschel started." It's also a steppingstone to a 15-meter THz telescope China hopes to build in Antarctica after 2015. Likewise, KDUST is a prelude to a 6- to 8-meter optical and near-infrared telescope. Long before those huge telescopes become reality, however, Chinese researchers will have put Dome A on the astronomy map.

–RICHARD STONE

CREDIT: COURTESY OF NANJING INSTITUTE OF ASTRONOMICAL OPTICS AND TECHNOLOGY

Published by AAAS

ScienceNOW

From *Science's* Online Daily News Site

The First Feast?

Whether it's Thanksgiving dinner or Mother's Day brunch, people around the world gather to pig out on special occasions. A new study finds that such feasts have been going on for at least 12,000 years.

Two years ago, archaeologists Natalie Munro of the University of Connecticut, Storrs, Leore Grosman of The Hebrew University of Jerusalem, and colleagues found the body of an approximately 45-year-old woman at Hilazon Tachtit, a cave west of the Sea of Galilee in Israel, which was occupied by hunter-gatherers during the transition between the prefarming Paleolithic and the agricultural Neolithic periods. Her skeleton was surrounded by animal remains, including the shells of 71 tortoises and the bones of at least three wild cattle.

In the new study, reported in the *Proceedings of the National Academy of Sciences*, the team finds that the wild cattle bones show clear signs of butchering and that the tortoise shells were broken in such a way as to make the meat easily accessible. The meat could have fed 35 or more people.

This is the "best documented case" of early feasting to date, says Brian Hayden, an archaeologist at Simon Fraser University in Burnaby, Canada. He says that feasting was key to the social transition between hunter-gatherer and farming societies. http://bit.ly/first-feast

The World's Smallest Refrigerator

You may have a $10,000 Sub-Zero fridge in your kitchen, but this is cooler. Theoretical physicists have dreamed up a scheme to make a refrigerator out of a pair of quantum particles such as ions or atoms.

Noah Linden, Sandu Popescu, and Paul Skrzypczyk of the University of Bristol in the United Kingdom will report in *Physical Review Letters* that, at least in principle, they can use two quantum particles called "qubits" to cool a third. The trick is to put two of the qubits—including the one to be cooled—in contact with a cold bath and the third one in contact with a hot bath. Arrange things just right and the qubits spontaneously "flip" between their excited and nonexcited quantum states in a way that siphons energy out of the target qubit and cools it toward absolute zero.

No word yet on when physicists might unveil the smallest possible beer. http://bit.ly/tiny-fridge

'Hunting for Conservation' Backfires

African lions are one step away from becoming an endangered species, and a measure designed to preserve them is to blame.

Lion populations have plummeted more than 90% over the last 70 years. In the 1980s and '90s, African nations proposed an unusual solution: trophy hunting. They hoped that by allowing rich game-chasers to shoot a few animals, landowners would have an incentive to conserve lion habitats and keep the species alive while boosting their local economies.

The strategy has backfired, according to an upcoming study in *Conservation Biology*. Led by Craig Packer of the University of Minnesota, Twin Cities, a team of biologists analyzed the amount of game brought back by hunters from 21-day safaris, the only legal way to hunt lions in Tanzania. They discovered that from 1996 to 2008, the number of lions hunters bagged in the East African nation decreased by half. Expanding agriculture, disease, and retaliatory killings might all play a role in the decline, the team concludes, but those threats paled in comparison to recreational hunting.

Although Packer acknowledges that the idea of hunting for conservation may work in theory, "there's no point in providing the animal with economic value and then overhunting them." http://bit.ly/trophy-hunting

A Pea-Sized Frog

The smallest frog on three continents has a loud voice, and that's the only way scientists were able to find it. Starting at dusk, the males emit a chorus of harsh, raspy calls. Researchers report in *Zootaxa* that they discovered the pea-sized amphibians on the side of the Gunung Serapi mountain in Borneo, chirping amid the tiny *Nepenthes* pitcher plants they call home. Named *Microhyla nepenthicola,* the male frogs measure only 10.6 to 12.8 mm long, making them the tiniest frogs in Europe, Asia, and Africa. (The females are almost twice as long.) The amphibians' high surface-to-volume ratio means that they lose water quickly, so they do most of their mating and eating near the moist pitcher plants. They're not the world's smallest frog, however: That record is currently held by two 9.8-mm-long amphibians in the New World, the gold frog in Brazil, and the Monte Iberia dwarf frog in Cuba. http://bit.ly/tiny-frog

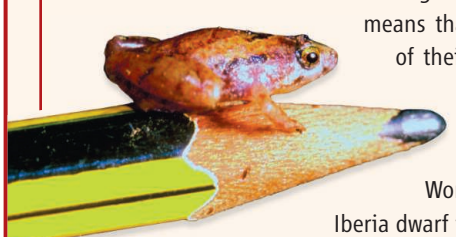

Read the full postings, comments, and more at **news.sciencemag.org/sciencenow**.

CREDITS (TOP TO BOTTOM): NAFTALI HILGER; THINKSTOCK; INDRANEIL DAS/INSTITUTE OF BIODIVERSITY AND ENVIRONMENTAL CONSERVATION

Published by AAAS

ENERGY INNOVATION

Novel Grant Promises Greener Buildings, Regional Growth

Civilian and military personnel working at the sprawling Philadelphia Navy Yard along the city's waterfront on the Delaware River went to Building 661 for exercise. But in 1995, the pool, basketball court, and fitness center inside the building were shuttered when the U.S. government closed the entire 500-hectare compound that since 1871 had helped the country go to war. Now the building itself is due for a workout.

Last week, a consortium led by Pennsylvania State University won a federal competition for $129 million over 5 years to spur efforts to develop technologies for making buildings more energy efficient. Building 661 will be retrofitted and reopened to help the country wage war against two 21st century opponents: global warming and energy profligacy. It's the centerpiece of an effort to transform the entire Navy Yard complex into a test bed for reducing the carbon footprint of a sector that accounts for roughly 40% of U.S. energy consumption. The grant also represents a novel approach by the U.S. government in funding energy research and development.

The Greater Philadelphia Innovation Cluster (GPIC) for Energy Efficient Buildings is the third Energy Innovation Hub that the Department of Energy (DOE) has funded this year. Last year, Energy Secretary Steven Chu proposed eight "Bell Lablets" that would bring large teams of scientists and engineers together to tackle complex and important energy problems. Congress gave him money for three hubs: One, for turning sunlight into fuels, is based at the University of California, Berkeley; the second, to develop the next generation of commercial nuclear reactors, is housed at DOE's Oak Ridge National Laboratory.

But GPIC, as its name implies, is more than a hub. It's also the first federally funded regional innovation cluster. A RIC is meant to raise the overall innovation IQ of a geographical area, and an E-RIC is supposed to do that by concentrating on clean energy technologies. Although DOE is the driver for the Philadelphia project—putting up $122 million of the total for the core research and technology activities—the Small Business Administration and three programs within the Department of Commerce are also chipping in money to promote economic redevelopment, strengthen manufacturing, and provide job training throughout the region. As Chu said in February when he announced the E-RIC competition, "energy efficient buildings represent one of our best and most immediate opportunities to create jobs, save money, and cut carbon pollution."

As early as this fall, scientists and engineers will begin swarming over the same ground once trod by steamfitters and ensigns. The idea of using an existing brownfield site is one of GPIC's more attractive features, says Henry Foley, Penn State's vice president for research and dean of its Graduate School, who's heading the new cluster.

"It's a city within a city," says Foley, a professor of chemical engineering with extensive industrial and academic experience, about the Navy Yard. "It has its own energy grid. We have more than 200 buildings to play with, of all sizes and shapes, and there's already a plan to rejuvenate it. We think it's a perfect place to begin."

The state is kicking in $30 million to help retrofit Building 661 and construct an adjacent integrated building sciences lab that together will serve as home for the hub. Each partner in the cluster—a far-flung alliance of 90 organizations that includes Purdue, Virginia Tech, Michigan, and Carnegie Mellon universities; IBM and United Technologies Corp.; and two DOE labs, Lawrence Livermore and the Princeton Plasma Physics Laboratory—will send scientists and engineers to work at the site, Foley explains.

Foley's job is to keep them marching toward the same, clear goal. "Look at all the progress we've made in other industries in design, building, and manufacturing processes," he begins. "Take automobiles. They've come up with new materials, better combustion engines, improved efficiency, reduced emissions. There's nothing comparable to that in the building industry."

The building sector needs to develop similar designs for superlow emissions and superhigh efficiencies, he argues. "Our first task is to do the science and engineering that's needed for innovations in how new buildings are constructed and how existing buildings can be rehabbed to meet higher standards," he says. "Then we'll try to put them into general use. … Retrofitting an existing structure and integrating it into the larger grid is a challenge that America faces. So we think it should be our challenge, too."

Foley says previous attempts ignored key components of what it takes to be green. "In the 1970s, we made buildings more energy efficient, but they were not always habitable because the materials that they used were harmful to people and to the environment," he says. "And in today's tough economic climate, no one would risk using something that hasn't been proven effective."

Although those who lost out to Penn State wish the decision had gone their way, they seem pleased that DOE is supporting interdisciplinary collaborations in building efficiency. "This is a field that has been chronically underfunded in the United States," says Leon Glicksman, a professor of building technology and mechanical engineering at the Massachusetts Institute of Technology (MIT) in Cambridge, the lead institution on a proposal from New England that would have converted an empty warehouse on campus into a testing and learning center. "It was amazing to see how many people at MIT from different fields were interested in the idea."

–JEFFREY MERVIS

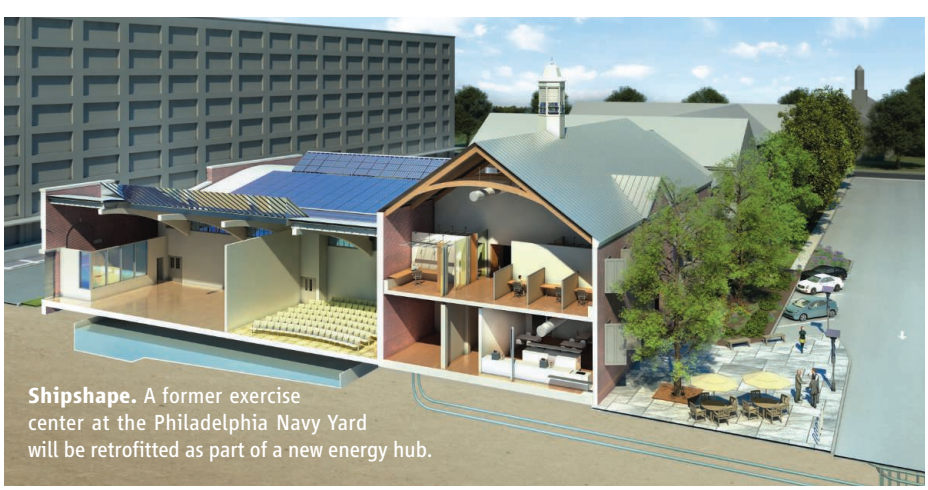

Shipshape. A former exercise center at the Philadelphia Navy Yard will be retrofitted as part of a new energy hub.

CREDIT: IMAGE COURTESY OF RE:VISION ARCHITECTURE

Published by AAAS

CREDIT: PHOTO BY JASON CLARKE, COURTESY OF SCIENCE FOUNDATION IRELAND

NEWSMAKER INTERVIEW: FRANK GANNON

Ireland's Departing Research Chief On Irish and European Science

In his early 60s and back in his native country after a decade-plus stint in Germany running the European Molecular Biology Organization, Frank Gannon probably could have finished out his career comfortably as director of the national funding agency Science Foundation Ireland (SFI), a position he's held since 2007. But after celebrating SFI's 10th anniversary in October, the biologist will resign his position at the end of the year and head off to Australia to become director of the Queensland Institute of Medical Research (QIMR) in Brisbane.

QIMR already has some 700 scientists working in about 60 research groups and is expanding thanks to state investment. Gannon's move will allow a return to the lab to conduct research on steroid hormone receptors and DNA methylation, something he gave up to direct SFI. "That's something that is a really attractive aspect of the [QIMR] job. I found I hadn't stopped wondering about some of the questions I was working on."

Gannon has been an active player in European science policy. He lobbied strongly, for example, for the creation of the European Research Council (ERC), which funds individual scientists in Europe. He says that ERC is off to a great start but notes that more than 95% of its grants go to just 15 of the European Union's 27 members. Perhaps, Gannon argues, ERC should create a new grant program "to build up strengths in places that are not fully competitive at the moment."

–JOHN TRAVIS

Q: There may be a perception that you are leaving SFI before Ireland is forced to make even more drastic cuts to its funding. Can you reassure SFI's scientists?

F.G.: This year has been a year of absolute economic stringency to make sure we could get the most out of the funds that were provided. There were cuts in our budget. Ireland is in a state where that was inevitable, unsurprising. … Will there be another cut next year, and is this the end of the strategy [to grow the economy through research and development]? The government has said in meetings and in the media here that the SFI budget will be increased next year, 2011. Then it will be back on track for some years to come. … There is a realization at the highest policy level that Ireland has to have a smart, or knowledge-based, economy. There is a recommitment to increased funding for research, development, and innovation.

Q: In terms of European science, are you optimistic or pessimistic about the region?

F.G.: By nature, I'm optimistic. I think the Irish story is being rerun at the European level. There was a time in many European countries where the research world felt it was sufficiently special that it didn't need to do anything other than good research. The new emphasis in Europe and on the national level is that knowledge is necessary but not sufficient. Getting linkages between the knowledge and the economy is something that is exercising many people's minds.

Q: Has the European Research Council lived up to your expectations?

F.G.: I think it has not only lived up to expectation but is now seen as a core component [of European science]. … The researchers that are being identified are setting standards for everyone else. [An ERC grant] has quickly become a symbol of excellence. The E.U. wasn't always associated with being a symbol of excellence. It was a symbol of effectiveness but not excellence.

ScienceInsider

From the *Science* Policy Blog

The editor of the journal *Cognition* says he believes that **fabrication is the most plausible explanation** for data in a 2002 paper by Harvard University's Marc Hauser involving cotton-top tamarins. The paper, which is being retracted, adds to growing doubts about the validity of Hauser's work on the cognitive gap between humans and monkeys. http://bit.ly/cognition-editor

Continuing an apparent **campaign to wipe out political dissent on campus**, the Iranian Ministry of Science has removed the founder-director of the Institute for Advanced Studies in Basic Sciences in Zanjan and the chancellor of Sharif University of Technology in Tehran and replaced them with scientists who are strong supporters of President Ahmadinijad. http://bit.ly/iran-firings

The European particle physics laboratory, CERN, has announced a **6% cut in spending over the next 5 years** that puts some projects on a longer time frame. It keeps open the world's largest atom smasher—the 27-kilometer-long, subterranean Large Hadron Collider—and avoids layoffs. http://bit.ly/cern-trims

China's self-appointed science fraud buster was assaulted outside his Beijing apartment this week. Police are investigating **the attack by two men on Fang Shimin**, better known by his pen name Fang Zhouzi. http://bit.ly/fang-assaulted

A new report from the Obama Administration on how last year's $787 billion stimulus package is helping to **transform the U.S. economy by fostering more innovation** puts a premium on applied renewable energy and genomics research. http://bit.ly/stimulus-innovation

A New York City public interest group has challenged **eight patents on the widely used HIV/AIDS drug ritonavir**, a protease inhibitor. It wants the U.S. Patent and Trademark Office to hold a formal reexamination of a string of awards made between 1996 and 2008 to Abbott Laboratories. http://bit.ly/ritonavir-patents

For more science policy news, visit **news.sciencemag.org/scienceinsider**.

Published by AAAS

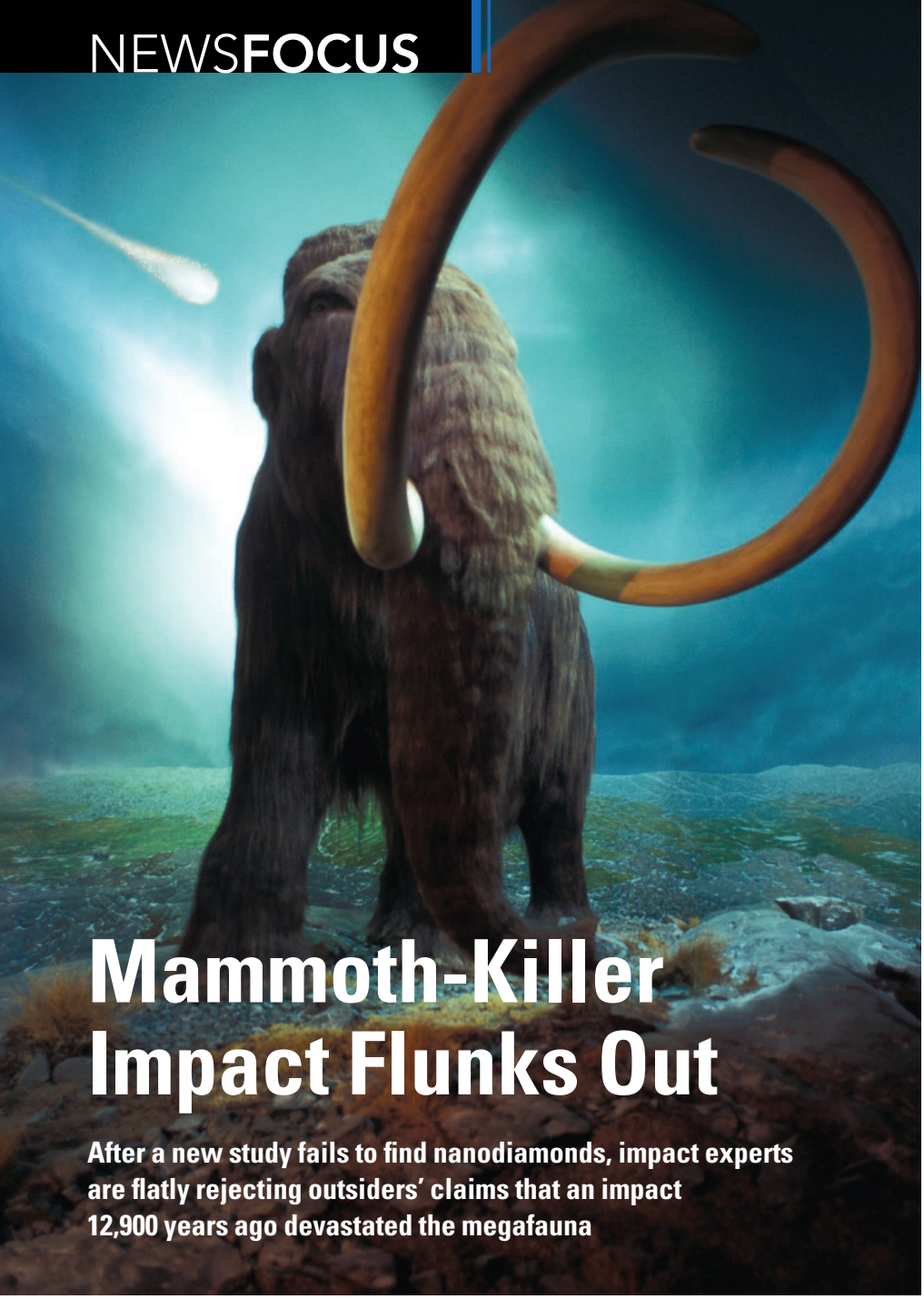

Mammoth-Killer Impact Flunks Out

After a new study fails to find nanodiamonds, impact experts are flatly rejecting outsiders' claims that an impact 12,900 years ago devastated the megafauna

DID A CONTINENT-SEARING COMET IMPACT wipe out the mammoths and other great beasts? Impact specialists have now weighed in on that widely publicized possibility. Their verdict: There never was a mammoth-killer impact. Proponents' evidence "is not internally consistent, not reproducible, and certainly not consistent with being produced by impact," says geochemist Christian Köberl of the University of Vienna, who has been publishing on impacts for 27 years.

Since impact specialists went looking on their own, Köberl says, "nobody has found anything." The final blow, in the eyes of some, comes this week in a paper reporting a failure to find proponents' most promising trace of an impact, a particular crystal form of nano-size diamond.

Core supporters of the impact scenario are sticking to their guns. "It's an hypothesis," says paleoceanographer James Kennett, professor emeritus at the University of California, Santa Barbara, and a prominent member of the loose confederation of assorted impact proponents. "If anything clearly shows it to be wrong, I'll abandon it," Kennett says—but not yet.

Evolutionary origins

The mammoth-killer impact hypothesis got its start in the late 1980s, says retired geophysical consultant Allen West of Prescott, Arizona, who became a prominent impact proponent. That's when William Topping, a retired archaeologist in New Mexico, went looking in sediments for evidence of a cosmic episode in Earth's history. He found unusual mineral grains—tiny magnetic spherules—at a pivotal point in the geologic and archaeological records: 12,900 years ago, about when the 1000-year-long cold snap called the Younger Dryas began, megafauna such as the mammoth disappeared, and the distinctive arrowheads and spear points crafted by the Paleo-Indian Clovis people vanished from the record.

By 2001, the Younger Dryas mineral grains had spawned the "nuclear catastrophe" hypothesis. Topping and nuclear chemist Richard Firestone of Lawrence Berkeley National Laboratory in California proposed that an earlier "nearby supernova or cosmic ray jet" had triggered "a sequence of events that may have included solar flares, impacts, and secondary cosmic ray bombardments" that did in the Clovis culture as well as the mammoths. Topping's magnetic "spherules," they proposed, had formed in the heat and pressure of the cataclysm.

Online
sciencemag.org
Podcast interview with author Richard A. Kerr.

By 2007, however, the supernova and its great irradiation had been put aside and a single North American impact had become the focus. And the cast of characters had grown. At the May meeting of the American Geophysical Union (AGU) (*Science*, 1 June 2007, p. 1264), a loose consortium of more than 25 people including Firestone, West, Kennett, and Topping presented a half-dozen chemical and mineralogical traces of an impact that were recovered from sediments laid down at the onset of the Younger Dryas—that is, at the Younger Dryas boundary (YDB). In their new scenario, a comet blew up in the atmosphere over North America or blasted into the lingering Laurentide Ice Sheet in Canada. They also presented soot, charcoal, and other carbonaceous debris from the YDB as evidence of continent-engulfing wildfires touched off by the impact.

Then, in an October 2007 paper in the *Proceedings of the National Academy of Sciences* (*PNAS*), 26 authors led by Firestone, West, and Kennett—a member of the National Academy of Sciences—made their case in the peer-reviewed literature. Only one of the 26 had previously worked on impact markers, and her specialty—molecular cages of carbon atoms containing trapped helium—remains unconfirmed as an impact marker (*Science*, 7 March 2008, p. 1331).

CREDIT: JEAN-PIERRE SYLVESTRE/PETERARNOLD

Published by AAAS

No impact, thank you

Now, 3 years later, of the 12 lines of evidence presented for an impact, "nanodiamonds are the last man standing. Everything else has failed to be corroborated," says geologist Nicholas Pinter of Southern Illinois University, Carbondale, who with colleagues has looked for YDB markers.

Supposed chemical evidence has withered under scrutiny, says impact geochemist Philippe Claeys of the Free University of Brussels. Claeys and colleagues probed YDB samples—both his own from Europe, and others from West—for claimed traces of an impacter. The targets included iridium, the exotic element that first put researchers on the trail of the dinosaur-killer impact. In a December 2009 *PNAS* paper, Claeys and colleagues reported their results: nil. "The geochemical story is finished; it's over," Claeys says. "There is nothing, no meteoritic signal. No one I know of has come to their defense."

Microscopic magnetic spherules—Topping's original find, later supported by Firestone and colleagues—haven't panned out either, say other researchers who have looked for them. Archaeologist Todd Surovell of the University of Wyoming in Laramie and colleagues found the minerals at four of seven YDB sites they searched, but the spherules occurred sporadically before, at, and after the YDB. Surovell and his team also looked for irregular magnetic mineral grains, reportedly one of the most reliable markers of the impact, but found "zero major peaks [of grains] associated with the onset of the Younger Dryas," says Surovell, who reported the result in *PNAS* in October 2009.

Lingering charred traces of impact-triggered wildfires are also in short supply, say researchers not proposing an impact. "I've done dozens of [YDB] sites, and charcoal is rare outside of Clovis cooking sites. It isn't there," says archaeologist C. Vance Haynes, professor emeritus at the University of Arizona in Tucson. Paleobotanist and fire scientist Andrew Scott of Royal Holloway, University of London, in Egham, U.K., goes further. "None of these people has spent their lives looking at carbon material in sediments," he says. "I've spent 35 years looking at it. I see no evidence of an exceptional fire event across North America."

The last nail?

None of those types of evidence is considered conclusive, however, specialists point out. Of the markers impact proponents have proposed, just one mineral bears the indelible signs of the crushing shock that in nature only an impact can create: high-pressure hexagonal diamond, or lonsdaleite. Using transmission electron microscopy (TEM), Douglas Kennett of the University of Oregon, Eugene (the son of James Kennett), James Kennett, West, and 14 colleagues reported the detection of such hexagonal nanodiamond at the YDB in a 20 July 2009 *PNAS* paper.

Two other groups have now looked for lonsdaleite at the YDB and found none. At the December 2009 AGU meeting, Claeys, microscopist Dominique Schryvers of the University of Antwerp in Belgium, and colleagues reported they could find no hexagonal diamond at a YDB in Belgium, only cubic diamond unrelated to an impact. And in a *PNAS* paper this week, physicist Tyrone Daulton of Washington University in St. Louis, Pinter, and Scott report searching samples from three YDB sites in the United States. Douglas Kennett and his co-authors had reported nanodiamonds at two of these sites, including hexagonal diamonds at one.

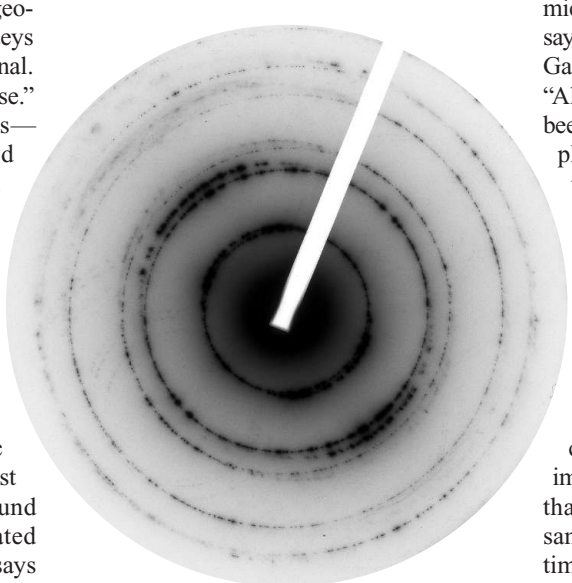

Diamond or dross? Transmission electron microscopy suggests to some there's no impact diamond.

Site of controversy. Proponents say traces of impact mark this 12,900-year-old dark layer.

On the basis of TEM analysis, "I'm convinced there's no [hexagonal] diamond present," says Daulton. TEM patterns of some material "matched closely what Kennett reported. I knew immediately this wasn't diamond." Instead, the material was aggregates of sheetlike forms of carbon, including graphene. "If you don't look too closely at it, you could convince yourself it is [lonsdaleite]. Theirs was a gross misidentification as lonsdaleite."

Daulton's judgment is reliable, other microscopists say. "He's a real TEM person," says meteoriticist and microscopist Laurence Garvie of Arizona State University, Tempe. "All the other [YDB] nanodiamond stuff has been written by people who aren't TEM people. If he says there are no nanodiamonds, there are no nanodiamonds."

Proponents of a Younger Dryas impact disagree. "The Daulton *et al*. claim that we have misidentified diamonds is false and misleading," writes Douglas Kennett in an e-mail. His complaints about Daulton *et al*. focus on sampling, sample processing, and interpretation. Impact proponents level similar criticisms at other outside studies of traces of impact and fire. Kennett sees little evidence that Daulton and his colleagues actually sampled the YDB, an often thin and sometimes hard-to-recognize layer. He also says that they probably analyzed too few carbonaceous particles—in which nanodiamonds reside—to find any diamond and that their sample processing may have destroyed diamond that was there. What's more, Kennett says, the TEM-determined crystalline structures of hexagonal diamond and graphene are so easily distinguished that misidentification is unlikely. "There's been a real problem of data quality," Kennett sums up.

This debate will likely go on for years. Impact specialist Köberl, for one, thinks it has already lasted too long. If impact proponents "had involved the mainstream community and listened to them, probably none of these papers would have been published," he says. Meanwhile, many researchers drawn from more mundane work to hunt for a killer impact are calling it quits."I spent 16 months in the lab and found very little evidence to support their hypothesis," says Surovell. "I have other things to worry about." **–RICHARD A. KERR**

CREDITS (TOP TO BOTTOM): TYRONE DAULTON/ WASHINGTON UNIVERSITY IN ST. LOUIS; ALLEN WEST

Published by AAAS

A doctor first. François Nosten treating a sick child at the Mae La refugee camp.

PROFILE: FRANÇOIS NOSTEN

The Dour Frenchman on Malaria's Frontier

When he arrived at the dangerous Thai-Burmese border in 1984, François Nosten barely knew what research was. Today, he's one of the world's top malaria scientists

MAE SOT, THAILAND—You'd think that a malaria scientist in François Nosten's position would need lots of charm and excellent diplomatic skills. He's a foreigner working in Thailand, a country where smiling seems a prerequisite for getting anything done. His work straddles the politically sensitive and occasionally violent border with Myanmar, formerly Burma, and he manages a health care system primarily for illegal immigrants from that country—people the Thai government largely ignores.

But as it happens, Nosten, 53, doesn't exude much charm, he rarely smiles, and one colleague calls him "famously undiplomatic." When *Science* came to visit him in this border town, a 7-hour drive from Bangkok, Nosten's long face bore a scowl. "I'm often grumpy," he confessed.

Yet despite his frequent sourness, Nosten has built an unmatched international resume in malaria. The Shoklo Malaria Research Unit (SMRU), which he founded 25 years ago, not only provides basic health services to tens of thousands of poor people, but it's also one of the most respected and prolific clinical malaria research centers in the world. With more than 230 published papers, including co-authorship of a report on page 1175 of this issue of *Science*, Nosten ranks as one of the 10 most-cited researchers in his field.

It was at SMRU that the so-called artemisinin-based combination therapies (ACTs), a class of new drugs that has become the standard worldwide, were pioneered. Most of the clinical trials of malaria treatment for pregnant women—who are especially vulnerable to dying from the disease—were done here. Epidemiologist Philippe Guérin, who worked with Nosten for 3 years in the late 1990s, calls his contribution "somewhere between enormous and critical." As to his demeanor, "people either love or hate François," says Guérin.

Those in the former category say you just have to get used to him. And indeed, Nosten seemed to thaw when, after a quick stop to pick up some cold beers, he invited this reporter to his wooden Thai house, set in a huge, private, fenced garden. "Welcome to Mae Sot," he said after popping open the first two cans. And as the evening went on, Nosten talked passionately about his unusual career. He even managed a smile or two.

True to his roots. After 25 years in Thailand, Nosten still feels "completely French."

Arms and legs

Nosten, who grew up in Toulouse, France, arrived in Thailand in the early 1980s as a long-haired doctor for Médecins Sans Frontières (MSF), the French charity. He knew next to nothing about malaria, and he wasn't trained as a scientist. It was his curiosity as a doctor that drove him to research. He quickly noticed that the standard malaria drugs weren't doing their job because the parasite had developed resistance, and he wondered whether mefloquine, a new drug developed by the U.S. Army, would do any better. So he embarked on his first clinical studies.

In 1985, he met Nicholas White, a British malariologist who had just set up shop in Bangkok, funded by the Wellcome Trust, and had a professorship at the University of Oxford. White was scouting for malaria research locations; Nosten was running a jungle hospital just across the border in Myanmar. "It was made out of wood and leaves, but it was a very good hospital," White recalls. Impressed, he convinced Nosten to leave MSF and do studies for him.

A quarter-century later, SMRU has five clinics serving an area roughly 200 kilometers long on the Thai-Burmese border, along with a research unit in the center of Mae Sot, a town of some 30,000 inhabitants. Nosten employs more than 350 people, 20 of them ex-pats from various Western countries. White, still in Bangkok, remains "the brain" behind this operation, he says. "I'm the arms and the legs. But I don't care. I'm very happy with him, and I'm his disciple." Guérin calls that false modesty, as Nosten has become an opinion leader himself.

To his staff members, Nosten is "like a demanding, old-fashioned father," says Marcus Rijken, a Dutch physician who came here 3 years ago to study the effects of malaria on unborn babies. Don't expect praise from him just for agreeing to come live in this dull, remote town, Rijken says: "He puts the bar very high, for himself and everybody else." Although some have left in frustration, those who stayed say Nosten is also a very helpful and witty mentor and an inspiration in his own peculiar way.

Porous border

When it comes to public health, border areas are often chaotic. Differing policies, language barriers, and human movement create messy

CREDITS (TOP TO BOTTOM): S. NOSTEN

Published by AAAS

circumstances where infectious diseases thrive. The Thai-Burmese border is a prime example, says Nosten, as he provides a tour in his Land Rover the next morning. Burma, just across the river, is dirt-poor and has a dismal health system. Tens of thousands of refugees have lived in semipermanent refugee camps on the Thai side for decades—most of them members of the Karen, an ethnic minority fighting for autonomy.

In addition, migrants from Myanmar continually cross the border looking for a better life. On any given day, dozens of people wade or raft across the Moei River. The Thai government is "in denial" about the influx, Nosten says, and the Thai health system is neither equipped nor financed to help people from Burma. "That's why we do it," he says. While the Wellcome Trust funds his research, Nosten is continuously hunting for funds for the health service, which has gradually expanded and now includes maternal care and treatment for HIV and tuberculosis.

Hybrid. SMRU is a research center as well as a health-care service for Karen refugees and migrants.

The conditions have long been harsh. For about a decade, the team lived in Shoklo, one of the camps, under primitive conditions and with little contact with the outside world. Massive floods almost swept away the hospital several times in the early 1990s, and Nosten nearly drowned while rescuing a Karen nurse. "Get the files! Get the files!" former SMRU researcher Christine Luxemburger recalls yelling during one such episode; the data from a malaria vaccine study were among the few items saved from the water. The camp also came under attack from the Burmese army, and in 1997, the Thai government decided that SMRU staff members could no longer stay there overnight. They had to move to Mae Sot.

Nosten says he's careful to stay out of politics. "If I started criticizing the Burmese generals or the Thai politicians, I couldn't survive here," he says. Nosten identifies strongly with the Karen and is well-known and beloved by them, says staff manager Honey Moon, who's been with SMRU for 25 years and is Karen herself. He married a Karen woman in 1989, and although he speaks Karen, his Thai is rudimentary. White, who's fluent in Thai, handles most of the bureaucratic and political hurdles, while Mahidol University in Bangkok—on whose faculty both Nosten and White serve—provides important backing.

Nosten says he's never tried that hard to integrate. "I was very happy to remain completely French," he says. So French, indeed, that he taught his housekeeper how to make baguettes, and he keeps an apartment near the Place de la Bastille in Paris, where he travels several times a year. He received an important recognition from his home country when he won the prestigious $400,000 Christophe Mérieux award in 2008.

Part of Nosten's appeal is that he has remained an MSF doctor at heart; his scientific curiosity is driven by the people he lives among, says Jean-René Kiechel of the Drugs for Neglected Diseases Initiative, a nonprofit in Geneva, Switzerland, with which Nosten has collaborated. It's also what led Nosten to explore the potential of ACTs. When mefloquine started failing soon after it was introduced, Nosten and White decided to try a new family of drugs called the artemisinin derivatives, isolated in China from a plant named *Artemisia annua*. To preempt resistance, they proposed combining a derivative called artesunate with another drug, a novel concept in malaria. In 1991, they started the first clinical trial of a combination of artesunate and mefloquine; by 1994 they were convinced that it was safe and effective.

SMRU has helped test every other ACT to come to the market since. But Nosten is frustrated that it took so long for combination therapies to become universally adopted. In Africa, in particular, ACTs weren't introduced broadly until about 5 years ago, despite evidence that older drugs were useless. "It's something strange about the malaria community," he says. "There are a lot of preconceived ideas, a lot of things preventing people from changing their minds." He says he's tried his best to change them—sometimes in not-so-subtle ways. "At meetings, I can be a bully," he admits.

Monstrosity

Nosten attributes SMRU's success to its hybrid nature: part humanitarian, part scientific. "We're not coming in big white vans, taking samples, and disappearing," he says. "We're embedded within the communities, so we have much better access to patients. And if treatment A works better than B, we can immediately implement that." Malaria rates, for instance, have plummeted in recent years in the border area.

But over a plate of spicy noodles at a roadside restaurant, he acknowledges that the model may not be sustainable. It's hard to attract people of international stature to the middle of nowhere for the long term. He says things might be easier if SMRU were split into a medical NGO, perhaps run by locals, and a research center where scientists could spend shorter amounts of time. "But if you do that the wrong way, then you break the link, and the research dies," he says.

"I guess I've created a monstrosity. I don't know what will happen with it after I'm gone," he concludes, as he musters another one of his rare smiles. **–MARTIN ENSERINK**

CREDIT: JOSS DIMOCK

Published by AAAS

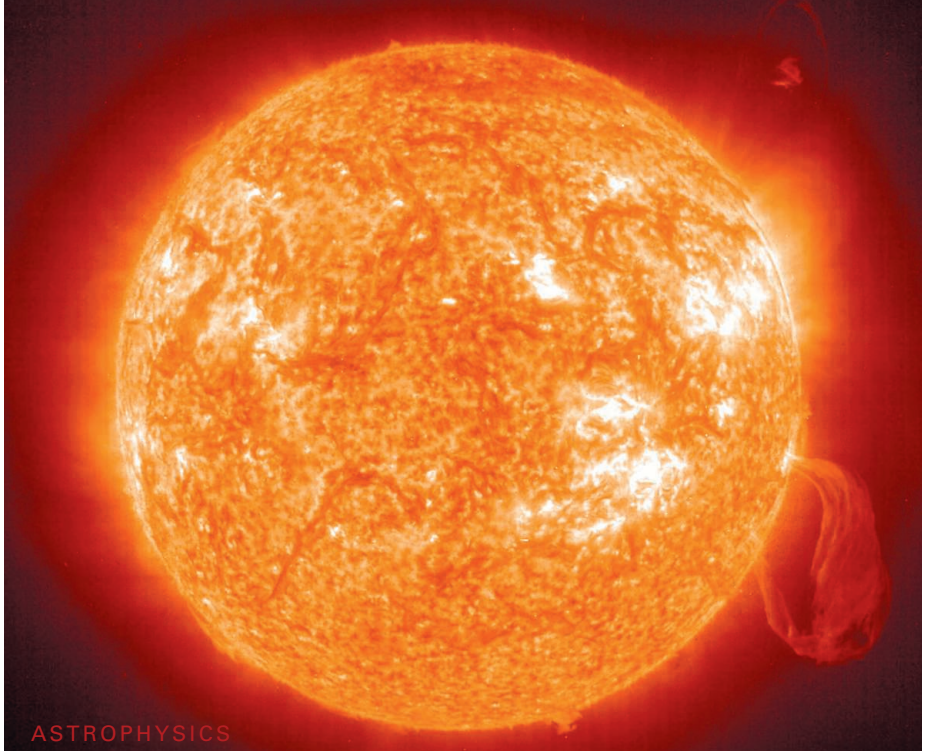

Hot topic. The sun's chemical composition is a key yardstick for astronomy.

CREDIT: NASA

ASTROPHYSICS

An Unsettled Debate About The Chemistry of the Sun

Researchers thought they knew the sun very well. Now, they are squabbling over the abundance of different elements in it

On a cloudless August morning, Martin Asplund is sitting in the sun, taking a coffee break from an astronomy conference. The day is so blazingly bright it makes Asplund squint and turn away from the sunlight. But the 40-year-old astrophysicist is not shying away from a heated solar debate that he ignited a few years ago.

In 2005, Asplund came out with a new picture of the chemical composition of the sun. His calculations showed that the abundances of carbon, nitrogen, oxygen, and neon in the star—the most plentiful elements in it besides hydrogen and helium—were about half as high as researchers had previously worked out. The new values solved a puzzle, because the previous calculations had always made the sun's chemistry seem oddly out of sync with that of its galactic environment. But when researchers plugged the new abundances into models of the solar interior, the resulting predictions about the sun's temperature profile no longer matched observations. The mismatch led to a debate over which of the two was right: the new abundances or the models.

Five years later, the question has not been resolved. "We're left with a conundrum," says Asplund, who is a director at the Max Planck Institute for Astrophysics in Garching, Germany.

Getting the abundances and the models correct is not just important for studies of the sun. It has implications for other fields of astronomy, such as how stars evolve and what interstellar gas is made of. That's because the sun's elemental composition is used as the yardstick for measuring the composition of everything else in the universe, from distant galaxies to blobs of gas inside the Milky Way.

Asplund's abundances have both fans and critics among other researchers. In the past 5 years, continued skepticism—mainly by astrophysicists who model the sun's interior—has forced Asplund's group to rework its calculations using more detailed physics. As a result, the values have shifted closer to the old abundances, as Asplund and colleagues reported in a 2009 paper in the *Annual Reviews in Astronomy and Astrophysics*. But the abundances are still only about two-thirds of the older ones, and the problems that creates remain fundamentally unchanged. Researchers have tried in vain to fine-tune models of the solar interior to match the new abundances.

The debate provides a glimpse into the messy world of modeling, where results are often fraught with uncertainty and temporary truths are hammered out by the tweaking of parameters and grudging consensus. "It makes us realize that we do not understand the sun—and by extension other stars—as well as we believed," says Aldo Serenelli, a solar modeler who works with Asplund at Garching. However, he is optimistic that the effort to reconcile solar models with the new abundances will eventually lead to new insights about the sun and other stars. "This is a very healthy exercise; it's what science is about, questioning our knowledge and understanding," he says.

A star is born

The sun was of no special interest to Asplund when he got his Ph.D. in theoretical astrophysics from Uppsala University in Sweden in 1997. He was developing models of the atmospheres of old stars so that he could use those stars as markers of galaxy formation and evolution.

Previous researchers had already modeled the sun's atmosphere, simplifying their computations by flattening the solar sphere into a disk. Asplund, however, thought three-dimensional modeling of stellar atmospheres would be more accurate. Taking advantage of advances in computing, he developed a 3D picture of the turbulent gas flows and energy transfer in a star's atmosphere, taking into account the interaction between radiation and plasma.

To test his models, Asplund turned to the star for which the most data are available: the sun. Over decades of study, researchers have developed a detailed picture of how this brilliant inferno works. At its core, millions of tons of hydrogen fuse into helium every second. The energy generated by this fusion radiates outward. At about two-thirds of the way to the sun's surface, the temperature becomes cool enough (about 2.3 million kelvin) to make the gas considerably more opaque to photons. Now, convection becomes dominant. Thermal columns carry hot material up to the surface, beyond which lies the solar atmosphere. Some of the energy eventually ends up as sunlight.

Asplund's models accurately predicted the variation in the sun's brightness across the solar disk (a function of the solar atmosphere) and the intensity of sunlight at different wavelengths. Then Asplund applied a third test: checking whether his models could generate a detailed solar spectrum that matched observations. To do so, he needed to combine his models with a scheme other researchers had developed, mapping the cascade of events that occurs as radiation emanates from deep inside the sun. This scheme, known as a line formation code, describes how photons of different

Published by AAAS

wavelengths interact with molecules and atoms in the gas; for example, getting absorbed by certain atoms that in turn emit other photons at new wavelengths. Together with the atmospheric models, it yields a unique spectrum for a given chemical composition.

Asplund's models passed this test as well, generating a spectrum that looked like the real one. But they also yielded abundances of carbon, nitrogen, oxygen, and neon radically lower than the previously accepted values. That was a surprise, Asplund says: "I thought things would only change a little bit as a result of 3D modeling of the atmosphere."

Asplund made a splash with the new abundances at a symposium in Austin in June 2004. The work appeared a year later in the proceedings of the conference; one of the co-authors was Nicolas Grevesse of the University of Liège in Belgium, who had been involved in calculating the earlier abundances. Stellar astrophysicists embraced the lower values, largely because they matched what researchers expected from a star that formed 4.5 billion years ago, when the galaxy was poorer in heavy elements than it is today.

Sound and fury

It wasn't long, however, before the new values came under attack from solar modelers. In the late 1990s and early 2000s, the old abundances had gained a foothold by helping astronomers solve a number of problems about the sun. Using them in models of the solar interior developed by Princeton University luminary John Bahcall and others, scientists had successfully predicted the characteristics of sound waves produced by the sun.

Helioseismologists can measure the speed and other features of these waves from minor changes either in solar brightness or in the position of spectral lines as the sun's surface expands and shrinks ever so slightly. From these measurements, they can infer how the temperature and density varies with depth below the solar surface. The same measurements help determine where the inner boundary of the convective envelope lies.

With the new abundances, researchers could no longer get the interior models to spit out sound speeds that matched observations. With less carbon, nitrogen, and oxygen in the mix, the material inside the sun became more transparent than previously thought. As a result, the boundary where the cooler gas became opaque to radiation—the base of the convection zone—was now pushed out toward the surface.

In August 2006, Asplund was an invited speaker at a helioseismology conference in Prague, at which the problems were discussed. "I knew that there would be some hostility," he says. Sure enough, his talk touched off a barrage of probing questions. It was clear that "they didn't believe our results, just as we didn't believe their models were correct," Asplund says. One of the skeptics in the audience—Marc Pinsonneault, an astrophysicist at Ohio State University in Columbus and an expert in modeling the sun's interior—suggested that Asplund and his colleagues had gone wrong by simulating only a small rectangular slab of the solar atmosphere instead of the whole thing.

"I decided we're going to redo everything," Asplund says. He and his colleagues developed "whole new atmospheric models" from scratch, this time simulating the entire solar atmosphere. "We tested them against even more observational constraints." By 2008, Asplund felt certain that his models were not the problem.

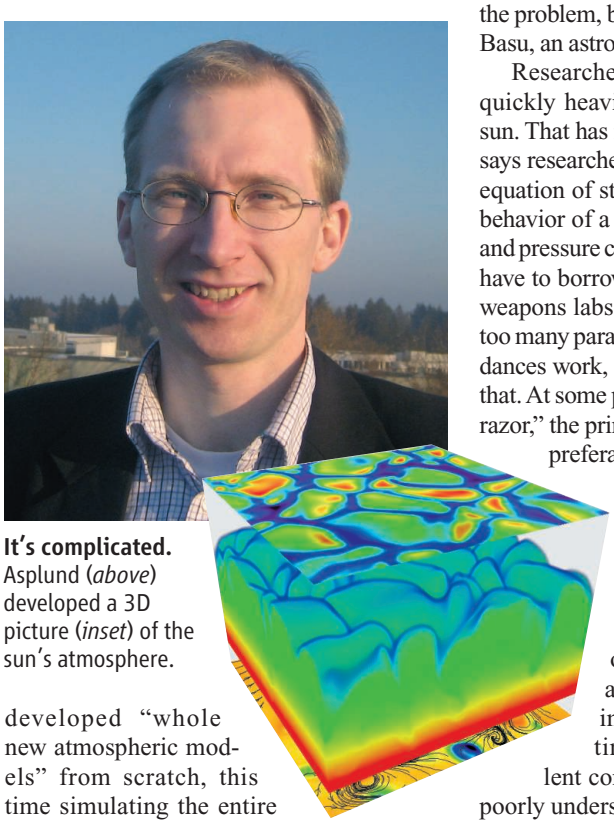

It's complicated. Asplund (*above*) developed a 3D picture (*inset*) of the sun's atmosphere.

That year, Aldo Serenelli, who had worked with Bahcall on interior models, applied for a position in Asplund's lab. Asplund was enthusiastic about working with somebody from the opposition camp, especially as he himself had no experience with modeling the interior. "I hired him not to convince him but to see whether we could find a solution that may have been overlooked," he says.

Serenelli says he joined Asplund with an open mind. "The agreement between solar models and helioseismology measurements was astonishingly good with older abundances, so it was hard to dismiss those results," he says. "On the other hand, Asplund's work was by far the most sophisticated and realistic study of the solar atmosphere."

In the past 2 years, Asplund and Serenelli have only grown more convinced of their respective positions. Meanwhile, Serenelli and others have tried a number of solutions to make the interior models work with the new abundances.

One approach assumes that elements such as neon and iron in the sun have a higher opacity (or lower transparency) than researchers have assumed. That shift would wipe out some of the gain in transparency resulting from the lower abundances. "It solves a fair amount of the problem, but it isn't enough," says Sarbani Basu, an astrophysicist at Yale University.

Researchers have also played with how quickly heavier elements sink down in the sun. That has not done the trick, either. Basus says researchers could also try modifying the equation of state describing the fundamental behavior of a gas under extreme temperature and pressure conditions, which astrophysicists have to borrow from experiments at nuclear-weapons labs. But that would be fine-tuning too many parameters to make Asplund's abundances work, she says. "I'm not willing to do that. At some point, you have to raise Occam's razor," the principle that simpler solutions are preferable to more-complex ones.

Others think the problem lies with models of the solar interior. "I think the standard solar model is missing something," says W. Dave Arnett, a researcher at the University of Arizona in Tucson. Arnett and colleagues are working to improve interior models by getting a better handle on turbulent convection in stars, which is still poorly understood.

Meanwhile, Asplund's 3D models of the sun's atmosphere are no longer the only game in town. Other researchers have developed sophisticated models of their own. One group, led by Hans-Günter Ludwig of the Paris Observatory, has produced abundance values somewhat higher than Asplund's, although still much smaller than the old values.

The continuing discrepancy "would suggest either new physics—exciting, if unlikely—or major errors in the existing physical ingredients of the models, which would have to be tracked down," says Pinsonneault. It's hard to predict what the outcome of such efforts would be, he adds, "but it could be very important for our understanding of the physics of stars."

–YUDHIJIT BHATTACHARJEE

CREDITS: COURTESY OF MARTIN ASPLUND

Published by AAAS

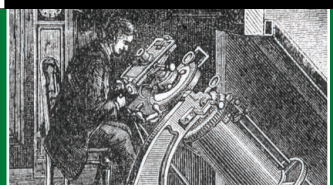

LETTERS

edited by Jennifer Sills

Give Beach Ecosystems Their Day in the Sun

THE INTERGOVERNMENTAL PANEL ON CLIMATE CHANGE FOURTH ASSESSMENT REPORT (*1*) LARGELY overlooked the impacts of climate change on marine ecosystems (*2*). In their Review ("The impact of climate change on the world's marine ecosystems," 18 June, p. 1523), O. Hoegh-Guldberg and J. F. Bruno redress this gap by synthesizing recent literature. In so doing, they made the disparities in research among ocean systems apparent. Specifically, there are no studies of climate change impacts to sandy beach ecosystems. Rather than any oversight by Hoegh-Guldberg and Bruno or previous authors (*3*), we believe that the omission of beaches from this and other assessments of anthropogenic impacts reflects a relative lack of appreciation of beaches as ecosystems.

This paucity of beach studies (*4*, *5*) is alarming, not only because beaches comprise ~70% of open-ocean coasts and have high socioeconomic and ecosystem value, but also because their position at the land-sea margin renders them highly vulnerable to climate change (*5*, *6*). Beaches are at risk of significant habitat loss and ecological impacts from warming, acidification, and erosion caused by sea-level rise and increased storms. Where landward retreat of beaches is restricted by development or topography, beach habitat may disappear. When engineering interventions seek to mitigate beach erosion, negative ecological consequences may be severe but are only beginning to be understood (*6*, *7*). The inadequacy of information on ecological impacts of climate change on this vulnerable and challenged coastal ecosystem must be addressed.

JENIFER E. DUGAN,[1]* OMAR DEFEO,[2] EDUARDO JARAMILLO,[3] ALAN R. JONES,[4] MARIANO LASTRA,[5] RONEL NEL,[6] CHARLES H. PETERSON,[7] FELICITA SCAPINI,[8] THOMAS SCHLACHER,[9] DAVID S. SCHOEMAN[10]

[1]Marine Science Institute, University of California, Santa Barbara, CA 93106–6150, USA. [2]UNDECIMAR, Facultad de Ciencias, Igua 4225, 11400 Montevideo, Uruguay. [3]Instituto de Ecología y Evolución, Universidad Austral de Chile, Valdivia, Chile. [4]Division of Invertebrates, The Australian Museum, Sydney, NSW 2010, Australia. [5]Department of Ecology and Animal Biology, Faculty of Marine Science, University of Vigo, 36310 Vigo, Spain. [6]Department of Zoology, Nelson Mandela Metropolitan University, Port Elizabeth, 6031, South Africa. [7]Institute of Marine Sciences, University of North Carolina, Chapel Hill, Morehead City, NC 28557, USA. [8]Department of Evolutionary Biology, University of Florence, 50125 Firenze, Italy. [9]Department of Marine Science, Faculty of Science, Health and Education, The University of the Sunshine Coast, Maroochydore DC, QLD 4558, Australia. [10]Centre for Coastal and Marine Research, School of Environmental Sciences, University of Ulster, Coleraine, BT52 1SA, Northern Ireland.

*To whom correspondence should be addressed. E-mail: j_dugan@lifesci.ucsb.edu

References

1. C. Rosenzweig *et al.*, in *Climate Change 2007: Impacts, Adaptation, and Vulnerability. Contribution of Working Group II to the Fourth Assessment Report of the Intergovernmental Panel on Climate Change*, M. L. Parry, O. F. Canziani, J. P. Palutikof, P. J. van der Linden, C E. Hanson, Eds. (Cambridge Univ. Press, Cambridge, 2007), pp. 79–131.
2. A. J. Richardson, E. S. Poloczanska, *Science* **320**, 1294 (2008).
3. A. S. Brierley, M. J. Kingsford, *Curr. Biol.* **19**, R602 (2009).
4. P. G. Fairweather, *Proc. Ecol. Soc. Aust.* **16**, 71 (1990).
5. T. A. Schlacher *et al.*, *Divers. Dist.* **13**, 556 (2007).
6. O. Defeo *et al.*, *Est. Coast. Shelf Sci.* **81**, 1 (2009).
7. C. H. Peterson *et al.*, *J. Exp. Mar. Biol. Ecol.* **338**, 205 (2006).

Methane from the East Siberian Arctic Shelf

IN THEIR REPORT "EXTENSIVE METHANE VENTing to the atmosphere from sediments of the East Siberian Arctic Shelf" (5 March, p. 1246), N. Shakhova *et al.* write that methane (CH_4) release resulting from thawing Arctic permafrost "is a likely positive feedback to climate warming." They add that the release of Arctic CH_4 was implied in previous climate shifts as well as in the recently renewed rise in atmospheric CH_4. These claims are not supported by all the literature they cite. Their reference 5 (*1*) presents measurements of emissions only of carbon dioxide, not CH_4. Their reference 8 (*2*), a study we conducted, suggests that a very large (~50%) increase in atmospheric CH_4 concentration associated with an abrupt warming event ~11,600 years ago was driven mainly by wetlands, without distinguishing between high and low latitudes. Their reference 9 (*3*) was published in 1993 and is not relevant to the renewed growth of atmospheric CH_4 that started in 2007. Their reference 10 (*4*) does not imply Arctic CH_4 releases in this renewed growth, and other recent work (*5*) also does not support sustained new emissions from the Arctic as the cause.

These findings of CH_4 emissions from the Arctic sea floor [in the Report and in (*6*)] add to our understanding of the atmospheric CH_4 budget, but they do not show that Arctic warming has produced a positive feedback

Letters to the Editor

Letters (~300 words) discuss material published in *Science* in the previous 3 months or issues of general interest. They can be submitted through the Web (www.submit2science.org) or by regular mail (1200 New York Ave., NW, Washington, DC 20005, USA). Letters are not acknowledged upon receipt, nor are authors generally consulted before publication. Whether published in full or in part, letters are subject to editing for clarity and space.

Published by AAAS

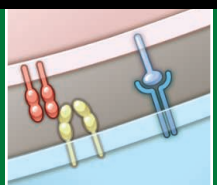

Skin sentinels
1154

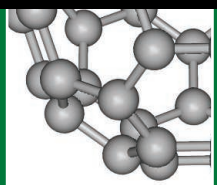

Carbon's fate in space
1159

in radiative forcing by causing these emissions to increase recently. A newly discovered CH_4 source is not necessarily a changing source, much less a source that is changing in response to Arctic warming. Shakhova *et al*. do acknowledge these distinctions, but in these times of enhanced scrutiny of climate change science, it is important to communicate all evidence to the scientific community and the public clearly and accurately.

VASILII V. PETRENKO,[1]* DAVID M. ETHERIDGE,[2] RAY F. WEISS,[3] EDWARD J. BROOK,[4] HINRICH SCHAEFER,[5] JEFFREY P. SEVERINGHAUS,[3] ANDREW M. SMITH,[6] DAVE LOWE,[7,8] QUAN HUA,[6] KATJA RIEDEL[5]

[1]Institute of Arctic and Alpine Research, University of Colorado, Boulder, CO 80309, USA. [2]Centre for Australian Weather and Climate Research, CSIRO Marine and Atmospheric Research, Aspendale, VIC 3195, Australia. [3]Scripps Institution of Oceanography, University of California, San Diego, La Jolla, CA 92093, USA. [4]Department of Geosciences, Oregon State University, Corvallis, OR 97331, USA. [5]National Institute of Water and Atmospheric Research, Kilbirnie, Wellington, New Zealand. [6]Australian Nuclear Science and Technology Organisation, PMB 1, Menai, NSW 2234, Australia. [7]Antarctic Research Centre, Victoria University of Wellington, Wellington, New Zealand. [8]Lowe NZ, Climate Change Education and Renewable Energy, Plimmerton–Porirua 5026, New Zealand.
*To whom correspondence should be addressed. E-mail: vasilii.petrenko@colorado.edu

References

1. E. A. G. Schuur *et al.*, *Nature* **459**, 556 (2009).
2. V. V. Petrenko *et al.*, *Science* **324**, 506 (2009).
3. W. C. Oechel *et al.*, *Nature* **361**, 520 (1993).
4. M. Rigby *et al.*, *Geophys. Res. Lett.* **35**, GL036037 (2008).
5. E. J. Dlugokencky *et al.*, *Geophys. Res. Lett.* **36**, GL039780 (2009).
6. G. K. Westbrook *et al.*, *Geophys. Res. Lett.* **36**, GL039191 (2009).

Response

WE THANK PETRENKO *ET AL*. FOR BRINGING attention to the community that, despite worrisome trends of warming in the Arctic with postulated positive climate-biogeochemistry feedback processes (*1*), there are still very few studies that can be cited for studying potentially relevant phenomena over extensive Arctic scales. Their criticism concerns the representativeness of some of our references.

We cited reference 5, Schuur *et al*. (*2*), because it shows that old C release increases as permafrost thawing increases, and that "emission rates will depend on the form of C gases released" (*2*). Strictly speaking, Schuur *et al*. did measure only CO_2, but we feel that the implications of their findings for methane budgets are clear.

It is correct that reference 8 (*3*) did not distinguish between high and low latitude, but the modeling of wetland emissions used radiocarbon signature of a thermokarst lake. We do not know of low-latitude wetlands or thermokarst lakes that could have provided such sudden and massive releases of methane. Given the ubiquity of subsea and land-fast wetlands and thermokarsts around the Arctic, we consider this citation fair.

References 9 and 10 (*4*, *5*) referred to the growth of contemporary (i.e., the time period in which we live) atmospheric CH_4 and CO_2. Data from both studies stand in contrast to data of the past. Growth in CH_4 concentrations was observed before the late 1990s (*4*) and after 2007 (*5*), in support of our assertions; thus, these references are appropriate.

Readers' Poll Results

The Time of Young Scientists

On 6 August, we asked what you thought about this question:
In the coming years, there is likely to be a growing focus on science communication; scientists will be asked to explain their science and the scientific process to the general public and policy-makers. How much time should the next generation of young scientists devote to these nonresearch activities?*

More than 3000 of you responded, from more than 60 countries. Here are your results:

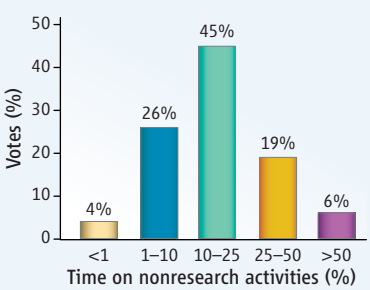

A selection of your thoughts:

"Communications skills, management skills, professionalism, and responsible conduct of research should balance the 'scientific theoretical' and 'research skill' components to develop the ideal young scientist. No one really learns how to 'communicate' without practice…"
—reader Emil Chuck

"[E]ach young scientist's career should first and foremost be driven by his or her passion for quality research. Yes, it is vital to be able to communicate about research, but the research must come first."
—reader Katrina Molland

Several readers based their responses on the assumption that nonresearch activities included all daily activities, not only science communication. Interpreting the results through this lens, these readers expressed concern that young scientists are subjected to unrealistic expectations, which in turn could lead to errors, exhaustion, and compromised creativity.

"[Y]oung scientists ought to get 8 hours of sleep per night, as a basic need for mental, physical, and emotional health. They should take at least one day per week off of their intellectual scientific pursuit, to leave room for unstructured reflection; to maintain their curiosity and inspiration; and, of course, to do laundry, garden, shop for groceries, etc. … Let's be realistic with regard to our expectations of young scientists, and foster an environment in which they might thrive, not just as counted in numbers of publications."
—reader Dr. S. Fischer

*See the poll, and links to the related Letters and Editorial, at www.sciencemag.org/extra/polls/20100806-1.dtl.

Polling results reflect the votes of those who chose to participate; they do not represent a random sample of the population.

Published by AAAS

Contrary to what is claimed by Petrenko *et al*., reference 10 (*5*) states, "we find that a substantial increase in [methane] emissions from both hemispheres was necessary between 2006 and 2007 to fit the observations." Given that Arctic/Subarctic wetlands are major contributors of northern hemisphere methane emissions, we maintain that this is a fair citation.

Unlike its land-fast cousin, subsea permafrost is not only changing in response to glacial/interglacial Arctic warming (~7°C), but is experiencing an additional ~10°C warming from overlying seawater since inundation in early Holocene. Hence, it must be understood that the greater vulnerability of the subsea permafrost methane pool may lead to an unfortunate coincidental timing with anthropogenic greenhouse gas releases. Whether additions of methane to the atmosphere can be linked to anthropogenic activities or are caused by nature, the radiative effect of the sources will be additive.

NATALIA SHAKHOVA,[1,2]* IGOR SEMILETOV,[1,2] ÖRJAN GUSTAFSSON[3]

[1]International Arctic Research Center, University of Alaska, Fairbanks, AK 99775, USA. [2]Russian Academy of Sciences, Far Eastern Branch, Pacific Oceanological Institute, Vladivostok, Russia. [3]Department of Applied Environmental Science and Bert Bolin Centre for Climate Research, Stockholm University, Stockholm, Sweden.
*To whom correspondence should be addressed. E-mail: nshakhov@iarc.uaf.edu

References

1. N. Gruber *et al.*, in *The Global Carbon Cycle; Integrating Humans, Climate, and the Natural World,* C. B. Field, M. R. Raupach, Eds. (Island Press, Washington, DC, 2004), pp. 45–76.
2. E. A. G. Schuur *et al*., *Nature* **459**, 556 (2009).
3. V. V. Petrenko *et al*., *Science* **324**, 506 (2009).
4. W. C. Oechel *et al*., *Nature* **361**, 520 (1993).
5. M. Rigby *et al*., *Geophys. Res. Lett*. **35**, GL036037 (2008).

Candidate Gene Approach's Missing Link

J. COUZIN-FRANKEL, IN HER NEWS FOCUS story "Major heart disease genes prove elusive" (4 June, p. 1220), presents an excellent summary of the scientific community's satisfaction and disappointment regarding genome-wide association studies. I would like to clarify one point that may have hampered the progress of those who use the candidate gene approach to investigate the genetics of complex human traits.

Given the many surveys of individuals of European ancestry, one might assume that the majority of common genetic variants are represented by at least one of the single-nucleotide polymorphisms (SNPs) in the genotyping platforms (*1*). However, this is not true. For instance, the immunoglobulin GM loci have at least 18 alleles, but none of the SNPs useful for indentifying these are included in the human diversity panel used in the HapMap project. Almost all GM markers are expressed on the Fc region of immunoglobulin gamma heavy chains, candidate genes for variation in immune responses because they interact with receptors expressed on effector cells (e.g., natural killer cells). They also contribute to antibody-dependent cell-mediated cytotoxicity, a major host mechanism for destroying virally infected cells as well as tumors. Yet genome-wide association analyses of infectious and malignant diseases are unlikely to detect these genes.

JANARDAN P. PANDEY

Department of Microbiology and Immunology, Medical University of South Carolina, Charleston, SC 29425–2230, USA. E-mail: pandeyj@musc.edu

Reference

1. The International HapMap Consortium, *Nature* **449**, 851 (2007).

Published by AAAS

SOCIAL PSYCHOLOGY

Mood Swings

Richard Taylor

The world makes money go round. This is John Casti's bold hypothesis in *Mood Matters*, which challenges both traditional financial theory and human gut reaction about how the world works. Most people believe that major world events, such as elections or the outbreak of war, influence the collective mood of society. Casti (a mathematician at the International Institute for Applied Systems Analysis, Austria) argues the opposite: social mood drives the events. In other words, social pessimism affects the likelihood of terrorist attacks rather than the other way around. By his account, the role of the financial market is as an accurate barometer of social mood, and a careful reading of the market's highs and lows might help predict how crucial world events will unfold.

Those within the field of social economics recognize that financial markets are more about understanding people, and in particular crowd psychology, than about money itself. Alan Greenspan, the former chairman of the U.S. Federal Reserve, described human nature's propensity to sway from fear to euphoria as "a condition that no economic paradigm has proved capable of suppressing without severe hardship" (*1*). The book departs from tradition when considering the relation between these mood swings and events. Casti promotes the picture of "socionomics" developed by Robert Prechter, which holds that social moods are driven by fundamental waves of optimism and pessimism that are surprisingly insensitive to world events.

To present the case, "sociometers" are needed to chart the social mood. Using his characteristic mix of clarity and humor, Casti takes the reader through the various measures that might be used. Rising birthrates are an obvious expression of optimism for the future. However, he also shows how more subtle signs reveal correlations as the social mood evolves. These include the construction of skyscrapers, the rise and fall of skirt length, car color, and music trends. Casti presents an effective argument for why the financial market serves as the optimal choice of sociometer.

The author reveals the tell-tale manifestations of socionomics through his meticulous detective work of the time lines involved in major events. In each case, he presents a compelling case for a mood change influencing the unfolding events. His conclusion often directly conflicts with flawed "event induces mood" sensations reported in the media. For example, the 2001 implosion of the U.S. energy company Enron was thought to have triggered a downswing in the financial market. Casti, however, argues that the sociometers at that time (including the financial market) indicated that the mood was already on a downswing. That trend blew in a societal climate of intolerance, which set the scene for the media's subsequent exposure of the Enron crisis.

Mood Matters
From Rising Skirt Lengths to the Collapse of World Powers

by John L. Casti
Springer, New York, 2010. 274 pp. $27.50.
ISBN 9783642048340.

Whereas readers will accept that mood can influence certain collective events in society, the second part of the socionomics account—that events have little feedback on mood—will, as Casti recognizes, meet with more skepticism. Thus, he asks for a suspension of disbelief while he runs through his comprehensive set of examples. These include the lack of long-term response of the financial markets (and therefore social mood) to dramatic events such as Pearl Harbor and John F. Kennedy's assassination.

This unexpected insensitivity to world events addresses a historic puzzle: why the financial market traces out recognizable patterns as a function of time. As Casti describes in the book's appendix, the peaks and troughs of the financial waves recur at increasingly fine time scales. First reported by Ralph N. Elliott in 1938 (*2*), this repetition at different scales represents one of the earliest noted fractal patterns in a physical system. If we believe the traditional view that the market is driven by irregular and diverse events, why would these cumulate in a distinct pattern? Instead, the fractal patterns provide an insight into human mood and behavior.

This timely book benefited from Casti's background in financial systems and complexity theory. The ten years he spent pondering the concepts and their consequences are evident in the volume of graphical evidence it includes. The author wisely declares his colors early on by stating that the work is deliberately one-sided and "opinionated," which is fair enough because his purpose is to trigger a reaction against the established beliefs of the financial world. The wealth of facts he presents should serve as valuable fuel for future scientific researchers arguing both for and against socionomics.

In these times of financial turmoil, many people will pick up *Mood Matters* with the hope of predicting financial markets. Although Casti includes a summary of Elliott Wave forecasting, his book is substantially more profound than this. By getting to grips with the relationship between events and social mood, he reveals the extent to which the latter determines our future. The last chapter discusses several questions that may help readers use socionomics to predict where our world is headed. The book emphasizes the importance of sociometers in signaling that fate.

Sign of upcoming downturn. Casti notes that construction of the next tallest building in the world (here, the Burj Dubai) starts while the local stock index is soaring, but a financial debacle arrives before the skyscraper is completed.

CREDIT: HAIDER YOUSUF/ISTOCKPHOTO.COM

The reviewer is at the Physics Department, University of Oregon, Eugene, OR 97403–1274, USA. E-mail: rpt@uoregon.edu

References
1. A. Greenspan, *Financial Times*, 5 February 2008, p. 11.
2. R. N. Elliott, *The Wave Principle* (New York, 1938).

10.1126/science.1194091

Published by AAAS

ASTRONOMY

Findings Brought to Ground

Gustav Holmberg

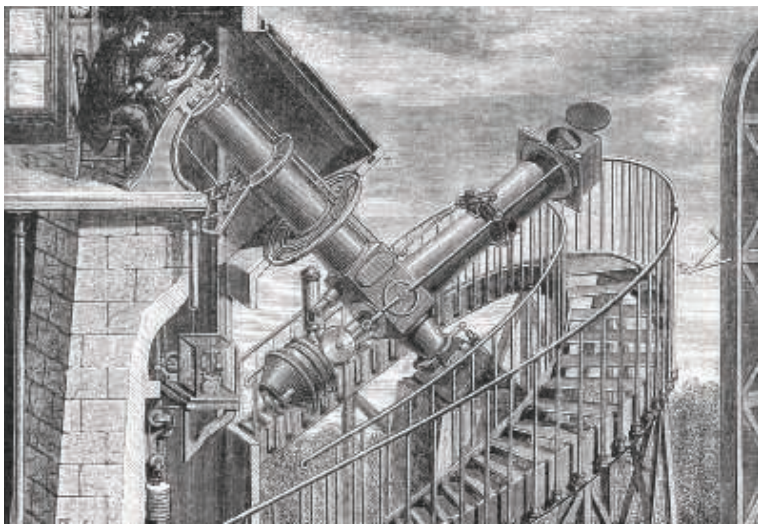

The Paris Observatory's grand equatorial coudé. Designed by Maurice Loewy, this 1890 telescope had a 60-cm lens.

Taking observatories as its unifying theme, *The Heavens on Earth* throws light on a variety of contexts, practices, and networks involving astronomy during the 19th century. The 12 articles grew out of a workshop at the Max Planck Institute for the History of Science in Berlin. By following the "observatory techniques" used by astronomers, meteorologists, geodesists, and physicists, the contributors look at observatories in Europe, Asia, America, and Australia at a time when astronomy and its allied sciences had a wide range of practical uses. Techniques for taking measurements, analyzing data, managing personnel, and representing Earth and the sky became useful for military, political, technological, societal, commercial, and colonial projects. The work of astronomers was connected to a diverse range of fields, and one of the volume's strengths is that it highlights many of the ways in which such a superficially celestial science actually was quite down to earth.

"The most precise observations," Carl Friedrich Gauss claimed in 1833, "can be expected only of those mathematicians who are familiar with the finest means of observation, namely the practical astronomer." Astronomers working at 19th-century observatories radiated precision to other sciences and also to other parts of society. Physicists such as Henry Rowland (Johns Hopkins University) and Albert Michelson (University of Chicago), as shown in Richard Staley's chapter, developed their work in collaboration with observatories and astronomers as well as with American industry. Number-crunching methods created at observatories were also aimed at society, and techniques for managing numerical data developed in astronomy figure in the history of statistics. Sven Widmalm discusses the many connections between astronomers and the military in 19th-century Sweden, where astronomers and their techniques for measurement and analysis were important parts of surveys, military cartography, and the statistical description of a nation.

Colonial observatories could, as Simon Schaffer shows in his study of the Paramatta Observatory in New South Wales, Australia, function as tools of colonial administration. Astronomers worked on navigation and the scientific mapping of Earth's surface, and their science was connected with processes of territorial power. Large-scale networks for geodetic measurement and the spread of navigation technologies were built up, sometimes with difficulty.

With its growing empire, 19th-century Russia presented another case where astronomy was used in large-scale administration. Pulkovo Observatory (established in 1839) would—in the words of its first director, Wilhelm Struve—increase "the efficiency of the ordinary governing of the land." Struve and his fellow astronomers participated in large-scale surveys of the Russian empire and ran extensive training programs for surveyors and officers of the Russian General Staff. But, as Simon Werrett demonstrates in his chapter, the observatory was not only a site for practical knowledge. Its founder Nicholas I also wanted it to bring prestige and honor to his country. He provided it with very generous funding, and it became known as the "astronomical capital of the world"—bringing international scientific recognition to Russia and the tsar, on whose estate and summer residence just outside St. Petersburg it was located. A century later and under a different political regime, its symbolic value was still apparent: after the observatory was demolished during the siege of Leningrad, the decision to rebuild it was quickly taken.

Tsars were not the only ones interested in stars, and several chapters explore the interface between science and the public. Charlotte Bigg writes about Norman Lockyer, who always seems to have been on his way to yet another public lecture or solar eclipse expedition. Lacking a secure institutional base for his projects in the early stages of British astrophysics (the "new astronomy" that emerged during the second part of the century), Lockyer turned instead to public science, which could provide various kinds of resources. The situation was a bit different in countries where astrophysics was institutionalized earlier. For François Arago at the Paris Observatory, as Theresa Levitt's contribution shows, the public was also a kind of platform—in his case for both astronomical and political programs. Arago held free astronomical lectures from 1813 to 1848 and was very active in debunking superstition: comets were not dangerous, he explained, and the Moon's rays could not destroy harvests. For Arago, the popularization of astronomy became a political tool; astronomy could help make people more reasonable, which was important in a republic founded on public opinion.

The Heavens on Earth demonstrates in a fruitful way the observatory's importance to 19th-century history, of both science and culture. A worthy addition to the literature of the history of science, the collection will inspire further mapping of the links between astronomy and other parts of society. It also gives at least this reviewer a feeling of a past golden age in which astronomers and their observatories were at the center of the world, their knowledge asked for by public and politicians alike, rather than being the poorer cousin of 20th- and 21st-century sciences.

10.1126/science.1192849

The Heavens on Earth
Observatories and Astronomy in Nineteenth-Century Science and Culture

David Aubin, Charlotte Bigg, and H. Otto Sibum, Eds.
Duke University Press, Durham, NC, 2010. 398 pp. $94.95, £74. ISBN 9780822346289. Paper, $25.95, £17.99. ISBN 9780822346401. Science and Cultural Theory.

The reviewer is at the Research Policy Institute, Lund University, Box 117, 221 00 Lund, Sweden. E-mail: gustav.holmberg@fpi.lu.se

CREDIT: FROM H. M. PAUL, *SCIENCE* **4**, 101 (1884)

SCIENCE EDUCATION

Growing Roles for Science Education in Community Colleges

To help meet economic challenges, 2- and 4-year colleges must collaborate to improve student completion and transfer.

George R. Boggs

In an increasingly global society and economy, education and training beyond compulsory primary and secondary education—especially in science, technology, engineering and mathematics (STEM)—is essential to a nation's competitiveness and its standard of living. Community colleges, originally developed at the turn of the 20th century as open-admissions junior colleges and offering the first two years of a baccalaureate education, help meet this need. These colleges have evolved into comprehensive institutions, preparing students to transfer to upper-division universities or to enter the workforce directly. Enrolling 43% of all U.S. undergraduates (*1*), community colleges play important roles in developing public scientific literacy, educating scientists and engineers, and addressing the nation's need for well-prepared technicians (*2*). But challenges remain.

Some challenges are cultural, such as misperceptions that community colleges serve only low-performing students or hire faculty who are unable to secure a position at a 4-year institution. Other challenges are systemic, such as high teaching loads, inadequate funding models, and industry hiring practices. This article will focus on the challenge of helping students to complete 2-year programs or transfer to 4-year programs.

Educating Diverse, Local Communities

Community colleges prepare a growing percentage of the U.S. technological workforce (*3*). In 1999 and 2000, almost half of the science and engineering baccalaureate recipients and almost one-third of the master's degree recipients had attended community colleges (*4*). Forty percent of U.S. teachers complete some of their mathematics or science courses at these institutions (*5*). Students who attend community colleges include 47% of first-generation college students, and 53% of Hispanic, 45% of Black, 52% of Native American, and 45% of Asian/Pacific Islander college students. Although the average age of community college students is 28, still 46% of them are age 21 or younger (*1*).

Community colleges develop curricula to respond to the needs of local economies, working closely with industry, government, and other education sectors. These colleges have become the institutions of choice for workers, including university graduates upgrading their skills and displaced workers preparing to reenter the workforce (*6*). By the year 2018, it is projected that 12.3% of STEM jobs will be filled by associate degree holders (the primary degree conferred by community colleges) (*7*). The Obama Administration, noting that jobs requiring at least an associate degree are projected to grow twice as fast as those requiring no college experience, has called on community colleges to increase the number of graduates and program completers by 5 million students over a 10-year period, a 50% increase (*8*).

Completion and Transfer Must Improve

Too many students do not make it successfully through remedial programs into college-level courses, and too many do not complete their college-level programs or are unable to transfer to 4-year programs because of insufficient financial support or poor institutional or state policies and practices (*9*, *10*). Problems are caused by failures to collaborate between institutions, as well as a lack of continuity and integration within programs resulting from overuse of adjunct faculty and graduate teaching assistants. Furthermore, when state requirements for attaining associate degrees differ or there is insufficient harmonization in course content, it is difficult for students to transfer credit from one institution to another.

Improving Practice and Policy

The first major effort to improve student completion in community colleges, set in motion in 2004, is Achieving the Dream: Community Colleges Count (ATD), a national initiative focusing on students of color, working adults, and students from low-income families. About 10% of community colleges across 22 states are now part of ATD. The initiative has increased student persistence rates by as much as 13% (*11*). Efforts have focused on precollege programs for underprepared students, improving performance in "gatekeeper" courses that allow students to continue along a course sequence, improving the experiences of first-year students, advising students on academic and personal issues that affect their ability to succeed, student support services, and tutoring. ATD colleges are also working to strengthen linkages to secondary schools, engage the community, and change state and federal policies that create barriers for students (*12*). ATD institutions share strategies and assess progress by noting trends in the percentage of students who successfully complete courses, advance from remedial to credit-bearing courses, enroll from one term to the next, and earn a degree or certificate.

The American Association of Community Colleges (AACC) is currently working with partners to define accountability metrics for community colleges (*13*). Success measures will likely include course completions, moving students from developmental education to college courses, transfer rates, graduation rates, and job-placement rates disaggregated by specific populations. Although ATD is focused on improving student success rates within the institution, Complete College America is dealing with interinstitutional and state policies and practices (*14*).

Four-year institutions do not yet play much of a role in community college initiatives to improve student success and completion. Any effort to improve communication across sectors would be beneficial. Programs like NSF's Advanced Technological Education (ATE) function in this capacity. Community college educators lead ATE programs that involve universities, secondary schools, and businesses to prepare and strengthen the skills of the nation's technological workforce in strategic fields (e.g., environmental technology and cybersecurity) (*3*).

Other issues need to be addressed for student success, e.g., improving the mathematics sequence (necessary for any STEM area). The Carnegie Foundation for the Advancement of Teaching has an initiative to revise

President and chief executive officer of the American Association of Community Colleges, Washington, DC 20036, USA. E-mail: gboggs@aacc.nche.edu

Published by AAAS

the content and teaching of developmental mathematics courses (*15*).

In April 2010, six national community college organizations committed member institutions to match President Obama's goal (*16*). But in the face of enrollment pressure, states have cut funding to public higher education, including community colleges.

Hundreds of thousands of students were turned away from classes last fall, roughly 140,000 in California alone (*17*), and the situation may get even worse. Financially needy community college students primarily rely on the federal Pell grant, as state aid policies vary considerably. Only 10% of community college students take out any type of federal student loan and are much less likely to access financial aid than are counterparts in other institutions. Although austere budgets may cause policy-makers to become more interested in eliminating duplication and waste across institutions, 2- and 4-year institutions might be forced to compete for scarce funding. Federal funds, other than student financial aid, are primarily directed toward research projects at 4-year institutions. Although university educators should be interested in developing the pipeline of students, current incentives in 4-year institutions reward research and attracting grants to campus more than teaching or working in other ways with undergraduates. Federal, state, and local resources should focus on the specific needs of community colleges so that they can realize their potential role in the preparation of STEM students. For example, resources and incentives should be provided to make it possible to enroll more students full-time and provide them with accelerated instruction, backed by rigorous faculty professional development.

But improving educational attainment in the United States can best be met if educators take the lead. If not, policy-makers may find less appropriate ways to force institutions to develop stronger policies, e.g., for transfer and articulation (promoting equivalence of course content, and transfer of credit, between institutions). College and university faculty and administrators need to work together to improve completion rates and facilitate the transfer of students from community colleges into upper-division course work through improved articulation and student advising.

Many 4-year institutions could increase their own overall graduation rates, while enrolling and graduating more students of low socioeconomic status, by increasing their numbers of community college transfers (*18*). Transfer students do better in 4-year universities than if they had come directly from high school with the same credentials (*18*). However, not enough community college students transfer.

Articulation is important: 82% of students who have all credits transfer from a community college to a 4-year institution graduate within a 6-year time frame; this number drops substantially to 42% when only some credits transfer (*19*). Community college and university faculty should agree on expectations and standards so that courses are more easily transferable. But articulation polices differ dramatically by state. Public institutions in some states share common course numbers and statewide transfer agreements. In other states, transfer of courses is very difficult, e.g., having only institution-by-institution transfer agreements, making degree completion more time consuming, difficult, and expensive both for students and taxpayers.

An International Movement

The need to open the doors of higher education beyond the relatively limited enrollments in selective universities has spawned an international movement to develop or expand institutions that are generally less expensive, more accessible, more flexible, and tied more closely to business. For example, several countries have followed the British model, developing Further Education (FE) or Technical and Further Education (TAFE) institutions to provide technical education beyond high school. These institutions are generally more centrally controlled than U.S. community colleges and are not considered part of higher education, which limits local flexibility and the ability of students to progress to a baccalaureate or higher degree level. Recently, international interest in the U.S. community college model has increased (*20*), many countries have established community colleges based on it, and/or sending (or receiving) delegations to (or from) U.S. community colleges to explain the U.S. model and how it might be adapted elsewhere.

Community colleges must be seen as part of an educational continuum that bridges secondary schools and 4-year colleges and universities. Their impact on STEM education can be greatly enhanced by collaboration of teachers and faculty across educational sectors. At education councils where regional stakeholders convene to address elementary, secondary, and higher education, participants appear to be helping break down barriers across this continuum, but much more is accomplished when administrators and faculty are directly involved.

What is being learned about helping students be successful in community colleges should help universities to be more successful with their students. Given recommendations that the science curriculum needs to be reformed to include project- or research-based experiences as early as possible, this undergraduate research model is one in which community colleges will likely play a much larger role over the next decade.

References and Notes

1. AACC, 2010 Fact Sheet (AACC, Washington, DC, 2010); www.aacc.nche.edu/AboutCC/Pages/fastfacts.aspx.
2. National Science Board, *Science and Engineering Indicators 2008* (National Science Foundation (NSF), Arlington, VA, 2008).
3. ATE Centers Impact 2008–2010 (NSF, Arlington, VA, 2008); http://atecenters.org/.
4. J. Tsapogas, The role of community colleges in the education of recent science and engineering graduates (NSF, Arlington, VA, 2004); www.nsf.gov/statistics/infbrief/nsf04315/.
5. G. Shkodriani, Seamless pipeline from two-year to four-year institutions for teacher training (Education Commission of the States, Denver, CO, 2004); www.ecs.org/html/Document.asp?chouseid=4957.
6. M. Van Noy, M. Zeidenberg, *Digital Learning* (India) **2009**, 42 (June 2009); http://ccrc.tc.columbia.edu/Publication.asp?UID=699.
7. A. Carnevale, N. Smith, J. Strohl, *Help Wanted: Projections of Jobs and Educational Requirements Through 2018* (Georgetown University Center on Education and the Workforce, Georgetown University, Washington, DC, 2010); http://cew.georgetown.edu/JOBS2018/.
8. B. H. Obama, Remarks by the President on the American Graduation Initiative (The White House, Office of the Press Secretary, Washington, DC, July 14, 2009); www.whitehouse.gov/the_press_office/Remarks-by-the-President-on-the-American-Graduation-Initiative-in-Warren-MI/.
9. "For example, after six years 23% earn a degree or certificate at the community college, 7% are still enrolled, and 32% transfer to another college" (*10*).
10. L. Berkner, S. He, E. F. Cataldi, *Descriptive Summary of 1995–96 Beginning Postsecondary Students: Six Years Later* (NCES 2003–151, National Center for Education Statistics, Washington, DC, 2002), p. 81; http://nces.ed.gov/pubs2003/2003151.pdf.
11. S. Jaschik, Inside Higher Ed: News (1 June 2010); www.insidehighered.com/news/2010/06/01/nisod.
12. Goal 2025 (Lumina Foundation for Education, Indianapolis, IN, 2010); www.luminafoundation.org/goal_2025/.
13. Voluntary Framework of Accountability, AAAC; www.aacc.nche.edu/Resources/aaccprograms/vfa/Pages/default.aspx.
14. Complete College America, www.completecollege.org/.
15. B. M. Bressoud, The problem of persistence (Mathematical Association of America, via Carnegie Foundation for the Advancement of Teaching); www.carnegiefoundation.org/carnegie-connections/in-the-news/problem-of-persistence.
16. National Organizations Sign Student Completion Call to Action, (AACC, Washington, DC, 2010); www.aacc.nche.edu/newsevents/News/articles/Pages/042020101.aspx.
17. California Community Colleges make concerted effort to meet demand [press release] (California Community College Chancellor's Office, 3 June 2010); www.cccco.edu/Portals/4/News/press_releases/2010/June%203%202010%20Media%20Briefing.pdf.
18. W. Bowen, M. Chingos, M. McPherson, *Crossing the Finish Line: Completing College at America's Public Universities* (Princeton Univ. Press, Princeton, NJ, 2009).
19. W. Doyle, *Change: The Magazine of Higher Learning* **38**, 56 (2006).
20. J. Biden, Keynote address at the UNESCO World Conference on Higher Education, Paris, France, 5 to 8 July 2009; www.unesco.org/education/wche/speeches/jill-biden-speech-2009WCHE.pdf.

10.1126/science.1194214

MICROBIOLOGY

Is the Tide Turning for New Malaria Medicines?

A return to traditional screening methods has rapidly produced a candidate malaria drug.

Timothy N. C. Wells

Every so often, the tide turns in a field of science. In malaria research, for a while an approach called "rational design" held sway, with great optimism that new drugs would emerge from understanding the biology of the malaria parasite at the molecular level. On page 1175 of this issue, however, Rottmann *et al*. (*1*) take our thinking back up to the level of the parasite.

Using older screening methods that involve whole malaria parasites and cells, the authors identify a new class of compounds, spiroindolones, that show promise for treating malaria. Low concentrations of one spiroindolone, NITD609, kill the parasite's erythrocytic (bloodstream) stages by blocking protein synthesis, and preliminary tests in animals suggest that it could be developed into a safe drug. The timing here is important: Researchers in Cambodia have reported the first signs of resistance to artemisinin, the essential ingredient of existing malaria treatments for 100 million patients annually (*2*). There is thus an urgent need for candidates for new drugs that can overcome the challenges of resistance.

In the past decade, the availability of genome data and high-throughput systems for screening compounds was heralded as a breakthrough for discovering new anti-infective drugs. These molecular-based approaches promised to identify new "hits," or compounds that could inhibit key enzymes or cell receptors at submicromolar concentrations. Unfortunately, this promise has not been fulfilled. Payne *et al*. (*3*), for instance, concluded that the molecular approach was not efficient in identifying validated "targets," such as specific genes or cellular pathways, for antimicrobial compounds. Targets are not validated until molecules can be tested in the clinic; and even then, getting the hits to kill the microbe was far from simple. Their recommendation was twofold: Researchers should either work on families of compounds already shown to be clinically active, or return to screening compounds against whole microorganisms.

This message was not lost on the industrial partners of the antiparasitic research community. Over the last few years, companies have screened several million compounds against the erythrocytic stages of the malaria parasite. They identified more than 20,000 compounds that, at submicromolar concentrations, show some effect on the parasites—a hit rate of 0.5% (*4*–*6*). This hit rate was startlingly higher than most predictions (*3*), and higher than the 0.1% hit rate that, in my experience, was considered a success for molecular-based screening programs. It also suggested that several years could be shaved off the drug development process (see the figure) if researchers could optimize, or further develop, the compounds identified by parasite-based screens without knowing exactly the molecular target they affected or the mechanism of action.

Rottmann *et al*. show that such "blind" optimization can be done rapidly. Their hit, initially identified by screening some 12,000 natural compounds and structurally similar synthetics against cells taken from malaria parasites, was optimized into a preclinical candidate in just 3 years. That is a turbocharged pace. Indeed, the first hints of NITD609's mechanism of action didn't come until the researchers studied how it acted against various mutant strains of the malaria parasite. These tests revealed that NITD609 blocks protein synthesis by inhibiting the gene that encodes the P-type cation-transporter ATPase4 (PfATP4).

One advantage of parasite-based screening is that it identifies compounds that may act on more than one molecular target. Clinical experience has shown that drugs targeting a single molecular pathway, such as folate synthesis (targeted by pyrimethamine) or electron transport (atovaquone), can rapidly generate resistant strains (*6*). Medicines that have a more ambiguous molecular target or targets, such as artemisinin or quinine, tend to fare better in the clinic. So it is reassuring that

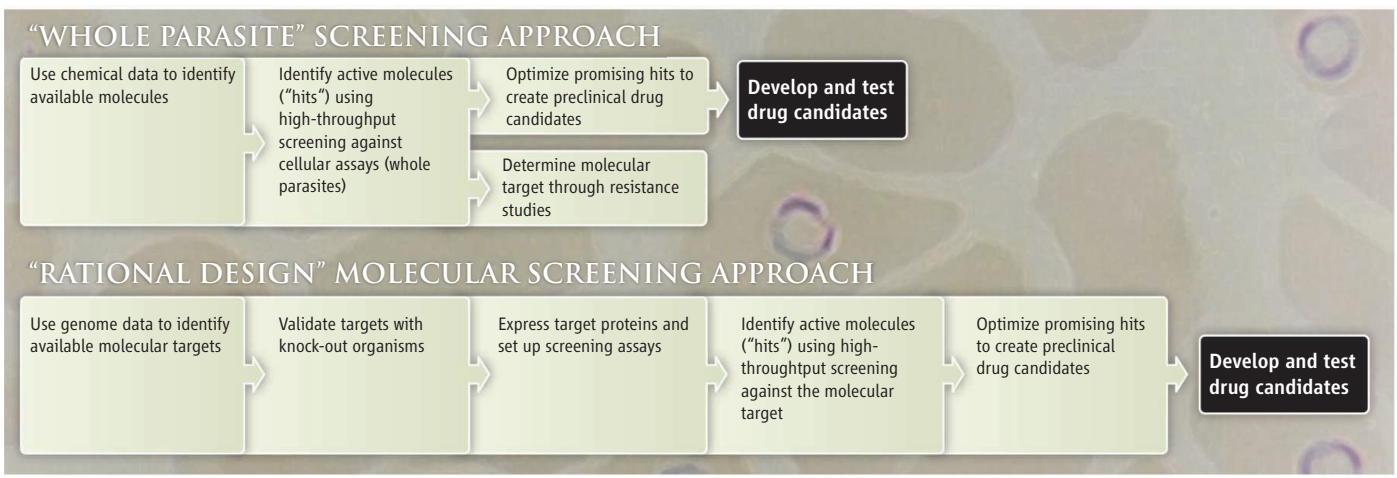

Making a comeback. Older "whole parasite" screening approaches (**top**) can develop antimalaria drug candidates more rapidly than newer "rational design" molecular approaches (**bottom**).

PHOTO CREDIT: WIKIMEDIA COMMONS

Medicines for Malaria Venture/MMV, 20, Route de Pré-Bois-Post Office Box 1826, Geneva, Switzerland. E-mail: wellst@mmv.org

Published by AAAS

Rottmann *et al*. had difficulty producing parasites resistant to NITD609 in vitro and that the molecule is active against malaria strains from Thailand, where resistance to artemisinin is a growing problem. Both results suggest that the compound may affect more than one cellular process.

A final twist in this story is that Rottmann *et al*.'s hit is a fully synthetic compound that was accidentally included in a collection of naturally occurring molecules; none of the other natural products were as interesting. Cell-based screening has not yet led us to new natural products that might replace artemisinin and quinine. It also suggests that future work on natural products should go back to its roots by focusing only on purifying natural molecules that have some clinical evidence of activity in humans.

Do these developments mean that the days of searching for molecular targets for antiparasitic drugs are over? Far from it. Target-based approaches are extremely useful once you know the target, and cell-based screening is one way of finding new molecular targets. Moreover, target-based approaches can help develop drugs that attack other stages of the malaria parasite's life cycle. This is important in the context of malaria eradication (*7*), which will require new classes of medicines that can stop transmission to other patients by blocking the sexual stages of the parasite (*8*, *9*). There is also a need for new medicines to block reactivation by dormant parasites in the liver, which occurs in the case of infection by *Plasmodium vivax* (*9*), the major strain in Asia and South America (*10*). Rational, molecular-based drug design also remains important in rapidly indentifying second-generation compounds that can overcome resistance.

Can NITD609 replace artemisinin? Unfortunately, as in most drug development, the answer is "wait and see." Artemisinin has two major strengths: It works quickly to reduce parasite levels in the bloodstream and resistance to it occurs less rapidly than for classical enzyme inhibitors. Meanwhile, NITD609's route to regulatory approval is a long one. In vitro and animal data are often poor surrogates for clinical reality. Even the most optimistic observer would note that less than 20% of new compounds make it to final approval, and that the process can take up to 8 years. The speed at which NITD609 has moved from a hit to a preclinical drug candidate, however, suggests that we may not have to wait too long.

References

1. M. Rottman *et al*., *Science* **329**, 1175 (2010).
2. A. M. Dondorp *et al*., *N. Engl. J. Med.* **361**, 455 (2009).
3. D. J. Payne, M. N. Gwynn, D. J. Holmes, D. L. Pompliano, *Nat. Rev. Drug Discov.* **6**, 29 (2007).
4. D. Plouffe *et al*., *Proc. Natl. Acad. Sci. U.S.A.* **105**, 9059 (2008).
5. F. J. Gamo *et al*., *Nature* **465**, 305 (2010).
6. W. A. Guiguemde *et al*., *Nature* **465**, 311 (2010).
7. T. N. Wells, P. L. Alonso, W. E. Gutteridge, *Nat. Rev. Drug Discov.* **8**, 879 (2009).
8. A. O. Talisuna, P. Bloland, U. D'Alessandro, *Clin. Microbiol. Rev.* **17**, 235 (2004).
9. N. J. White, *Malar. J.* **7** (suppl. 1), S8 (2008).
10. T. N. C. Wells, J. N. Burrows, J. K. Baird, *Trends Parasitol.* **26**, 145 (2010).

10.1126/science.1194923

IMMUNOLOGY

CAR'ing for the Skin

Andrey S. Shaw and Yina Huang

Epidermal T cell responses to injury and infection require stimulation by a protein that maintains cell adhesion and normal dermal integrity.

The innate immune system provides the first line of defense against pathogens through major barriers like the skin and mucosa. Specialized sentinel cells embedded in these barriers sound the alarm when they sense that the barrier has been breached (*1*). What these sentinel cells recognize and how they are activated have perplexed immunologists for over a decade. Two papers in this issue, by Verdino *et al*. on page 1210 (*2*) and by Witherden *et al*. on page 1205 (*3*), demonstrate that part of the mechanism involves the recognition of a tight junction protein expressed in the skin.

The impermeable barrier of the skin is mediated by adhesive cellular structures called tight junctions that prevent the passage not only of fluid but also of pathogens. Composed mainly of proteins such as cadherins, claudins, and occludins, they also contain proteins of the immunoglobulin superfamily (IgSF). In tight junctions, the latter proteins fall into three families: JAM, CTX, and Nectins. An important role of IgSF proteins in tight junctions is to facilitate the transient opening of epithelial barriers to permit the passage of cells. This is important for allowing immune cells to pass through endothelial and epithelial barriers during an inflammatory response (*4*) and spermatogonia to cross the blood-testis barrier (*5*). Curiously, these proteins also act as receptors for viruses like polio, herpes, adeno-, coxsackie, and reovirus (*6*–*8*). Whether binding to these IgSF proteins is directly used by viruses to cross epithelial barriers is not known, as uninjured epithelium is generally resistant to adenoviral infection.

An important sentinel cell in the skin is the γδ T cell. In contrast to the classical αβ T cell, which recognizes foreign antigens, it is not known what molecules are recognized by a γδ T cell. The latter expresses a limited number of T cell receptors (TCRs), suggesting that they may bind to conserved ligands whose expression is triggered by cell injury or stress. In the skin, a γδ T cell is known as a dendritic epidermal T cell (DETC) because of its unusual octopus-like shape, extending processes that contact many cells in the skin (see the figure). Once activated, a DETC secretes cytokines that promote inflammation and stimulate repair of the barrier (*9*).

Naïve T cells cannot be activated merely through the association of a ligand with the TCR, but require engagement of a second costimulatory receptor (*10*). The need for two signals is thought to prevent inappropriate activation of the immune system. Witherden *et al*. characterized a monoclonal antibody that costimulated TCR signaling in mouse DETCs. Although antibodies to the TCR weakly activated DETCs, addition of this monoclonal antibody potentiated proliferation and cytokine production. Mass spectroscopy revealed that the antibody recognized a JAM family protein called junctional adhesion molecule–like protein (JAML) (*11*). JAML is important for neutrophil chemotaxis across endothelial cells by binding to another member of the JAM/CTX/Nectin family called coxsackievirus and adenovirus receptor (CAR) (*12*).

Witherden *et al*. found that in mice, JAML is weakly expressed on naïve DETCs but not on other lymphocytes, including αβ T cells, B cells, or splenic γδ T cells. Activation strongly induced JAML expression in all γδ T cells, as well as on a subpopulation of $CD8^+$ T cells. However, JAML costimulated TCR signaling only in epidermal and

Department of Pathology and Immunology and Howard Hughes Medical Institute, Washington University School of Medicine, St. Louis, MO 63110, USA. E-mail: shaw@pathology.wustl.edu

intestinal γδ T cells but not in $CD8^+$ T cells or splenic γδ T cells. JAML thus functions as a specific costimulatory receptor only in γδ T cells in skin and mucosal barriers. Blocking JAML engagement substantially delayed wound healing in mice, demonstrating the physiological relevance of the JAML-CAR interaction.

To examine the interaction in greater detail, Verdino *et al*. crystallized the ectodomain of JAML as well as the JAML-CAR ectodomain complex. Both molecules possess two tandem Ig domains. Whereas CAR has a typical flexible linkage between these domains, the two Ig domains in JAML interact with each other, making the structure more rigid. In addition, whereas Ig domains typically interact with their ligands via the loops at the ends of the β sheets, JAML interacts with CAR via the sides of their two Ig domains, similar to the interaction between the immune cell adhesion molecules CD2 and CD58 (*13*).

Because viruses interact at the same interface, structural features of the interface between JAML and CAR are of interest. The interface is unusual because it is mainly hydrophilic and composed of numerous salt bridges and hydrogen bonds. The large number of interactions allows the interface to impart a high specificity but may also be responsible for the large number of virus interactions. Adenovirus interacts with 16 of the 18 key residues of CAR, whereas coxsackie virus interacts with 6 critical residues. Because the JAML-CAR interaction involves so many residues, changing any one of them to evade viral binding would probably also impair JAML-CAR function.

The presence of dimers in the crystal structure suggested that JAML dimers that are formed by CAR binding might trigger JAML signaling in the γδ T cell. Indeed, Verdino *et al*. found that the binding of phosphatidylinositol 3-kinase (PI 3-kinase) to a conserved motif in the JAML cytoplasmic domain occurred only when JAML dimerized. Mutational studies showed that this binding motif, as well as an adjacent proline motif important for activation of Src kinases (*14*), is important for PI 3-kinase binding. Proof that these sequences are important for the costimulatory function of JAML, however, requires further analysis because the role of PI 3-kinase in DETC costimulation was not directly examined. Although it was long assumed to be important, it was recently shown that the PI 3-kinase binding site in CD28, the best-studied costimulatory receptor, is not necessary for costimulation in αβ T cells (*15*).

Because CAR is constitutively expressed on keratinocytes, what is the sequence of events that results in the activation of DETCs? Activation increases JAML expression, so TCR recognition of its unknown ligand should stimulate JAML production, allowing it to potentiate TCR signaling. Yet, CAR is sequestered in tight junctions in normal skin and is not likely to be accessible to JAML expressed on DETCs. Viruses are known to cause tight junction disassembly, releasing CAR to allow for further infection (*16*). This released CAR may be sensed by the DETC. Definitive answers to these questions await the identification of a bona fide ligand for TCR of γδ T cells, but the identification of JAML as a costimulatory receptor is a critical step in that direction.

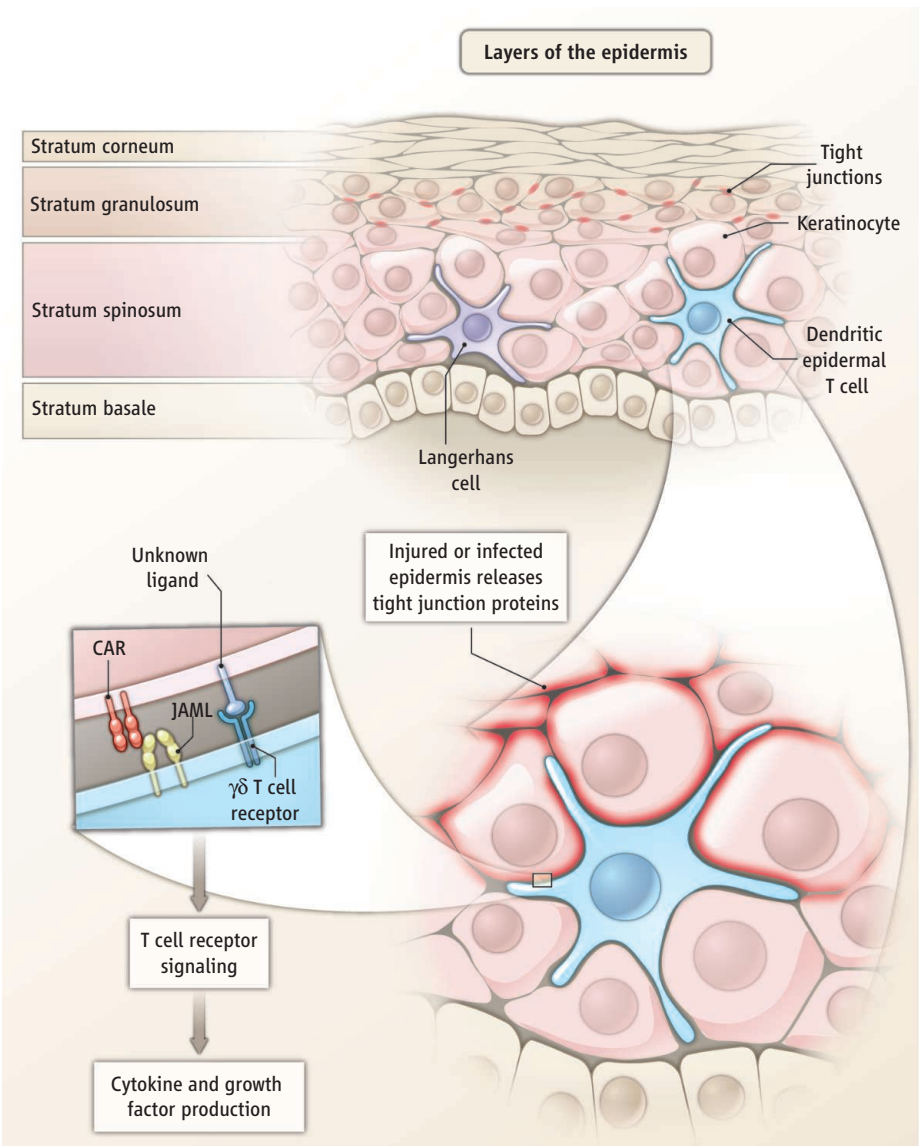

CREDIT: Y. GREENMAN/*SCIENCE*

Alerting injury to the skin. In normal human skin epidermis, tight junctions are mainly found in the SG, whereas DETCs are located in the layer below. The engagement of tight junction proteins prevents them from being bound by viruses or T cells. Injury by, for example, a virus disrupts tight junctions in the skin, freeing junctional components so that they can bind to viruses as well as DETCs.

References

1. J. Strid *et al*., *Semin. Immunol.* **21**, 110 (2009).
2. P. Verdino *et al*., *Science* **329**, 1210 (2010).
3. D. A. Witherden *et al*., *Science* **329**, 1205 (2010).
4. T. Chavakis *et al*., *Thromb. Haemost.* **89**, 13 (2003).
5. C. Q. Wang *et al*., *J. Cell Biol.* **178**, 549 (2007).
6. E. S. Barton *et al*., *Cell* **104**, 441 (2001).
7. J. M. Bergelson *et al*., *Science* **275**, 1320 (1997).
8. R. J. Geraghty *et al*., *Science* **280**, 1618 (1998).
9. L. L. Sharp *et al*., *Crit. Rev. Immunol.* **25**, 1 (2005).
10. J. S. Boomer *et al*., *Cold Spring Harb. Perspect. Biol.* **2**, a002436 (2010).
11. C. Moog-Lutz *et al*., *Blood* **102**, 3371 (2003).
12. K. Zen *et al*., *Mol. Biol. Cell* **16**, 2694 (2005).
13. J. H. Wang *et al*., *Cell* **97**, 791 (1999).
14. A. D. Holdorf *et al*., *Nat. Immunol.* **3**, 259 (2002).
15. L. F. Dodson *et al*., *Mol. Cell. Biol.* **29**, 3710 (2009).
16. R. W. Walters *et al*., *Cell* **110**, 789 (2002).

10.1126/science.1195337

Published by AAAS

PALEONTOLOGY

Marine Biodiversity Dynamics over Deep Time

Analysis of a large fossil database puts a new curve on the history of marine life.

Charles R. Marshall

The fossil record provides our only direct window into how Earth's biodiversity has changed over the past 530 million years. Efforts to dissect diversity dynamics, however, have been impeded by gaps in the fossil record and uneven sampling by paleontologists. As a result, two of the most fundamental questions in paleobiology remain contentious. How, in detail, has diversity changed over geologic time? And what is the nature of the rules that governed these diversity changes? More specifically, was the diversification of most groups of organisms unconstrained, or was it subject to some sort of limit? On page 1191 of this issue, Alroy (*1*) presents a new analysis of the marine fossil record that goes to the heart of these questions. The results are unlikely to be universally accepted, but they help to pinpoint the critical issues.

Alroy is not the first to attempt to graph the historic ebb and flow of marine biodiversity. One early effort came in 1860 (*2*), and in the 1980s Sepkoski combed the paleontology literature to develop a massive compendium that listed the first and last occurrences of known marine genera (*3*) and drew what has become the standard diversity curve (see the figure, panel A). This approach left many unsatisfied, however, because it did not account for biases in sampling. One problem, for instance, is that older fossils may be underrepresented because they are less likely than younger fossils to have survived erosional processes and to be found by paleontologists. Another problem is that investigators have collected more heavily in some geographic areas and rock strata than others. In an attempt to overcome such biases, Alroy and colleagues (including Sepkoski) created the Paleobiology Database (PBDB) (*4*), a large and growing compilation of data from nearly 100,000 fossil collections. Over the past decade, researchers have used statistical techniques to "subsample" the PBDB and draw "sample-standardized" diversity curves (*5*), including one published by Alroy and colleagues in 2008 (*6*) (see the figure, panel B).

Department of Integrative Biology, University of California Museum of Paleontology, University of California, Berkeley, Berkeley, CA 94720, USA. E-mail: crmarshall@berkeley.edu

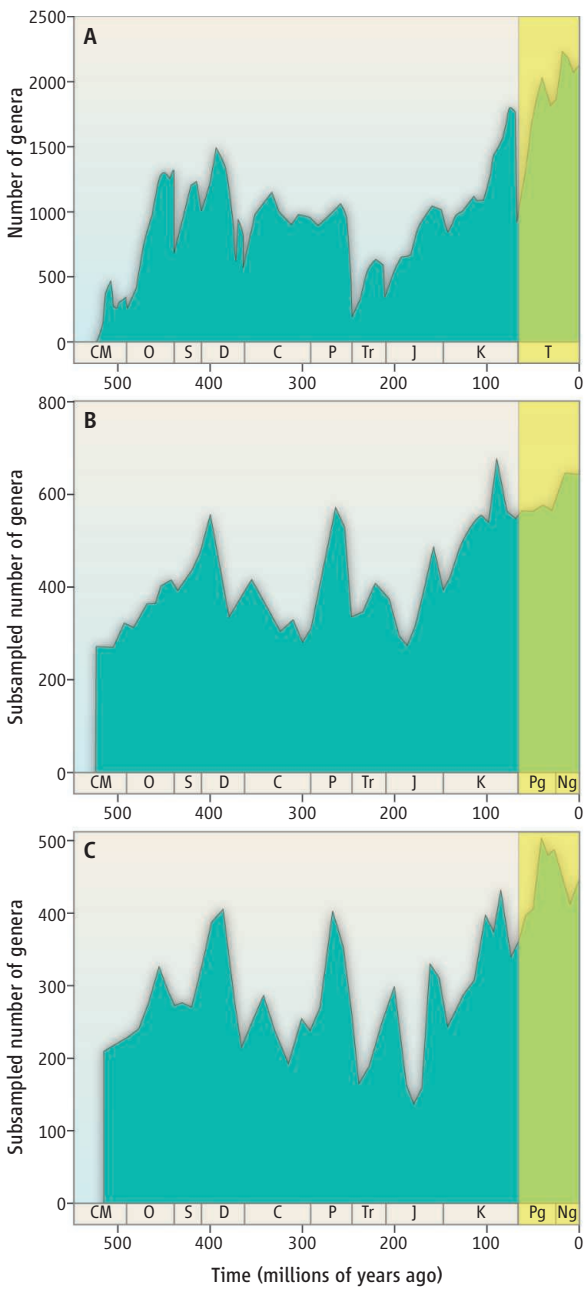

Alroy has now used the PBDB to produce a diversity curve (panel C) with some features that were seen in Sepkoski's original uncorrected curve (*3*), but were absent from earlier PBDB curves (*5*, *6*). Using this curve, Alroy reaches the unsurprising conclusion that the rules governing diversification of major groups were not fixed over time. The end-Permian mass extinction, for example, "reset" the rules for crinoids and "articulate" brachiopods, which led to lower diversity in these groups after the mass extinction. A second conclusion, more controversial and more dependent on the details of the new curve, is that most groups have caps on their diversity, although those caps varied at different times. That is, Alroy's analysis appears to refute some previous work that argues for unconstrained, or exponential, diversification of the marine biota (*7*, *8*).

To place Alroy's results in context, it helps to note that the first results from the PBDB in 2001 (*5*) were contentious in part because they showed an almost complete absence of a diversity increase in the Cenozoic (~65 million years ago to the present). This absence of a diversity rise, however, was challenged by other data; for example, researchers had reported that the average number of species found per locality increased dramatically toward the present (*9*). Furthermore, doubts arose over the veracity of the subsampling methods used to

Diverse views of diversity. (**A**) Sepkoski's marine animal diversity curve has long been the standard, but lacks correction for uneven temporal or spatial sampling. (**B**) A more recent diversity curve based on the Paleobiology Database (PBDB) attempted to correct for uneven sampling and offers a different view of diversity dynamics (*6*). (**C**) The latest diversity curve from the PBDB uses a new method for correcting for uneven sampling (*1*) and, for the Cenozoic (yellow), is strikingly similar to Sepkoski's. The challenge now is to reach agreement on the methods for correcting for uneven sampling and for rigorously demonstrating that the PBDB provides a balanced reflection of the fossil record.

Published by AAAS

create the first PBDB curve (*10*). The 2008 PBDB curve rested on essentially the same methods but reflected data from about eight times as many collections (*6*). Nonetheless, the curve remained flatter over the Cenozoic than many expected.

One important reason for the differences in the PBDB curves, at least in the Cenozoic, seems to be the use of a new method of sample standardization. Alroy calls it shareholder sampling and asserts that, unlike previous methods, it ensures that uncommon taxa are fairly represented in the results. This method suggests that previous sample-standardized curves were indeed severely "damped" or showed less diversity than actually was present. Now, other similarly damped curves will need to be reexamined. For example, a sample-standardized study of phytoplankton has produced a remarkably flat trajectory toward the present that may understate diversity trends (*11*).

This is not likely to be the last word on marine diversity patterns over the past 530 million years. First, shareholder sampling needs to be further vetted by the scientific community. A second, deeper question is whether the PBDB is currently an accurate reflection of the fossil record. Some feel that it is not (*12*–*14*). For example, most groups of living organisms show a pronounced latitudinal diversity gradient, with diversity decreasing from the equator to the poles. The PBDB's fossil record of bivalves over the past 11 million years, however, does not show a similar pattern. In part, this is because some key literature is missing from the PBDB, and also we have poor knowledge of the fossil record of the tropical realm, particularly of the diverse Indo-West Pacific, relative to temperate regions (*12*). These and similar deficiencies might be biasing the PBDB toward curves that support the view that there were constraints on diversification for groups such as bivalves. To further reduce such biases, projects such as the recent €2.7 million (U.S. $3.4 million) effort by the European Union to describe Indonesia's tropical marine fossil record will be of critical importance.

Although Alroy's curve represents the latest contribution to our understanding of diversity dynamics on geologic time scales, there will be no immediate consensus on the details of the pattern of diversity. Still, the pieces are falling into place for rigorously understanding the dynamics that have shaped, and continue to shape, the biosphere.

References

1. J. Alroy, *Science* **329**, 1191 (2010).
2. J. Phillips, *Life on the Earth: Its Origins and Succession* (Macmillan, Cambridge, 1860).
3. J. J. Sepkoski Jr., *J. Paleontol.* **71**, 533 (1997).
4. Paleobiology Database (http://paleodb.org).
5. J. Alroy *et al.*, *Proc. Natl. Acad. Sci. U.S.A.* **98**, 6261 (2001).
6. J. Alroy *et al.*, *Science* **321**, 97 (2008).
7. S. M. Stanley, *Paleobiology* **33** (suppl.), 1 (2007).
8. M. J. Benton, *Science* **268**, 52 (1995).
9. A. M. Bush, R. K. Bambach, *J. Geol.* **112**, 625 (2004).
10. A. M. Bush *et al.*, *Paleobiology* **30**, 666 (2004).
11. D. L. Rabosky, U. Sorhannus, *Nature* **457**, 183 (2009).
12. A. Z. Krug *et al.*, *Astrobiology* **9**, 113 (2009).
13. J. B. C. Jackson, K. G. Johnson, *Science* **293**, 2401 (2001).
14. D. H. Erwin, *Curr. Biol.* **19**, R575 (2009).

10.1126/science.1194924

CHEMISTRY

Just Add Water

A graphene overlayer is used to map the structure of water from ice to liquid, one atomic layer at a time.

Mikhail I. Katsnelson

The discovery of graphene (*1*–*3*), a two-dimensional allotrope of carbon, has initiated huge activity in physics, chemistry, and materials science. The peculiar character of charge carriers in this material makes it a "CERN on the desk," allowing some of the subtle effects of high-energy physics to be simulated in a microscopic, solid-state sample. Graphene is the simplest possible membrane, a sheet of carbon atoms just one atom thick—an ideal testbed for statistical physics in two dimensions. It also promises brilliant perspectives for the next generation of electronics researchers, who have mainly been limited to the surfaces of materials. However, graphene is not only interesting in itself. On page 1188 of this issue, Xu *et al.* (*4*) present a new use of graphene that may be a breakthrough in studies of the physics and chemistry of wetting.

The interaction of water with surfaces of solids is a process of extraordinary importance in many natural phenomena (including corrosion, atmospheric processes such as rain precipitation, and geological processes such as erosion), as well as in catalytic reactions used by the chemical industry (*5*). Wetting processes are determined essentially by the structure of the first water molecular layer formed at the surface (*6*). Ideally, we would like to be able to watch growth of the water layer step by step, with atomic resolution. In principle, modern local probe techniques such as scanning tunneling microscopy (STM) or atomic force microscopy (AFM) are the appropriate tools (*7*). The problem is that, at least at room temperature (which is, naturally, the most interesting case for most applications), the water molecules are too weakly coupled to the surface. The probe tip can easily push the molecules and affect the measurements. We know the atomic struc-

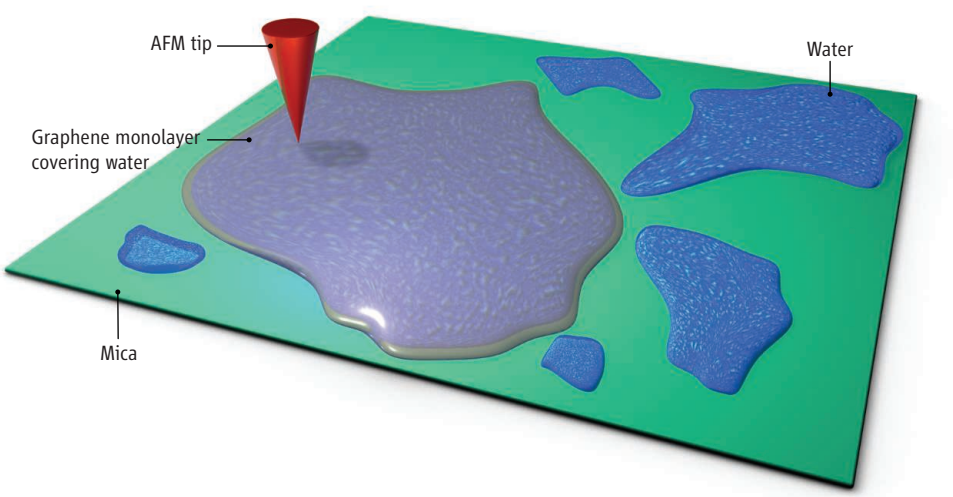

CREDIT: ADAPTED BY P. HUEY/*SCIENCE*

On the surface. The mica surface is partially covered by water. Xu *et al.* show that the graphene monolayer covering the surface does not disturb the structure of water clusters and protects them from disturbance by the AFM tip.

Radboud University Nijmegen, Institute for Molecules and Materials, 6525 AJ Nijmegen, the Netherlands. E-mail: m.katsnelson@science.ru.nl

ture of water monolayers at low temperatures from STM measurements (*7*), but at ambient conditions the available experimental data are less direct.

Although graphene is extremely thin, it is a mechanically very strong (*8*) and impermeable membrane, even for the smallest atoms and molecules (*9*), and interacts with insulating substrates by rather weak van der Waals forces (*10*). For water on a mica surface, Xu *et al*. show that an overlayer of graphene protects the water layer and does not disturb its structure. Using AFM, they were able to probe the water structure at different thicknesses with atomic-scale resolution. The scheme of the system is quite simple (see the figure). Because mica is hydrophilic, its surface is naturally covered by water, at least, partially. Graphene follows the atomic relief of the wet substrate, showing the first, second, and further water layers. As a result, the structure of the water layer at room temperature and different humidity can be imaged. It turns out that the first monolayer of water on mica has an ice structure, as does the second layer forming at higher humidity. Subsequent layers, however, seem to be already liquid-like. The atomic resolution allows us also to study the role of specific nucleation centers in the wetting process.

This method can be applied to other surfaces with different types of chemical bonding, which would give us a deeper understanding of differences between hydrophilic and hydrophobic substrates. Although graphene was used only as a cover layer, knowledge of the structure of water under graphene is very important to better understand the mechanisms responsible for the behavior of the electron mobility in graphene on various substrates. In such cases, the complex interaction between the graphene, substrate, and water can influence the doping of the graphene and the electron scattering processes within it (*11*).

Up to now, the main interest in graphene has been related to its own properties (*1*–*3*), but it can be also used as a scaffold material (*8*); one can put large molecules on this very stiff, transparent, and conducting membrane and study them by various methods. The work of Xu *et al*. is the first application of graphene as a cover material in surface science to protect a surface from effects of the measuring devices. The ability to understand wetting at atomic resolution is the first demonstration of the importance of this approach; others are sure to follow.

References

1. A. K. Geim, K. S. Novoselov, *Nat. Mater.* **6**, 183 (2007).
2. M. I. Katsnelson, *Mater. Today* **10**, 20 (2007).
3. A. K. Geim, *Science* **324**, 1530 (2009).
4. K. Xu, P. Cao, J. R. Heath, *Science* **329**, 1188 (2010).
5. P. A. Thiel, T. E. Madey, *Surf. Sci. Rep.* **7**, 211 (1987).
6. P. J. Feibelman, *Phys. Today* **63**, 34 (2010).
7. A. Verdaguer, G. M. Sacha, H. Bluhm, M. Salmeron, *Chem. Rev.* **106**, 1478 (2006).
8. T. J. Booth *et al*., *Nano Lett.* **8**, 2442 (2008).
9. J. S. Bunch *et al*., *Nano Lett.* **8**, 2458 (2008).
10. J. Sabio *et al*., *Phys. Rev. B* **77**, 195409 (2008).
11. T. O. Wehling, A. I. Lichtenstein, M. I. Katsnelson, *Appl. Phys. Lett.* **93**, 202110 (2008).

10.1126/science.1195392

TRANSCRIPTION

Targeting the Core of Transcription

An enzyme that senses metabolic stress phosphorylates a chromatin protein to control gene expression and adaptive responses.

D. Grahame Hardie

Adenosine 5′-monophosphate–activated protein kinase (AMPK) is a cellular energy sensor expressed across eukaryotes (*1*). It is switched on by stresses that disturb energy balance and triggers both acute responses and longer-term adaptations by affecting gene expression. It was thought that its transcriptional effects were mediated largely via phosphorylation of transcription factors (*2*) or coregulators (*3*, *4*) that recruit RNA polymerase II to gene promoters. However, on page 1201 of this issue, Bungard *et al*. (*5*) suggest that AMPK might cause additional effects by phosphorylating a chromatin protein, histone H2B.

AMPK is activated by both genotoxic and metabolic stresses, and Bungard *et al*. found that mouse embryonic fibroblasts lacking functional AMPK were less viable and showed reduced expression of genes controlled by the transcription factor p53 in response to such stresses. Using chromatin immunoprecipitation, they report evidence that AMPK associated with promoters targeted by p53 in stressed cells, along with liver kinase B1 (LKB1), an enzyme required for its activation. One puzzle here is that LKB1 accessory subunits (STRAD and MO25), which are essential for its activity (*6*), also sequester it in the cytoplasm (*7*), so it remains unclear whether nuclear LKB1 is active.

The budding yeast AMPK ortholog is known to phosphorylate histone H3 (*8*), but Bungard *et al*. show that in mammalian cells AMPK phosphorylates histone H2B [at serine residue 36 (Ser^{36})] in response to metabolic stress or treatment with AMPK-activating drugs. The optimal motif for phosphorylation by AMPK was previously defined (*9*–*11*) as a serine flanked by hydrophobic and basic residues (see the figure). The sequence around Ser^{36} on H2B has conserved basic residues that are five and three residues before the serine, which is a variation on the canonical rec-

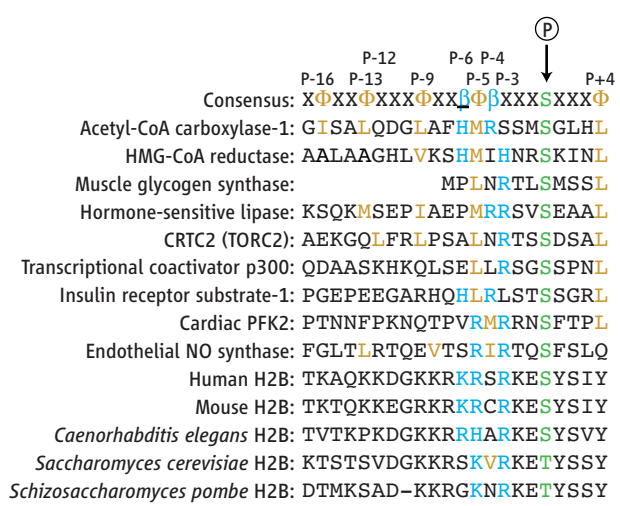

AMPK recognition motif. An alignment is shown of the generic recognition motif of AMPK and the amino acid sequences on human proteins that are known to be phosphorylated by AMPK, including Ser^{36} on H2B. The phosphorylation site (denoted P, in green), and critical flanking hydrophobic (orange) and basic (blue) residues are shown (numbers representing their positions relative to the phosphorylation site). Some substrates (e.g., ACC1) also have regularly spaced hydrophobic residues at P–5, P–9, P–12/13, and P–16, which form an amphipathic helix (*10*).

College of Life Science, University of Dundee, Dow Street, Dundee DD1 5EH, Scotland, UK. E-mail: d.g.hardie@dundee.ac.uk

ognition motif also seen in two established substrates, cardiac phosphofructokinase and endothelial nitric oxide synthase. However, the last-named substrates (unlike H2B) have hydrophobic residues between the two basic residues. Moreover, in H2B, the residue four positions after the serine is tyrosine, which was found to be unfavorable in a peptide library approach (*11*). Despite this imperfect fit to the recognition motif, AMPK may phosphorylate Ser^{36} on H2B because it is recruited to these promoters through other interactions.

Both AMPK and phosphorylated H2B (at Ser^{36}) associated not only with the promoters, but also with transcribed regions of target genes, which suggests a possible effect on elongation of transcription. When Ser^{36} was changed to alanine (which prevented phosphorylation) and the mutated protein expressed, less RNA polymerase II associated with transcribed regions of a p53 target gene compared with cells expressing wild-type H2B. Moreover, expression of several other p53 targets in response to a metabolic stress decreased, and fewer cells survived the insult.

How general is this mechanism across eukaryotes? Activation of the budding yeast AMPK ortholog (SNF1) enhances transcription at a promoter at which RNA polymerase II is already recruited (*12*), although it is not clear whether this requires H2B phosphorylation. In budding and fission yeast H2B, the critical basic residues are conserved, but Ser^{36} itself is replaced by threonine. Although threonine residues can be phosphorylated by yeast SNF1, serine is preferred (*9*). Thus, it remains unclear whether H2B would be a target for the yeast kinase.

The findings of Bungard *et al*. suggest that AMPK can modulate stages in transcription beyond RNA polymerase II recruitment by phosphorylating core components of chromatin. One possibility is that Ser^{36} phosphorylation introduces two negative charges that destabilize wrapping of DNA around nucleosomes, and so directly facilitates the elongation phase of transcription. Structures of the nucleosome reveal that Ser^{36} is not in a location particularly accessible to the kinase, so it is likely that phosphorylation would have to occur on histones when they are not present in a nucleosome, or DNA may have to dissociate to allow the modification.

AMPK has generated much interest recently because of its importance in metabolism and its potential as a drug target in diabetes and cancer. The finding that it modifies chromatin adds another interesting facet to the varied effects it has on cellular function.

References

1. D. G. Hardie, *Nat. Rev. Mol. Cell Biol.* **8**, 774 (2007).
2. T. Kawaguchi, K. Osatomi, H. Yamashita, T. Kabashima, K. Uyeda, *J. Biol. Chem.* **277**, 3829 (2002).
3. W. Yang *et al*., *J. Biol. Chem.* **276**, 38341 (2001).
4. S. H. Koo *et al*., *Nature* **437**, 1109 (2005).
5. D. Bungard *et al*., *Science* **329**, 1201 (2010); published online 15 July 2010.
6. S. A. Hawley *et al*., *J. Biol.* **2**, 28 (2003).
7. J. Boudeau *et al*., *EMBO J.* **22**, 5102 (2003).
8. W.-S. Lo *et al*., *Science* **293**, 1142 (2001).
9. S. Dale, W. A. Wilson, A. M. Edelman, D. G. Hardie, *FEBS Lett.* **361**, 191 (1995).
10. J. W. Scott, D. G. Norman, S. A. Hawley, L. Kontogiannis, D. G. Hardie, *J. Mol. Biol.* **317**, 309 (2002).
11. D. M. Gwinn *et al*., *Mol. Cell* **30**, 214 (2008).
12. C. Tachibana, R. Biddick, G. L. Law, E. T. Young, *J. Biol. Chem.* **282**, 37308 (2007).

10.1126/science.1195447

ASTRONOMY

Fullerenes and Cosmic Carbon

Hydrogen-poor conditions in a planetary nebula enable the detection of carbon-cage molecules C_{60} and C_{70}, confirming the existence of fullerenes in space.

Pascale Ehrenfreund[1] and Bernard H. Foing[2]

Carbon is formed by fusion reactions in the cores of stars, and in the late stages of stellar evolution, massive stellar winds expel it into interstellar space. Atomic carbon participates in gas and solid-state chemical reactions to form a variety of organic compounds within circumstellar regions and interstellar clouds (*1*). Spectroscopic studies of these regions have long provided tantalizing clues to the presence of large carbon molecules that contain many aromatic rings. Candidate molecules include polycyclic aromatic hydrocarbons (PAHs), in which the rings join in flat sheets, and fullerenes, in which they form closed cages. New spectroscopic observational and analytical tools are helping to pin down which molecules are present, as well as characterize the environments that lead to their formation. On page 1180 of this issue, Cami *et al*. (*2*) report the detection, by means of the Infrared Spectrograph (IRS) onboard the Spitzer Space Telescope, of vibrational bands of the fullerenes C_{60} and C_{70} as neutral molecules, likely attached to dust grains, in the young planetary nebula Tc 1. There was no evidence of other major carbon compounds, such as PAHs, in this hydrogen-poor environment. These observations raise important questions about the formation and evolution of fullerene compounds in circumstellar regions.

Fullerenes became candidates for interstellar carbon molecules only after their laboratory discovery by Kroto *et al*. (*3*). A few years later, Krätschmer *et al*. (*4*) reported the synthesis of macroscopic quantities of C_{60} from condensed soot. Since then, the presence of soot material in carbon-rich stars, along with the spontaneous formation and remarkable stability of the fullerene cage, strongly suggested the existence of fullerene compounds in interstellar space. Fullerenes are now made in the lab either by vaporization of graphite in a hydrogen-poor atmosphere or by photochemical processing of hydrogenated amorphous carbon.

Monitoring of soot formation shows that polyyne chains (carbon chains with alternating single and triple bonds) act as intermediates and can form different products. PAHs form in the presence of sufficient hydrogen, but when hydrogen is absent, polyynes cross-link to form fullerenes (*5*). Recent laboratory studies forming carbon particles by gas-phase condensation reactions, such as laser pyrolysis and laser ablation, show that the temperature in the condensation zone plays a key role. Below 1700 K, the condensation by-products are mainly PAHs with three to five aromatic rings (*6*). At condensation temperatures above 3500 K, fullerene-like carbon grains and fullerene compounds are formed. Molecular synthesis may occur in the circumstellar environment on time scales as short as several hundred years (*7*).

The two strongest electronic bands, fingerprints of the C_{60}^{+} ion, were discovered in the near-infrared spectra of more than 15 distant stars whose light is absorbed through diffuse interstellar clouds (*8*–*10*). The abundance of C_{60}^{+} has been inferred from optical measurements to be 0.3 to 0.9% of the cosmic carbon (*8*, *10*). Until the study by Cami *et al*., the search in mid-infrared wavelengths for vibrational transitions in emission of C_{60}

[1]Space Policy Institute, Washington, DC 20052, USA. [2]European Space Agency, ESTEC SRE-S, 2200 AG Noordwijk, Netherlands. E-mail: pehren@gwu.edu; bernard.foing@esa.int

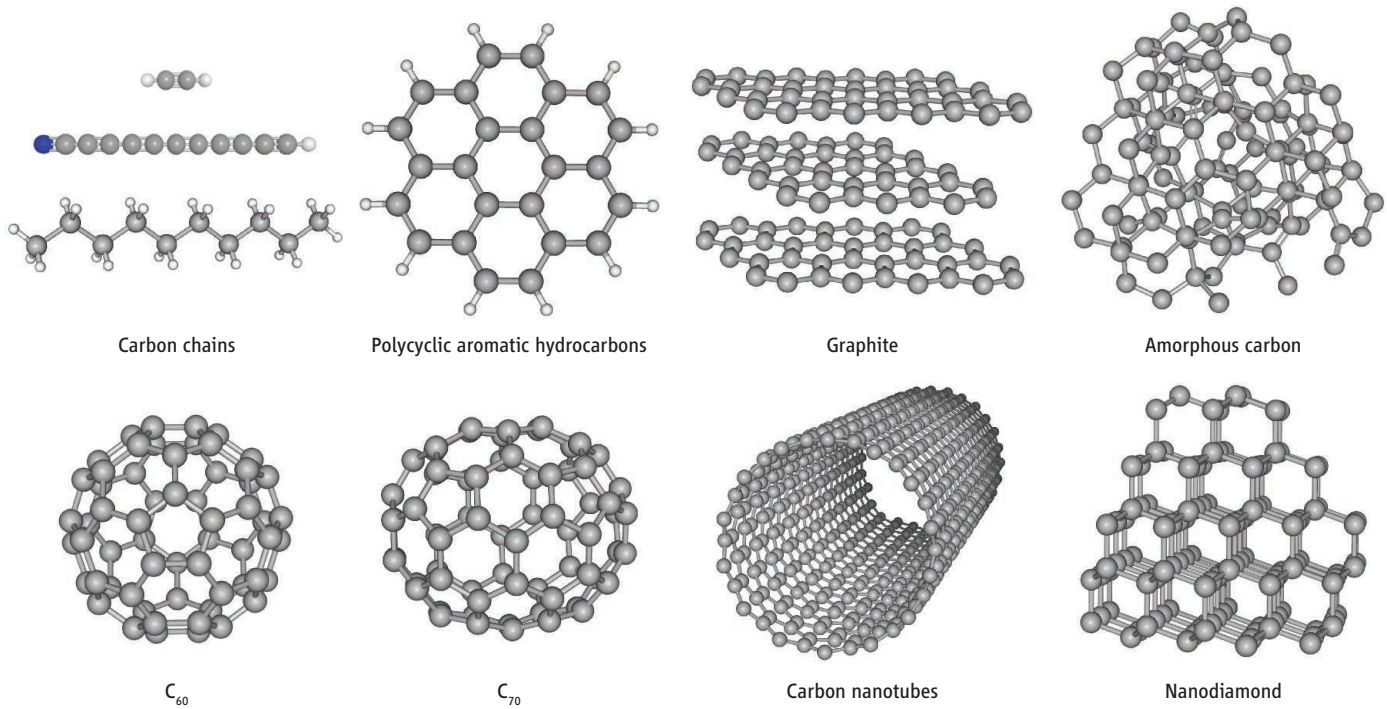

Carbon in space. The evidence for interstellar C_{60}^+ and detection of neutral C_{60} and C_{70} fullerene compounds in Tc 1 boosts the number of carbon allotropes present in space. Nanodiamonds and graphite are found in meteorites. Amorphous carbon may represent the main component of the solid-state carbon fraction in low-density interstellar regions. Future observations and laboratory data may lead to the identification of other fullerene compounds, such as carbon nanotubes or carbon onions. Polyynes (carbon chains) and polycyclic aromatic hydrocarbons (PAHs) are observed ubiquitously in space and are likely involved in the process of fullerene formation.

and C_{60}^+ yielded spectra that could provide only uncertain upper limits. The spectrum of Tc 1 displays clean symmetric bands that confirm the presence of fullerenes in space. The profiles of the bands, their position, and their width indicate that C_{60} and C_{70} molecules are in a neutral state. Gas-phase fullerenes ionize readily, so these molecules are likely trapped on dust grains.

The progenitors of planetary nebulae are red giant stars that have expelled gas and dust and formed a circumstellar envelope. Thermal pulses cause the ejection of their outer envelopes and create shells that cool and become regions for active gas-phase and solid-state chemistry leading to molecule formation. The core of Tc 1 provides optimal conditions for detecting the prevalence of C_{60} and C_{70} fullerene compounds in terms of temperature, recent ejection of hydrogen-poor precursor material, and a compact shell where ultraviolet excitation is low. This short phase that favors fullerene evolution may occur in the evolution of other planetary nebulae. In the outer shell of Tc 1, hydrogen emission lines are observed at optical wavelengths, and a search for PAHs in this region could prove fruitful.

Although C_{60} and C_{70} represent only ~1% of the cosmic carbon, the analysis by Cami *et al*. and future observations will lead to a better understanding of physical and chemical processes in space, including the formation of carbon allotropes (*1*) (see the figure). Fullerene-like structures are present in "terrestrial" lab soot, and apart from circumstellar regions such as Tc 1, they are likely a component of the interstellar refractory dust fraction that dominates the inventory of cosmic carbon in diffuse clouds (*11*, *12*). Fullerene onions (formed of concentric shells of carbon) or nanotubes may also contribute to this reservoir. Direct and long-term exposure of fullerenes to cosmic rays when attached onto grain surfaces may lead to complete carbon amorphization in a few billion years. The stability of C_{60} and C_{70} fullerenes in the solid state in the interstellar medium and in solar system objects has recently been simulated with γ irradiation and He^+ ion bombardment (*13*).

In the interstellar gas, fullerenes may have a rich chemistry. C_{60} and C_{70} are highly electronegative and readily form compounds with electron-donating atoms (*14*). Ultraviolet irradiation in low-density interstellar clouds will ionize C_{60}, but the corresponding C_{60} dication is very stable. Hydrogenated fullerenes, as well as fullerenes forming complexes with atoms or molecules in and outside their cages, may be present in circumstellar and interstellar environments.

The detection and analysis of Tc 1 provides a stimulus for further optical and infrared spectroscopic observations of circumstellar and interstellar fullerenes. Continued astronomical observations following these high-quality Spitzer data and related laboratory data will open a way for exploring the fascinating chemistry of these fullerenes in space environments.

References

1. Th. Henning, F. Salama, *Science* **282**, 2204 (1998).
2. J. Cami, J. Bernard-Salas, E. Peeters, S. E. Malek, *Science* **329**, 1180 (2010); published online 22 July 2010 (10.1126/science.1192035).
3. H. W. Kroto, J. R. Heath, S. C. O'Brien, R. F. Curl, R. E. Smalley, *Nature* **318**, 162 (1985).
4. W. Krätschmer, L. Lamb, K. Fostiropoulos, D. R. Huffman, *Nature* **347**, 354 (1990).
5. F. Cataldo, in *Astrobiology: Future Perspectives*, P. Ehrenfreund *et al*., Eds. (Kluwer Academic, Dordrecht, Netherlands, 2004), pp. 97–126.
6. C. Jäger, H. Mutschke, Th. Henning, F. Huisken, *Astrophys. J.* **689**, 249 (2008).
7. S. Kwok, *Nature* **430**, 985 (2004).
8. B. H. Foing, P. Ehrenfreund, *Nature* **369**, 296 (1994).
9. G. A. Galazutdinov, J. Krelowski, F. A. Musaev, P. Ehrenfreund, B. H. Foing, *Mon. Not. R. Astron. Soc.* **317**, 750 (2000).
10. B. H. Foing, P. Ehrenfreund, *Astron. Astrophys.* **317**, L59 (1997).
11. P. Ehrenfreund, S. B. Charnley, *Annu. Rev. Astron. Astrophys.* **38**, 427 (2000).
12. Y. J. Pendleton, L. J. Allamandola, *Astrophys. J. Suppl. Ser.* **138**, 75 (2002).
13. F. Cataldo, G. Strazzulla, S. Iglesias-Groth, *Mon. Not. R. Astron. Soc.* **394**, 615 (2009).
14. D. K. Bohme, *Mass Spectrom. Rev.* **28**, 672 (2009).

10.1126/science.1194855

CREDIT: ZAN PEETERS

Heavy Fermions and Quantum Phase Transitions

Qimiao Si[1]* and Frank Steglich[2]*

Quantum phase transitions arise in many-body systems because of competing interactions that promote rivaling ground states. Recent years have seen the identification of continuous quantum phase transitions, or quantum critical points, in a host of antiferromagnetic heavy-fermion compounds. Studies of the interplay between the various effects have revealed new classes of quantum critical points and are uncovering a plethora of new quantum phases. At the same time, quantum criticality has provided fresh insights into the electronic, magnetic, and superconducting properties of the heavy-fermion metals. We review these developments, discuss the open issues, and outline some directions for future research.

Quantum mechanics not only governs the subatomic world but also dictates the organization of the microscopic particles in bulk matter at low temperatures. The behavior is strikingly different depending on the spin (the internal angular momentum) of the constituent particles. Particles whose spin is an integer multiple of $\hbar$ (Planck's constant h divided by 2π) are bosons. When cooled down to sufficiently low temperatures, they will be described by the same wave function, forming a "condensate." Particles whose spin is a half-integer of $\hbar$, on the other hand, are fermions satisfying the Pauli exclusion principle; no two particles can have the same state. At absolute zero, they occupy the states with the lowest energies, up to an energy referred to as the Fermi energy. In the momentum space, this defines a Fermi surface, enclosing a Fermi volume in which all the states are occupied.

When the particle-particle interactions are included, the behavior of such quantum systems becomes even richer. These strongly correlated systems have taken the center stage in the field of quantum matter over the past two decades (*1*). High-temperature superconductors, fractional quantum Hall systems, colossal magnetoresistive materials, and magnetic heavy-fermion metals are a few prominent examples. The central question for all these systems is how the electrons are organized and, in particular, whether there are principles that are universal among the various classes of these strongly correlated materials. One such principle, which has come to the forefront in recent years, is quantum criticality (*2*).

A quantum critical point (QCP) arises when matter undergoes a continuous transition from one phase to another at zero temperature. A nonthermal control parameter, such as pressure, tunes the amount of zero-point motion of the constituent particles. In other words, such a parameter controls quantum-mechanical tunneling dictated by Heisenberg's uncertainty principle, changing the degree of quantum fluctuations. This is the analog of varying the thermal fluctuations in the case of temperature-driven classical phase transitions, such as the melting of ice or the loss of ferromagnetic order in iron.

The temperature-pressure phase diagram observed in the heavy-fermion intermetallic compound $CePd_2Si_2$ is illustrated in Fig. 1A (*3*). At ambient pressure, $CePd_2Si_2$ orders into an antiferromagnet, below the Néel temperature T_N of about 10 K. Applying pressure reduces T_N monotonically, eventually suppressing the antiferromagnetic order altogether and turning the system into a paramagnetic metal. The putative critical pressure p_c is around 2.8 GPa, at which point an antiferromagnetic QCP is implicated. The QCP, however, is not explicitly observed. Instead, a "dome" emerges at very low temperatures in the vicinity of p_c, under which the system is a superconductor.

This phase diagram exemplifies a general point. It suggests that antiferromagnetic quantum criticality can provide a mechanism for superconductivity—an observation that may be of relevance to a range of other strongly correlated systems, such as high–critical temperature (T_c) cuprates, organic superconductors, and the recently discovered high-T_c iron pnictides. The formation of new phases near a QCP may be considered the consequence of an accumulation of entropy, which is a generic feature of any QCP (*4*) and has recently been observed experimentally (*4*–*6*).

A good example for such an antiferromagnetic QCP is the one observed in the compound $YbRh_2Si_2$ (*4*). Here, the nonthermal control parameter is a (small) magnetic field. The studies of heavy-fermion antiferromagnets have shown that accompanying the QCP at zero temperature is a finite parameter range at nonzero temperatures, in which the metallic state is anomalous (Fig. 1B) (*7*, *8*). Over this quantum critical regime, the electrical resistivity is linear in temperature—a telltale sign for an unusual metallic state. This non-Fermi liquid behavior (*9*), which goes beyond the standard theory of metals [Fermi-liquid theory (*10*)], is another phenomenon that is broadly relevant to the physics of strongly correlated systems (*11*, *12*).

Quantum criticality has been implicated to one degree or another in a host of other heavy-fermion metals (*4*, *13*, *14*). These include $CeCu_2Si_2$, the first superconductor to be observed among heavy-fermion metals (*15*), and $CeRhIn_5$ (Fig. 1C) (*16*). Extensive theoretical studies have led to unconventional quantum criticality (*17*–*20*). More recently, a plethora of phases have been uncovered in heavy-fermion metals near a QCP [such as in Ir-doped $YbRh_2Si_2$ (*8*) and in β-$YbAlB_4$ (*21*)]. Together with the theoretical studies of the global phase diagram of the heavy-fermion metals (*22*, *2*), these developments open up an entirely new frontier on the interplay between quantum criticality and unusual phases.

Quantum Phase Transitions

Quantum phase transitions result from the variation of quantum fluctuations. Tuning a control parameter at absolute zero temperature tilts the balance among the competing ground states associated with conflicting interactions of quantum matter.

Heavy-fermion metals comprise a lattice of localized magnetic moments and a band of conduction electrons (*10*). The exchange interaction between the local moments is primarily that mediated by the conduction electrons: the familiar Ruderman-Kittel-Kasuya-Yoshida (RKKY) interaction. This interaction drives the local moments into an ordered pattern, much like H_2O molecules are condensed into an ordered arrangement in ice. The Kondo-exchange interaction between the local moments and conduction electrons introduces spin flips, which is a tunneling process enabled by quantum mechanics. Correspondingly, increasing the Kondo interaction amounts to enhancing quantum fluctuations, which eventually destroys the magnetic order and yields a paramagnetic phase (*23*, *24*).

The theory of classical phase transitions, formulated by Landau (*25*), is based on the principle of spontaneous symmetry breaking. Consider $CePd_2Si_2$ at ambient pressure. In the paramagnetic phase, at $T > T_N$, the spins are free to rotate. Upon entering the magnetically ordered phase, this continuous spin-rotational symmetry is spontaneously broken; the spins must choose preferred orientations. In the Landau formulation, this symmetry distinction is characterized by a quantity called order parameter; in our case, this is the staggered magnetization of the antiferromagnet. The order parameter is nonzero in the magnetically ordered phase but vanishes in the paramagnetic phase. The critical point arises when the phase transition is continuous—when the order parameter goes to zero smoothly. It is described in terms of the spatial fluctuations of the order parameter. These fluctuations occur over a char-

[1]Department of Physics and Astronomy, Rice University, Houston, TX 77005, USA. [2]Max Planck Institute for Chemical Physics of Solids, 01187 Dresden, Germany.

*To whom correspondence should be addressed. E-mail: qmsi@rice.edu (Q.S.); steglich@cpfs.mpg.de (F.S.)

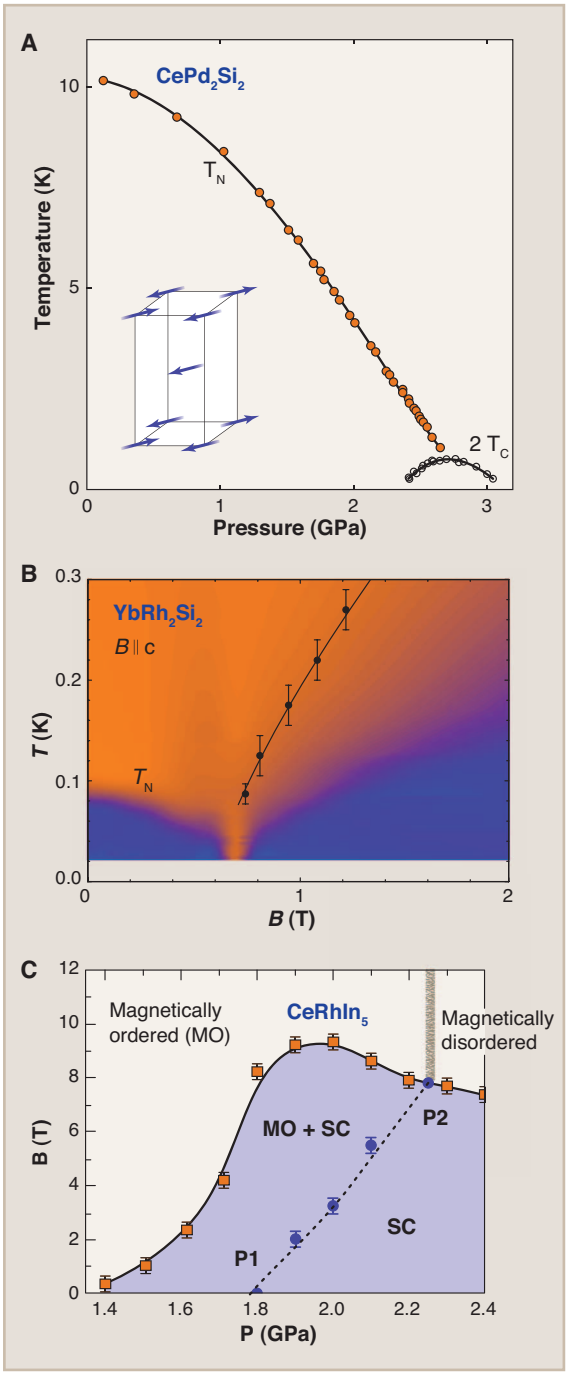

Fig. 1. Quantum phase transitions in heavy-fermion metals. (**A**) Suppression of antiferromagnetic order through pressure in $CePd_2Si_2$. T_N is the Néel transition temperature, and the corresponding antiferromagnetic order is illustrated in the inset. At the boundary of the antiferromagnetism, a phase of unconventional superconductivity arises. T_c corresponds to the superconducting transition temperature (*3*). (**B**) Field-induced quantum phase transition in $YbRh_2Si_2$. The blue regions label the Fermi-liquid behavior observed with measurements of electrical resistivity and other transport and thermodynamic properties; they correspond to $T < T_N$ at $B < B_N$ and $T < T_{FL}$ at $B > B_N$, where B_N is the critical field at $T = 0$. The orange region describes non-Fermi liquid behavior that is anchored by the QCP at $B = B_N$ (*7*). The (T^*) line delineates crossover behavior associated with the destruction of the Kondo effect (*8*). (**C**) The pressure-field phase diagram at the lowest measured temperature ($T = 0.5$ K) in $CeRhIn_5$. The antiferromagnetic order, denoted by MO, at ambient pressure gives way to superconductivity, specified by SC, at higher pressures. At $B = 0$, the antiferromagnetic order goes away when the pressure exceeds P_1. When the magnetic field exceeds just enough to suppress superconductivity, the system is antiferromagnetically ordered at lower pressures ($P < P_2$) but yields a nonmagnetic phase at higher pressures ($P > P_2$). The hatched line refers to the transition at P_2, between these two phases (*37*).

acteristic length scale, which increases on approaching the critical point. At the critical point, the correlation length is infinite. Correspondingly, physical properties are invariant under a mathematical operation that dilates the lengths; in other words, they are scale-invariant.

A straightforward generalization of the Landau paradigm to QCPs gives rise to essentially the same theoretical description (*26*). Quantum mechanics introduces a "time" axis: Quantum states evolve in time. (For quantum systems in equilibrium, the relevant quantum evolution is along an imaginary time of length $\hbar/k_BT$, where k_B is the Boltzmann constant.) This introduces a time scale that accompanies the divergent correlation-length scale. When the transition takes place at a finite temperature T_N, $\hbar/k_BT_N$ serves as the upper bound of the correlation time, and the ultimate critical behavior is still determined by the fluctuations in space only. When T_N is driven to zero temperature, however, a divergent correlation time ξ_τ accompanies the divergent correlation length ξ, and both must be taken into account even for equilibrium properties. Hence, the quantum critical fluctuations of the order parameter take place both in space and in time. The effective dimensionality of the fluctuations is $d + z$, where d is the spatial dimensionality, and z, the dynamic exponent defined in terms of the relationship $\xi_\tau \propto \xi^z$, describes the number of effective spatial dimensions to which the time dimension corresponds.

However, it has been appreciated that this Landau paradigm can break down for QCPs. Consider the effect of the Kondo-exchange coupling. In addition to destabilizing the magnetic order, the Kondo interaction also introduces quantum coherence between the local moments and conduction electrons. Indeed, inside the paramagnetic phase a process called Kondo screening takes place, which leads to a qualitatively new ground state in which the local moments and conduction electrons are entangled. Just as a continuous onset of magnetic order at zero temperature introduces quantum fluctuations of the magnetic order parameter, a critical onset of Kondo entanglement also yields its own quantum critical degrees of freedom. When that happens, a new type of QCP ensues.

Kondo Effect and Heavy Fermions

Historically, the Kondo screening effect was introduced for dilute magnetic impurities in metallic hosts (*10*). By the 1970s, the notion that the Kondo phenomenon operates in a dense periodic array of magnetic Ce ions in intermetallic compounds, such as $CeAl_2$ (*27*), was already in place. A characteristic scale, at which the Kondo screening initially sets in, is the Kondo temperature T_K.

The list of heavy-fermion materials is long, and they are typically compounds containing rare earths or actinides (including Yb, U, and Np, in addition to Ce) with partially filled 4f- or 5f-orbitals. Their defining characteristic is that the effective mass of the charge carriers at the lowest accessible temperatures is hundreds of times the bare electron mass.

Microscopically, heavy-fermion systems can be modeled as a lattice of localized f-electron moments that are coupled to a band of conduction electrons. In the early 1980s, the description of the Kondo effect in the ground state of this Kondo lattice was formulated (*10*). The local moments lose their identity by forming a many-body spin singlet with all the conduction electrons, leading to an entangled state (Fig. 2A). The Kondo entanglement in the ground state makes the local moments, which are charge-neutral to begin with, acquire the quantum numbers of the conduction electrons, namely spin-$\hbar/2$ and charge-e. Correspondingly, "Kondo resonances" appear as charge carriers, and they remember their localized-moment origin by possessing a heavy mass. Because the Kondo resonances are part of the electronic-excitation spectrum, they must be accounted for in the Fermi surface, leading to the notion of a large Fermi surface (Fig. 2B)—the picture of a heavy Fermi liquid.

The Kondo resonances can alternatively be thought of as the remnants of the original f-electrons. They are delocalized because the 4f- or 5f-wave function has a finite overlap with the ligand orbitals that form the conduction electrons. In other words,

the f-electrons and conduction electrons are hybridized.

QCPs in Heavy Fermions

Two types of QCPs. The Kondo singlet in the ground state of a heavy-fermion paramagnet represents an organized macroscopic pattern of the quantum many-body system (Fig. 2A). It endows the paramagnetic phase at zero temperature with a quantum order. This characterization of the phase goes beyond the Landau framework. The Kondo-singlet state does not invoke any spontaneous breaking of symmetry because the spins can orient in arbitrary directions; no Landau order parameter can be associated to the Kondo effect. Two types of QCPs arise, depending on the behavior of the Kondo singlet as we approach the QCP from the paramagnetic side.

When the Kondo singlet is still intact across the antiferromagnetic transition at zero temperature, the only critical degrees of freedom are the fluctuations of the magnetic order parameter. In this case, the antiferromagnetically ordered phase in the immediate proximity to the QCP can be described in terms of a spin-density-wave (SDW) order of the heavy quasiparticles of the paramagnetic phase. The QCP is referred to as of the SDW type, which is in the same class as that already considered by Hertz (*26*, *28*–*30*). On the other hand, when the Kondo singlet exists only in the paramagnetic phase, the onset of magnetic order is accompanied by a breakdown of the Kondo effect. The quantum criticality incorporates not only the slow fluctuations of the antiferromagnetic order parameter but also the emergent degrees of freedom associated with the breakup of the Kondo singlet. The corresponding transition is referred to as locally critical (*17*, *18*); the antiferromagnetic transition is accompanied by a localization of the f-electrons.

This distinction of the two types of QCPs can also be made in terms of energetics. The key quantity to consider is the energy scale E^*, which dictates the breakup of the entangled Kondo singlet state as the system moves from the heavy-Fermi-liquid side toward the quantum critical regime. A reduction of the E^* scale upon approaching the magnetic side is to be expected because the development of antiferromagnetic correlations among the local moments reduces the strength of the Kondo singlet (*17*–*20*). When E^* remains finite at the antiferromagnetic QCP, the Kondo singlet is still formed, and the quantum criticality falls in the universality class of the SDW type. When the E^* scale continuously goes to zero at the antiferromagnetic QCP, a critical Kondo breakdown accompanies the magnetic transition. The T_K scale, in which the Kondo screening initially sets in, is always nonzero near the QCP, even when E^* approaches zero.

The consequence of the Kondo breakdown for the change of the Fermi surface is illustrated in Fig. 2. When E^* is finite, the Kondo-singlet ground state supports Kondo resonances, and the Fermi surface is large. When the E^* scale becomes zero, the ground state is no longer a Kondo singlet, and there are no fully developed Kondo resonances. Correspondingly, the Fermi surface is small, incorporating only the conduction electrons.

In the Kondo-screened paramagnetic phase (Fig. 2A), the large Fermi surface is where the heavy quasiparticles are located in the momentum space (Fig. 2B). As usual, such sharply defined Fermi surfaces occur below an effective Fermi temperature, T_{FL}. Below this temperature, standard Fermi-liquid properties—such as the inverse quasiparticle lifetime and the electrical resistivity being quadratically dependent on temperature—take place.

In the Kondo-destroyed antiferromagnetic phase (Fig. 2C), there is no Kondo singlet in the ground state, and correspondingly, static Kondo screening is absent. Kondo screening still operates dynamically, leading to an enhancement of the mass of the quasiparticles. The quasiparticles still have a Fermi-liquid form at low temperatures. In contrast to the case of the Kondo-singlet ground state, these quasiparticles are adiabatically connected to the ordinary conduction electrons and are located at the small Fermi surface (Fig. 2D).

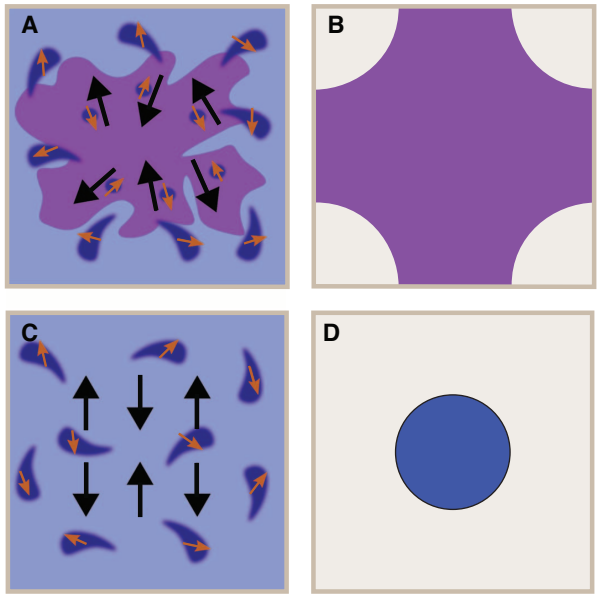

Fig. 2. Kondo entanglement and its breakdown in heavy-fermion metals. (**A**) Kondo-singlet ground state in a paramagnetic phase, giving rise to a heavy Fermi liquid. The shapes with orange arrows indicate the mobile conduction electrons, and the thick black arrows indicate localized magnetic moments. The purple profile describes the Kondo singlet in the ground state. (**B**) The Kondo singlet in the ground state gives rise to Kondo resonances, which must be incorporated into the Fermi volume. Correspondingly, the Fermi surface is large, with a volume that is proportional to 1 + x, where 1 and x, respectively, refer to the number of local moments and conduction electrons per unit cell. An SDW refers to an antiferromagnetic order that develops from a Fermi-surface instability of these quasiparticles. (**C**) Kondo breakdown in an antiferromagnetic phase. The local moments arrange into an antiferromagnetic order among themselves, and they do not form static Kondo singlets with the conduction electrons. (**D**) Kondo resonances do not form in the absence of static Kondo screening. Correspondingly, the Fermi surface is small, enclosing a volume in the paramagnetic Brillouin zone that is proportional to x. Dynamical Kondo screening, however, still operates, giving rise to an enhancement of the quasiparticle mass near the small Fermi surface.

The large number of available compounds is a key advantage in the study of quantum critical heavy-fermion systems. At the same time, it raises an important question: Can we classify the quantum critical behavior observed in these heavy-fermion compounds? Below, we summarize the evidence for such a classification in the systems that have been most extensively studied in the present context.

QCP of the SDW type. The phase diagram for $CePd_2Si_2$ (Fig. 1A) (*3*) is reminiscent of theoretical discussions of unconventional superconductivity near an SDW instability. Unfortunately, because of the high pressure necessary to access the QCP in this compound, it has not yet been possible to study either the order or the fluctuation spectrum near the QCP. $CeCu_2Si_2$ is an ideal system for such an investigation because, here, heavy-fermion superconductivity forms in the vicinity of an antiferromagnetic QCP at ambient/low pressure. Neutron diffractometry revealed the antiferromagnetically ordered state to be an incommensurate SDW with small ordered moment (~0.1 μ_B/Ce) because of the nesting of the renormalized Fermi surface (*31*). Inelastic neutron-scattering studies on paramagnetic $CeCu_2Si_2$ have identified fluctuations close to the incommensurate ordering wave vector of the nearby SDW and have shown that such fluctuations play a dominant role in driving superconducting pairing (*32*), confirming earlier theoretical predictions.

Another compound is $CeNi_2Ge_2$, for which the magnetic instability may be achieved by slight volume expansion. The critical Grüneisen ratio in this system diverges as T^{-1}, which lends support for a nearby SDW QCP (*4*).

There are also a few examples of magnetic quantum phase transitions induced by alloying that appear to fall in the category of the SDW QCP. In $Ce_{1-x}La_xRu_2Si_2$, for instance, recent inelastic neutron-scattering experiments have provided such evidence near its critical concentration $x_c \approx 0.075$ (*33*).

QCP involving a Kondo breakdown. As shown in Fig. 3A, inelastic neutron-scattering

experiments on the quantum critical material $CeCu_{5.9}Au_{0.1}$ revealed an energy over temperature (E/T) scaling (*34*) of the dynamical susceptibility, with a fractional exponent (*35*). The same critical exponent is found to govern the magnetic susceptibility at wave vectors far away from the antiferromagnetic wave vector. These features are incompatible with the predictions of the SDW theory (*26*, *28*–*30*) and have provided the initial motivation for the development of local quantum criticality (*17*). Because such a QCP involves a breakdown of the Kondo effect, it must be manifested in the charge carriers and their Fermi surfaces as well.

Direct measurements of Fermi surfaces are typically done by using angle-resolved photoemission spectroscopy (ARPES). In spite of impressive recent developments, ARPES still does not have the resolution to study heavy-fermion metals in the required sub-Kelvin low-temperature range. The other well-established means to probe Fermi surfaces is the de Haas–van Alphen (dHvA) technique, which, however, requires a large magnetic field of several teslas. A rare opportunity arises in $CeRhIn_5$, in which a magnetic field of about 10 T is in fact needed to suppress superconductivity and expose a quantum phase transition (Fig. 1C). From dHvA measurements performed in the field range of 10 to 17 T, a pronounced jump in the Fermi surface was seen in $CeRhIn_5$ at the critical pressure of 2.3 GPa (Fig. 3B) (*36*). This, together with the observation of a seemingly diverging cyclotron mass of the heavy charge carriers, is commonly considered as evidence for a Kondo-breakdown QCP (*37*). We caution that for $CeRhIn_5$, this issue remains to be fully settled; an alternative explanation that is based on a change of the valence state of the Ce ions has also been made (*38*).

The heavy-fermion metal $YbRh_2Si_2$ has provided an opportunity to probe the electronic properties near an antiferromagnetic QCP involving a breakdown of the Kondo effect. As mentioned earlier, the very weak antiferromagnetic order of $YbRh_2Si_2$ is suppressed by a small magnetic field, giving way to non-Fermi liquid behavior (*7*). Furthermore, the magnetic field induces a substantial change of the isothermal Hall coefficient. The latter has been shown to probe, at low temperatures, the properties of the Fermi surface (*39*). A new temperature scale, $T^*(B)$, was identified in the T–B phase diagram of $YbRh_2Si_2$ (Fig. 1B); across this scale, the isothermal Hall coefficient exhibits a crossover as a function of the applied magnetic field (B). This crossover sharpens upon cooling. Extrapolation to $T = 0$ suggests an abrupt change of the Fermi surface at the critical magnetic field B_N, the field where T_N approaches zero (*39*). Further evidence for the inferred change of Fermi surface has come from thermotransport measurements (*40*). Across the T^* line, the low-temperature thermopower shows a sign change, suggesting an evolution between hole-like and electron-like Fermi surfaces, as illustrated in Fig. 2, B and D.

Further thermodynamic and transport investigations confirmed $T^*(B)$ to be an intrinsic energy scale that vanishes at the antiferromangetic QCP (Fig. 4A) (*41*). The T^* scale is distinct from the Fermi-liquid scale T_{FL}, below which a T^2 resistivity is observed (Fig. 4A). These properties are naturally interpreted as signatures of a breakdown of the Kondo effect at the QCP, with the Fermi surface being large at $B > B_N$ (Fig. 2, A and B) and being small at $B < B_N$ (Fig. 2, C and D); T^* refers then to the temperature scale accompanying the Kondo-breakdown energy scale E^* introduced earlier. Notably, the E^* scale is distinct from the aforementioned T_K scale, which serves as the upper cut-off of the quantum-critical scaling regime and should therefore remain finite near the QCP. For instance, at the critical concentration of $CeCu_{6-x}Au_x$ T_K has been observed in photoemission spectroscopy to be nonzero (*42*), even though E^* is expected to vanish.

A recent thorough study of the Hall crossover on $YbRh_2Si_2$ single crystals of substantially improved quality showed unequivocally that the width of the crossover at $T^*(B)$ is strictly proportional to temperature (Fig. 4B) (*43*). This indicates that the E/T scaling also operates in this compound. Furthermore, it provides evidence that the Kondo-breakdown effect indeed underlies such quantum critical scaling (*43*).

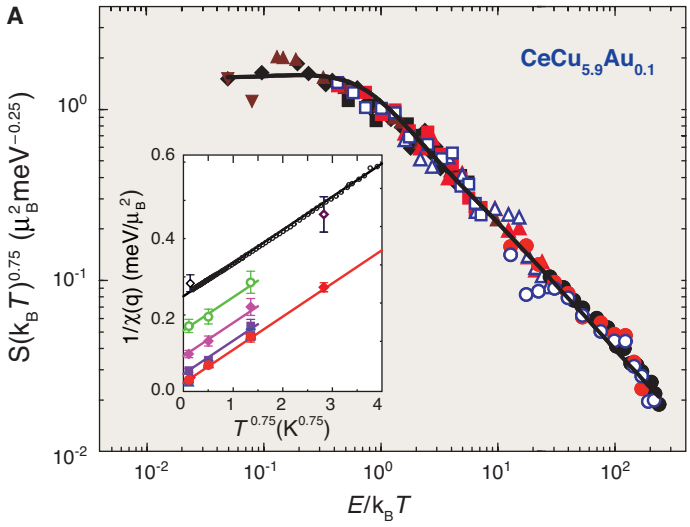

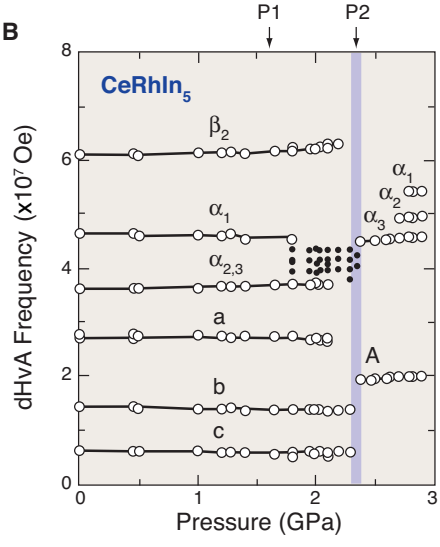

Fig. 3. Quantum critical properties of $CeCu_{6-x}Au_x$ and $CeRhIn_5$. (**A**) Quantum-dynamical E/T scaling of the inelastic neutron-scattering cross-section S in $CeCu_{5.9}Au_{0.1}$. The measurements were performed at the antiferromagnetic wave vectors (where S is maximized), and the scaling collapse is constructed in the form of $T^{\alpha}S$ as a function of E/T. The temperature and energy exponent is fractional: $\alpha = 0.75$. The different symbols represent data taken in different spectrometers at the different peak wave vectors. (Inset) The inverse of the bulk magnetic susceptibility, $1/\chi(\mathbf{q} = 0) \equiv H/M$, and that of the static susceptibility at other wave vectors derived from the dynamical spin susceptibility through the Kramers-Kronig relation (*35*). (**B**) Several dHvA frequencies as a function of pressure in $CeRhIn_5$. The applied magnetic field ranges between 10 T and 17 T. P_1 and P_2 have the same meaning as in Fig. 1C. The symbols denote different branches of the Fermi surface (*36*).

Global Phase Diagram

The fact that in $YbRh_2Si_2$, the multiple lines defining the Kondo-breakdown scale T^*, the Fermi-liquid scale T_{FL}, and the Néel-temperature scale T_N all converge at the same magnetic field in the zero-temperature limit raises the question of what happens when some additional control parameter is varied. This global phase diagram has recently been explored by introducing chemical pressure to $YbRh_2Si_2$ (*8*). The antiferromagnetic order is stabilized or weakened by means of volume compression or expansion, respectively (Fig. 4, C to E), in accordance with the well-established fact that pressure reinforces magnetism in Yb-based intermetallics. Unexpectedly however, the $T^*(B)$ line is only weakly dependent on chemical pressure. Under volume compression (3% Co-doping), the antiferromagnetic QCP occurs at a field substantially higher than B^*, at which $T^* \rightarrow 0$ (Fig. 4E). In this situation, T^* is

finite at the antiferromagnetic QCP. One therefore expects that the SDW description will apply, and this is indeed observed (*8*). Under a small volume expansion (2.5% Ir-doping), B_N and B^* continue to coincide within the experimental accuracy (Fig. 4D). With a large volume expansion (17% Ir-doping), on the other hand, B_N has vanished, but B^* remains finite (Fig. 4C). This opens up a range of magnetic field in which not only any magnetic ordering is absent but also the Kondo-breakdown scale vanishes, suggesting a small Fermi surface. Hydrostatic-pressure experiments (*44*) on undoped $YbRh_2Si_2$ give results comparable with those of the Co-doped materials with a similar average unit-cell volume, indicating that the crossing of $T_N(B)$ and $T^*(B)$ as observed (*8*) for 7% Co-doped $YbRh_2Si_2$ originates from the alloying-induced volume compression rather than disorder.

The results can be summarized in the global phase diagram shown in Fig. 4F. The transition from the small-Fermi-surface antiferromagnet to the heavy-Fermi-liquid state has three types. It may go through a large-Fermi-surface antiferromagnet, such as in the Co-doped cases. The transition can also occur directly, such as in the pure and 2.5% Ir-doped compounds. Or, it may go through a small-Fermi-surface paramagnetic phase, such as in the case of the 6% Ir-doped $YbRh_2Si_2$ (*8*). In this phase, the electrical resistivity shows a quasi-linear temperature dependence (*8*).

Theoretically, two kinds of antiferromagnet–to–heavy-Fermi-liquid transitions were already considered in the previous section. One way to connect them is to invoke a $T = 0$ global phase diagram (*22*), spanned by two parameters associated with two types of quantum fluctuations. One parameter, J_K, describes the Kondo coupling between the conduction electrons and the local moments; increasing J_K enhances the ability of the conduction electrons to screen the local moments and reduces the magnetic order. The other parameter, G, is associated with the interactions among the local moments and refers to, for instance, the degree of geometric frustration (*45*) or simply the dimensionality (*17*, *46*); raising the parameter G boosts the inherent quantum fluctuations of the local-moment system and correspondingly weakens the magnetism. In the two-parameter global phase diagram of (*22*), each kind of transition appears as a line of critical points: One line is associated with local quantum criticality, with the breakdown of the Kondo effect occurring at the antiferromagnetic-ordering transition; the other one is associated with SDW quantum criticality, in which case the Kondo breakdown can only take place inside the antiferromagnetically ordered region. This is consistent with Fig. 4F, in which B_N and B^* coincide for a finite range of small Ir concentrations. The extension of this global phase diagram is currently being pursued theoretically (*2*). When the quantum fluctuations among the local moments are even stronger, a possibility exists for a paramagnetic phase with a suppressed Kondo entanglement and a concomitant small Fermi surface; this can be compared with the region highlighted by the question marks in Fig. 4F. This phase could be a spin liquid or could be an ordered state (such as a spin-Peierls phase) that preserves the spin-rotational invariance. Understanding the nature of the phase represents an intriguing problem worthy of further study, both theoretically and experimentally.

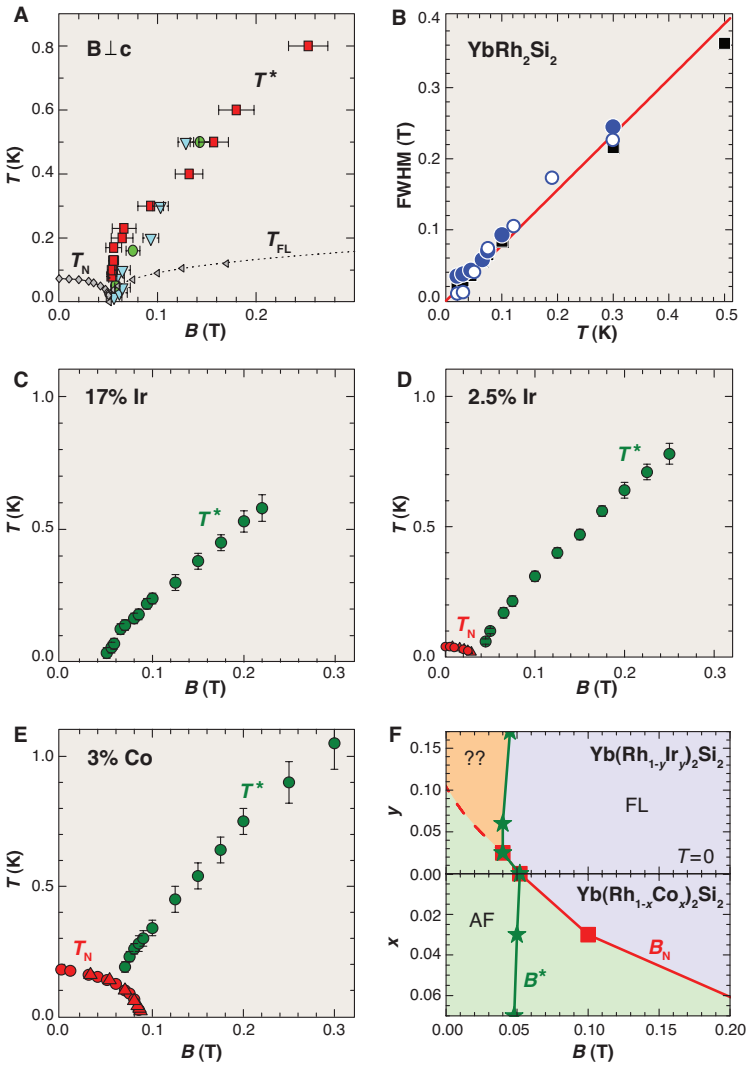

Fig. 4. Quantum criticality and global phase diagram in pure and doped $YbRh_2Si_2$. (**A**) Multiple energy scales in pure $YbRh_2Si_2$. T^* is extracted from isothermal crossovers in the Hall effect and thermodynamic properties, which is interpreted in terms of a Kondo breakdown. T_{FL} is the scale below which Fermi-liquid properties occur. Both crossover lines merge with the line that specifies the magnetic phase boundary T_N in the zero-temperature limit, at B_N (*41*). (**B**) Full width at half maximum (FWHM) of the crossover in the Hall coefficient of a high-quality single crystal (*RRR* = 120). It extrapolates to zero in the $T = 0$ limit, implying a jump of the Hall coefficient and other properties. It is proportional to temperature, suggesting a quantum-dynamical *E*/*T* scaling (*43*). (**C** to **E**) $T^*(B)$ and $T_N(B)$ lines for Ir- and Co-doped $YbRh_2Si_2$, determined via AC susceptibility measurements (*8*). Data for the 7% Co-doped $YbRh_2Si_2$ show an intersection of the two lines (*8*). (**F**) The $T = 0$ phase diagram, doping-concentration versus magnetic field, for $Yb(Rh_{1-x}M_x)_2Si_2$, M=Co,Ir (*8*).

Other heavy-fermion systems may also be discussed in this two-parameter global phase diagram. The zero-temperature transition in $CeCu_{6-x}Au_x$ as a function of doping or pressure can be described in terms of local quantum criticality. As a function of magnetic field, for both $CeCu_{6-x}Au_x$ (*47*) and $CeIn_3$ (*48*) the Kondo breakdown seems to take place inside the antiferromagnetic part of the phase diagram. It will be instructive to see whether other heavy-fermion materials can be used to map the global phase diagram and, in particular, display a paramagnetic non-Fermi liquid phase near a Kondo-breakdown QCP.

Conclusions and Outlook

Studies in the last decade have firmly established the existence of QCPs in heavy-fermion metals. These transitions arise from the suppression of long-range antiferromagnetic ordering by means of tuning pressure, chemical composition, or magnetic field. An important property of QCPs is the accumulation of entropy. Correspondingly, the Grüneisen ratio or the magnetocaloric effect diverges, which serves as an important thermodynamic characterization of the QCPs.

Two types of QCPs have been developed for antiferromagnetic heavy-fermion systems. When a breakdown of the Kondo entanglement occurs inside the antiferromagnetically ordered phase, the QCP has the standard SDW form that conforms to Landau's paradigm of order-parameter fluctuations. When such a Kondo breakdown

happens at the onset of antiferromagnetism, a new class of QCP arises. Evidence for this local quantum criticality has come from the quantum-dynamical scaling and mass divergence in $CeCu_{6-x}Au_x$ and $YbRh_2Si_2$, the multiple energy scales observed in $YbRh_2Si_2$, and the jump of the Fermi surface in $YbRh_2Si_2$ and $CeRhIn_5$.

A strong case has been made that in $CeCu_2Si_2$, the critical fluctuations of a SDW QCP promote unconventional superconductivity. It is likely that the superconductivity in $CePd_2Si_2$ has a similar origin. Whether the Kondo-breakdown local QCPs also favor superconductivity is less clear. $CeRhIn_5$ under pressure and β-$YbAlB_4$ could be examples in this category, although the nature of QCPs in these systems remains to be firmly established.

More recent studies have focused attention, both experimentally and theoretically, on the global phase diagram of antiferromagnetic heavy-fermion metals. Tantalizing evidence has emerged for a non-Fermi liquid phase without any magnetic ordering and with suppressed Kondo entanglement. Whether such a state can in fact arise within the Kondo-lattice model is an intriguing open theoretical question. In the process of addressing such issues, it is becoming clear that quantum fluctuations in heavy-fermion systems can be tuned in more ways than one. Different phases and QCPs may arise when a magnetic disordering is induced by the Kondo coupling between the local moments and conduction electrons or when it is caused by reduced dimensionality and/or magnetic frustration.

Theoretically, an important notion that has emerged from studies in heavy-fermion systems is that quantum criticality can go beyond the Landau paradigm of fluctuations in an order parameter associated with a spontaneous symmetry breaking. This notion has affected the developments on quantum criticality in other systems, including insulating magnets. More generally, quantum criticality in heavy-fermion metals epitomizes the richness and complexity of continuous quantum phase transitions as compared with their classical counterparts. New theoretical methods are needed to study strongly coupled quantum critical systems. One promising new route is provided by an approach that is based on quantum gravity (*49*). Using a charged black hole in a weakly curved space-time to model a finite density of electrons, this approach has provided a tantalizing symmetry reason for some fermionic spectral quantities to display an anomalous frequency dependence when its momentum dependence is smooth. Whether a related symmetry principle underlies the dynamical scaling of the spin response at the Kondo-breakdown local quantum criticality is an intriguing issue for future studies.

The insights gained from these studies on the well-defined QCPs in various heavy-fermion metals have implications for other members of this class of materials as well as for other classes of strongly correlated electronic systems. For example, an outstanding issue is the nature of the hidden-order phase in the heavy-fermion compound URu_2Si_2 (*50*, *51*). This phase is in proximity to some low-temperature magnetically ordered phases, raising the question of the role of quantum phase transitions in this exciting system. In the cuprates, Fermi-surface evolution as a function of doping has also been playing a prominent role in recent years. In light of the discussions on the possible role of doping-induced QCPs, it appears likely that some of the physics discussed for heavy-fermion quantum criticality also comes into play in the cuprates (*52*). For the iron pnictides, the magnetic/superconducting phase diagram has also been observed to show a striking resemblance to Fig. 1A. The interplay between magnetic quantum criticality, electronic localization, and unconventional superconductivity, which has featured so prominently in the systems considered here, is probably pertinent to heavy-fermion metals in general as well as other classes of correlated-electron materials, including the iron pnictides and organic charge-transfer salts. Quantum phase transitions are also being discussed in broader settings, such as ultracold atomic gases and quark matter. It is conceivable that issues related to our discussion here will come into play in those systems as well.

References and Notes

1. I. Osborne, R. Coontz, *Science* **319**, 1201 (2008).
2. Special Issue, *Phys. Status Solidi B* **247**, 457 (2010).
3. F. M. Grosche *et al.*, *J. Phys. Condens. Matter* **13**, 2845 (2001).
4. P. Gegenwart, Q. Si, F. Steglich, *Nat. Phys.* **4**, 186 (2008).
5. Y. Tokiwa, T. Radu, C. Geibel, F. Steglich, P. Gegenwart, *Phys. Rev. Lett.* **102**, 066401 (2009).
6. A. W. Rost, R. S. Perry, J.-F. Mercure, A. P. Mackenzie, S. A. Grigera, *Science* **325**, 1360 (2009).
7. J. Custers *et al.*, *Nature* **424**, 524 (2003).
8. S. Friedemann *et al.*, *Nat. Phys.* **5**, 465 (2009).
9. M. B. Maple *et al.*, *J. Low Temp. Phys.* **95**, 225 (1994).
10. A. C. Hewson, *The Kondo Problem to Heavy Fermions* (Cambridge Univ. Press, Cambridge, 1993).
11. R. A. Cooper *et al.*, *Science* **323**, 603 (2009).
12. S. A. Grigera *et al.*, *Science* **294**, 329 (2001).
13. G. R. Stewart, *Rev. Mod. Phys.* **73**, 797 (2001).
14. H. v. Löhneysen, A. Rosch, M. Vojta, P. Wölfle, *Rev. Mod. Phys.* **79**, 1015 (2007).
15. F. Steglich *et al.*, *Phys. Rev. Lett.* **43**, 1892 (1979).
16. H. Hegger *et al.*, *Phys. Rev. Lett.* **84**, 4986 (2000).
17. Q. Si, S. Rabello, K. Ingersent, J. L. Smith, *Nature* **413**, 804 (2001).
18. P. Coleman, C. Pépin, Q. Si, R. Ramazashvili, *J. Phys. Condens. Matter* **13**, R723 (2001).
19. T. Senthil, M. Vojta, S. Sachdev, *Phys. Rev. B* **69**, 035111 (2004).
20. I. Paul, C. Pépin, M. R. Norman, *Phys. Rev. Lett.* **98**, 026402 (2007).
21. S. Nakatsuji *et al.*, *Nat. Phys.* **4**, 603 (2008).
22. Q. Si, *Physica B* **378**, 23 (2006).
23. S. Doniach, *Physica B* **91**, 231 (1977).
24. C. M. Varma, *Rev. Mod. Phys.* **48**, 219 (1976).
25. S.-K. Ma, *Modern Theory of Critical Phenomena* (Addison-Wesley, Redwood City, CA, 1976).
26. J. A. Hertz, *Phys. Rev. B* **14**, 1165 (1976).
27. C. D. Bredl, F. Steglich, K. D. Schotte, *Z. Phys. B* **29**, 327 (1978).
28. A. J. Millis, *Phys. Rev. B* **48**, 7183 (1993).
29. T. Moriya, *Spin Fluctuations in Itinerant Electron Magnetism* (Springer, Berlin, 1985).
30. M. A. Continentino, *Phys. Rev. B* **47**, 11587 (1993).
31. O. Stockert *et al.*, *Phys. Rev. Lett.* **92**, 136401 (2004).
32. O. Stockert *et al.*, *Physica B* **403**, 973 (2008).
33. W. Knafo, S. Raymond, P. Lejay, J. Flouquet, *Nat. Phys.* **5**, 753 (2009).
34. M. C. Aronson *et al.*, *Phys. Rev. Lett.* **75**, 725 (1995).
35. A. Schröder *et al.*, *Nature* **407**, 351 (2000).
36. H. Shishido, R. Settai, H. Harima, Y. Ōnuki, *J. Phys. Soc. Jpn.* **74**, 1103 (2005).
37. T. Park *et al.*, *Nature* **440**, 65 (2006).
38. S. Watanabe, A. Tsuruta, K. Miyake, J. Flouquet, *J. Phys. Soc. Jpn.* **78**, 104706 (2009).
39. S. Paschen *et al.*, *Nature* **432**, 881 (2004).
40. S. Hartmann *et al.*, *Phys. Rev. Lett.* **104**, 096401 (2009).
41. P. Gegenwart *et al.*, *Science* **315**, 969 (2007).
42. M. Klein *et al.*, *Phys. Rev. Lett.* **101**, 266404 (2008).
43. S. Friedemann *et al.*, *Proc. Natl. Acad. Sci. U.S.A.* (2010).
44. Y. Tokiwa, P. Gegenwart, C. Geibel, F. Steglich, *J. Phys. Soc. Jpn.* **78**, 123708 (2009).
45. L. Balents, *Nature* **464**, 199 (2010).
46. H. Shishido *et al.*, *Science* **327**, 980 (2010).
47. O. Stockert, M. Enderle, H. v. Löhneysen, *Phys. Rev. Lett.* **99**, 237203 (2007).
48. S. E. Sebastian *et al.*, *Proc. Natl. Acad. Sci. U.S.A.* **106**, 7741 (2009).
49. I. R. Klebanov, J. M. Maldacena, *Phys. Today* **62**, 28 (2009).
50. A. R. Schmidt *et al.*, *Nature* **465**, 570 (2010).
51. P. Aynajian *et al.*, *Proc. Natl. Acad. Sci. U.S.A.* **107**, 10383 (2010).
52. N. Doiron-Leyraud *et al.*, *Nature* **447**, 565 (2007).

53. We thank E. Abrahams, M. Brando, P. Coleman, S. Friedemann, P. Gegenwart, C. Geibel, F. M. Grosche, S. Kirchner, C. Krellner, M. Nicklas, T. Park, J. Pixley, O. Stockert, J. D. Thompson, S. Wirth, and S. Yamamoto for useful discussions. This work has been supported by NSF and the Robert A. Welch Foundation grant C-1411 (Q.S.) and by the DFG Research Unit 960 "Quantum Phase Transitions" (F.S.).

10.1126/science.1191195

Chlorine Isotope Fractionation in the Stratosphere

J. C. Laube,[1]* J. Kaiser,[1] W. T. Sturges,[1] H. Bönisch,[2] A. Engel[2]

The isotopic compositions of only a few stratospheric gases have been investigated to date (*1*, *2*). One known effect is the relative enrichment of heavier isotopologues (isotopically distinct species of a compound) for gases that are destroyed in the stratosphere (*2*). Such isotope effects are often characteristic for specific reactions and can help improve our understanding of the transport and reaction pathways of gases in this climate-sensitive atmospheric region (*3*–*6*). For example, position-dependent nitrogen isotope fractionation in nitrous oxide is different for photolysis and photooxidation of N_2O by O^1D (*4*). Similarly, the strong isotope effect in the reaction of chlorine radicals with methane leaves a "fingerprint" of stratospheric chemistry in the reaction product carbon monoxide (*7*).

Here, we present chlorine isotope ratio measurements of CF_2Cl_2 in air samples collected in 2005 and 2008 on board balloons flying in the tropical stratosphere. CF_2Cl_2 is the most abundant chlorofluorocarbon (CFC) in the atmosphere and commonly known as CFC-12. It is a key anthropogenic greenhouse gas with an atmospheric lifetime of about 100 years (*8*) and plays a major role in stratospheric ozone depletion (*9*). A recent reanalysis of the retrieved trace gas data (*10*, *11*) revealed that the isotopic composition of chlorine in CF_2Cl_2 changes with altitude. Chlorine has two stable isotopes, ^{37}Cl and ^{35}Cl, which occur in a ratio of about 24.24:75.76 (*12*, *13*). Here, the isotopic composition is given as the relative $^{37}Cl/^{35}Cl$ isotope ratio difference, $\delta(^{37}Cl)$, between the sample and tropospheric air. We observed $\delta(^{37}Cl)$ values up to 27 per mil (‰) ± 4‰ (SE) in the stratospheric air samples (Fig. 1), almost double the total previously reported range of 16‰ for $\delta(^{37}Cl)$ in naturally occurring samples of any form (*13*–*17*). Furthermore, our data show that stratospheric $\delta(^{37}Cl)$ values increase with altitude, which is probably most due to the faster decomposition of $CF_2{}^{35}Cl_2$ relative to $CF_2{}^{37}Cl^{35}Cl$ and $CF_2{}^{37}Cl_2$ by photolysis and by reaction with O^1D.

If such irreversible sinks with a constant isotopic fractionation were the causing process, the $\delta(^{37}Cl)$ values should follow a Rayleigh-type fractionation with a linear correlation of the form $\ln[1 + \delta(^{37}Cl)] \approx \varepsilon_{app}\ln(y_{sample}/y_{entry})$ (*4*), where y_{sample}/y_{entry} is the ratio of stratospheric to tropospheric mixing ratios and ε_{app} is the apparent isotopic fractionation in the stratosphere. We observed a tight correlation with $\varepsilon_{app} = -12.1‰ \pm 1.7‰$. The apparent isotope fractionation observed in the stratosphere is expected to be lower than that caused by the fractionating reaction because of slow stratospheric transport and mixing (*4*). On the basis of N_2O, which shares the same sinks as CF_2Cl_2 and has a similar lifetime of 120 years, the magnitude of the intrinsic photochemical fractionation could be twice as large as ε_{app}, that is, ≤–24‰. Predictions from simple zero-point energy theory calculations give only about –6 to –8‰ (*18*) for photolytic isotope fractionation. More advanced theories are needed to quantitatively explain the observed effects but have only been developed for molecules with three atoms or fewer (*19*–*21*).

Moreover, the instruments used here (*18*) are not typical for carrying out isotope ratio studies. Their successful application overcomes the insufficient sensitivity of conventional isotope ratio mass spectrometers for very low (parts per trillion, 10^{-12}) abundances of trace gases and the difficulty of obtaining large stratospheric samples. Many important greenhouse and ozone-depleting gases contain chlorine and should show similar enrichment. This could enable the quantification of the relative magnitudes of their stratospheric sinks. For CF_2Cl_2, laboratory experiments suggest that between 93 and 97% is destroyed by photolysis, the remainder by O^1D (*22*). Because the altitude profile of the O^1D loss is different from that of the photolysis sink, further measurements may be used to confirm and constrain the relative contribution of the O^1D to the total loss of CF_2Cl_2 and other important ozone-depleting substances. A subsequent reduction in the uncertainties of their atmospheric lifetimes [ranging from 79 to 113 years for CF_2Cl_2 (*9*)] would then lead to improvements in ozone recovery predictions. In addition, the explored measurement capabilities to detect chlorine isotope effects might help identifying and quantifying remaining sources of CFCs via their individual signatures. Lastly, chlorine isotope measurements could help unravel the human contribution to compounds that have both natural and anthropogenic sources, such as methyl chloride.

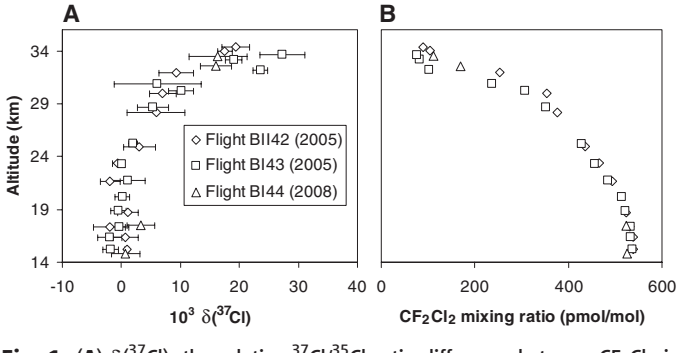

Fig. 1. (**A**) $\delta(^{37}Cl)$, the relative $^{37}Cl/^{35}Cl$ ratio difference between CF_2Cl_2 in the stratosphere and the troposphere (average 1σ standard deviation of samples: ± 2.3‰) and (**B**) the corresponding mixing ratios of CF_2Cl_2 (all 1σ standard deviations less than size of the symbols).

References and Notes

1. M. S. Johnson, K. L. Feilberg, P. von Hessberg, O. J. Nielsen, *Chem. Soc. Rev.* **31**, 313 (2002).
2. C. A. M. Brenninkmeijer *et al.*, *Chem. Rev.* **103**, 5125 (2003).
3. S. S. Cliff, C. A. M. Brenninkmeijer, M. H. Thiemens, *J. Geophys. Res.* **104**, 16171 (1999).
4. J. Kaiser, A. Engel, R. Borchers, T. Röckmann, *Atmos. Chem. Phys.* **6**, 3535 (2006).
5. J. A. Smith, A. S. Ackerman, E. J. Jensen, O. B. Toon, *Geophys. Res. Lett.* **33**, L06812 (2006).
6. D. Krankowsky *et al.*, *J. Geophys. Res.* **112**, D08301 (2007).
7. C. A. M. Brenninkmeijer *et al.*, *Geophys. Res. Lett.* **23**, 2125 (1996).
8. V. R. P. Forster *et al.*, in *Climate Change 2007: The Physical Science Basis. Contribution of Working Group I to the Fourth Assessment Report of the Intergovernmental Panel on Climate Change*, S. Solomon *et al.*, Eds. (Cambridge Univ. Press, Cambridge, 2007), chap. 2.
9. C. Clerbaux *et al.*, in *Scientific Assessment of Ozone Depletion: 2006* (report no. 50, Global Ozone Research and Monitoring Project, World Meteorological Organization, Geneva, 2007), chap. 3.
10. J. C. Laube *et al.*, *Atmos. Chem. Phys.* **8**, 7325 (2008).
11. J. C. Laube *et al.*, *Atmos. Chem. Phys.* **10**, 1093 (2010).
12. W. R. Shields, T. J. Murphy, E. L. Garner, V. H. Dibeler, *J. Am. Chem. Soc.* **84**, 1519 (1962).
13. J. R. De Laeter *et al.*, *Pure Appl. Chem.* **75**, 683 (2003).
14. M. A. Stewart, A. J. Spivack, in *Geochemistry of Non-Traditional Stable Isotopes*, C. M. Johnson, B. L. Beard, F. Albarède, Eds. (Mineralogical Society of America, Washington, DC, 2004), chap. 7.
15. T. B. Coplen *et al.*, *Pure Appl. Chem.* **74**, 1987 (2002).
16. S. M. Lev, R. D. Vocke Jr., contribution 971 of the V. M. Ninth Annual Goldschmidt Conference, Lunar Planetary Institute, Cambridge, MA, 22 to 27 August 1999, p. 169.
17. H. E. Gaudette, *Geol. Soc. Am. Abstr. Prog.* **22**, A173 (1990).
18. Information on materials and methods is available on *Science* Online.
19. S. Nanbu, M. S. Johnson, *J. Phys. Chem. A* **108**, 8905 (2004).
20. M. C. Liang, G. A. Blake, Y. L. Yung, *J. Geophys. Res.* **109**, D10308 (2004).
21. M. K. Prakash, R. A. Marcus, *J. Chem. Phys.* **123**, 174308 (2005).
22. P. K. Patra, S. Lal, *J. Atmos. Sol. Terr. Phys.* **59**, 1149 (1997).

23. We thank the Centre National d'Etudes Spatiales (CNES) balloon team and the anonymous reviewers and acknowledge funding from Natural Environment Research Council (fellowship NE/F015585/1), Royal Society (WM052632), European Space Agency, European Union (project GOCE-CT-2003-505390), Deutsches Zentrum für Luft- und Raumfahrt (project 50EE0016), and Deutsche Forschungsgemeinschaft (project EN 367/4).

Supporting Online Material

www.sciencemag.org/cgi/content/full/329/5996/1167/DC1
Materials and Methods
Fig. S1
References

4 May 2010; accepted 13 July 2010
10.1126/science.1191809

[1]School of Environmental Sciences, University of East Anglia, Norwich NR47TJ, UK. [2]Institute for Atmosphere and Environment, University of Frankfurt, 60438 Frankfurt (Main), Germany.

*To whom correspondence should be addressed. E-mail: j.laube@uea.ac.uk

Effectiveness and Safety of Tenofovir Gel, an Antiretroviral Microbicide, for the Prevention of HIV Infection in Women

Quarraisha Abdool Karim,[1,2]*† Salim S. Abdool Karim,[1,2,3]* Janet A. Frohlich,[1] Anneke C. Grobler,[1] Cheryl Baxter,[1] Leila E. Mansoor,[1] Ayesha B. M. Kharsany,[1] Sengeziwe Sibeko,[1] Koleka P. Mlisana,[1] Zaheen Omar,[1] Tanuja N. Gengiah,[1] Silvia Maarschalk,[1] Natasha Arulappan,[1] Mukelisiwe Mlotshwa,[1] Lynn Morris,[4] Douglas Taylor,[5] on behalf of the CAPRISA 004 Trial Group‡

The Centre for the AIDS Program of Research in South Africa (CAPRISA) 004 trial assessed the effectiveness and safety of a 1% vaginal gel formulation of tenofovir, a nucleotide reverse transcriptase inhibitor, for the prevention of HIV acquisition in women. A double-blind, randomized controlled trial was conducted comparing tenofovir gel (n = 445 women) with placebo gel (n = 444 women) in sexually active, HIV-uninfected 18- to 40-year-old women in urban and rural KwaZulu-Natal, South Africa. HIV serostatus, safety, sexual behavior, and gel and condom use were assessed at monthly follow-up visits for 30 months. HIV incidence in the tenofovir gel arm was 5.6 per 100 women-years (person time of study observation) (38 out of 680.6 women-years) compared with 9.1 per 100 women-years (60 out of 660.7 women-years) in the placebo gel arm (incidence rate ratio = 0.61; P = 0.017). In high adherers (gel adherence > 80%), HIV incidence was 54% lower (P = 0.025) in the tenofovir gel arm. In intermediate adherers (gel adherence 50 to 80%) and low adherers (gel adherence < 50%), the HIV incidence reduction was 38 and 28%, respectively. Tenofovir gel reduced HIV acquisition by an estimated 39% overall, and by 54% in women with high gel adherence. No increase in the overall adverse event rates was observed. There were no changes in viral load and no tenofovir resistance in HIV seroconverters. Tenofovir gel could potentially fill an important HIV prevention gap, especially for women unable to successfully negotiate mutual monogamy or condom use.

Women are disproportionately affected by the Acquired Immunodeficiency Syndrome (AIDS) epidemic in Africa, the region that accounts for 70% of global burden of Human Immunodeficiency Virus (HIV) infection (*1*). Current HIV prevention behavioral messages on abstinence, faithfulness, and condom promotion have had limited impact on HIV incidence rates in women, especially in sub-Saharan Africa, where young women bear the greatest HIV burden (*2*). The search for new technologies to prevent sexually transmitted HIV infection over the past three decades has had limited success. Only five of 37 randomized controlled trials, which tested 39 HIV prevention strategies, have demonstrated protection against sexual transmission of HIV infection (*3*). The successful trials tested medical male circumcision in South Africa (*4*), Kenya (*5*), and Uganda (*6*) (combined effectiveness in reducing HIV acquisition was 57%), sexually transmitted infection (STI) treatment in Tanzania (effectiveness in reducing HIV acquisition was 42%) (*7*), and a HIV vaccine combination in Thailand (effectiveness in reducing HIV acquisition was 31%) (*8*). Hence, HIV prevention technologies that women can use and control remain a pressing priority (*9*).

Microbicides are products that can be applied to the vagina or rectum with the intention of reducing the acquisition of STIs, including HIV. An effective microbicide has the potential to alter the trajectory of the global HIV pandemic (*10*). Over the last 20 years of microbicide research, none of the 11 effectiveness trials of six candidate products have demonstrated meaningful protection against HIV infection (*11*).

Tenofovir, an adenosine nucleotide analog with potent activity against retroviruses (*12*), was initially developed and tested as a prophylactic in monkeys and was subsequently formulated for oral use as tenofovir disoproxil fumarate (Viread), which is now widely used for HIV treatment. Tenofovir's efficacy in suppressing viral replication, favorable safety profile, and long half-life (*13*) made it an ideal choice as the first antiretroviral drug to be formulated as a microbicide gel. In vitro and in vivo assessments of the 1% concentration of tenofovir in a gel formulation have demonstrated its potential as a microbicide (*13*). Tenofovir has shown efficacy against viral challenge in animal models when administered as pre- or post-exposure prophylaxis (*14*, *15*). In monkey challenge studies, tenofovir gel has shown protection with intermittent dosing and with a single pre-exposure dose (*16*). In early-stage clinical trials, tenofovir gel was well tolerated in both HIV-negative and HIV-positive women (*17*), with both daily and coitally related use of the gel being found to be acceptable and safe (*18*).

The purpose of this study was to assess the effectiveness and safety of tenofovir gel for the prevention of HIV infection in women.

Study design and population. Centre for the AIDS Program of Research in South Africa (CAPRISA) 004, a two-arm, double-blind, randomized, placebo-controlled trial, was conducted from May 2007 to March 2010. Women were enrolled at an urban and a rural clinic in KwaZulu-Natal, South Africa, but the study was not designed to assess the effectiveness of tenofovir in each clinic separately. Urban women were enrolled at the CAPRISA eThekwini Research Clinic, which is adjacent to an STI clinic located in the Durban city center. Rural women were enrolled at the CAPRISA Vulindlela Research Clinic adjacent to a comprehensive primary health care clinic in Vulindlela, which is a rural community of approximately 90,000 people and about 150 km northwest of Durban. Before the CAPRISA 004 trial, feasibility studies were conducted in order to assess HIV incidence and sexual behavior at both sites. Extrapolated HIV incidence rates from prevalence studies in the urban (*19*) and rural (*20*) sites were 15.6 and 11.2%, respectively. Reported anal sex rates were substantially lower at these two sites than we had observed in previous microbicide trials (*21*) in female sex workers in this region. Data from these feasibility studies were used as the basis for selecting these sites for the trial, as well as for the design and sample size calculations for the CAPRISA 004 trial.

HIV-negative women, from 18 to 40 years old, who were sexually active (defined as having engaged in vaginal sex at least twice in the 30 days before screening), not pregnant, and using a nonbarrier form of contraceptive were eligible for enrollment. Participants who had a history of adverse reactions to latex, planned to either travel away from the study site for more than 30 consecutive days, relocate away from the study site, become pregnant, or enroll in any other behavioral or investigational product study were excluded. Participants who had a creatinine clearance of <50 ml/min (*22*), had evidence of genital deep epithelial disruption, had in the past year participated in any research related to any vaginally applied product or products, or had an untreated STI or reproductive tract infection were also excluded. Women who met eligibility criteria and demonstrated adequate understanding of the trial (through a comprehension checklist) were enrolled after providing written informed consent. From May 2007 to January 2009, 2160 women were screened and 1085 were enrolled, of whom

[1]Centre for the AIDS Program of Research in South Africa (CAPRISA), Durban 4013, South Africa. [2]Department of Epidemiology, Mailman School of Public Health, Columbia University, NY 10032, USA. [3]University of KwaZulu-Natal, Durban 4013, South Africa. [4]National Institute for Communicable Diseases (NICD), Johannesburg 2131, South Africa. [5]Family Health International (FHI), Durham, NC 27713, USA.

*These authors contributed equally to this work.
†To whom correspondence should be addressed. E-mail: caprisa@ukzn.ac.za
‡The members of the CAPRISA 004 Trial Group appear at the end of this paper.

889 were included in the analysis (Fig. 1). Further information on the enrollment process and exclusions can be found in (*23*).

Enrolled women were randomly assigned in equal proportions to one of two study arms: tenofovir gel or placebo gel. Tenofovir gel comprised 40 mg of 9-[(R)-2-phosphonomethoxy) propyl]adenine monohydrate (PMPA) in a solution of purified water with edetate disodium, citric acid, glycerin, methylparaben, propylparaben, and hydroxyethycellulose (HEC). The placebo gel was the "universal" HEC placebo gel, which has been shown to have minimal anti-HIV activity (*24*). Tenofovir and placebo gels appeared identical and were dispensed in the same prefilled vaginal applicators with identical packaging.

A coitally related dosing strategy was selected to achieve high adherence on the basis of in-depth consultations with the communities involved. Sexual behavior data showed that women in the key study population had infrequent high-risk sex with migrant partners. Monkey challenge data and perinatal transmission studies informed the timing of doses in relation to sex. The "before and after" sex doses were modeled on the timing of nevirapine in its proven strategy for preventing mother-to-child HIV transmission (*25*). Women were requested to insert one dose of gel within 12 hours before sex and a second dose of gel as soon as possible within 12 hours after sex and no more than two doses of gel in a 24-hour period. Hence, the dosing strategy is referred to as "BAT24." The latter restriction was imposed because of the lack of human safety data on more than two doses of gel per day.

Gel adherence was defined as the estimated proportion of reported sex acts covered by two gel doses and calculated for each woman by dividing half the number of returned used applicators each month by the number of reported sex acts that month. Applicators that were not returned were regarded as unused for the purposes of calculating adherence. When we conducted a sensitivity analysis treating unreturned applicators as used, the results did not change materially. The median of each woman's monthly adherence estimates was assigned as her overall gel adherence. This approach assumed that every reported sex act used two doses of gel. Although this assumption was not always applicable, adjusting for multiple sex acts within 24 hours made no material difference.

At enrollment and monthly follow-up visits, participants were provided with comprehensive HIV prevention services (HIV pre- and post-test counseling, HIV risk reduction counseling, condoms, and STI treatment), reproductive health services, and assigned study gel.

Participants were requested to return their used (from October 2007 onward) and unused applicators at every visit. Each month, the applicators returned by women as used and unused were counted, reconciled against the number dispensed, and thereafter discarded, in accordance with standard requirements for medical waste.

A comprehensive adherence support program assisted participants with the mechanics of applicator use, timing and dosing, avoidance of gel sharing, and incorporation of gel use into their daily routines. From October 2008, individualized motivational interviewing (*26*, *27*) was introduced to assist participants so as to overcome obstacles to gel use and set goals for optimal adherence in the upcoming month. This included individualized adherence support and counseling, customized on the previous month's experience of gel use, which was provided throughout the study. The women in this study were specifically and repeatedly counseled to only use the gel vaginally, and the lack of safety with rectal use was highlighted.

Each participant had monthly HIV and urine pregnancy testing [QuickVue One-Step hCG Urine Test (Quidel Corporation, San Diego, California)] performed before gel was dispensed. Because of a lack of pregnancy safety data, gel use was temporarily discontinued after a positive pregnancy test and resumed when the pregnancy test returned to negative. Self-reported data on gel use and sexual frequency during the last 30 days were collected at monthly visits, together with gel and condom use on the day of the last sex act, by means of a brief interviewer-administered questionnaire. Two months after study exit, participants attended a posttrial visit to assess HIV status and safety after product withdrawal.

Drug safety was assessed at every study visit by evaluating, grading, and recording adverse events experienced by participants. Participants underwent quarterly pelvic examinations and, if needed, colposcopy. Serology was performed for hepatitis B virus [Abbott Architect C8200 (Abbott Laboratories, Detroit, Michigan)] and herpes simplex type 2 virus [Kalon Enzyme Immunoassay (Kalon Biologicals, Ashgate, UK)]. Hematological, hepatic, and renal abnormalities were assessed at study months 3, 12, and 24; additionally when clinically indicated; and at study exit. Adverse events were graded for severity via the Division of AIDS Table for Grading Adult and Pediatric Adverse Events, 2004. Product use was temporarily discontinued for an adverse event at the discretion of the

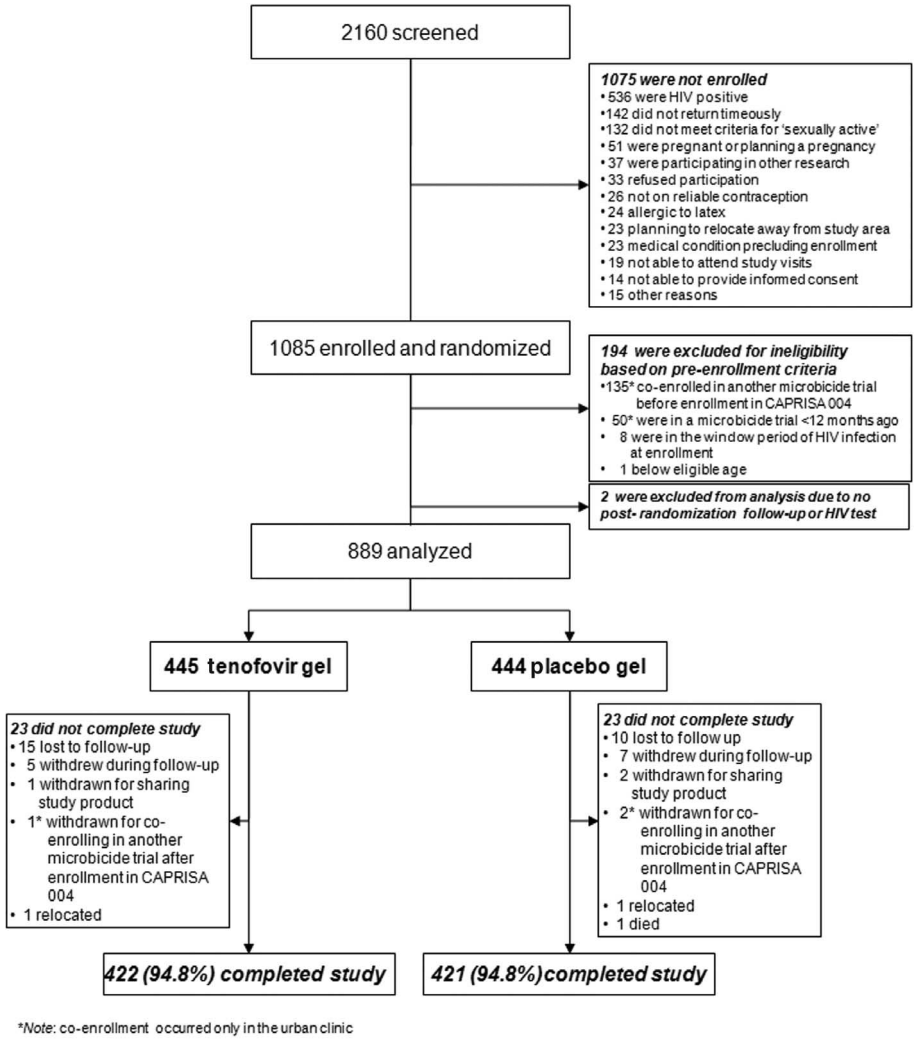

Fig. 1. Screening, enrollment, randomization, and follow-up of the study participants.

study clinician. The trial (NCT00441298) was approved by the University of KwaZulu-Natal's Biomedical Research Ethics Committee (E111/06), Family Health International (FHI)'s Protection of Human Subjects Committee (9946), and the South African Medicines Control Council (20060835).

HIV, viral load, and genotypic resistance assays. Two HIV rapid tests, Determine HIV 1/2 (Abbott Laboratories, Chicago, Illinois) and Uni-Gold Recombigen® HIV test (Trinity Biotech, Wicklow, Ireland), were performed at each study visit. Participants with concordantly positive, discordant, or indeterminate results were assessed for possible seroconversion by means of two separate RNA polymerase chain reaction (PCR) [Roche Cobas TaqMan HIV-1 Monitor v1.0 (Roche Diagnostics, Branchburg, New Jersey)] assays, about 1 week apart. When HIV seroconversion was established, product use was discontinued, and women were referred to local AIDS treatment services, including the CAPRISA AIDS Treatment Program, which provides free antiretroviral therapy. Stored plasma, available from prior study visits by each seroconverter, was tested by means of RNA PCR so as to identify the window period for HIV infection (RNA PCR–positive but rapid HIV test–negative) at prior visits. By protocol, only eligibly enrolled women with HIV infection during study follow-up, as confirmed by two independent RNA PCR results, were defined as HIV endpoints. Participants in the HIV window period at study exit were included as HIV endpoints if seropositivity was confirmed after the study. Thus, HIV infections were categorized as follows: (i) HIV endpoints, (ii) HIV infections not meeting the protocol definition for an HIV endpoint (did not have the two independent RNA PCR tests), (iii) window period HIV infections at enrollment (infected before study entry), (iv) posttrial HIV infections (infected after study exit), and (v) HIV infections among women who were enrolled and later found to be ineligible (*23*).

Tenofovir resistance testing and Western Blot [Genetics systems HIV-1 Western Blot kit (Bio-Rad Laboratories, Hercules, California)] were performed at the post-seroconversion visit. The HIV-1 *pol* gene was population sequenced by means of a certified (*28*) in-house assay. Viral RNA was extracted, and a 1.7-kb fragment spanning the *pol* gene was amplified by means of nested PCR with the Expand Long Template PCR System (Roche Diagnostics), as described previously (*28*). PCR products were sequenced (codons 1 to 99 of protease and codons 1 to 350 of reverse transcriptase) by using a BigDye Terminator v3.1 cycle sequencing kit and an ABI 3130XL DNA sequencer (Applied Biosystems, Foster City, California). Consensus sequences were aligned and manually edited by using the Sequencher version 4.5 program (GeneCodes, Ann Arbor, Michigan) and submitted to the Stanford University HIV Drug Resistance Database (http://hivdb.stanford.edu) to identify mutations.

Statistical analyses. In this endpoint-driven trial, participants were followed until 92 HIV infections were observed, providing 90% power to detect a 50% effect (two-sided $\alpha = 0.05$). Originally, the study was designed with 80% power. Before their first data review, the Data Safety and Monitoring Board (DSMB) ratified a change to 90% power adjusted for two preplanned interim reviews, with stringent stopping guidelines.

Upon enrollment, a participant was assigned a sequential identification number, which corresponded to a unique envelope (accessible only to each study site pharmacist) that allocated her randomly, by using permuted block randomization of sizes 12 and 18, with no stratification, to one of six codes. The three codes assigned randomly to each of tenofovir and placebo gels were held in confidence by the product manufacturer and independent DSMB statistician.

The primary intent-to-treat analysis was based on a log-rank test, stratified by site. Duration of time on study was calculated from randomization to estimated date of HIV infection or date of withdrawal, whichever occurred first. A Poisson distribution was assumed for confidence intervals (CIs) of incidence rates and incidence rate ratios (IRRs). Fisher's exact test and the unpaired *t* test/Wilcoxon two-sample test were performed where appropriate. Proportional hazards regression models were used to calculate hazard ratios while adjusting for potentially important covariates. All reported *P* values are two-sided, and all CIs are 95%. The statistical analysis was performed using SAS (SAS Institute, Cary, North Carolina) version 9.1.3.

Table 1. Baseline demographic characteristics, sexual history, and contraceptive use by study participants in the CAPRISA 004 tenofovir gel trial.

	Site			Study arms		
	Rural (*n* = 611 women)	Urban (*n* = 278 women)	*P* value	Tenofovir (*n* = 445 women)	Placebo (*n* = 444 women)	*P* value
Demographic characteristics						
Mean age (years)	23.3	25.1	<0.001	24.2	23.6	0.131
Monthly income <1000 South African rand	86.1%	69.1%	<0.001	81.1%	80.4%	0.799
Married	6.5%	3.6%	0.085	5.8%	5.4%	0.884
Stable partner	77.0%	93.1%	<0.001	87.6%	88.5%	0.756
Sexual behavior						
Mean age sexual debut	17.3	17.7	0.014	17.4	17.4	0.782
Mean number sexual partners (lifetime)	2.1	6.0	<0.001	3.0	3.6	0.780
Mean age of oldest partner (past 30 days)	26.4	29.6	<0.001	27.7	27.1	0.299
Reported sex in the past 7 days	58.9%	68.3%	0.007	63.6%	60.1%	0.301
Always use condom during sex	22.9%	42.8%	<0.001	28.8%	29.5%	0.825
New partner (past 30 days)	0.5%	2.5%	0.014	1.3%	0.9%	0.753
Anal sex (past 30 days)	0.5%	0.4%	1.000	0.4%	0.5%	1.000
HSV-2 prevalence	47.6%	59.6%	0.001	53.5%	49.2%	0.202
Contraception						
Injectable	83.1	79.9	0.606*	80.7%	83.6%	0.288*
Oral	14.6	17.6		16.4%	14.6%	
Tubal ligation	2.1	2.5		2.9%	1.6%	
Hysterectomy	0.2	0.0		0	0.2%	

**P* value applicable to comparison for all forms of contraception.

Results. A total of 611 rural and 278 urban women met eligibility criteria, were enrolled, and followed up, for a total of 1341 women-years (mean = 18 months) and an overall study retention rate of 94.8%. Rural women were younger and poorer, with fewer lifetime sexual partners, and had lower sexual frequency and lower condom use (Table 1). At enrollment, there were no significant differences in the demographic characteristics and sexual behavior of women in the tenofovir ($n = 445$ women) and placebo ($n = 444$ women) gel arms (Table 1).

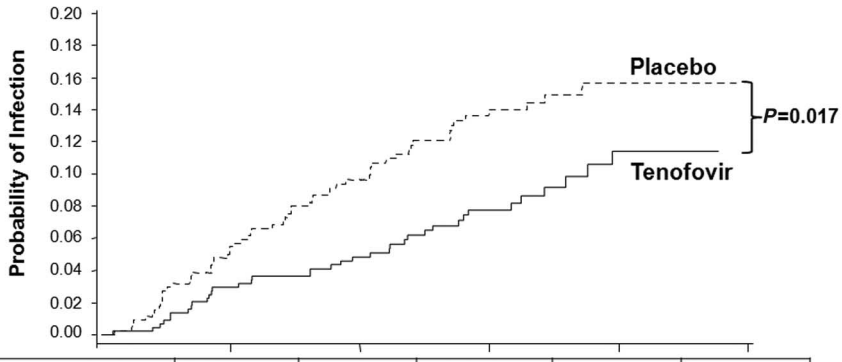

Months of follow-up	6	12	18	24	30
Cumulative HIV endpoints	37	65	88	97	98
Cumulative women-years	432	833	1143	1305	1341
HIV incidence rates (Tenofovir vs Placebo)	6.0 vs 11.2	5.2 vs 10.5	5.3 vs 10.2	5.6 vs 10.2	5.6 vs 9.1
Effectiveness (*P*-value)	**47% (0.064)**	**50% (0.007)**	**47% (0.004)**	**40% (0.013)**	**39% (0.017)**

Fig. 2. Kaplan-Meier estimates of cumulative probability of HIV infection in the tenofovir and placebo gel arms. The table provides the cumulative number of HIV endpoints, corresponding HIV incidence rates, and effectiveness of tenofovir gel for each additional 6 months of follow-up.

HIV incidence and effectiveness. The tenofovir and placebo gel arms had 38 and 60 HIV endpoints, respectively. The HIV incidence rate in the tenofovir gel arm was 5.6 per 100 women-years (CI, 4.0 and 7.7) compared with 9.1 per 100 women-years (CI, 6.9 and 11.7) in the placebo gel arm (IRR = 0.61; CI, 0.40 and 0.94; $P = 0.017$).

HIV infection trends (Fig. 2) show that the tenofovir gel effect was evident soon after initiation of gel use. The steadily declining HIV incidence rates in placebo gel arm were 11.2, 10.5, 10.2, 9.4, and 9.1 per 100 women-years after follow-up for 6, 12, 18, 24, and 30 months, respectively (Fig. 2). In contrast, the HIV incidence rate in the tenofovir gel arm remained in a narrow range between 5.2 and 6.0 per 100 women-years during the study. The HIV incidence rate in the tenofovir gel arm, when compared with the placebo gel arm, was 50% ($P = 0.007$) lower after 12 months of follow-up and 40% ($P = 0.013$) lower after 24 months of follow-up (Fig. 2).

After adjusting for baseline covariates including, age, site, anal sex history, contraceptive method, HSV-2 antibody status, and condom use, the hazard ratio was 0.63 (CI, 0.42 and 0.94; $P = 0.025$). All 98

Table 2. Impact of adherence and non-endpoint HIV infections on the effectiveness of tenofovir gel in HIV prevention in the CAPRISA 004 tenofovir gel trial.

	No. of HIV infections/women years		N	HIV incidence					
	Tenofovir	Placebo		Tenofovir gel (95% CI)	Placebo gel (95% CI)	Incidence rate ratio	Effectiveness	95% CI	*P* value
Overall effectiveness of tenofovir gel									
HIV endpoints	38/680.6	60/660.7	889	5.6 (4.0, 7.7)	9.1 (6.9, 11.7)	0.61	39%	6, 60	0.017
Site-specific effectiveness									
Rural	25/484.7	42/461.2	611	5.2 (3.3, 7.6)	9.1 (6.6, 12.3)	0.57	43%	5, 67	0.023
Urban	13/195.9	18/199.5	278	6.6 (3.5, 11.3)	9.0 (5.3, 14.3)	0.74	26%	-59, 67	0.380
HIV endpoints by levels of adherence*									
High adherers (>80% gel adherence)	11/259.2	25/269.4	336	4.2 (2.1, 7.6)	9.3 (6.0, 13.7)	0.46	54%	4, 80	0.025
Intermediate adherers (50–80% adherence)	10/159.8	10/99.7	181	6.3 (3.0, 11.5)	10.0 (4.8, 18.4)	0.62	38%	-67, 77	0.343
Low adherers (<50% gel adherence)	16/258.5	25/290.6	367	6.2 (3.5, 10.1)	8.6 (5.6, 12.7)	0.72	28%	-40, 64	0.303
Sensitivity analyses									
HIV endpoints plus									
HIV infection not meeting protocol definition	39/680.6	60/660.7	889	5.7 (4.1, 7.8)	9.1 (6.9, 11.7)	0.63	37%	4, 59	0.023
HIV endpoints plus ineligibly enrolled	40/720.1	63/698.6	1075	5.6 (4.0, 7.6)	9.0 (6.9, 11.5)	0.62	38%	7, 60	0.015
HIV endpoints plus women with post-trial infection	39/680.6	64/660.7	889	5.7 (4.1, 7.8)	9.7 (7.5, 12.4)	0.59	41%	11, 61	0.015
Per protocol analysis†	32/589.2	53/575.4	889	5.4 (3.7, 7.7)	9.2 (6.9, 12.0)	0.59	41%	7, 63	0.017
All HIV infections‡	43/720.1	76/698.8	1085	6.0 (4.3, 8.0)	10.9 (8.6, 13.6)	0.55	45%	19, 63	0.003
Adjusted analysis§	38	60	889		Hazard ratio = 0.63		37%	6, 58	0.025

*Adherence could not be calculated for the five women who reported no sex during their follow-up in the study. †Excludes all visits after 3 month's interruption of drug supply. ‡All HIV infections = protocol-defined HIV endpoints ($n = 98$ women) + HIV infection not meeting protocol definition ($n = 1$ woman who did not have 2 RNA PCR results) + HIV infections among ineligibly enrolled women ($n = 5$ women) + posttrial HIV infections ($n = 5$ women) + window period HIV infections in eligible women ($n = 8$ women) + window period HIV infections in ineligibly enrolled women ($n = 2$ women). §Adjusted for the following baseline covariates: age, site, parity, number of sexual partners (past 30 days), presence of STI, anal sex, contraceptive method, HSV-2 antibody status, and condom use; HSV-2 status is indeterminate in four women and missing in five women.

HIV endpoints were Western Blot–positive. One additional HIV infection did not meet the protocol endpoint requirement of two independent RNA PCR results. There were five HIV infections among ineligibly enrolled women, 10 window-period HIV infections (two among ineligibly enrolled women), and five posttrial HIV infections. Sensitivity analyses (Table 2), which include these additional HIV infections, do not differ appreciably from the overall 39% level of effectiveness.

Gel adherence and sexual behavior. Over the entire duration of the study, 181,340 applicators were dispensed, and 95.2% of these were returned. Each month, study participants returned an average of 6.0 used applicators and reported a mean of 5.0 sex acts. Coital frequency, gel adherence, and condom use during the trial were similar in the tenofovir and placebo gel arms. Gel acceptability was high; 97.4% of the study participants found the gel to be acceptable, and 97.9% indicated that they would use it if it prevented HIV.

Five women reported having no sex during follow-up in the study. Adherence estimates based on applicator returns for the remaining 884 women indicate that, on average, 72.2% (median = 60.2%) of self-reported sex acts in the last 30 days were covered by two doses of gel. In the 336 high gel adherers, HIV incidence was 54% lower (IRR = 0.46; CI, 0.20 and 0.94; $P = 0.025$) in the tenofovir gel arm (Table 2). In intermediate gel adherers and low gel adherers, the HIV incidence reduction was 38% ($P = 0.343$) and 28% ($P = 0.303$), respectively. The mean number of sex acts in the high, intermediate, and low gel adherers was 3.2, 5.0, and 6.7 per month, respectively.

Over the 30 months of follow-up, reported coital frequency declined steadily (Fig. 3), from 7.2 sex acts per month in the first 6 months to 3.1 sex acts per month in months 18 to 24 ($P < 0.001$). In women who did not acquire HIV, overall median gel adherence was 61.3%, increasing from 55.0% in the first 6 months to 75.0% in months 18 to 24 ($P < 0.001$). In HIV seroconverters, overall median adherence (until product discontinuation after HIV infection) was 59.2%, ranging from 56.9% in the first 6 months to 61.3% in months 18 to 24 ($P = 0.735$). Overall, condoms were reportedly used in 80.3% of sex acts, increasing from 78.5% in the first 6 months to 84.3% in months 18 to 24 ($P < 0.001$) (Fig. 3).

Safety and pregnancy outcomes. There were 4692 adverse events reported during the study, with 94.3% (838 out of 889) of the study participants reporting at least one adverse event. Adverse event rates were 3.55 per women-year in the tenofovir and 3.44 per women-year in the placebo gel arms ($P = 0.265$). Women in the tenofovir gel arm reported more instances of diarrhea (Table 3) than those using placebo gel (16.9 versus 11.0%, $P = 0.015$). There were 39 serious adverse events, including one death. In the 37 hepatitis B virus carriers (20 randomized to tenofovir gel and 17 to placebo gel), there were two cases of "hepatic flares" (alanine aminotransferase > 5 times the upper limit of normal) in each arm. Further information on grading of the hepatic, renal, and bone-adverse events can be found in (*23*).

Five participants discontinued gel use for a total of 1.04 women-years because of adverse events; four were due to genital findings, and one was due to congestive cardiac failure.

The overall pregnancy rate was 4.0 per 100 women-years: 3.2 per 100 women-years in the tenofovir arm and 4.7 per 100 women-years in the placebo arm ($P = 0.183$) (Table 3). At the time of analysis, there were six ongoing pregnancies, and 58.3% of the remaining 48 pregnancies had resulted in a full-term live birth. There were no significant differences in pregnancy outcomes by study arm, and there were no congenital anomalies. A total of 20.9 women-years of follow-up occurred while women were not using gel because of pregnancy.

Viral load and tenofovir resistance. The mean log HIV viral load at the time when HIV seroconversion was identified was 4.65 [interquartile range (IQR), 4.04 to 5.39] and 4.30 (IQR, 3.56 to 5.17) log copies per milliliter in the tenofovir gel arm ($n = 38$ HIV seroconverters) and placebo gel arm ($n = 60$ HIV seroconverters), respectively ($P = 0.147$).

It is estimated that the HIV seroconverters were exposed to gel episodically for about 3 to 4 weeks after infection and the resistance assays ($n = 35$ HIV seroconverters) were performed on average 20 weeks after the estimated date of infection. There were no tenofovir-related resistance mutations (K65R or K70E) detected, and none of the women had thymidine analog mutations (M41L, L210W, T215Y/F, D67N, K70R, and K219Q/E) or mutations that confer multiple–nucleoside reverse transcriptase inhibitor resistance (*29*).

Discussion. Tenofovir gel reduced HIV infection by an estimated 39%. The protective effect of coitally related tenofovir gel use was evident soon after initiation and peaked at 50% after 12 months of gel use. This protective effect is evident irrespective of sexual behavior, condom use, herpes simplex type 2 virus infection, or urban/rural differences. A trend of higher effectiveness was observed as gel adherence improved; high adherers had a 54% lower HIV incidence rate in the tenofovir gel arm.

The observed level of effectiveness is dependent on both the efficacy of the product and the participants' willingness and ability to use it as prescribed. Inadequate adherence is the most serious challenge to obtaining an accurate estimate of product efficacy (*30*). To address this, we implemented an intensive adherence support program with motivational strategies that depended on reliable measurement of adherence. Monitoring of this key behavior in the trial included an objective count of used and unused applicators returned each month and did not rely solely on self-reported use. Despite this adherence program and high gel acceptability, about 40% of the women in this study had below 50% gel adherence. Future trials will need to place greater emphasis on enhancing and objectively measuring adherence, in light of its substantial influence on the trial outcome.

In this study population, women with the highest gel adherence tended to have the lowest reported coital frequency. Despite their lower coital frequency, these women had HIV incidence rates comparable (in the placebo gel arm) with those in women with much higher coital frequencies, highlighting the importance of infrequent but very high-risk sex with migrant men. The impact of coitally related tenofovir gel was substantial in this group, indicating its potential to alter the course of the HIV epidemic in southern Africa, where young women engaging in sex with

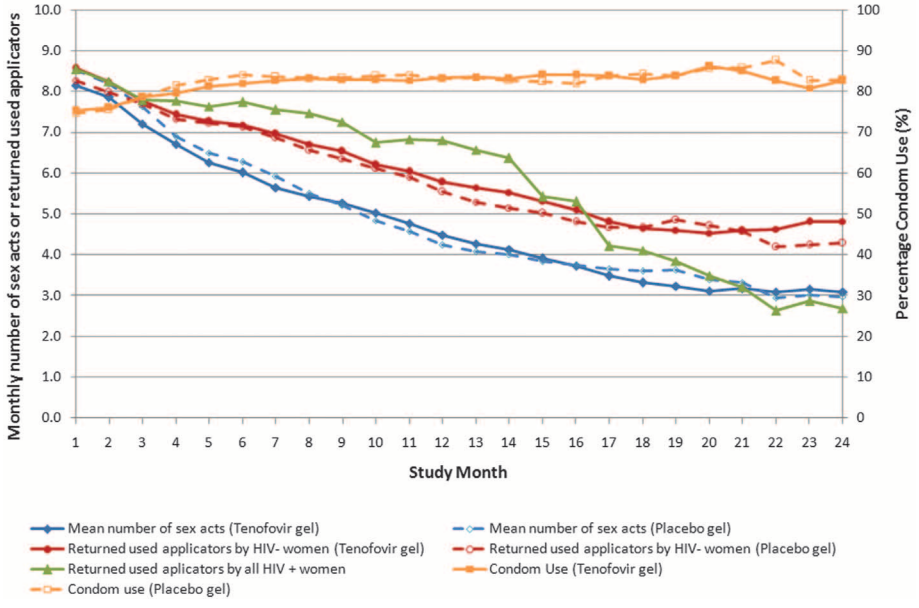

Fig. 3. Trends in coital frequency, condom use, and gel use (gel use by HIV status) in relation to duration of follow-up.

migrant men is the key driver in the spread of HIV infection (*31*). On a cautionary note, the effectiveness of coitally related tenofovir gel appeared to decline after 18 months; reasons for this are unclear, and factors, including the possibility of declining number of gel applications and/or adherence over time, need further investigation.

HIV incidence rates observed in this study population were high because KwaZulu-Natal province is at the epicenter of South Africa's "explosive" HIV epidemic (*32*). Although the women in the tenofovir gel arm had a substantially lower HIV incidence rate than that of the placebo arm, they still had an unacceptably high HIV incidence rate, consistently above 5 per 100 women-years. This highlights the need to seek higher levels of adherence and effectiveness with tenofovir gel and to develop other effective prevention strategies for use in combination with tenofovir gel. Encouragingly, there was no evidence of risk compensation (*33*), in which individuals increase their HIV risk by reducing their use of proven prevention modalities, such as condoms, in favor of less effective or unproven prevention strategies. Instead, we observed declining HIV incidence rates in the placebo gel arm. This may have been due to their declining coital frequency and increasing condom use. However, the consistently high levels of self-reported condom use in the last sex act need to be interpreted cautiously because these may be affected by inaccurate recall and may be indicative of condom use in only the last sex act and not all sex acts.

We found no empirical evidence for the theoretical concern that tenofovir gel may mask HIV infection and that withdrawal of tenofovir gel use after study exit may lead to the unmasking of these infections.

Coitally related tenofovir gel use was safe. There were no increases in renal, hepatic, pregnancy-related, or genital-adverse events. The increased risk of diarrhea in women using tenofovir gel may possibly have been due to a local tenofovir effect; further investigation is needed to establish the mechanism for this observed adverse effect. The reported cases of diarrhea were mild and self-limiting, rarely requiring medication.

There was no renal toxicity—the most important tenofovir-related safety concern (*34*)—although the study excluded women with compromised creatinine clearance at enrollment. Increases in hepatic flares, which have been reported upon cessation of oral tenofovir use in hepatitis B–infected individuals (*35*), was not observed in this study, possibly because of the low systemic absorption of tenofovir from the gel formulation (*17*). No safety concerns were identified in the 22

Table 3. Adverse events and other safety markers in the CAPRISA 004 tenofovir gel trial.

	Tenofovir gel	Placebo gel	*P* value
	Events/participants/ (percent with ≥ 1 event)	**Events/participants/ (percent with ≥ 1 event)**	
Number of adverse events	2419/423/(95.1)	2273/415/(93.5)	0.32
Deaths	0/0/(0)	1/1/(0.2)	0.50
Serious adverse events:	23/21/(4.7)	16/16/(3.6)	0.50
total serious adverse events			
Pregnancy-related serious adverse events	8/8/(1.8)	8/8/(1.8)	1.00
Grade 3* adverse events	19/15/(3.4)	18/16/(3.6)	0.86
Grade 4* adverse events	4/4/(0.9)	4/3/(0.7)	1.00
Common adverse events			
Influenza	365/216/(48.5)	314/220/(49.5)	0.79
Vaginal discharge	203/156/(35.1)	239/156/(35.1)	1.00
Headache	126/93/(20.9)	133/102/(23.0)	0.53
Urinary tract infection	135/100/(22.5)	120/93/(20.9)	0.63
Diarrhea and gastrointestinal infections	91/75/(16.9)	65/49/(11.0)	0.02
Upper respiratory tract infections	162/114/(25.6)	145/100/(22.5)	0.31
Genital adverse events			
Disrupted epithelium, e.g., genital ulceration	18/18/(4.0)	14/13/(2.9)	0.47
Intact epithelium, e.g., erythema	48/41/(9.2)	42/33/(7.4)	0.40
Urogenital symptoms (such as menorrhagia)	312/210/(47.2)	394/238/(53.6)	0.06
Vaginal candidiasis	156/114/(25.6)	187/130/(29.3)	0.23
Other	182/131/(29.4)	176/123/(27.7)	0.60
Laboratory parameters: any abnormality after randomization			
Hepatic			
Aspartate aminotransferase (AST)	29/21/(4.7)	36/29/(6.5)	0.25
Alanine transaminase (ALT)	42/33/(7.4)	50/40/(9.0)	0.38
Renal			
Raised creatinine	3/3/(0.7)	1/1/(0.2)	0.62
Low potassium	119/95/(21.3)	99/83/(18.7)	0.36
Abnormal sodium	54/48/(10.8)	43/41/(9.2)	0.50
Hematological			
Anemia	52/34/(7.6)	46/29/(6.5)	0.60
Neutropenia	19/16/(3.6)	13/11/(2.5)	0.44
Bone			
Low phosphate	79/62/(13.9)	65/51/(11.5)	0.31
Abnormal calcium	16/15/(3.4)	14/13/(2.9)	0.85
Fractures	5/4/(0.9)	2/2/(0.5)	0.69
Pregnancy rate per 100 women-years	3.2	4.7	0.18
Proportion of pregnancies resulting in live births	66.7	51.9	0.38

*Grade 3 and 4 adverse events refer to the grading for severity according to the Division of AIDS Table for Grading Adult and Pediatric Adverse Events, 2004 (http://rsc.tech-res.com/safetyandpharmacovigilance/).

women exposed to tenofovir gel in early pregnancy, providing further evidence to support the analysis of the Antiretroviral Pregnancy Register (*36*), which showed no increases in congenital anomalies. No tenofovir-related resistance was found in the 35 women exposed to tenofovir gel early in acute HIV infection. Further studies to identify tenofovir resistance at earlier time points after infection, in both the genital and systemic compartments, are needed. Coitally related tenofovir gel use showed no impact on viral load in HIV seroconverters.

This test-of-concept study had several limitations; the relatively small sample size and the small number of study sites restrict the broad generalizability of the results. The study's adherence program needed to attain higher and sustained levels of adherence. The co-enrollment challenge was a setback at the urban site. It did not, however, affect the estimated effectiveness of tenofovir gel when infections in co-enrolled women were included in the analysis. It is not possible to derive from this study any conclusions on the safety and effectiveness of tenofovir gel for anal sex. Similarly, it is not possible to make any conclusions on the effectiveness of tenofovir gel in relation to the timing of gel applications because when gel was applied, BAT24 was usually followed.

Currently, there are five large-scale trials assessing oral pre-exposure prophylaxis with tenofovir or tenofovir-emtricitabine (*37*) in men who have sex with men, intravenous drug users, and heterosexual men and women. One of these, the Microbicide Trials Network (MTN) 003 trial (*38*), is assessing the effectiveness of daily tenofovir gel for HIV prevention. This critically important study will provide urgently needed evidence on whether more frequent dosing can improve adherence and effectiveness of tenofovir gel without compromising safety. Additional studies are needed to corroborate the findings of the CAPRISA 004 trial and to assess the safety, effectiveness, adherence, and cost advantages or disadvantages of coitally related tenofovir gel as compared with daily tenofovir in either the gel or oral formulation for HIV prevention in women.

Conclusion. Coitally related tenofovir gel appears safe and effective in preventing HIV infection. Once these promising findings have been corroborated, this antiretroviral microbicide could potentially fill an important HIV prevention gap, especially for women unable to successfully negotiate mutual monogamy or condom use.

References and Notes

1. UNAIDS, WHO, *AIDS Epidemic Update* (Joint United Nations Programme on HIV/AIDS and World Health Organization, Geneva, 2009).
2. S. S. Abdool Karim, G. J. Churchyard, Q. Abdool Karim, S. D. Lawn, *Lancet* **374**, 921 (2009).
3. N. S. Padian, S. I. McCoy, J. E. Balkus, J. N. Wasserheit, *AIDS* **24**, 621 (2010).
4. B. Auvert *et al*., *PLoS Med.* **2**, e298 (2005).
5. R. C. Bailey *et al*., *Lancet* **369**, 643 (2007).
6. R. H. Gray *et al*., *Lancet* **369**, 657 (2007).
7. H. Grosskurth *et al*., *Lancet* **346**, 530 (1995).
8. S. Rerks-Ngarm *et al*.; MOPH-TAVEG Investigators, *N. Engl. J. Med.* **361**, 2209 (2009).
9. Z. A. Stein, *Am. J. Public Health* **80**, 460 (1990).
10. C. Watts, P. Vickerman, *AIDS* **15**, S43 (2001).
11. S. S. Abdool Karim, C. Baxter, *HIV Ther.* **3**, 3 (2009).
12. E. De Clercq, *Biochem. Pharmacol.* **73**, 911 (2007).
13. L. C. Rohan *et al*., *PLoS ONE* **5**, e9310 (2010).
14. R. A. Otten *et al*., *J. Virol.* **74**, 9771 (2000).
15. C.-C. Tsai *et al*., *Science* **270**, 1197 (1995).
16. U. M. Parikh *et al*., *J. Virol.* **83**, 10358 (2009).
17. K. H. Mayer *et al*.; HPTN 050 Protocol Team, *AIDS* **20**, 543 (2006).
18. S. L. Hillier, paper presented at the Microbicide 2008, New Delhi, India, 2008.
19. A. B. Kharsany, Q. A. Karim, S. S. Abdool Karim, *AIDS Care* **22**, 533 (2010).
20. A. B. Kharsany *et al*., *HIV Med.*; published online 17 May 2010.
21. L. Van Damme *et al*.; COL-1492 Study Group, *Lancet* **360**, 971 (2002).
22. D. W. Cockcroft, M. H. Gault, *Nephron* **16**, 31 (1976).
23. Materials and methods are available as supporting material on *Science* Online.
24. D. Tien *et al*., *AIDS Res. Hum. Retroviruses* **21**, 845 (2005).
25. J. B. Jackson *et al*., *Lancet* **362**, 859 (2003).
26. R. A. Ferrer, K. M. Morrow, W. A. Fisher, J. D. Fisher, *AIDS Care* **22**, 997 (2010).
27. W. R. Miller, S. Rollnick, *Motivational Interviewing* (Guilford, New York, 1991).
28. V. Pillay *et al*., *Antivir. Ther.* **13** (suppl. 2), 101 (2008).
29. Single-letter abbreviations for the amino acid residues are as follows: A, Ala; C, Cys; D, Asp; E, Glu; F, Phe; G, Gly; H, His; I, Ile; K, Lys; L, Leu; M, Met; N, Asn; P, Pro; Q, Gln; R, Arg; S, Ser; T, Thr; V, Val; W, Trp; and Y, Tyr. In the mutants, other amino acids were substituted at certain locations; for example, K65R indicates that lysine at position 65 was replaced by arginine.
30. S. W. Lagakos, A. R. Gable, Eds., *Methodological Challenges in Biomedical HIV Prevention Trials* (National Academy of Sciences, Washington, DC, 2008).
31. M. N. Lurie *et al*., *AIDS* **17**, 2245 (2003).
32. Q. Abdool-Karim, S. S. Abdool-Karim, *Int. J. Epidemiol.* **31**, 37 (2002).
33. M. M. Cassell, D. T. Halperin, J. D. Shelton, D. Stanton, *BMJ* **332**, 605 (2006).
34. B. Schaaf, S. P. Aries, E. Kramme, J. Steinhoff, K. Dalhoff, *Clin. Infect. Dis.* **37**, e41 (2003).
35. M. Crane *et al*., *J. Infect. Dis.* **199**, 974 (2009).
36. R. S. Brown, D. Goodwin, S. Zhang, E. Fagan, paper presented at the 13th International Symposium on Viral Hepatitis and Liver Disease (ISVHLD), Washington, DC, 20 to 24 March 2009.
37. AVAC, Pre-Exposure Prophylaxis (PrEP), available at www.avac.org/ht/d/sp/i/262/pid/262/cat_id/458/cids/453,458 (2010) (accessed 12 June 2010).
38. Microbicide Trials Network, "Phase 2B safety and effectiveness study of tenofovir 1% gel, tenofovir disoproxil fumarate tablet, and emtricitabine/tenofovir disoproxil fumarate tablet for the prevention of HIV infection in women," available at www.mtnstopshiv.org/node/70 (2010) (accessed 12 June 2010).

39. We pay tribute to the women who participated in this trial; their dedication and commitment made this study possible. We thank the Health Department of the City of Durban, the traditional leadership of Vulindlela, specifically N. Sondelani Zondi and N. Nsikayezwe Zondi, and members of the Community Advisory Boards at the Vulindlela and eThekwini Research Clinics. Q.A.K. is the co-principal investigator of the HIV Prevention Trials Network (HPTN) Prevention Leadership Group [NIH/National Institute of Allergy and Infectious Diseases (NIAID) U01 AI068619]. S.S.A.K. was the protocol chair of the HPTN 035 trial, which was supported by NIH (grants U01AI46749 and U01AI068633). The other authors have no financial conflicts of interest. By arrangement with Gilead Sciences and CONRAD, LIFE*lab*—a biotechnology center of the South African Department of Science and Technology—acquired a voluntary nonexclusive royalty-free license for tenofovir gel for low-cost distribution in Africa. The CAPRISA 004 Tenofovir gel trial was supported by CAPRISA, the United States Agency for International Development (USAID), FHI (cooperative agreement GPO-A-00-05-00022-00 and contract 132119), and LIFE*lab*. Support from CONRAD for the product manufacturing and packaging, as well as support from Gilead Sciences for the tenofovir used in the production of gel, is gratefully acknowledged. We thank NIH's Comprehensive International Program of Research on AIDS (CIPRA grant AI51794) and the Columbia University–Southern African Fogarty AIDS International Training and Research Programme (AITRP grant D43TW00231) for the research infrastructure and training that made this trial possible. The Trial Oversight Committee included Q.A.K., S.S.A.K. (CAPRISA), L. Claypool, J. Manning, J. Spieler (USAID), H. Gabelnick (CONRAD), B. Okole, C. Montague (LIFE*lab*), J. Rooney (Gilead Sciences), W. Cates, L. Dorflinger, and D.T. (FHI). The study monitors were S. Combes, C. Katz, L. McNeil, and A. Troxler and the DSMB members were E. Bukusi, M. Chen (independent statistician), K. Dickson, C. Lombard, K. Mayer (chair), and S. Self.

The CAPRISA 004 Trial Group includes (in alphabetical order)
Principal Investigators: Q. Abdool Karim and S. S. Abdool Karim
Site Directors: J. A. Frohlich, A. B. M. Kharsany, and K. P. Mlisana
Project Coordinators: C. Baxter and L. E. Mansoor
Site Coordinators: N. A. Arulappan and S. Maarschalk
Assistant Site Coordinators: H. Humphries, G. Parker, J. Richards, and J. Upton
Study Gynecologist: S. Sibeko
Clinicians: B. Mdluli, N. Miya, L. Mtongana, N. Naicker, Z. Omar, and D. Sokal (FHI)
Nurses: D. D. Chetty, F. Dlamini, S. D. Gumede, Z. Gumede, N. E. Khambule, N. Langa, B. T. Madlala, N. Madlala, N. Mkhize, Z. L. Mkhize, M. Mlotshwa, C. Ndimande, N. Ngcobo, C. Ntshingila, B. Phungula, and T. E. Vumase
Counselors: N. B. Biyela, N. Dladla, T. Dlamini, C. T. Khwela, N. Mayisela, M. R. Mlaba, J. Mchunu, Z. Msimango, D. Nkosi, and T. Shange
Pharmacists: L. Chelini, T. N. Gengiah, A. Gray, B. Maharaj, G. I. Masinga, A. Naidoo, and M. Upfold
Pharmacist's Assistants: B. Moodley, Y. Naidoo, C. Ngcobo, T. Nzimande, and L. Zondi
Statisticians: A. C. Grobler, D. Taylor (FHI), L. Werner, and N. Yende
Data Management: R. Lallbahadur, M. Mdladla, K. Naidoo, T. Nala, C. Pillay, P. Sikakane, and T. Zondo
Quality Assurance: T. Govender, N. Mvandaba, F. van Loggerenberg, and I. van Middelkoop
Laboratory: J. Naicker, V. Naranbhai, N. Ndlovu, N. Samsunder, S. Sidhoo, P. Tshabalala, J. Ledwaba (NICD), and L. Morris (NICD),
Behavioral Science: J. Fisher (University of Connecticut) and K. MacQueen (FHI)
Cohort Coordinators: L. R. Luthuli and F. Ntombela
Cohort Administrators: P. F. Chonco, D. P. Magagula, P. C. Majola, T. Ndlovu, L. Ngobese, N. Ngubane, and N. M. Zwane
Community Outreach: N. Bhengu, P. Buthelezi, P. D. Lembethe, B. F. Mazibuko, S. F. Mdluli, W. N. Mkhize, S. P. Ndlovu, S. Ngubane, R. M. Ogle, and R. B. Xulu
Administrative Staff: N. Amla, S. A. Barnabas, T. Malembe, M. Matthews, Y. T. Miya, A. Mqadi, S. Panday, S. Sibisi, M. Swart, and B. Zulu

Supporting Online Material

www.sciencemag.org/cgi/content/full/science.1193748/DC1
Materials and Methods
Table S1
References

14 June 2010; accepted 13 July 2010
Published online 20 July 2010;
10.1126/science.1193748
Include this information when citing this paper.

Spiroindolones, a Potent Compound Class for the Treatment of Malaria

Matthias Rottmann,[1,2*] Case McNamara,[3*] Bryan K. S. Yeung,[4*] Marcus C. S. Lee,[5] Bin Zou,[4] Bruce Russell,[6,7] Patrick Seitz,[1,2] David M. Plouffe,[3] Neekesh V. Dharia,[8] Jocelyn Tan,[4] Steven B. Cohen,[3] Kathryn R. Spencer,[8] Gonzalo E. González-Páez,[8] Suresh B. Lakshminarayana,[4] Anne Goh,[4] Rossarin Suwanarusk,[6] Timothy Jegla,[9] Esther K. Schmitt,[10] Hans-Peter Beck,[1,2] Reto Brun,[1,2] Francois Nosten,[11,12,13] Laurent Renia,[6] Veronique Dartois,[4] Thomas H. Keller,[4] David A. Fidock,[5,14] Elizabeth A. Winzeler,[3,8]† Thierry T. Diagana[4*]†

Recent reports of increased tolerance to artemisinin derivatives—the most recently adopted class of antimalarials—have prompted a need for new treatments. The spirotetrahydro-β-carbolines, or spiroindolones, are potent drugs that kill the blood stages of *Plasmodium falciparum* and *Plasmodium vivax* clinical isolates at low nanomolar concentration. Spiroindolones rapidly inhibit protein synthesis in *P. falciparum*, an effect that is ablated in parasites bearing nonsynonymous mutations in the gene encoding the P-type cation-transporter ATPase4 (PfATP4). The optimized spiroindolone NITD609 shows pharmacokinetic properties compatible with once-daily oral dosing and has single-dose efficacy in a rodent malaria model.

Almost half the world's population is exposed to malaria, which causes over 800,000 deaths each year and kills more under-5-year-olds than any other infectious agent (*1*). Fifty years ago, malaria had been eliminated from many areas of the world through a combination of drug treatments and vector control interventions (*2*). However, the global spread of drug resistance together with a collapse of vector control programs resulted, by the 1980s, in a resurgence in disease incidence and mortality. Today, epidemiological data suggest that the introduction of new drugs (notably the artemisinin-based combination therapies or ACTs) may have reversed that trend (*3*). Recent reports suggest that resistance to derivatives of the endoperoxide artemisinin is now emerging (*4*–*6*). These observations have triggered a concerted search for new drugs that could be deployed if artemisinin resistance were to spread.

Many of the therapies currently in development use known antimalarial pharmacophores (e.g., aminoquinolines and/or peroxides) chemically modified to overcome the liabilities of their predecessors (*7*). Although these compounds may become important in the treatment of malaria, it would be preferable to discover chemotypes with novel mechanisms of actions (*8*). However, despite important advances in our understanding of the *Plasmodium* genome, the identification and validation of new drug targets have been challenging (*9*).

To identify novel antimalarial leads, we and others have screened diverse chemical libraries using *Plasmodium* whole-cell proliferation assays with cultured intraerythrocytic parasites (*10*–*12*). From a library of about 12,000 pure natural products and synthetic compounds with structural features found in natural products, our screen identified 275 primary hits with submicromolar activity against *Plasmodium falciparum*. We discarded those hits whose activity was not reconfirmed against multidrug-resistant parasites and/or that displayed some cytotoxicity against mammalian cells (more than 50% viability inhibition at 10 μM). Pharmacokinetic and physical properties were then determined for the remaining 17 compounds. From this, a synthetic compound related to the spiroazepineindole class, having a favorable pharmacological profile, stood out as a starting point for a medicinal chemistry lead optimization effort. Synthesis and evaluation of about 200 derivatives yielded the optimized spirotetrahydro-β-carboline (or spiroindolone) compound NITD609 (Fig. 1A). This compound is synthesized in eight steps, including chiral separation of the active enantiomer, and is amenable to large-scale manufacturing. NITD609 has good drug-like attributes (see below) and displays physicochemical properties compatible with conventional tablet formulation.

There is general agreement that a new antimalarial should ideally meet the following criteria: (i) kills parasite blood stages; (ii) is active against drug-resistant parasites; (iii) is safe (i.e., no cytotoxicity, genotoxicity, and/or cardiotoxicity); and (iv) has pharmacokinetic properties compatible with once-daily oral dosing. NITD609 meets all these criteria. We also gained insight into a mechanism of drug resistance involving the P-type cation-transporter ATPase4 (PfATP4).

Activity against drug-resistant *Plasmodium*. Antimalarial blood-stage activity was evaluated in vitro against a panel of culture-adapted *P. falciparum* strains. NITD609 displayed single-digit nanomolar average 50% inhibitory concentration values (IC_{50} range, 0.5 to 1.4 nM; table S1), with no evidence of diminished potency against drug-resistant strains (table S1) (*13*). This compound was also tested in ex vivo assays with fresh isolates of *P. falciparum* and *P. vivax* (*14*), collected from malaria patients on the Thai-Burmese border where chloroquine resistance has been widely reported (*15*, *16*). NITD609 was found to be as effective as artesunate, with potency in the low nanomolar range (IC_{50} values consistently <10 nM) against all *P. vivax* (Fig. 1B) and *P. falciparum* (Fig. 1C) isolates. NITD609 was also similar to artesunate in its ability to kill both mature trophozoite and immature *P. vivax* ring stages, in contrast to the trophozoite stage-specific activity observed with chloroquine (*17*). Regardless of their initial developmental stages, NITD609-treated parasites displayed morphological hallmarks of dying parasites, including pycnotic nuclei and abnormal digestive vacuoles and/or nuclear segmentation. Collectively, our in vitro and ex vivo data showed that spiroindolones were potent against the intraerythrocytic stages of the major human malarial pathogens *P. falciparum* and *P. vivax*, including a range of drug-resistant strains.

The rapid activity of artemisinin derivatives against all *Plasmodium* asexual erythrocytic stages is a key feature of their therapeutic efficacy (*6*). To precisely determine which parasite blood stages are most sensitive to the spiroindolones, and to evaluate the time required for these drugs to act, we conducted in vitro drug sensitivity assays with synchronized parasites treated at ring, trophozoite, and schizont stages for various durations (1, 6, 12, and 24 hours) before removal of drug and continuation of culture for 24 hours in the presence of [^{3}H]hypoxanthine. At a high concentration of NITD609 (≈100 × IC_{50} value), all stages (rings, trophozoites, and schizonts) were similarly sensitive (fig. S1). However, at low concentrations (≈1 or 10 × IC_{50} value), schizonts were the most susceptible. We speculate that the target is present in all asexual blood stages but might be particularly vulnerable in schizonts. Although clearly faster-acting than the former first-line antifolate agent pyrimethamine, NITD609 did not inhibit parasite growth as quickly as the artemisinin derivative artemether (fig. S1). Strong growth inhibition (>90%) was achieved with artemether treatment at 8 nM for only 6 hours, whereas similar activity was achieved with NITD609 at 1.6 nM for 24 hours.

Although at least 12 hours of continuous drug exposure was required to reduce by 90% the in-

[1]Swiss Tropical and Public Health Institute, Parasite Chemotherapy, CH-4002 Basel, Switzerland. [2]University of Basel, CH-4003 Basel, Switzerland. [3]Genomics Institute of the Novartis Research Foundation, San Diego, CA 92121, USA. [4]Novartis Institute for Tropical Diseases, 138670 Singapore. [5]Department of Microbiology and Immunology, Columbia University Medical Center, New York, NY 10032, USA. [6]Laboratory of Malaria Immunobiology, Singapore Immunology Network, Agency for Science Technology and Research (A*STAR), Biopolis, 138648, Singapore. [7]Department of Microbiology, National University of Singapore, 117597, Singapore. [8]Department of Cell Biology, The Scripps Research Institute, La Jolla, CA 92037, USA. [9]Department of Biology and Huck Institute of Life Sciences, Pennsylvania State University, University Park, PA 16802, USA. [10]Natural Products Unit, Novartis Pharma AG, CH-4002 Basel, Switzerland. [11]Shoklo Malaria Research Unit, Mae Sot, Tak 63110, Thailand. [12]Faculty of Tropical Medicine, Mahidol University, Bangkok, Thailand. [13]Centre for Tropical Medicine, Nuffield Department of Clinical Medicine, University of Oxford, Oxford OX3 7LJ, UK. [14]Department of Medicine (Division of Infectious Diseases), Columbia University Medical Center, New York, NY 10032, USA.

*These authors contributed equally to this work.
†To whom correspondence should be addressed. E-mail: winzeler@scripps.edu (E.A.W.); thierry.diagana@novartis.com (T.T.D.)

corporation of [^{3}H]-hypoxanthine into parasite DNA (fig. S1), a ^{35}S-radiolabeled methionine and cysteine ([^{35}S]-Met/Cys) incorporation assay revealed that NITD609 blocked protein synthesis in *P. falciparum* parasites within 1 hour (Fig. 2A). A similar effect was observed with the known protein translation inhibitors anisomycin (an inhibitor of peptidyl transferase) and cycloheximide (an inhibitor of translocation activities during polypeptide elongation). In contrast, the antimalarial drugs artemisinin and mefloquine showed a nominal (<25%) decrease in [^{35}S]-Met/Cys incorporation within 1 hour. We suggest that NITD609 has a mechanism of action different from those of artemisinin and mefloquine.

Selectivity index and safety profile. Safety is paramount when considering that the malaria patient population is composed mostly of young children living in places where there are very limited resources for providing adequate medical supervision. To assess the intrinsic cytotoxic activity of NITD609, we measured the concentration leading to 50% cell death (CC_{50}) in vitro with cell lines of neural, renal, hepatic, or monocytic origin. No significant cytotoxicity was observed at any concentration (CC_{50} > 10 μM; table S2). Given that NITD609 had an IC_{50} of ~1 nM against *P. falciparum* (table S1), the cytotoxicity data established a selectivity index (CC_{50}/IC_{50}) > 10,000. Multiple antimalarial drugs (e.g., 4-aminoquinolines) have cardiotoxicity liabilities due to hERG channel inhibition, resulting in withdrawal in the extreme case of halofantrine (*18*, *19*). hERG (human Ether-a-go-go Related Gene) binding and patch-clamp assays with NITD609 yielded IC_{50} values >30 μM, consistent with a low risk of cardiotoxicity (table S3). Using a miniaturized Ames assay (*20*), we also established that NITD609 lacked intrinsic mutagenic activity. Finally, we observed no significant binding with a panel of human G-protein coupled receptors, enzymes, and ion channels (table S4).

Male rats tolerated oral administration of NITD609 daily for 14 days at a dose yielding daily exposure ($AUC_{0\text{-}24h}$) values between 29,400 and 56,500 ng·hour/ml. This is equivalent to 10- to 20-fold the daily exposure to a dose that reduced parasitemia by 99% in a malaria mouse model [99% effective dose (ED_{99}) = 5.3 mg/kg; see below]. Under these conditions, no adverse events or notable histopathological findings were observed. Overall, these data show that NITD609 has a safety profile that is acceptable for an antimalarial drug.

Pharmacokinetic and pharmacodynamic properties. Upon oral and intravenous administration in mice and rats, NITD609 displayed a moderate volume of distribution (V_{ss} = 2.11 and 3.04 liter/kg) and a low total systemic clearance (CL= 9.75 and 3.48 ml min^{-1} kg^{-1}) (table S5). Orally administered NITD609 displayed a long half-life ($T_{1/2}$ = 10 and 27.7 hours) and excellent bioavailability (F =100%). On the basis of our in vitro metabolic stability data, this profile is likely to extend to humans, because the predicted metabolic clearance for this compound was low across several species (table S6). Taken together, these data show that NITD609 displays pharmacokinetic properties consistent with once-daily oral dosing. We tested this drug candidate by oral dosing in a virulent *P. berghei* malaria mouse model (*21*, *22*). The results showed that

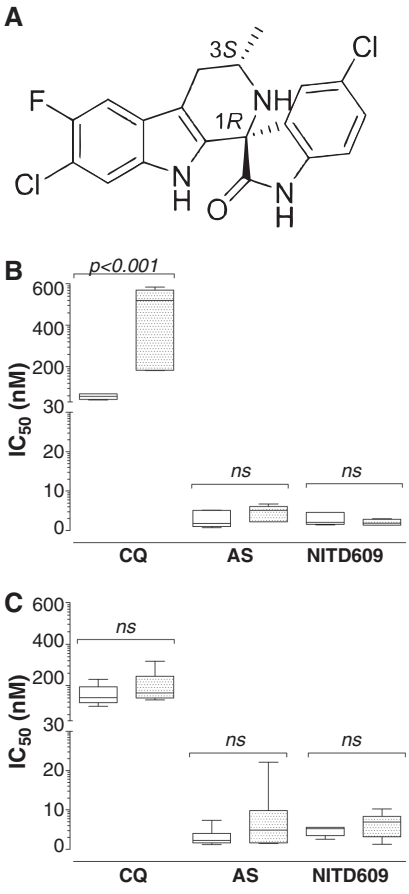

Fig. 1. (**A**) Chemical structure of NITD609, showing the 1*R*,3*S* configuration that is essential for antimalarial activity. Key physicochemical properties: solubility (pH 6.8), 39 μg/ml; logP (pH 7.4), 4.7; logD (pH 7.4), 4.6; pK_a^1, 4.7; pK_a^2, 10.7; polar surface area, 56.92 Å^2. (**B**) Ex vivo sensitivity of *P. vivax* and (**C**) *P. falciparum* (9 and 10 clinical isolates, respectively) to NITD609 compared with the reference drugs chloroquine (CQ) and artesunate (AS). The antimalarial sensitivity of these two species was measured after exposing ring (unshaded boxes) and trophozoite stages (shaded boxes) to drug for 20 hours. Data are shown as box plots. Maximum-minimum IC_{50} values are indicated, respectively, by the top and bottom horizontal thin bars, with the solid internal line indicating the median. Boxed areas indicate 75% confidence intervals. Inhibition of parasite growth was determined after 42 hours. Only chloroquine-treated *P. vivax* displayed a significant stage-specific sensitivity (P < 0.001). ns, not significant.

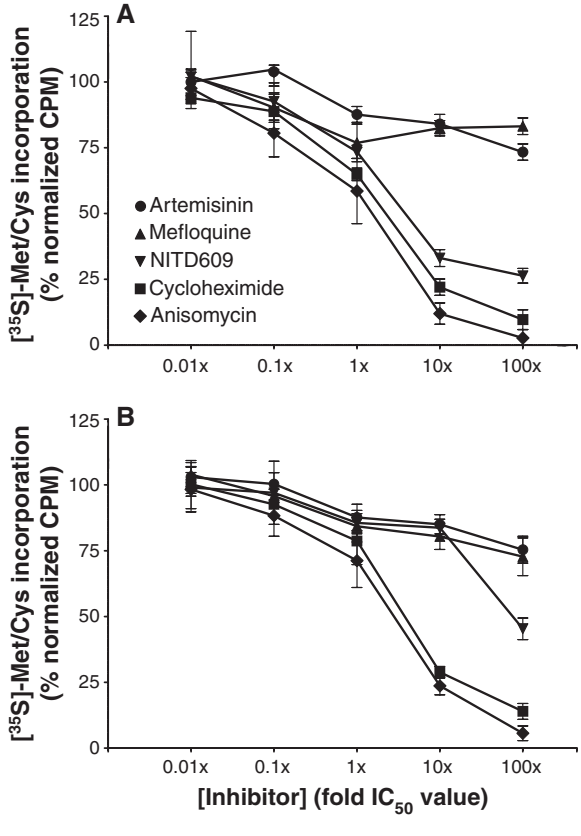

Fig. 2. Spiroindolones rapidly diminish protein synthesis in the parasite. The rate of parasite protein synthesis was evaluated by monitoring ^{35}S-radiolabeled methionine and cysteine ([^{35}S]-Met/Cys) incorporation into asynchronous cultures. Parasites were assayed for 1 hour in the presence of NITD609 (inverted triangle), anisomycin (diamond), cycloheximide (square), artemisinin (circle), or mefloquine (triangle), then extracted for radiographic measurements. Radiolabel incorporation was measured against inhibitor dosed over a five-log concentration range, and percent incorporation was calculated by comparison to cultures assayed in the absence of inhibitor. Anisomycin and cycloheximide were included as positive controls. (**A**) Spiroindolone treatment rapidly diminishes protein synthesis in Dd2; however, this effect is mostly absent in (**B**) NITD609-R^{Dd2} clone #2 except at very high concentration. Fifty percent inhibition of [^{35}S]-Met/Cys incorporation was observed with 3× and 78× IC_{50} of NITD609 on the NITD609-treated Dd2 wild type and NITD609-R^{Dd2} drug-resistant clones, respectively. Data are expressed as means ± SD and represent three independent experiments performed in triplicate. Similar losses of protein synthesis inhibition upon NITD609 treatment were observed in the resistant clones NITD609-R^{Dd2} #1 and #3, respectively (see fig. S2).

Table 1. In vivo efficacy data in the *P. berghei* rodent malaria model. "Activity": average parasitemia reduction; "Survival": average life span after infection (6 to 7 days for untreated mice); "Cure": no parasite present at day 30.

Compound	1 × 10 mg/kg oral		1 × 30 mg/kg oral			1 × 100 mg/kg oral		
	Activity (%)	Survival (%)	Activity (%)	Survival (days)	Cure (%)	Activity (%)	Survival (days)	Cure (%)
NITD609*	99.6	13.3	99.6	24.1	50	99.2	>30	100
Artesunate†	70	7.3	89	7.2	–	97	6.7	–
Artemether†	81	6.2	97	6.9	–	99	7.6	–
Chloroquine†	99.6	8	99.7	8.7	–	>99.9	12	–
Mefloquine†	95	15.2	98	18.2	–	89	28	–

*Methylcellulose 0.5%/0.1% Solutol HS15 formulation (n = 10 mice). †Tween 80 7%/3% ethanol formulation ($n \geq 10$ mice).

NITD609 was efficacious at doses ($ED_{50/90/99}$ = 1.2, 2.7, and 5.3 mg/kg) lower than those of the reference antimalarial drugs chloroquine, artesunate, and mefloquine (table S7). A single oral dose of NITD609 at 100 mg/kg completely cleared a *P. berghei* infection in all treated mice, and a 50% cure rate was achieved with a single oral dose at 30 mg/kg (Table 1). Three daily oral doses of 50 mg/kg also afforded complete cure (table S8). At similar dosing regimens, none of the reference drugs tested could cure infection in this lethal malaria mouse model. To our knowledge, among the drug candidates currently in development, only the new-generation synthetic

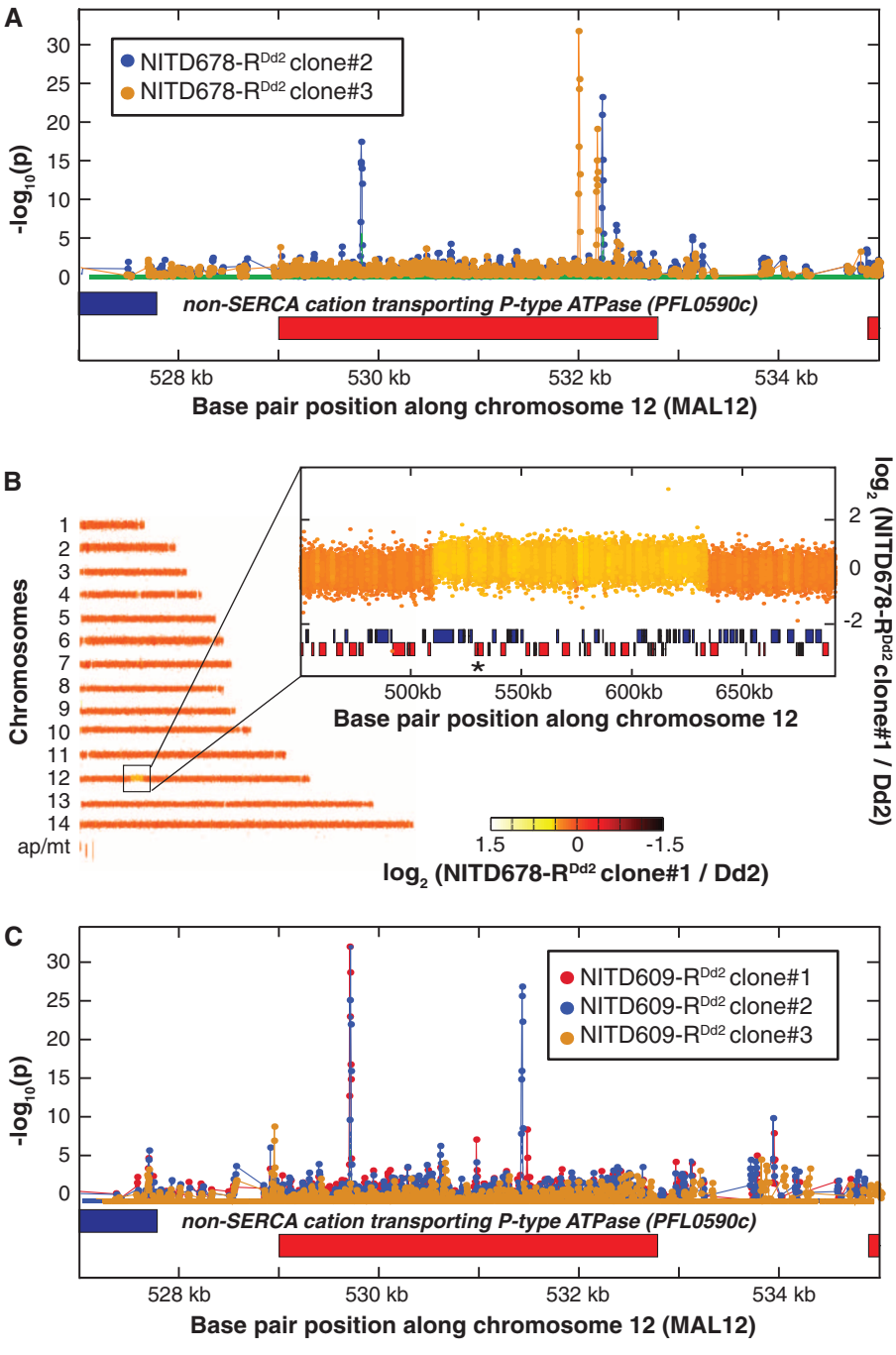

Fig. 3. Genomic tiling arrays identified shared mutations in the *pfatp4* gene (PFL0590c) in all drug-resistant parasites. (**A**) Distinct pairs of SNPs in *pfatp4* were detected in NITD678-R^{Dd2} clones #2 (blue) and #3 (orange). *P* values were calculated for all probes covering *pfatp4* and flanking regions; a spike in the *P* value reflects a difference in hybridization between the parental clone and the drug-selected clone, a hallmark of a SNP. Direct sequencing of *pfatp4* from each clone confirmed that these SNPs cause nonsynonymous changes in the coding region, indicated by the red boxes. (**B**) A 120-kb copy number variation covering 37 genes in chromosome 12 was detected in the genome of NITD678-R^{Dd2} clone #1. The *pfatp4* gene (asterisk) was contained within this amplification. Direct sequencing of *pfatp4* from this clone identified an additional nonsynonymous SNP at amino acid position 223 (G223R). This mutation was continuously observed throughout numerous sequencing reads of subcloned *pfatp4* PCR products of NITD678-R^{Dd2} clone #1, suggesting that the mutation occurred before the amplification event and, thus, resides in all *pfatp4* gene copies in the genome. (**C**) The three NITD609-R^{Dd2} clones showed no evidence of copy number variants; however, each clone contained nonsynonymous SNPs in *pfatp4* (clone#1, red; clone#2, blue; clone#3, orange).

peroxide compounds (e.g., OZ439) have been reported to have this level of curative activity upon single-dose oral administration (*7*). Considering NITD609 pharmacokinetic and pharmacodynamic properties, we speculate that sustained parasitemia reduction will be achievable at low doses in humans.

Drug resistance mediated by a P-type cation-transporter ATPase4. The rapid development of drug resistance has plagued malaria control programs in almost all endemic regions. In vitro selection of resistance is a powerful predictor of the molecular determinants used by parasites in field settings (*23*, *24*). To evaluate the potential for drug resistance and gain insight into the mechanism of action, we applied drug pressure to a cultured clone of Dd2, a multidrug-resistant parasite strain believed to have a higher propensity to mutate (*25*) (fig. S3A). Six independent cultures were exposed to incrementally increasing sublethal concentrations of two compounds: NITD609 and the less potent derivative NITD678 (fig. S3, B and C). After 3 to 4 months of constant drug pressure, the IC_{50} values had increased 7- to 24-fold (attaining a mean of 3 to 11 nM) for NITD609-selected parasites, and 7- to 11-fold (mean of 162 to 241 nM) for NITD678-selected parasites (fig. S3, D and E, and table S9). The high number of passages required to yield drug-resistant parasites, together with the low level of resistance that was achieved, suggests that spiroindolones do not readily select for high-level resistance in vitro. Subsequent passaging of drug-selected parasites in drug-free media for 4 months showed no evidence of revertants, indicating that resistance was stable (fig. S4). None of the selected mutants showed cross-resistance to a panel of antimalarial agents with diverse modes of action, including artemisinin and mefloquine (table S10).

To determine the molecular basis of in vitro resistance, we prepared genomic DNA (gDNA) from each of the six drug-resistant clones. gDNA samples were then fragmented, labeled, and hybridized to a high-density tiling array that contains ~6 million single-stranded 25-oligonucleotide probes complementary to the *P. falciparum* genome. We compared the hybridization data for each haploid clone, using software that identifies regions on the array that showed a loss or gain of hybridization relative to the nonresistant parental reference line (*26*), and that calculated a probability of a genomic change based on the number of consecutive probes that showed a hybridization difference. The microarray covers ~90% of coding regions and 60% of noncoding regions, with probes spaced every two or three bases. Sequence coverage is limited only by the high AT content of *P. falciparum* that causes some 25-oligonucleotide sequences to be represented more than once throughout the genome, rendering those noninformative (*27*). Former studies showed that this genome-tiling analysis can identify 90% of the differences that distinguish two strains in unique regions of the genome (*26*).

Detectable genomic changes include single-nucleotide polymorphisms (SNPs), insertion/deletion events, and copy number variations. Using a permissive *P*-value cutoff of 1×10^{-5}, we identified 7 to 95 genomic differences, localized to within 2 or 3 nucleotides, in each resistant clone. A similar comparison between two highly diverged strains such as Dd2 and 3D7 would yield >13,000 genomic differences (*26*). Using a stricter cutoff ($P < 10^{-10}$) that should give fewer false-positives at the expense of more false-negatives, we found 27 total differences among all six mutants. Seven of these mapped to a single gene, *pfatp4* (PFL0590c; Fig. 3, A and C), with the remainder found largely in randomly assorted subtelomeric or intergenic regions. Inspection of the hybridization patterns showed that one strain carried a copy number variant that encompassed the *pfatp4* locus (Fig. 3B). These data strongly suggest that treatment with spiroindolones specifically selects for mutations in *pfatp4*.

Sequencing of the entire *pfatp4* gene from the different resistant strains revealed 11 non-synonymous mutations (table S9), with at least one in every clone. Nine of these were considered true genomic alterations for the thresholds used with the microarray analysis ($P < 10^{-5}$). One exception resulted from a SNP lying within the copy number variant (NITD678-R^{Dd2} clone#1). The second exception (NITD609-R^{Dd2} clone#1) was the result of an emergent mixed population that had been cultured for several weeks after cloning in order to obtain enough DNA for hybridization. Sequencing of different polymerase chain reaction (PCR) products from this clone showed that some fragments contained three mutations (Ile^{398}→Phe, Pro^{990}→Arg, and Asp^{1247}→Tyr) in *pfatp4*, whereas others harbored only two mutations (Ile^{398}→Phe and Pro^{990}→Arg). The probability of 11 nonsynonymous mutations occurring in *pfatp4* by chance is extremely unlikely. Sequencing of 14 different isolates of *P. falciparum* from different continents (*28*, *29*) revealed only 7 non-synonymous SNPs and 6 synonymous SNPs for *pfatp4* (from a total of ~32,000 SNPs), placing the gene at

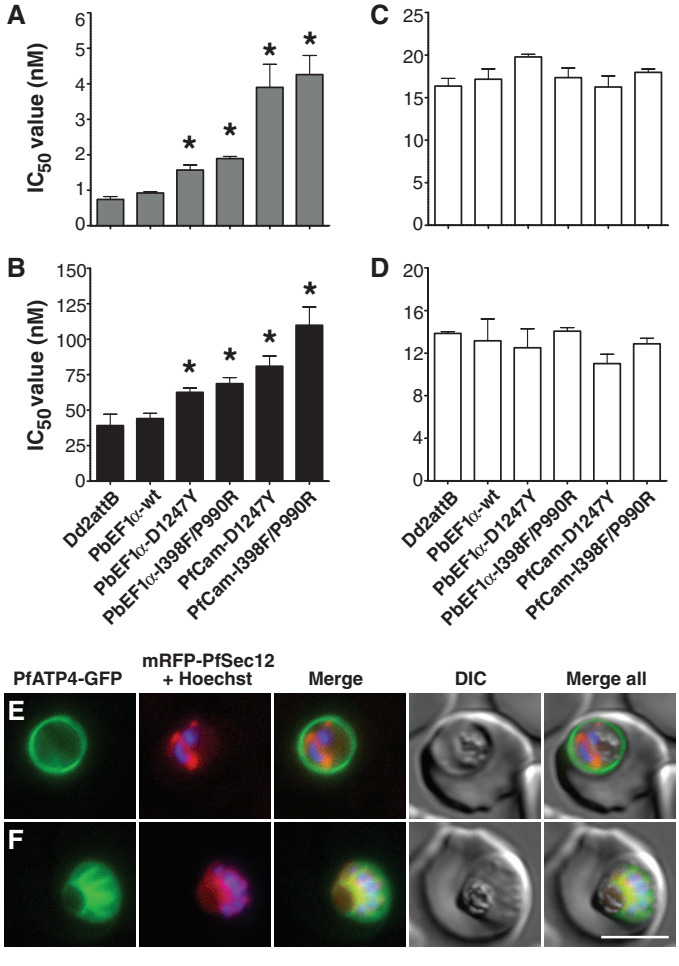

Fig. 4. Introduction of mutant *pfatp4* into $Dd2^{attB}$ parasites decreases susceptiblity to spiroindolones. *pfatp4* transgenes harboring mutations identified in either NITD609-R^{Dd2} clone #1 (I398F/P990R) or clone #3 (D1247Y) were individually introduced into the parental Dd2 background to evaluate the ability of the mutant protein to protect against spiroindolone activity. As a control, wild-type *pfatp4* was also introduced. Expression of *pfatp4* was regulated by either the *P. berghei* EF1α promoter (PbEF1α) or the stronger *P. falciparum* calmodulin promoter (PfCam). IC_{50} values were determined for (**A**) NITD609, (**B**) NITD678, (**C**) artemisinin, and (**D**) mefloquine. IC_{50} values are shown as means ± SD and were derived from three independent experiments performed in quadruplicate with the SYBR Green–based cell proliferation assay (*12*). Statistical significance was calculated using a two-tailed unpaired *t* test, comparing transgenic *pfatp4* lines to the $Dd2^{attB}$ parental line: *$P < 0.0001$. (**E** and **F**) Localization of PfATP4 to the parasite plasma membrane. Transgenic parasites coexpressing PfATP4-GFP and an ER marker, mRFP-PfSec12, were labeled with Hoechst 33382 to visualize the nucleus. PfATP4-GFP was observed at the parasite plasma membrane in (E) early schizont (two nuclei) and (F) late-segmented schizont parasites. DIC, differential interference contrast. Bar, 5 μm.

about the 70th percentile in terms of diversity. In contrast, none of the genes with the highest number of nonsynonymous SNPs from sequencing field isolates (*28*, *29*) showed any differences in our tiling array analysis. Thus, our data are indicative of selective pressure operating on this single gene.

To confirm that drug resistance was conferred directly by these mutations, we amplified the full-length *pfatp4* gene from either wild-type or resistant lines, and cloned it into an expression vector that allows for site-specific integration in transgenic parasites (fig. S5). Following integrase-mediated recombination (*30*) to introduce these genes stably into parasites, we evaluated transgenic lines for inhibition of parasite growth as a function of drug concentration. Lines expressing mutant PfATP4 harboring either the single Asp^{1247}→Tyr (D1247Y) or double Ile^{398}→Phe/Pro^{990}→Arg (I398F/P990R) mutations showed an increase in IC_{50} values relative to the parental line (Fig. 4, A and B, and table S11). This effect was enhanced when either mutant was placed under the control of the strong *P. falciparum* calmodulin (PF14_0323) promoter, conferring a fivefold increase in the IC_{50} value against NITD609. The reduced level of resistance compared to the original drug-selected mutants can be attributed to the coexpression of variant *pfatp4* and the endogenous wild-type allele in our transfected lines. Artemisinin (Fig. 4C) and mefloquine (Fig. 4D) displayed equivalent potency against the wild-type and transgenic strains (table S11), confirming that resistance was specific to the spiroindolones.

Molecular characterization of PfATP4. The *pfatp4* gene product is annotated as a cation-transporting P-type adenosine triphosphatase (ATPase) (PfATP4) (*31*–*33*). This family of ATP-consuming transporters can be inhibited by chemically diverse compounds, including thapsigargin, cyclopiazonic acid, and lansoprazole, and thereby constitutes an attractive set of drug targets [reviewed in (*34*)]. P-type ATPases are ubiquitous in eukaryotic organisms, and those involved in divalent cation transport appear to maintain a conserved structural mechanism for ion translocation (*35*). PfATP4 shows a high level of homology to *Saccharomyces cerevisiae* PMR1, a P-type ATPase required for high-affinity Ca^{2+} and Mn^{2+} transport. The human ortholog (hSPCA1) is associated with Hailey-Hailey disease, an acantholytic skin condition. The structural elucidation of a related rabbit SERCA (sarco/endoplasmic reticulum calcium ATPase) pump (*36*), which shares 30% amino acid identity with PfATP4, enabled us to generate a homology model (Fig. 5). This localizes most of the eight resistance-associated mutations to transmembrane domains. The transmembrane region is predicted to act as a funnel to translocate cations across biological membranes, and includes eight conserved residues required for cation coordination (*37*, *38*). None of those residues were altered in our resistant lines. A number of P-type ATPase inhibitors, including cyclopiazonic acid and thapsigargin, bind to the transmembrane region (*39*–*41*). However, no cross-resistance to either inhibitor was observed in our spiroindolone-selected mutant parasite lines (table S10).

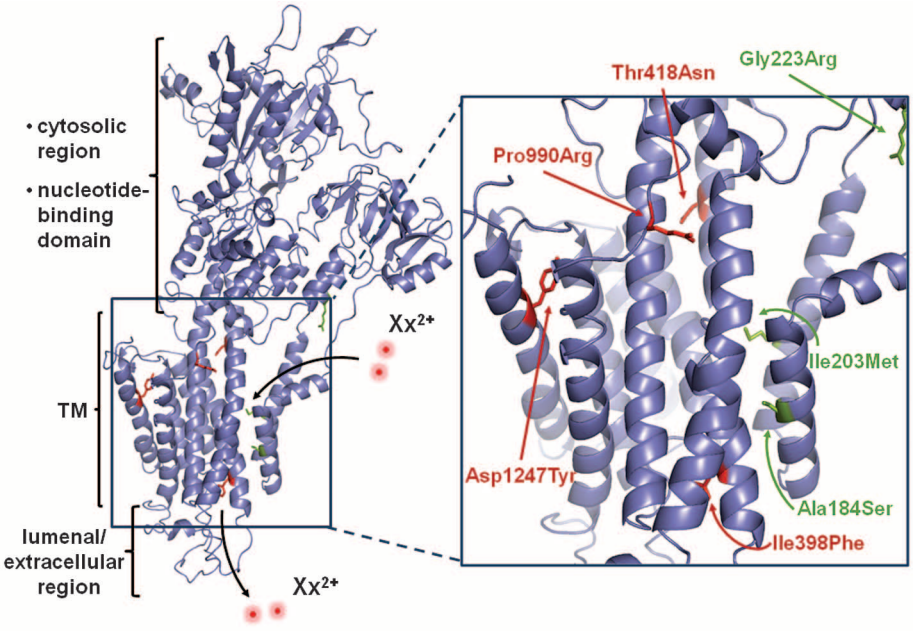

Fig. 5. Resistance-associated SNPs map to the predicted transmembrane region of PfATP4. A homology model of PfATP4 was generated in SWISS-MODEL based on the crystal structure of the rabbit SERCA pump. Amino acid alignment analysis by EMBOSS (*43*) revealed 30% identity and 48% similarity between these proteins. Residues corresponding to resistance-associated mutations are indicated in red for NITD609-R^{Dd2} and in green for NITD678-R^{Dd2}. These mutations mapped to the putative transmembrane (TM) helices. The sites of divalent cation entry and exit are indicated as Xx^{2+}.

To characterize PfATP4 further, we generated a PfATP4-GFP (green fluorescence protein) fusion that was cotransfected into Dd2 parasites along with mRFP-PfSec12, an endoplasmic reticulum (ER) marker (*42*). Live cell imaging of transgenic parasites localized PfATP4-GFP to the parasite plasma membrane throughout the intraerythrocytic life cycle (Fig. 4, E and F, and fig. S6). In late-stage segmented schizonts, this fusion protein was invaginated and surrounded the developing daughter merozoites, confirming a parasite plasma membrane distribution rather than delivery to the surrounding parasitophorous vacuole (Fig. 4F). This finding is supported by earlier immunofluorescence data that localized PfATP4 at or near the plasma membrane (*32*).

Several possibilities may explain how mutations in PfATP4 could confer resistance to spiroindolones. First, the protein could play a role in drug transport; however it shows no homology to known transporters. Alternatively, PfATP4 mutations could attenuate the spiroindolone-induced disruption of cellular homeostasis through an indirect mechanism that remains to be determined. Finally, PfATP4 may be the target of spiroindolones because cation-transporting ATPases are druggable targets (*34*). It is difficult to distinguish between these possibilities as little is known about the molecular function of PfATP4. We have been unable to reproduce results suggesting that PfATP4 plays a role in calcium transport (*33*) (fig. S7), and it is unlikely that the protein regulates calcium transport of the ER calcium stores, given its localization to the plasma membrane. It is possible, nonetheless, that the protein regulates the trafficking of other cations. Although further functional characterization of PfATP4 is clearly warranted, the mutations we identified will be useful molecular markers of drug resistance once NITD609 enters clinical trials.

Conclusions. These studies define the spiroindolones as an antimalarial drug candidate that acts through a mechanism of action distinct from that of existing antimalarial drugs. In contrast to mefloquine and artemisinin, spiroindolones rapidly suppress protein synthesis in the parasite. Our genome-wide investigations revealed that resistance is mediated by the P-type ATPase PfATP4 and showed at single-base resolution how a small eukaryotic genome adapts to sublethal drug pressure. Our lead compound, NITD609, displays good antimalarial activity and meets the criteria required for an antimalarial drug candidate. Further safety and pharmacological preclinical evaluation is currently ongoing to support the initiation of human clinical trials.

References and Notes

1. WHO, World Malaria Report 2009; www.who.int/malaria/world_malaria_report_2009/en/.
2. B. M. Greenwood *et al.*, *J. Clin. Invest.* **118**, 1266 (2008).
3. R. T. Eastman, D. A. Fidock, *Nat. Rev. Microbiol.* **7**, 864 (2009).

4. A. M. Dondorp *et al.*, *N. Engl. J. Med.* **361**, 455 (2009).
5. H. Noedl *et al.*, *N. Engl. J. Med.* **359**, 2619 (2008).
6. N. J. White, *Science* **320**, 330 (2008).
7. P. Olliaro, T. N. Wells, *Clin. Pharmacol. Ther.* **85**, 584 (2009).
8. T. N. C. Wells, P. L. Alonso, W. E. Gutteridge, *Nat. Rev. Drug Discov.* **8**, 879 (2009).
9. E. A. Winzeler, *Nature* **455**, 751 (2008).
10. F. J. Gamo *et al.*, *Nature* **465**, 305 (2010).
11. W. A. Guiguemde *et al.*, *Nature* **465**, 311 (2010).
12. D. Plouffe *et al.*, *Proc. Natl. Acad. Sci. U.S.A.* **105**, 9059 (2008).
13. See supporting material on *Science* Online.
14. B. M. Russell *et al.*, *Antimicrob. Agents Chemother.* **47**, 170 (2003).
15. J. P. Guthmann *et al.*, *Trop. Med. Int. Health* **13**, 91 (2008).
16. N. J. White, *J. Antimicrob. Chemother.* **30**, 571 (1992).
17. W. W. Sharrock *et al.*, *Malar. J.* **7**, 94 (2008).
18. M. Traebert, B. Dumotier, *Expert Opin. Drug Saf.* **4**, 421 (2005).
19. N. J. White, *Lancet Infect. Dis.* **7**, 549 (2007).
20. B. N. Ames, F. D. Lee, W. E. Durston, *Proc. Natl. Acad. Sci. U.S.A.* **70**, 782 (1973).
21. D. A. Fidock, P. J. Rosenthal, S. L. Croft, R. Brun, S. Nwaka, *Nat. Rev. Drug Discov.* **3**, 509 (2004).
22. J. L. Vennerstrom *et al.*, *Nature* **430**, 900 (2004).
23. K. Hayton, X. Z. Su, *Curr. Genet.* **54**, 223 (2008).
24. A. Nzila, L. Mwai, *J. Antimicrob. Chemother.* **65**, 390 (2010).
25. P. K. Rathod, T. McErlean, P. C. Lee, *Proc. Natl. Acad. Sci. U.S.A.* **94**, 9389 (1997).
26. N. V. Dharia *et al.*, *Genome Biol.* **10**, R21 (2009).
27. M. J. Gardner *et al.*, *Nature* **419**, 498 (2002).
28. S. K. Volkman *et al.*, *Nat. Genet.* **39**, 113 (2007).
29. D. C. Jeffares *et al.*, *Nat. Genet.* **39**, 120 (2007).
30. L. J. Nkrumah *et al.*, *Nat. Methods* **3**, 615 (2006).
31. F. Trottein, J. Thompson, A. F. Cowman, *Gene* **158**, 133 (1995).
32. M. Dyer, M. Jackson, C. McWhinney, G. Zhao, R. Mikkelsen, *Mol. Biochem. Parasitol.* **78**, 1 (1996).
33. S. Krishna *et al.*, *J. Biol. Chem.* **276**, 10782 (2001).
34. L. Yatime *et al.*, *Biochim. Biophys. Acta* **1787**, 207 (2009).
35. W. Kühlbrandt, *Nat. Rev. Mol. Cell Biol.* **5**, 282 (2004).
36. A. M. Jensen, T. L. Sørensen, C. Olesen, J. V. Møller, P. Nissen, *EMBO J.* **25**, 2305 (2006).
37. D. M. Clarke, T. W. Loo, G. Inesi, D. H. MacLennan, *Nature* **339**, 476 (1989).
38. C. Toyoshima, M. Nakasako, H. Nomura, H. Ogawa, *Nature* **405**, 647 (2000).
39. C. Toyoshima, H. Nomura, *Nature* **418**, 605 (2002).
40. K. Moncoq, C. A. Trieber, H. S. Young, *J. Biol. Chem.* **282**, 9748 (2007).
41. M. Takahashi, Y. Kondou, C. Toyoshima, *Proc. Natl. Acad. Sci. U.S.A.* **104**, 5800 (2007).
42. M. C. Lee, P. A. Moura, E. A. Miller, D. A. Fidock, *Mol. Microbiol.* **68**, 1535 (2008).
43. P. Rice, I. Longden, A. Bleasby, *Trends Genet.* **16**, 276 (2000).
44. We thank A. Matter, M. Tanner, and P. Herrling for their foresight and support in establishing a malaria drug discovery program in the context of a public-private partnership. We thank T. A. Smith (SwissTPH) for the statistical analysis of the stage and rate of action studies. We thank S. Rao (Novartis Institute for Tropical Diseases) and M. Traebert (Novartis-preclinical safety), respectively, for the cytotoxicity and hERG inhibition data. We also thank M. Weaver (Novartis-preclinical safety) for the interpretation of the preclinical toxicology data. The team acknowledges P. Schultz, who had the vision to see the potential of the drug resistance experiments in the exploratory phase. In addition, we are grateful to R. T. Eastman for providing guidance to establish the in vitro drug-selection protocol and for providing the cloned Dd2 parasites. Finally, the scientific expertise provided by S. E. R. Bopp and S. K. Sharma and their helpful discussions throughout this project are greatly appreciated. Funding for the PfATP4 transfectants was provided to the Fidock laboratory in part by the Medicines for Malaria Venture (MMV08/0015; PI D. Fidock). The Shoklo Malaria Research Unit is sponsored by the Wellcome Trust of Great Britain, as part of the Oxford Tropical Medicine Research Programme of Wellcome Trust–Mahidol University. Laurent Renia's laboratory is supported by a core grant from the Singapore Immunology Network, A*STAR. This work was supported by a grant from the Medicines for Malaria Venture and a translational research grant (WT078285) from the Wellcome Trust to the Novartis Institute for Tropical Diseases, the Genomics Institute of the Novartis Research Foundation and the Swiss Tropical Institute, and by grants to E.A.W. from the W. M. Keck Foundation and the NIH (R01AI059472). NITD609 is described in the Novartis patent application WO2009/132921. All requests for spiroindolones or related compounds are subject to a Material Transfer Agreement. T.H.K. and E.A.W. own shares in Novartis (Switzerland).

Supporting Online Material

www.sciencemag.org/cgi/content/full/329/5996/1175/DC1
Materials and Methods
Figs. S1 to S10
Tables S1 to S13
References

3 June 2010; accepted 30 June 2010
10.1126/science.1193225

REPORTS

Detection of C_{60} and C_{70} in a Young Planetary Nebula

Jan Cami,[1,2]* Jeronimo Bernard-Salas,[3,4] Els Peeters,[1,2] Sarah Elizabeth Malek[1]

In recent decades, a number of molecules and diverse dust features have been identified by astronomical observations in various environments. Most of the dust that determines the physical and chemical characteristics of the interstellar medium is formed in the outflows of asymptotic giant branch stars and is further processed when these objects become planetary nebulae. We studied the environment of Tc 1, a peculiar planetary nebula whose infrared spectrum shows emission from cold and neutral C_{60} and C_{70}. The two molecules amount to a few percent of the available cosmic carbon in this region. This finding indicates that if the conditions are right, fullerenes can and do form efficiently in space.

Interstellar dust makes up only a small fraction of the matter in our galaxy, but it plays a crucial role in the physics and chemistry of the interstellar medium (ISM) and star-forming regions (*1*). The bulk of this dust is created in the outflows of old, low-mass asymptotic giant branch (AGB) stars; such outflows are slow (5 to 20 km/s) but massive (10^{-8} to 10^{-4} solar masses per year) (*2*–*4*). Once most of the envelope is ejected, the AGB phase ends and the stellar core—a hot white dwarf—becomes gradually more exposed. When this white dwarf ionizes the stellar ejecta, they become visible as a planetary nebula (PN).

Chemical reactions and nucleation in the AGB outflows transform the atomic gas into molecules and dust grains. For carbon-rich AGB stars (sometimes called carbon stars), this results in a large variety of carbonaceous compounds; to date, more than 60 individual molecular species and a handful of dust minerals have been identified in these outflows (*5*), including benzene, polyynes, and cyanopolyynes up to about 13 atoms in size (*6*, *7*).

These environments are also thought to be the birthplace for large aromatic species such as polycyclic aromatic hydrocarbons (PAHs) and fullerenes (*8*, *9*), a class of large carbonaceous molecules that were discovered in laboratory experiments aimed at understanding the chemistry in carbon stars (*10*). Fullerenes have unique physical and chemical properties, and the detection of fullerenes and the identification of their formation site are therefore considered a priority in the field of interstellar organic chemistry (*11*). However, astronomical searches for fullerenes in interstellar and circumstellar media have not resulted in conclusive evidence (*12*–*14*). The most promising case to date is the detection of two diffuse interstellar bands (DIBs) in the near-infrared (*15*) whose wavelengths are close to laboratory spectra of C_{60}^+ in solid matrices (*16*); this finding awaits confirmation from comparison to a cold, gas-phase spectrum.

Here, we report on the detection of the fullerenes C_{60} and C_{70} in the circumstellar environment of Tc 1. Tc 1 is a young, low-excitation PN where the white dwarf is still enshrouded by the dense stellar ejecta. At optical wavelengths, Tc 1 shows Hα emission up to ~50 arc sec away from the central star, but the PN also has a much smaller (~9 arc sec) and more compact core that was observed with the Infrared Spectrograph (IRS) (*17*) onboard the Spitzer Space Telescope (*18*). This inner region turns out to be carbon-rich, hydrogen-poor, and dusty.

The Spitzer IRS spectrum of Tc 1 (Fig. 1) (*19*) shows numerous narrow forbidden emission

[1]Department of Physics and Astronomy, University of Western Ontario, London, Ontario N6A 3K7, Canada. [2]SETI Institute, 515 North Whisman Road, Mountain View, CA 94043, USA. [3]222 Space Sciences Building, Cornell University, Ithaca, NY 14853, USA. [4]Institut d'Astrophysique Spatiale, CNRS/Université Paris-Sud 11, 91405 Orsay, France.

*To whom correspondence should be addressed. E-mail: jcami@uwo.ca

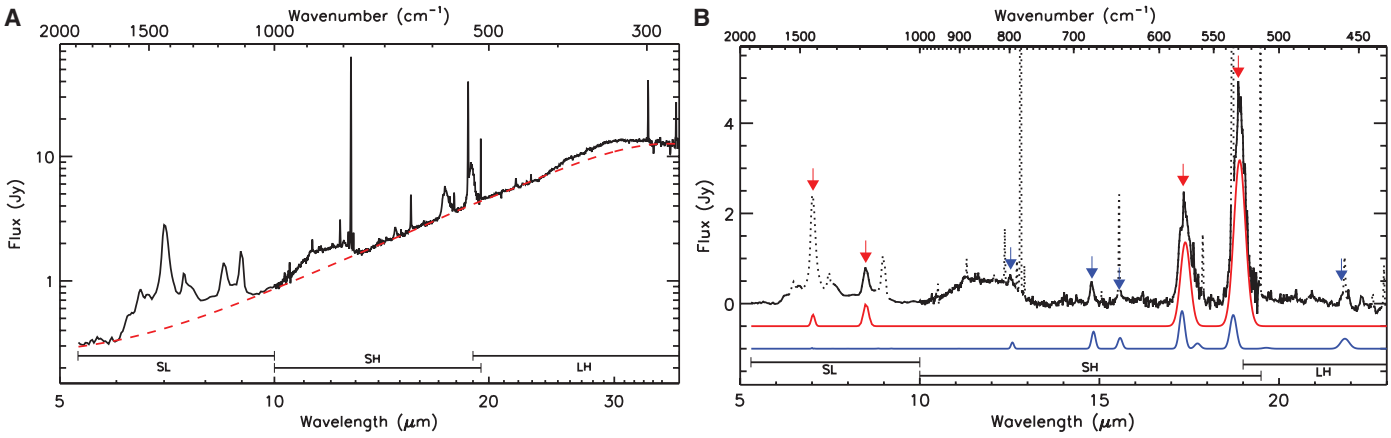

Fig. 1. The Spitzer IRS spectrum of Tc 1. (**A**) The entire range, 5 to 37 μm. (**B**) Continuum-subtracted spectrum between 5 and 23 μm, where known forbidden emission lines are masked (*19*). We fitted a cubic spline to spectral ranges devoid of features to determine the dust continuum (red dashed line). The broad plateau between 11 and 13 μm is attributed to emission from SiC dust (*34*, *35*), and the well-known broad feature longward of 23 μm is believed to be due to MgS (*36*). Red arrows mark the wavelengths of all infrared active modes for C_{60}; blue arrows denote those of the four strongest, isolated C_{70} bands. The red and blue curves below the data are thermal emission models for all infrared active bands of C_{60} and C_{70} at temperatures of 330 K and 180 K, respectively (*19*). We convolved the bands with a Gaussian profile ($\sigma = 2.55$ cm^{-1} for all C_{70} bands, $\sigma = 4.5$ cm^{-1} for the C_{60} bands in the SH/LH module, and $\sigma = 10$ cm^{-1} for those in the SL module). Apparent weak emission bumps near 14.4, 16.2, 20.5, and 20.9 μm are artifacts. The nature of the weak feature near 22.3 μm is unclear because it appears differently in both nods.

lines that are characteristic for the low-density gas environment of PNe. The infrared continuum is due to emission from circumstellar dust. For carbon-rich environments, this dust is typically amorphous carbon, which results in a featureless continuum. Other common dust components reveal their presence through emission bands.

The spectra of most carbon-rich PNe are generally dominated by strong emission features due to PAHs. These features are completely absent in the spectrum of Tc 1. In addition, there is no trace of even the simplest H-containing molecules (such as HCN and C_2H_2) that are often observed in carbon-rich proto-PNe. The Spitzer IRS spectrum does show a few weak hydrogen recombination lines, but these most likely originate from the halo material farther out, where Hα emission is also observed. Instead, the spectrum is dominated by the prominent C_{60} bands at 7.0 (*20*), 8.5, 17.4, and 18.9 μm, and furthermore exhibits weaker features that are due to C_{70} (Fig. 1).

Emission processes result in band intensities that are proportional to the Einstein A coefficients for spontaneous emission and to the population of the excited states. We scaled the experimentally obtained relative absorption coefficients for the C_{60} bands (1, 0.48, 0.45, and 0.378 for the bands at 18.9, 17.4, 8.5, and 7.0 μm, respectively) (*21*, *22*) to absolute values by adopting a value of 25 km/mol for the band at 8.5 μm (*23*) and converted them to Einstein A coefficients. Using these, we calculated the population distribution over the excited vibrational states from the total emitted power in each of the C_{60} bands and found them to be consistent with thermal emission, in which case they are fully determined by a single parameter—the excitation temperature—which we derived to be ~330 K (*19*). The relative intensities of the infrared C_{60} bands in Tc 1 thus match what is expected for thermal emission at 330 K when using experimentally obtained absorption coefficients.

It is well established from laboratory experiments that the peak wavelengths and bandwidths are temperature-dependent (*24*). The peak wavelengths in Tc 1 agree, within uncertainty, with those found in laboratory experiments obtained at temperatures comparable to our derived excitation temperature (*19*, *25*). We measured widths (full width at half maximum) of ~10 cm^{-1} for the bands at 18.9 and 17.4 μm, which agrees with laboratory results (*24*–*26*); the bands at 7.0 and 8.5 μm are unresolved (*19*). We performed a similar analysis for the C_{70} bands using appropriate laboratory results (*24*, *27*, *28*) and obtained an excitation temperature of ~180 K (*19*).

For comparison, we used the derived excitation temperatures to construct thermal emission models for both molecules (Fig. 1). The correspondence between the laboratory-based emission model and the observations supports the identification of these bands with fullerenes. The absence of the corresponding spectral features of fullerene cations or anions (e.g., 7.1 and 7.5 μm for C_{60}^{+}) implies that the fullerenes are in the neutral state. All infrared active bands of both species are fully accounted for in Tc 1; no other clear spectral features remain unidentified in the spectrum (*19*). The environment of Tc 1 thus results in a unique dust composition, but not in a wide variety of dust components.

Our results suggest that the emission does not originate from free molecules in the gas phase, but from molecular carriers attached to solid material. With an effective temperature for the central object of ~30,000 K, the radiation field peaks for photon energies in the range 6 to 10 eV, which would result in excitation temperatures of 800 to 1000 K for large gas-phase species. The much lower temperatures derived for the fullerenes thus imply that these species are in direct contact with a much cooler material. In this environment, the most likely solid material is the surface of the abundant carbonaceous grains present in the outflow. These solids are in radiative equilibrium with the stellar radiation field, and thus their temperature is determined by the distance from the central object. If the fullerenes are in direct contact with this material, they must be at the same temperature and display a thermal population distribution over the excited vibrational states, such as we observe in Tc 1. The difference in temperature between C_{60} and C_{70} then implies different spatial locations, with C_{60} located closer to the illuminating source than C_{70}. This could happen if C_{70} forms from C_{60} as it moves out.

The presence of only neutral fullerenes is in agreement with an origin on grain surfaces, in which case charge effects on individual molecules are unimportant. In contrast, gaseous C_{60} would be largely in cationic form in this environment. Some observational support for an origin in the solid state is also provided by the broad and generally symmetric (Gaussian) band profiles. For gas-phase species, vibrational anharmonicities (and possibly ro-vibrational structure) would result in asymmetric bands. Only a small fraction of such gaseous material could be hidden in the observed bands. The absence of gas-phase species is puzzling and could indicate that the fullerenes form on (or from) the dust grains and never fully evaporate.

On Earth, fullerenes can be synthesized by vaporizing graphite in a hydrogen-poor atmosphere that contains helium as a buffer gas. The fullerene formation process is very efficient, and C_{60} is by far the dominant and most stable species among the large cluster population formed in

these experiments, followed by C_{70} (*10*, *25*). However, fullerene formation is inhibited by the presence of hydrogen (*29*, *30*). The circumstellar environment of Tc 1 seems to be the astrophysical analog of such a laboratory setup. The dust is clearly carbonaceous—as is also expected from the overabundance of C in the gas phase, with a C/O ratio of ~3.2 (*31*)—but the absence of any H-containing species indicates that the dust environment must be very H-poor. About 5.8×10^{-8} solar masses of pure C_{60} and $\sim 4.7 \times 10^{-8}$ solar masses of C_{70} are required to reproduce the emission bands. The Spitzer IRS observations are sensitive to dust only at temperatures of at least ~100 K, and given the measured expansion velocity of 20 km/s (*32*), this corresponds to mass loss from only the past 100 years. At the measured carbon abundance (*31*) and adopting a mass loss rate of 10^{-4} solar masses per year, this means that each of the fullerene species represents at least ~1.5% of the available carbon. This is roughly consistent with abundance estimates from the two DIBs associated with C_{60}^{+} (*15*) and matches the fraction of graphite that is converted into fullerenes in laboratory experiments (*25*). Fullerenes can also be created by photochemical processing of hydrogenated amorphous carbon (*33*). However, such processes generally also result in large amounts of PAHs, which are absent in Tc 1. The role of photochemistry in the fullerene formation process in Tc 1 is thus unclear.

The unusual circumstellar environment of Tc 1 indicates that it must have ejected its entire hydrogen envelope at least a few thousand years ago, exposing the helium intershell material. Presumably, a late thermal pulse then caused the ejection of this material, which now makes up the warm, dusty, and hydrogen-poor PN core where fullerenes are abundant. Tc 1 is thus not necessarily an unusual object, although we evidently have observed it during a short (and possibly unusual) phase. The presence or absence of hydrogen in this type of carbon-rich environment then clearly determines whether the chemical pathways favor the formation of PAH molecules or fullerenes as large aromatic species. Within the context of carbon-rich PNe, the PAH route is generally dominant; only those objects that completely remove their hydrogen envelope and undergo a late thermal pulse can then create the hydrogen-poor environment where fullerenes flourish.

References and Notes

1. A. G. G. M. Tielens, *The Physics and Chemistry of the Interstellar Medium* (Cambridge Univ. Press, Cambridge, 2005).
2. H. J. Habing, *Astron. Astrophys. Rev.* **7**, 97 (1996).
3. L. A. Willson, *Annu. Rev. Astron. Astrophys.* **38**, 573 (2000).
4. F. Herwig, *Annu. Rev. Astron. Astrophys.* **43**, 435 (2005).
5. S. Kwok, *Int. J. Astrobiol.* **8**, 161 (2009).
6. J. Cernicharo *et al.*, *Astrophys. J.* **546**, L123 (2001).
7. J. R. Pardo, J. Cernicharo, J. R. Goicoechea, M. Guélin, A. Asensio Ramos, *Astrophys. J.* **661**, 250 (2007).
8. M. Frenklach, E. D. Feigelson, *Astrophys. J.* **341**, 372 (1989).
9. I. Cherchneff, Y. H. Le Teuff, P. M. Williams, A. G. G. M. Tielens, *Astron. Astrophys.* **357**, 572 (2000).
10. H. W. Kroto, J. R. Heath, S. C. Obrien, R. F. Curl, R. E. Smalley, *Nature* **318**, 162 (1985).
11. E. Herbst, E. F. van Dishoeck, *Annu. Rev. Astron. Astrophys.* **47**, 427 (2009).
12. G. H. Herbig, *Astrophys. J.* **542**, 334 (2000).
13. C. Moutou, K. Sellgren, L. Verstraete, A. Léger, *Astron. Astrophys.* **347**, 949 (1999).
14. G. C. Clayton *et al.*, *Astron. J.* **109**, 2096 (1995).
15. B. H. Foing, P. Ehrenfreund, *Nature* **369**, 296 (1994).
16. J. Fulara, M. Jakobi, J. P. Maier, *Chem. Phys. Lett.* **211**, 227 (1993).
17. J. R. Houck *et al.*, *Astrophys. J.* **154** (suppl.), 18 (2004).
18. M. W. Werner *et al.*, *Astrophys. J.* **154** (suppl.), 1 (2004).
19. See supporting material on *Science* Online.
20. The emission at 7.0 μm is much higher than expected for C_{60} emission alone because of a blend with a strong [ArII] line.
21. M. C. Martin, D. Koller, L. Mihaly, *Phys. Rev. B* **47**, 14607 (1993).
22. J. Fabian, *Phys. Rev. B* **53**, 13864 (1996).
23. N. Sogoshi *et al.*, *J. Phys. Chem. A* **104**, 3733 (2000).
24. L. Nemes *et al.*, *Chem. Phys. Lett.* **218**, 295 (1994).
25. W. Krätschmer, L. D. Lamb, K. Fostiropoulos, D. R. Huffman, *Nature* **347**, 354 (1990).
26. C. I. Frum *et al.*, *Chem. Phys. Lett.* **176**, 504 (1991).
27. A. von Czarnowski, K. H. Meiwes-Broer, *Chem. Phys. Lett.* **246**, 321 (1995).
28. R. Stratmann, G. Scuseria, M. Frisch, *J. Raman Spectrosc.* **29**, 483 (1998).
29. M. S. De Vries *et al.*, *Geochim. Cosmochim. Acta* **57**, 933 (1993).
30. X. K. Wang *et al.*, *J. Mater. Res.* **10**, 1977 (1995).
31. Y. V. Milanova, A. F. Kholtygin, *Astron. Lett.* **35**, 518 (2009).
32. A. Acker, K. Gesicki, Y. Grosdidier, S. Durand, *Astron. Astrophys.* **384**, 620 (2002).
33. A. Scott, W. W. Duley, G. P. Pinho, *Astrophys. J.* **489**, L193 (1997).
34. A. K. Speck, A. B. Corman, K. Wakeman, C. H. Wheeler, G. Thompson, *Astrophys. J.* **691**, 1202 (2009).
35. J. Bernard-Salas *et al.*, *Astrophys. J.* **699**, 1541 (2009).
36. S. Hony, L. B. F. M. Waters, A. G. G. M. Tielens, *Astron. Astrophys.* **390**, 533 (2002).

37. We thank M. Houde and A. Tielens for commenting on earlier versions of the manuscript, G. Fanchini for stimulating discussions on various properties of fullerene materials, and G. C. Sloan for discussions on carbonaceous species in PNe. Supported by a Discovery grant from the National Science and Engineering Research Council of Canada (J.C., E.P., and S.E.M.) and by the Spitzer Space Telescope General Observer Program.

Supporting Online Material

www.sciencemag.org/cgi/content/full/science.1192035/DC1
Materials and Methods
Fig. S1
Table S1
References

10 May 2010; accepted 7 July 2010
Published online 22 July 2010;
10.1126/science.1192035
Include this information when citing this paper.

Real-Time Dynamics of Single Vortex Lines and Vortex Dipoles in a Bose-Einstein Condensate

D. V. Freilich,* D. M. Bianchi,† A. M. Kaufman,‡ T. K. Langin, D. S. Hall§

Understanding the behavior of quantized vortices is essential to gaining insight into diverse superfluid phenomena, from critical-current densities in superconductors to quantum turbulence in superfluids. We observe the real-time dynamics of quantized vortices in trapped dilute-gas Bose-Einstein condensates by repeatedly imaging the vortex cores. The precession frequency of a single vortex is measured by explicitly observing its time dependence and is found to be in good agreement with theory. We further characterize the dynamics of vortex dipoles in two distinct configurations: (i) an asymmetric configuration, in which the vortex trajectories are dynamic and nontrivial, and (ii) a stable, symmetric configuration, in which the dipole is stationary.

Quantized vortices are topological defects that carry angular momentum and are among the most conspicuous characteristics of a superfluid (*1*, *2*). Although superfluid phenomena have been recognized for more than a century, it is only in the past few decades that the motion of quantized vortex lines has been detected in real time through magnetic resonance techniques, including the precession of a single vortex line (*3*), the propagation of vortices from a rotating superfluid into a nonrotating superfluid (*4*, *5*), and the phase transition of vortex lines into vortex sheets (*6*). The dynamical behavior of quantized vortex lines has also been imaged directly in real time in superfluid helium (*7*) and type II superconductors (*8*). These studies have yielded a wealth of information about how vortices influence superfluid behavior through their pinning, transport, and reconnection properties.

Dilute-gas Bose-Einstein condensates (BECs) (*9*–*11*) are a natural choice for fundamental studies

Department of Physics, Amherst College, Amherst, MA 01002–5000, USA.

*Present address: Department of Mechanical and Aerospace Engineering, University of California, San Diego, La Jolla, CA 92093–0411 USA.

†Present address: Department of Linguistics and Philosophy, Massachusetts Institute of Technology, Cambridge, MA 02139–4307 USA.

‡Present address: JILA, National Institute of Standards and Technology and Department of Physics, University of Colorado, Boulder, CO 80309–0440, USA.

§To whom correspondence should be addressed. E-mail: dshall@amherst.edu

of superfluid vortex dynamics, because they are highly controllable and can be described by tractable theories (*12*). Real-time vortex dynamics have been studied indirectly through an examination of condensate collective excitations (*13*, *14*); to date, however, experiments have generated, at most, two sequential images of individual vortex lines (*13*, *15*). The primary challenge to observing vortices in a trapped condensate is that the radius of a vortex core is ordinarily several times smaller than the wavelength of light used for imaging, making direct, in situ observation difficult. Extinguishing the trapping potential and permitting the condensate to expand to a point at which vortex lines can be resolved (*16*), on the other hand, irrevocably disrupts the time evolution. Despite substantial recent progress (*17*), reproducing precisely the initial conditions of the vortices also remains challenging.

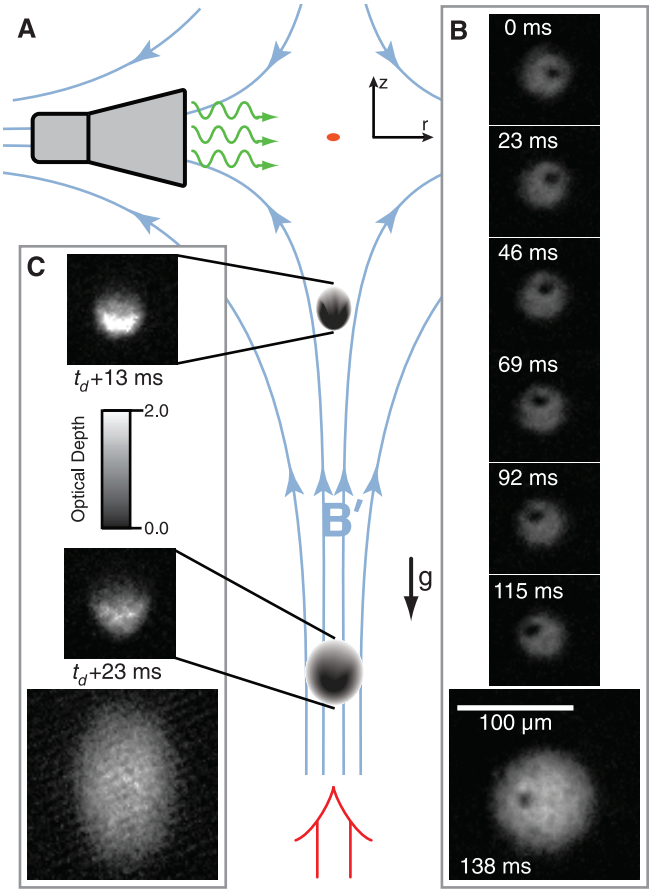

Fig. 1. (**A**) A small fraction (typically 5%) of the trapped condensate (red dot) is extracted by a brief microwave pulse (green arrows) that transfers it to an untrapped state at time t_d. No longer confined and supported against gravity (g), the extracted atoms fall and expand in a magnetic field gradient B' (light blue), at which point they are absorptively imaged from below (red arrow). (**B**) Several images from the same condensate, in units of optical depth, showing the counterclockwise precession of a vortex line. (Bottom) Image of the remnant condensate after release and expansion. (**C**) Atomic density distributions of atoms viewed from the side 13 and 23 ms after the microwave pulse. (Bottom) Side view of a remnant condensate containing a single vortex line.

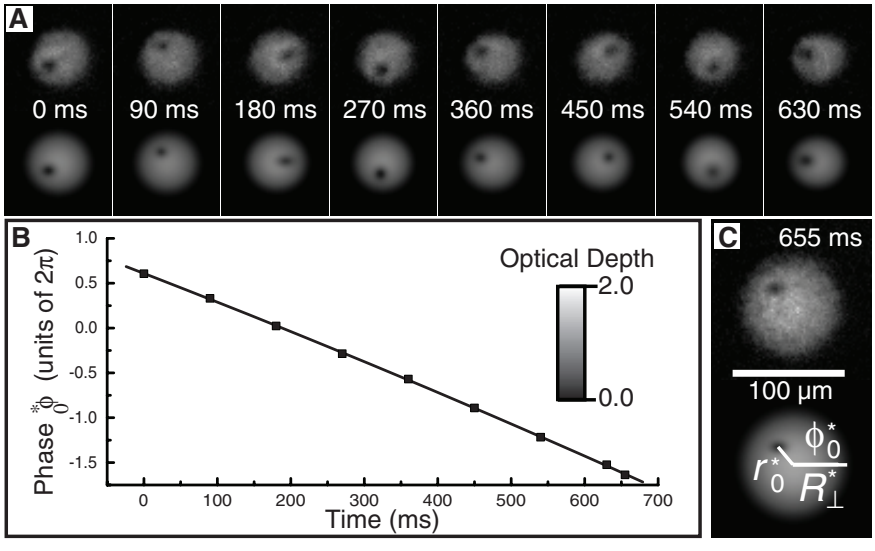

Fig. 2. Quantitative analysis of typical vortex precession data. (**A**) (Upper row) Images of the extracted atoms (in units of optical depth) at eight time points. (Lower row) Best fits to the surface profile. (**B**) Dependence of ϕ_0^* on time (squares), along with the best fit to a second-order polynomial (black line). The sense of precession is unambiguously determined by comparing the image taken at 630 ms with that of the remnant condensate at 655 ms (**C**), which are separated by a shorter time interval.

The single-shot nature of our imaging method opens up a wide variety of new vortex-dynamics experiments, including those in which the vortices are generated irreproducibly or even stochastically (*21*), as they are in this work. Our vortices arise during evaporation via a Kibble-Zurek mechanism (*22*, *23*), in which the rapid quench of a cold thermal gas through the BEC phase transition results in the formation of topological defects (*21*, *24*, *25*). With our evaporation parameters, we obtain, on average, a vortex line in one of every three or four experimental runs, and we observe vortices of topological charge ±1 (see below) in roughly equal number. The observed vortex lines are parallel to the symmetry axis of the trap, and we have seen no convincing evidence of bent or tilted lines.

A sequence of images derived by extracting 5% of the atoms from a single condensate at 23-ms intervals is shown in Fig. 1B, along with the image of the released remnant condensate. The vortex line, viewed along its axis, appears clearly in each of the images as a roughly circular minimum in the atomic density (*16*). As a function of time, the vortex line precesses in a counterclockwise sense about the center of the atomic density distribution. We immediately infer its topological charge, or sense of circulation, which is the same as its sense of precession (*26*). The extracted sample interacts briefly with the remaining trapped condensate as it falls, modifying its axial density profile (Fig. 1C). Although such interactions hinder a three-dimensional reconstruction of the vortex line, we note that vortex lines are not usually visible in the axial profile, even in the image of the remnant condensate after expansion (Fig. 1C, bottom panel). Fortunately, interactions between trapped and untrapped atoms are not observed to affect the radial density profile.

Quantitative information about vortex motion is obtained by fitting the images to a surface consisting of a Gaussian superimposed on a parabola; the former captures the center of the vortex line, and the latter captures the center and radial extent of the extracted atoms, which retain an approximately Thomas-Fermi profile after expansion. Together, these quantities yield the polar coordinate of the vortex line (r_0^*,ϕ_0^*). The image and fit to the remnant condensate also yield final observables such as the number of atoms N, the radial extent of the expanded condensate $R_\perp^*$, and the temperature T. A typical data set and its accompanying fits are shown in Fig. 2A. In all of the data we present, there is no discernible thermal component ($T/T_c < 0.4$, where T_c is the Einstein condensation temperature at which the BEC phase transition occurs).

The behavior of a solitary precessing vortex is an important benchmark for studies of vortex dynamics in a BEC. The core of a vortex line is a region of vanishing atomic density within the inhomogeneous density profile of the condensate; it therefore experiences a radial (outward) buoyant force. In addition, it experiences a gyroscopic Magnus force directed perpendicular to the direction of fluid flow. These forces lead to circular precession of the vortex line about the center of the condensate (*26*, *27*). Vortex precession in a dilute-gas condensate was first observed directly in a landmark experiment a decade ago (*15*), with the use of a method that identified the position of a single vortex core at two distinct times. The experiment achieved a precision of a few percent after averaging many such measurements and matched the theoretical precession frequency to ~10%.

Our precession-frequency measurements achieve a precision of a few percent in a single sequence of images. Moreover, we can easily observe any time dependence that arises from processes such as interactions with thermal atoms or reduction in atom number. In Fig. 2B, we plot ϕ_0^* as a function of time to extract the precession frequency $\dot{\phi}_0^*$. The reduction in atom number is nonnegligible (see below); we therefore fit the data to a quadratic polynomial as an elementary correction for the small degree of expected change in $\dot{\phi}_0^*$. For the data set of Fig. 2, we find $\dot{\phi}_0^* = 2\pi \cdot 3.67\,(6)$ Hz at time $t = 655$ ms, increasing 16(4)% from a value of $2\pi \cdot 3.17(13)$ Hz at $t = 0$ ms.

The predicted precession frequency for a straight vortex line in a disk-shaped condensate confined in a nonrotating axisymmetric trap may be written (*28*)

$$\dot{\phi}_0 = \frac{2\hbar\omega_r^2}{8\mu(1 - r_0^2/R_\perp^2)}\left(3 + \frac{\omega_r^2}{5\omega_z^2}\right)\ln\left(\frac{2\mu}{\hbar\omega_r}\right) \quad (1)$$

where ω_r and ω_z are the radial and axial trap frequencies, respectively; μ is the chemical potential; r_0 is the radial coordinate of the vortex line; $R_\perp$ is the radial Thomas-Fermi extent of the condensate; and $\hbar$ is Planck's constant h divided by 2π. The predicted precession frequency depends on N, largely through the chemical potential $\mu \propto N^{2/5}$. Eight images, each extracting 5% of the atoms from the condensate, reduce the number of atoms by one-third. Atoms are also lost on a longer time scale to dipolar relaxation and three-body recombination (*29*). Together, extraction and loss leave us with ~60% of the initial sample by 655 ms (*18*).

We use our measured trap frequencies $[\{\omega_r,\omega_z\} = 2\pi \cdot \{35.8(2),101.2(5)\}$ Hz (*18*)], $\mu = h \cdot 1.30(6)$ kHz for $N = 3.5(4) \times 10^5$ atoms and $r_0/R_\perp = r_0^*/R_\perp^* = 0.36(2)$, assuming linear scaling during expansion (*15*, *30*), to obtain a predicted frequency $\dot{\phi}_0 = 2\pi \cdot 3.7(2)$ Hz at $t = 655$ ms, in good agreement with the measured value. We further note that $\dot{\phi}_0$ increases by 18% for the change of N considered, which is also in good agreement with the observed increase in $\dot{\phi}_0^*$. The agreement between measured and predicted precession frequencies is maintained at the ~5% level in experiments with a variety of different N and $r_0^*/R_\perp^*$ values.

We also study the more complicated dynamics of two interacting vortices, which we observe in a few percent of our condensates. Vortices of opposite topological charge, or vortex dipoles (*17*), dominate our observations. Dipoles typically survive the evaporative quench in one of two configurations. The first is spatially asymmetric (Fig. 3), with one vortex line near the center of the condensate and the other close to the periphery. The vortex lines exert forces on one another that vary with their relative separation and positions within the condensate, substantially complicating their trajectories. Nevertheless, our imaging method yields a representation of their motion.

Whereas the inner vortex line can move along paths resembling precessing ellipses (Fig. 3, C and D), the outer vortex line continues to follow a roughly circular trajectory at an average speed that is markedly less than that of a solitary precessing vortex at the same radius. For the data sets shown in Fig. 3, where the average number of atoms $N_{avg} \sim 0.5 \times 10^6$ and $r_0^* \sim 0.5R_\perp^*$, the expected average period of precession for a solitary vortex line is $2\pi(\dot{\phi}_0^*)^{-1} \sim 260$ ms (Eq. 1).

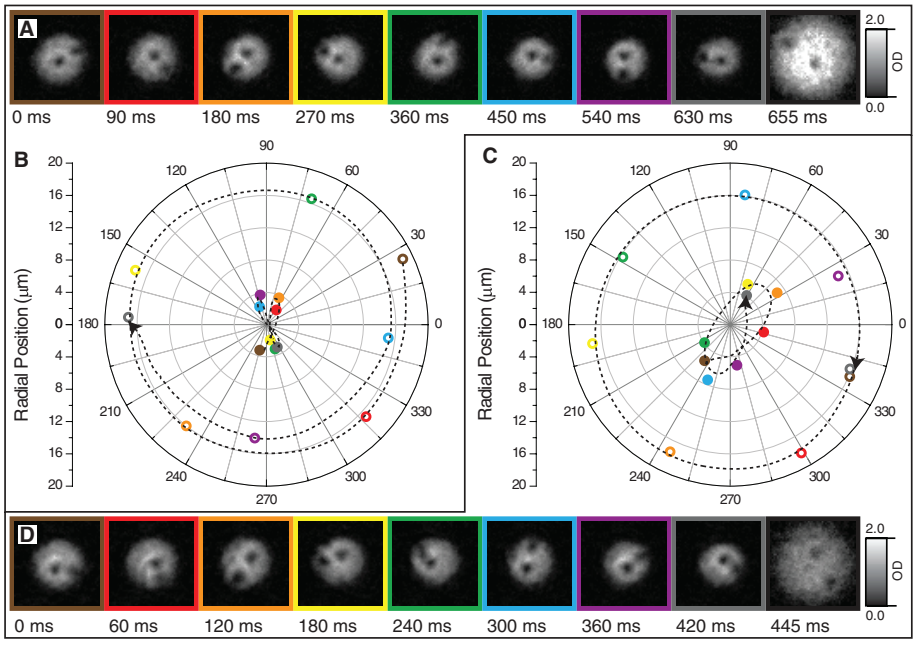

Fig. 3. Examples of the asymmetric vortex-dipole configuration. (**A**) Images of the atomic density in units of optical depth (OD). (**B**) Fit positions of the vortex lines in polar coordinates. The outer and inner vortex positions are designated by the open and solid circles, respectively, and the colors correspond to the image frames in (A). The directed lines indicate an estimate of the motion of the vortex lines and are intended to guide the eye. (**C**) Same as in (B) for the second data set (**D**). Each image is 100 μm per side.

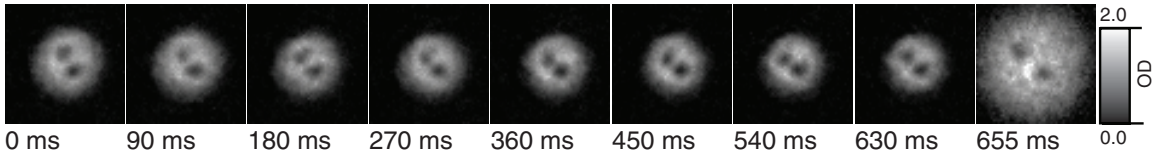

Fig. 4. Images of a stationary vortex dipole in units of optical depth. Each image is 100 μm per side.

This is considerably shorter than the observed average period of ~400 ms of the outer vortex line. The effect may be explained by noting that the outer vortex line experiences an additional inward Magnus force due to the countercirculating flow generated by the inner vortex line. Thus, the outer vortex line is not required to move as swiftly to maintain its approximately circumferential motion. (In the presence of an inner vortex line of the same topological charge, the outer vortex line would increase its speed.)

A particularly compelling demonstration of the second, symmetric dipole configuration is shown in Fig. 4. This unusual, time-independent topological structure is a stationary vortex dipole (*31*–*33*), the simplest example of a stable vortex cluster in an inhomogeneous superfluid. The stationary vortex dipole arises at the particular vortex separation distance (d_{sep}) at which the Magnus and buoyant forces on each vortex line balance. We find that d_{sep} is essentially constant for $N \sim 4$ to 6×10^5, the range of atomic number in the sequence shown. Averaging the nine measurements of d_{sep} from the images shown in Fig. 4, we find $d_{sep} = 0.432(17)\ R_{\perp}^{*}$. Published predictions for d_{sep} (*32*, *33*) consider only small, weakly interacting systems in two dimensions, unfortunately precluding a straightforward comparison with this measurement.

Small perturbations from the stationary–vortex-dipole configuration are predicted to display a variety of rich behavior, including oscillations of the vortices about their equilibrium positions and a slow precession of the vortices around their axis of symmetry (*33*). Although a systematic experimental study of this state is difficult due to its low probability of formation, our imaging method can, in principle, be combined with other experimental techniques that consistently generate this or other related (*17*) topological structures.

Future experiments may examine in detail the dynamics of one-, two-, and many-vortex systems, from their formation during evaporation to their termination at the edge of the condensate (*28*). For single vortices, the dependence of vortex precession frequencies on the many tunable-system parameters, including temperature and interatomic interaction strength, will permit a close test of theory under a variety of interesting experimental conditions. For vortex dipoles and particularly stationary vortex dipoles, a wealth of predicted interaction dynamics becomes experimentally accessible (*33*). We expect that dynamical studies of more complicated vortex configurations will be particularly fruitful, from individual vortex motion in disordered arrays to collective behavior in regular lattices (see fig. S1), as well as in the transitions between the two. These fundamental studies promise to deepen our understanding of the important roles that quantized vortices play in diverse superfluid phenomena, including critical-current densities, resistance, and quantum turbulence.

References and Notes

1. D. R. Tilley, J. Tilley, *Superfluidity and Superconductivity* (Institute of Physics Publishing, Philadelphia, ed. 3, 1990).
2. R. J. Donnelly, *Quantized Vortices in Helium II* (Cambridge Univ. Press, New York, 1991).
3. R. E. Packard, *Rev. Mod. Phys.* **70**, 641 (1998).
4. V. B. Eltsov *et al.*, *Phys. Rev. Lett.* **96**, 215302 (2006).
5. V. B. Eltsov *et al.*, *Phys. Rev. Lett.* **99**, 265301 (2007).
6. V. B. Eltsov *et al.*, *Phys. Rev. Lett.* **88**, 065301 (2002).
7. G. P. Bewley, D. P. Lathrop, K. R. Sreenivasan, *Nature* **441**, 588 (2006).
8. K. Harada *et al.*, *Nature* **360**, 51 (1992).
9. M. H. Anderson, J. R. Ensher, M. R. Matthews, C. E. Wieman, E. A. Cornell, *Science* **269**, 198 (1995).
10. K. B. Davis *et al.*, *Phys. Rev. Lett.* **75**, 3969 (1995).
11. C. C. Bradley, C. A. Sackett, J. J. Tollett, R. G. Hulet, *Phys. Rev. Lett.* **75**, 1687 (1995).
12. F. Dalfovo, S. Giorgini, L. P. Pitaevskii, S. Stringari, *Rev. Mod. Phys.* **71**, 463 (1999).
13. P. C. Haljan, B. P. Anderson, I. Coddington, E. A. Cornell, *Phys. Rev. Lett.* **86**, 2922 (2001).
14. P. Engels, I. Coddington, P. C. Haljan, E. A. Cornell, *Phys. Rev. Lett.* **89**, 100403 (2002).
15. B. P. Anderson, P. C. Haljan, C. E. Wieman, E. A. Cornell, *Phys. Rev. Lett.* **85**, 2857 (2000).
16. K. W. Madison, F. Chevy, W. Wohlleben, J. Dalibard, *Phys. Rev. Lett.* **84**, 806 (2000).
17. T. W. Neely, E. C. Samson, A. S. Bradley, M. J. Davis, B. P. Anderson, *Phys. Rev. Lett.* **104**, 160401 (2010).
18. Supporting material is available on *Science* Online.
19. K. M. Mertes *et al.*, *Phys. Rev. Lett.* **99**, 190402 (2007).
20. W. Petrich, M. H. Anderson, J. R. Ensher, E. A. Cornell, *Phys. Rev. Lett.* **74**, 3352 (1995).
21. C. N. Weiler *et al.*, *Nature* **455**, 948 (2008).
22. T. W. B. Kibble, *J. Phys. A Math. Gen.* **9**, 1387 (1976).
23. W. H. Zurek, *Nature* **317**, 505 (1985).
24. V. M. H. Ruutu *et al.*, *Nature* **382**, 334 (1996).
25. V. B. Eltsov, T. W. B. Kibble, M. Krusius, V. M. H. Ruutu, G. E. Volovik, *Phys. Rev. Lett.* **85**, 4739 (2000).
26. A. L. Fetter, *Rev. Mod. Phys.* **81**, 647 (2009).
27. D. S. Rokhsar, *Phys. Rev. Lett.* **79**, 2164 (1997).
28. A. L. Fetter, A. A. Svidzinsky, *J. Phys. Condens. Matter* **13**, R135 (2001).
29. E. A. Burt *et al.*, *Phys. Rev. Lett.* **79**, 337 (1997).
30. F. Dalfovo, M. Modugno, *Phys. Rev. A* **61**, 023605 (2000).
31. L.-C. Crasovan *et al.*, *Phys. Rev. A* **68**, 063609 (2003).
32. M. Möttönen, S. M. M. Virtanen, T. Isoshima, M. M. Salomaa, *Phys. Rev. A* **71**, 033626 (2005).
33. W. Li, M. Haque, S. Komineas, *Phys. Rev. A* **77**, 053610 (2008).

34. We thank J. R. Friedman, R. P. Anderson, and P. G. Kevrekidis for interesting conversations and A. Dewan, E. Altuntas, and A. W. Eddins for experimental assistance. This work was supported by the NSF through grant PHY-0855475.

Supporting Online Material

www.sciencemag.org/cgi/content/full/329/5996/1182/DC1
SOM Text
Fig. S1
References

21 April 2010; accepted 26 July 2010
10.1126/science.1191224

Plastic Accumulation in the North Atlantic Subtropical Gyre

Kara Lavender Law,[1]* Skye Morét-Ferguson,[1,2] Nikolai A. Maximenko,[3] Giora Proskurowski,[1,2] Emily E. Peacock,[2] Jan Hafner,[3] Christopher M. Reddy[2]

Plastic marine pollution is a major environmental concern, yet a quantitative description of the scope of this problem in the open ocean is lacking. Here, we present a time series of plastic content at the surface of the western North Atlantic Ocean and Caribbean Sea from 1986 to 2008. More than 60% of 6136 surface plankton net tows collected buoyant plastic pieces, typically millimeters in size. The highest concentration of plastic debris was observed in subtropical latitudes and associated with the observed large-scale convergence in surface currents predicted by Ekman dynamics. Despite a rapid increase in plastic production and disposal during this time period, no trend in plastic concentration was observed in the region of highest accumulation.

Plastics are a major contaminant in the world's oceans. Their chemically engineered durability and slow rate of biodegradation (*1*) allow these synthetic polymers to withstand the ocean environment for years to decades or longer (*2*). Environmental impacts of ocean plastic are wide-ranging (*3*) and include entanglement of marine fauna (*4*), ingestion by seabirds and organisms ranging in size from plankton to marine mammals (*4*, *5*), dispersal of microbial and colonizing species to potentially non-native waters (*6*, *7*), and concentration and transport of organic contaminants to marine organisms at multiple trophic levels (*8*–*10*). In the open ocean, the abundance, distribution, and temporal and spatial variability of plastic debris are poorly known, despite an increasing awareness of the problem. Although high concentrations of floating plastic debris have been found in the Pacific Ocean (*11*–*14*), only limited data exist to quantify and explain the geographical range and integrated plastic content. In the Atlantic Ocean, the subject has been all but ignored since the earliest studies of marine debris (*15*–*17*).

[1]Sea Education Association, Post Office Box 6, Woods Hole, MA 02543, USA. [2]Department of Marine Chemistry and Geochemistry, Woods Hole Oceanographic Institution, 266 Woods Hole Road, Woods Hole, MA 02543, USA. [3]International Pacific Research Center, School of Ocean and Earth Science and Technology, University of Hawai'i, Honolulu, HI 96822, USA.

*To whom correspondence should be addressed. E-mail: klavender@sea.edu

Here, we present an analysis of 22 years of ship-survey data collected in the western North Atlantic Ocean and Caribbean Sea. We examine the abundance, spatial distribution, and temporal variability of plastic debris from samples collected and archived by more than 7000 undergraduate students and faculty scientists at Sea Education Association (SEA) from October 1986 to December 2008. More than 6100 surface plankton net tows were conducted onboard SEA's sailing research vessels, from which more than 64,000 plastic pieces were hand-picked and enumerated (*18*, *19*).

Sixty-two percent of all net tows contained detectable amounts of plastic debris. The highest plastic concentrations were observed between 22° and 38°N (Fig. 1 and figs. S1 and S2), where 83% of total plastic pieces were collected. The largest sample collected in a single 30-min tow was 1069 pieces at 24.6°N, 74.0°W in May 1997, equivalent to 580,000 pieces km^{-2}. The maximum sample size reported in Atlantic studies from the 1970s ranged from 12,000 pieces km^{-2} (*15*) to 167,000 pieces km^{-2} (*16*). Comparatively low plastic concentrations were measured in tows closest to land, such as along the Florida coast and Florida Keys, in the Gulf of Maine, and near Caribbean islands. The average plastic concentration measured within the Caribbean Sea was only 1414 ± 112 pieces km^{-2}, while that in the Gulf of Maine was 1534 ± 200 pieces km^{-2}, both more than an order of magnitude lower than the average concentration near 30°N (20,328 ± 2324 pieces km^{-2}, 29° to 31°N). Although in our study region the latitudinal bounds of the highest plastic concentration are well defined, the eastern extent has not yet been determined because of a lack of direct observations.

The region of highest plastic concentration is clearly associated with the large-scale subtropical convergence in the surface velocity field created by wind-driven Ekman currents and geostrophic circulation (Fig. 2). This convergence zone, indicated by converging streamlines and current velocities less than 2 cm s^{-1}, extends across most of the subtropical North Atlantic basin (*20*) and coincides with the highest observed plastic concentrations. This correspondence not only explains the plastic distribution but also illustrates how floating debris acts as a tracer of large-scale mean surface currents.

While the convergence acts to concentrate floating debris, the geographic origin of the debris cannot be easily determined from current patterns or from the recovered plastic samples themselves. To address this question, we used data from satellite-tracked drifting surface buoys (drifters) (*21*) to examine pathways into and out of the "central region" of high plastic concentration (26° to 34°N, 60° to 70°W). Of 1666 drifters broadly deployed in the North Atlantic (0° to 76°N, 0° to 90°W) from 1989 to 2009, 24 drifters were deployed in the central region and 116 others passed through this region. The trajectories of these "central region" drifters were strongly confined to the western subtropical gyre; before entering the central region, 66% (92 drifters) originated west of 50°W and between 18° and 42°N, whereas only 10% (14 drifters) ultimately drifted outside of this area (fig. S3). This suggests that floating plastic debris, similarly transported by surface currents, may have originated in the subtropical western North Atlantic where currents also act to retain it. This is further supported by a numerical model based on drifter statistics (*22*). The model was initialized with a homogeneous concentration of a passive tracer and integrated forward in time. After 10 years, the tracer converged in the North Atlantic subtropical gyre with a maximum concentration 15 times its initial value. This convergence, centered at approximately 30°N, directly corresponds to the observed high plastic accumulation region (fig. S2).

Further, the model indicates that the minimum time for surface tracer (i.e., drifter or plastic) to reach the collection center from the U.S. eastern seaboard is less than 60 days, at least half the time required to travel from Europe or Africa. The influence of the Gulf Stream is particularly evident in some of the fastest propagation times—40 days from Washington, D.C., and Miami, Florida, for example—in which tracer traveled along the coast before entering the gyre interior. Although not indicative of the size or location of land-based sources, or of the age of debris, these estimates demonstrate how quickly plastic entering the ocean near major U.S. population centers could affect an area more than 1000 km offshore.

We observed no strong temporal trends in plastic concentration in the 22-year data set (Fig. 3). Large interannual variability was observed within the high plastic concentration region, and a linear fit to annual mean plastic concentration had a slope not different from zero (–20 ± 217 pieces km^{-2} $year^{-1}$; $r^2 = 0.00$, $P > 0.1$). Although the average concentration in this region did show a statistically significant increase from the 1990s to 2000s ($P = 0.0097$, 962 DOF), this increase disappeared when concentrations greater than 200,000 pieces km^{-2} (less than 1% of values) were removed ($P = 0.6947$, 1382 DOF). To address a potential sampling bias, the analysis was also performed with data from the most spatially consistent, annually repeated cruise track from Woods Hole, Massachusetts, to St. Croix, U.S. Virgin Islands. In this case, a weak but not statistically significant decreasing trend (–573 ± 265 pieces km^{-2} $year^{-1}$; $r^2 = 0.21$, $P > 0.1$) was observed in the high plastic concentration region (fig. S4). Although the nonuniform sampling in this data set cannot resolve short spatial or temporal scale variability, no robust trend was observed in the broadest region of plastic accumulation on interannual time scales and longer.

Although no direct estimates of plastic input to the ocean exist, the increase in global production of plastic materials [fivefold increase from 1976 to 2008 (*23*)] together with the increase in discarded plastic in U.S. municipal solid waste (MSW) [fourfold increase from 1980 to 2008 (*24*) (Fig. 3)] suggest that the land-based source of plastic into the ocean increased during the study period. Ocean-based sources may have decreased in response to international regulations prohibiting dumping of plastic at sea (*25*). Given the measured steady plastic concentration in the western North Atlantic, loss terms must exist to offset the presumed increase in plastic input to the ocean.

A change in the type of plastic material entering the ocean could affect the observed amount of floating debris. Density analysis of plastic samples collected at the sea surface revealed that 99% were less dense than seawater, and ele-

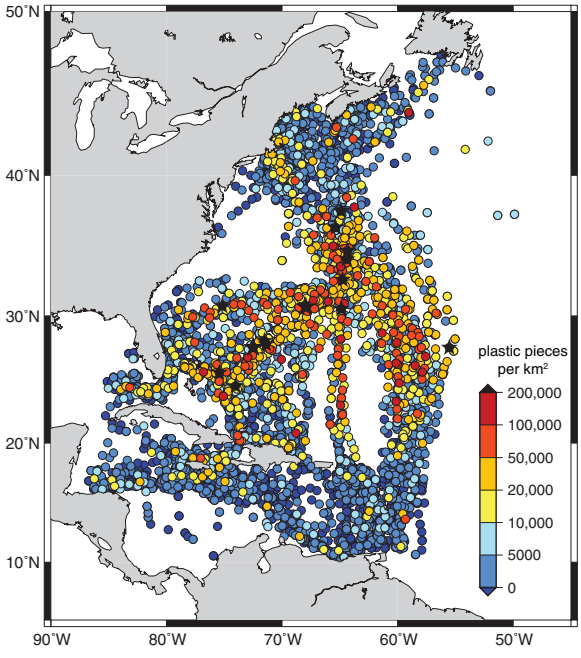

Fig. 1. Distribution of plastic marine debris collected in 6136 surface plankton net tows on annually repeated cruise tracks from 1986 to 2008 in the western North Atlantic Ocean and Caribbean Sea. Symbols indicate the location of each net tow; color indicates the measured plastic concentration in pieces km^{-2}. Black stars indicate tows with measured concentration greater than 200,000 pieces km^{-2}. Symbols are layered from low to high concentration.

mental analysis indicated properties consistent with the buoyant plastic materials high- and low-density polyethylene, and polypropylene (*26*). Between 1993 and 2008, a 24% increase in discarded buoyant plastics was estimated in U.S. MSW, totaling 14.5 million tons in 2008 (*24*, *27*). Assuming that plastic input into the ocean followed a similar trend, a measurable increase in floating plastic is expected.

Industrial resin pellets, the "raw material" of consumer plastic products, are an additional source of plastic to the ocean. In 1991, in response to a U.S. Environmental Protection Agency (EPA) study (*28*), the plastics industries voluntarily instituted a program to prevent or recapture spilled pellets (*29*). Between 1986 and 2008, we observed a statistically significant decrease in the average concentration of resin pellets in the entire region sampled (-32 ± 4 pieces km^{-2} year^{-1}; $r^2 = 0.79$, $P < 0.01$); however, the pellet concentration was only a small fraction of the total plastic material collected (annually averaged concentration ranged from 200 to 1000 pellets km^{-2}, or 1 to 16% of total pieces). This trend suggests that efforts to reduce plastic input at a land-based source may be measurably effective.

Spatial and temporal variability in surface ocean currents could result in an export of debris from the high concentration region in anomalous currents or eddies, or could alter the distribution through a shift in the large-scale circulation pattern. The convergence of modeled tracer into the subtropical gyre suggests a long residence time (10 to 100 years) (*22*), and therefore a relatively small removal by anomalous currents. Long-term shifts in the large-scale circulation pattern are driven by changes in wind forcing. Surface wind estimates (*30*) during three intervals spanning the study period (1988 to 1992, 1995 to 1999, and 2004 to 2008) showed only small variations in wind speed and direction across the North Atlantic. Therefore, it is unlikely that ocean circulation could account for an export of plastic from the region large enough to offset the presumed increase in input.

Possible sinks for floating plastic debris include fragmentation, sedimentation, shore deposition, and ingestion by marine organisms. In the marine environment, photodegradation and oxidative and hydrolytic degradation cause many common plastics to become embrittled and suffer mechanical breakdown on time scales of months (*31*, *32*). Analysis of a subset of samples (*26*) indicated that 88% were less than 10 mm in largest dimension, and most had characteristics suggesting physical deterioration such as brittleness, rough edges, or cracks. It is likely that plastic pieces ultimately become small enough to pass through the 335-μm mesh net used in this study, although the rate of mechanical degradation is not expected to vary on the time scale of the study.

In ocean conditions, the density of buoyant plastic debris may increase over time due to rapid biofilm formation and subsequent aggregation of fouling organisms (*26*, *33*). Elemental analysis of plastic samples revealed the presence of nitrogen (*26*), which is absent in virgin polyethylenes and polypropylene and thus indicative of bioaccumulation. The fate of plastic particles that become dense enough to sink below the sea surface is unknown, and we are unaware of any studies of seafloor microplastics offshore of the continental shelf. However, analysis of particle trap data in the center of the high plastic region near Bermuda shows no evidence of plastic as a substantial contributor to trapped sinking material at depths of 500 to 3200 m (*34*).

Plastic debris is a common feature of beaches on the U.S. east coast (*26*, *35*) and on island beaches in Bermuda (*17*, *36*) and the Bahamas (*17*). However, there are no published records of temporal trends in island beach deposition, and 10-year records from U.S. east coast beaches show regionally variable seasonal and long-term trends in marine debris (*35*). Finally, ingestion of plastic debris has been well documented in seabirds and large marine animals (*4*), and manipulative feeding experiments have revealed ingestion of microplastics by much smaller organisms (*5*, *37*). Because the cohort of pelagic organisms that ingest plastic, their ingestion rates, and the fate of ingested plastics are unknown, it is impossible to estimate the size of this sink.

A study of plastic microdebris in waters from the British Isles to Iceland (*5*) revealed a statistically significant increase in plastic abundance from the 1960s and 1970s to the 1980s and 1990s. However, similar to this study, no significant increase was observed between the later decades despite a large increase in plastic production and disposal. Together, our studies illustrate how poorly constrained are the sources and sinks of plastic debris in the ocean. The 22-year data set presented here provides evidence that floating plastic debris acts as a passive tracer of ocean circulation, accumulating in the large-scale subtropical

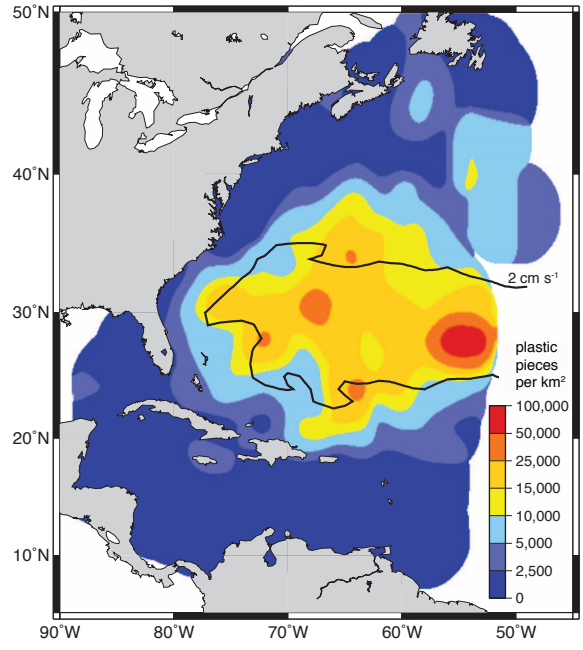

Fig. 2. Average plastic concentration (color shading, units of pieces km^{-2}) computed in 0.5° bins and smoothed with a 700-km width Gaussian filter. Black line indicates the 2 cm s^{-1} contour of the 10-year (1993 to 2002) mean surface circulation (Ekman and geostrophic components), which was computed using data from drifters, satellite altimetry, hydrographic profiles, and reanalysis winds, and assuming a surface horizontal momentum balance [data from figure 2b in (*20*)]. The highest plastic concentration is encompassed by the velocity contour, which is indicative of the subtropical convergence. This strong correspondence suggests that the convergence acts to concentrate plastic debris and demonstrates that floating plastic acts as a tracer of large-scale mean surface currents. The estimated total amount of plastic in the domain is 8×10^{10} pieces or 1100 metric tons, computed by integrating the contoured field (concentrations >2500 pieces km^{-2}) and multiplying by the average mass (1.36×10^{-5} kg) of measured plastic pieces (*26*).

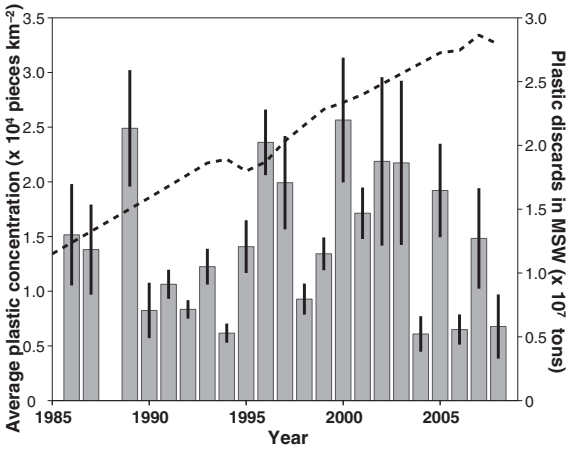

Fig. 3. Annually averaged plastic concentration in the region of highest accumulation (22° to 38°N, 54° to 79°W) from 1986 to 2008, with standard error bars. Heavy dashed line indicates concurrent time series of plastic discarded in the U.S. municipal solid waste stream (*24*). Despite a strong increase in discarded plastic, no trend was observed in plastic marine debris in the 22-year data set.

convergence as predicted by ocean physics. This analysis provides an important baseline for future monitoring efforts, as well as a quantitative assessment to accurately inform the public and policymakers of the scope of this environmental problem.

References and Notes

1. M. Sudhakar *et al.*, *Polym. Degrad. Stabil.* **92**, 1743 (2007).
2. D. Shaw, R. Day, *Mar. Pollut. Bull.* **28**, 39 (1994).
3. M. R. Gregory, *Philos. Trans. R. Soc. London Ser. B* **364**, 2013 (2009).
4. D. W. Laist, *Mar. Pollut. Bull.* **18**, 319 (1987).
5. R. C. Thompson *et al.*, *Science* **304**, 838 (2004).
6. H. Webb, R. Crawford, T. Sawabe, E. Ivanova, *Microbes Environ.* **24**, 39 (2009).
7. D. K. Barnes, *Nature* **416**, 808 (2002).
8. Y. Mato *et al.*, *Environ. Sci. Technol.* **35**, 318 (2001).
9. E. L. Teuten, S. J. Rowland, T. S. Galloway, R. C. Thompson, *Environ. Sci. Technol.* **41**, 7759 (2007).
10. E. L. Teuten *et al.*, *Philos. Trans. R. Soc. London Ser. B* **364**, 2027 (2009).
11. C. S. Wong, D. R. Green, W. J. Cretney, *Nature* **247**, 30 (1974).
12. D. G. Shaw, G. A. Mapes, *Mar. Pollut. Bull.* **10**, 160 (1979).
13. R. H. Day, D. G. Shaw, *Mar. Pollut. Bull.* **18**, 311 (1987).
14. R. H. Day, D. G. Shaw, S. E. Ignell, The quantitative distribution and characteristics of marine debris in the North Pacific Ocean, 1984–88. *Proceedings of the Second International Conference on Marine Debris U.S. Dept. Commerce, NOAA Tech. Memo* NOAA-TM-NMFS-SWFCC-154, pp. 182–211 (1990).
15. E. J. Carpenter, K. L. Smith Jr., *Science* **175**, 1240(1972).
16. J. B. Colton Jr., B. R. Burns, F. D. Knapp, *Science* **185**, 491 (1974).
17. R. J. Wilber, *Oceanus* **30**, 61 (1987).
18. Materials and methods are available as supporting material on *Science* Online.
19. The 22-year data set has been deposited with the Marine Geoscience Data System, www.marine-geo.org/tools/search/entry.php?id=NorthAtlantic_Law, and is also available at www.geomapapp.org.
20. N. Maximenko *et al.*, *J. Atmos. Ocean. Technol.* **26**, 1910 (2009).
21. Drifters are drogued at 15-m depth; only those whose drogue was attached for its full lifetime were used in this analysis. Data courtesy of (*38*).
22. International Pacific Research Center, Tracking ocean debris. *IPRC Climate* **8**, 14 (2008) (http://iprc.soest.hawaii.edu/newsletters/iprc_climate_vol8_no2.pdf).
23. PlasticsEurope Market Research Group, *The Compelling Facts About Plastics 2009* (PEMRG, Brussels, Belgium, 2009); www.plasticseurope.org/Documents/Document/20100225141556-Brochure_UK_FactsFigures_2009_22sept_6_Final-20090930-001-EN-v1.pdf.
24. U.S. Environmental Protection Agency, *Municipal Solid Waste Generation, Recycling, and Disposal in the United States: Detailed Tables and Figures for 2008* (EPA, Washington, DC, 2009); www.epa.gov/osw/nonhaz/municipal/msw99.htm.
25. International Convention for the Prevention of Pollution from Ships (MARPOL), *Annex V: Prevention of Pollution by Garbage from Ships* (1988); www.imo.org/Environment/mainframe.asp?topic_id=297
26. S. Morét-Ferguson *et al.*, *Mar. Pollut. Bull.* 10.1016/j.marpolbul.2010.07.020 (2010).
27. Polystyrene foam is buoyant in seawater, but solid polystyrene is not. The U.S. EPA report does not distinguish between the two forms; thus, polystyrene was not included in the calculation. Discarded polystyrene in MSW increased 6% from 1993 to 2008.
28. U.S. Environmental Protection Agency, *Plastic Pellets in the Aquatic Environment: Sources and Recommendations: Final Report* (EPA 842-S-93-001) (EPA, Washington, DC, 1993); www.epa.gov/owow/oceans/debris/plasticpellets/plasticpellets.pdf.
29. American Chemistry Council, *Operation Clean Sweep Pellet Handling Manual* (www.opcleansweep.org).
30. National Centers for Environmental Prediction reanalysis data are provided by the NOAA/OAR/ESRL PSD, Boulder, CO, USA, and are available at www.esrl.noaa.gov/psd.
31. A. Andrady, *J. Appl. Polym. Sci.* **39**, 363 (1990).
32. D. Feldman, *J. Polym. Env.* **10**, 163 (2002).
33. S. Ye, A. Andrady, *Mar. Pollut. Bull.* **22**, 608 (1991).
34. Since 2003, routine analysis of particle trap data from the Oceanic Flux Program time series (*39*) has found no evidence of the presence of microplastic either in visual analysis using stereo microscopy for fractions >125 μm or in carbon-to-nitrogen ratios for the <125-μm size fraction.
35. C. A. Ribic, S. B. Sheavly, D. J. Rugg, E. S. Erdmann, *Mar. Pollut. Bull.* **60**, 1231 (2010).
36. M. Gregory, *Mar. Environ. Res.* **10**, 73 (1983).
37. E. R. Graham, J. T. Thompson, *J. Exp. Mar. Biol. Ecol.* **368**, 22 (2009).
38. Global Drifter Program, www.aoml.noaa.gov/phod/dac/gdp.html.
39. Oceanic Flux Program time series; http://ecosystems.mbl.edu/conte/ofp/index.html.

40. We thank the thousands of students and staff at Sea Education Association who collected plastic samples onboard the research vessel *Westward* and the sailing school vessel *Corwith Cramer*. This work was supported by the National Science Foundation (OCE-0842727) and the Hollis and Ermine Lovell Charitable Foundation. N.A.M. and J.H. were supported by the National Fish and Wildlife Foundation (2008-0066-006); the NASA Physical Oceanography Program through membership in its Ocean Surface Topography Science Team (NNX08AR49G); and the Japan Agency for Marine-Earth Science and Technology (JAMSTEC), NASA (NNX07AG53G), and the National Oceanic and Atmospheric Administration (NA17RJ1230), which sponsor research at the International Pacific Research Center.

Supporting Online Material

www.sciencemag.org/cgi/content/full/science.1192321/DC1
Materials and Methods
Figs. S1 to S4
References

14 May 2010; accepted 30 July 2010
Published online 19 August 2010;
10.1126/science.1192321
Include this information when citing this paper.

Graphene Visualizes the First Water Adlayers on Mica at Ambient Conditions

Ke Xu,*† Peigen Cao,* James R. Heath‡

The dynamic nature of the first water adlayers on solid surfaces at room temperature has made the direct detection of their microscopic structure challenging. We used graphene as an atomically flat coating for atomic force microscopy to determine the structure of the water adlayers on mica at room temperature as a function of relative humidity. Water adlayers grew epitaxially on the mica substrate in a layer-by-layer fashion. Submonolayers form atomically flat, faceted islands of height 0.37 ± 0.02 nanometers, in agreement with the height of a monolayer of ice. The second adlayers, observed at higher relative humidity, also appear icelike, and thicker layers appear liquidlike. Our results also indicate nanometer-scale surface defects serve as nucleation centers for the formation of both the first and the second adlayers.

Water coats all hydrophilic surfaces under ambient conditions, and the first water adlayers on a solid often dominate the surface behavior (*1*–*4*). Although scanning tunneling microscopy (STM) and other ultrahigh vacuum surface characterization techniques have been extensively used to study water (ice) adlayers on solids at cryogenic temperatures (*1*, *2*), such techniques are not applicable to room-temperature studies because of the high vapor pressure of water (*2*, *3*). Various optical methods have been used at ambient conditions to probe the averaged properties of water adlayers over macroscopic areas (*3*, *5*–*7*). Atomically resolved studies have remained challenging. For example, although thin ice layers have been studied with atomic force microscopy (AFM) below freezing temperatures (*8*, *9*), reliable AFM imaging of water adlayers under ambient conditions is confounded by tip-sample interactions (*2*). For example, the capillary menisci formed between the tip and the sample strongly perturb the water adlayers on solids (*10*).

Scanning polarization force microscopy (SPFM) has been used to image water adlayers (*2*, *11*, *12*). For SPFM, the tip-sample distance is kept at tens of nanometers. By briefly contacting the tip on a mica surface to induce capillary condensation, metastable islandlike structures were observed in SPFM images. These islands were interpreted as a second adlayer on a monolayer of water (*2*, *12*). However, the lateral resolution of SPFM is relatively low, and the measured apparent heights reflect local polarizability instead of actual heights. Furthermore, the structure of the first adlayer was not observed, likely because of the low lateral resolution and/or the dynamic nature of the first adlayer (*12*).

Kavli Nanoscience Institute and Division of Chemistry and Chemical Engineering, California Institute of Technology, MC 127-72, Pasadena, CA 91125, USA.

*These authors contributed equally to this work.
†Present address: Department of Chemistry and Chemical Biology, Harvard University, 12 Oxford Street, Cambridge, MA 02138, USA.
‡To whom correspondence should be addressed. E-mail: heath@caltech.edu

Here, we report on the use of monolayer graphene sheets as ultrathin coatings for enabling an AFM study of the first water adlayers on mica. Sputtered carbon is commonly used to coat biological systems, such as cells, for electron microscopy imaging. The carbon enables the imaging experiments by providing a protective (and conductive) coating. The graphene coating used here plays a somewhat similar role; graphene can tightly seal what are otherwise elusive adlayers and, stably "fix" the water adlayer structures, thus permitting the detection of the structure of the first water adlayers under ambient conditions. Humidity-dependent experiments further reveal how the structure of the water adlayers evolves at the nanometer and molecular scale.

Graphene sheets were deposited onto the (001) surface of muscovite mica through the standard method of mechanical exfoliation of Kish graphite flakes (*13*, *14*). We readily identified graphene monolayers, as well as bilayers and multilayers, on mica through a back-illuminated optical microscope [the mica substrate is translucent, and the graphene layers absorb white light (*15*); see fig. S1 (*16*)]. The numbers of graphene layers were unambiguously confirmed through spatially resolved Raman spectroscopy (*17*, *18*) (fig. S2).

In Fig. 1, we present typical AFM images of graphene deposited on mica at ambient conditions [room temperature; relative humidity (RH) ~ 40%]. In agreement with a recent study (*14*), we found that graphene sheets spread atomically flat on mica over areas of 100 to 200 nm on a side (fig. S6). Over larger areas, however, islandlike plateaus varying from a couple nanometers to a few micrometers in lateral size were observed across all the graphene samples (Fig. 1 and figs. S3 and S5). These plateaus appear atomically flat (fig. S6), and plateaus from different samples have the same height of 0.37 ± 0.02 nm (SE) (Fig. 1, E and G) regardless of the lateral dimensions. Although dotlike thicker features were occasionally present, no plateaus with heights smaller than ~0.35 nm were observed.

The observed plateaus are not flakes of graphene or mica layers; such structures were not observed on the exfoliated surfaces of graphite and mica or graphene deposited on SiO_2 substrates (fig. S3). In addition, the ~0.37-nm height is not consistent with the layer thicknesses of graphene (0.335 nm) or mica (0.99 nm), and, as described below, the structures themselves depended on the RH of the experimental conditions. For the case in which the edge of a monolayer graphene sheet is folded underneath itself (Fig. 1, F and G), a ~0.34-nm step height was observed for the folded graphene, whereas the same ~0.37-nm height was observed for plateaus both in and out of the folded region. Plateaus with the same height were also observed in bilayer graphene sheets, and the plateaus appeared to be continuous across monolayer-bilayer borders (fig. S3). Our phase images further indicated that the plateau structures were under the graphene sheets (fig. S4). Plateaulike structures a few tenths of nanometers in height have been noticed for multilayer graphene on mica and were also identified as gases or moisture trapped under graphene (*19*). Indeed, albeit only one atom thick, monolayer graphene is known to be robust and impermeable to liquid and gas (*20*, *21*).

The observation of atomically flat plateaus that have well-defined heights and depend on the RH indicates that the observed structures are not random gas molecules trapped between the graphene and mica surfaces but instead are ordered water adlayers (Fig. 1A). Previous SPFM studies have observed water layers on mica surfaces forming two-dimensional islands tens of nanometers to several micrometers in lateral size (*2*, *11*, *12*). The shapes and size distribution of those water islands are in good agreement with the trapped structures in Fig. 1, except that the presence of water islands smaller than a few tens of nanometers were not previously known, likely because of the ~10-nm lateral resolution of SPFM. The heights of the water islands were also not accurately determined with SPFM. The ~0.37-nm height we measured is in good agreement with the height of a monolayer of a "puckered bilayer" of ice ($c/2$ = 0.369 nm, where c is the lattice constant indicated in Fig. 1B) (*22*), a widely assumed model for how water molecules arrange in the first adlayer on a solid (*1*, *4*, *23*).

We emphasize that, although morphologically similar, the islands observed in the previous SPFM studies were the second water adlayer artificially induced on top of the first adlayer (*2*, *12*). The nature of the first adlayer was largely unknown because of the high mobility of water molecules at room temperature (*12*). As will become more evident in the RH-dependent experiments (Figs. 2 and 3), the plateaus we observed on samples prepared at ambient conditions (Fig. 1) are the first water adlayer on the mica surface: The second adlayer appears only with high frequency at RH $\gtrsim$ 90%. For our case, graphene serves as an ultrathin coating that locks the first water adlayer into fixed patterns for AFM imaging. The fixed patterns are remarkably stable: Besides preventing any appreciable changes of morphology during the several hours of our AFM operation, we found that the patterns are stable for weeks under ambient conditions (fig. S5). However, the water adlayer can become mobile again when the mica substrate is subjected to extensive bending (fig. S5). Bending causes shear and displacement of graphene on the mica surface, thus releasing the locked water. The adlayer reorganizes accordingly, reflecting its dynamic nature.

The boundaries of the islands formed by the first water adlayer often exhibited fascinating polygonal shapes with preferred angles of ~120°.

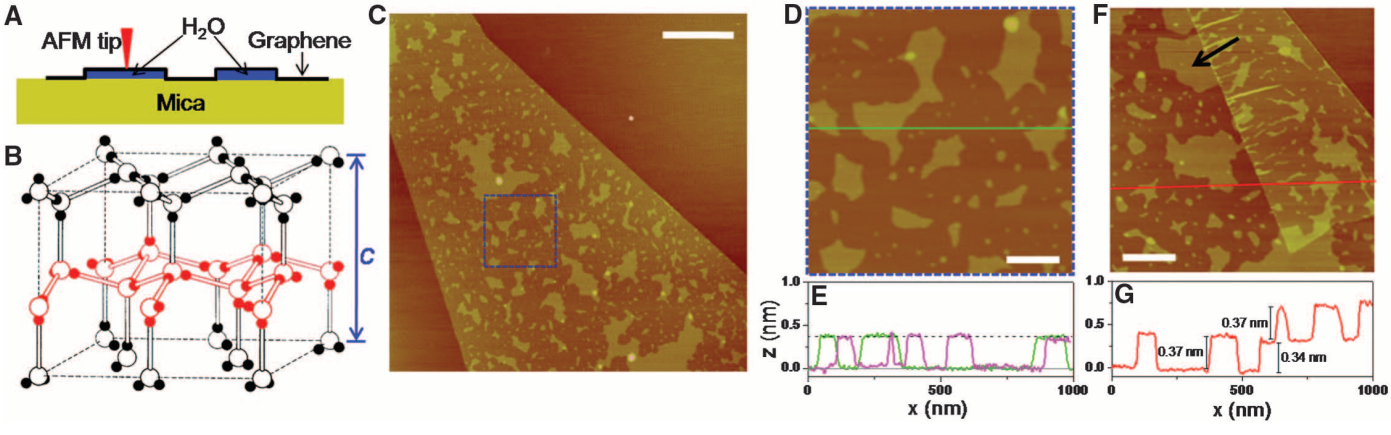

Fig. 1. Graphene visualizes the first water adlayer on mica surface at ambient conditions. (**A**) A schematic of how graphene locks the first water adlayer on mica into fixed patterns and serves as an ultrathin coating for AFM. (**B**) The structure of ordinary ice (ice I_h). Open balls represent O atoms, and smaller, solid balls represent H atoms. A single puckered bilayer is highlighted with red. Interlayer distance is $c/2$ = 0.369 nm when close to 0°C. Adapted from (*22*). (**C**) AFM image of a monolayer graphene sheet deposited on mica at ambient conditions. (**D**) A close-up of the blue square in (C). (**E**) Height profiles along the green line in (D) and from a different sample (fig. S3). The dashed line indicates z = 0.37 nm. (**F**) AFM image of another sample, where the edge of a monolayer graphene sheet is folded underneath itself. The arrow points to an island with multiple 120° corners. (**G**) The height profile along the red line in (F), crossing the folded region. Scale bars indicate 1 μm for (C) and 200 nm for (D) and (F). The same height scale (4 nm) is used for all images.

For example, the arrow in Fig. 1F points to an island with multiple 120° corners. This geometry suggests that, at ambient conditions, the first water adlayer has an icelike structure that grew epitaxially on the substrate, similar to what was previously observed for the second water adlayer (*2*, *11*). We also note that all the islands had the same height as a single layer of ice. These results are consistent with previous sum-frequency-generation spectroscopy results obtained over large areas (*6*). By contrast, we also imaged adlayers of tetrahydrofuran on mica by using graphene templating, and we observed monolayer island structures that did not exhibit polygonal shapes (fig. S7). For water, the observed sub-monolayer coverage at ambient conditions is also consistent with previous macroscopic optical studies (*3*, *5*, *7*), which indicated one statistical monolayer coverage at RH ~75% and a surface coverage of ~50% at RH ~40%. In stark contrast to mica, graphitic surfaces (including graphene) are highly hydrophobic (*24*, *25*), and water is known to only adsorb on graphitic surfaces below ~150 K (*26*). Thus, in the sandwich structure (Fig. 1A) no water is expected to come from the graphene side. The occasionally observed dotlike thicker features are possibly caused by surface defects that attract water, as discussed below.

To investigate how the water adlayers evolved as the environmental humidity varies, we deposited graphene onto mica under controlled RH (*16*) and characterized the samples with AFM at ambient conditions. These studies also permitted investigations into the role that surface defects play in the initial formation of water adlayers. Figure 2A presents an AFM image of graphene deposited on mica under dry conditions (RH ~ 2%). No islandlike structures are observed for most samples prepared in this way: Graphene lies atomically flat (*14*) (fig. S6) without observable features, except for sporadic dotlike structures ~2 nm in height, which are likely due to surface defects. This result agrees with previous optical studies (*5*, *7*), which indicated no reliably detectable water adsorption on mica surfaces at RH ~ 2%.

The measured height of monolayer graphene on bare mica surface was sensitive to the specific settings of AFM and could vary from 0.4 to 0.9 nm. We attributed this observation and similar height variations observed for monolayer graphene on SiO_2 (0.5 to 1 nm) (*17*, *27*) to the large chemical contrast between graphene and the substrate (*17*). This is why Raman spectroscopy provides such a useful probe for distinguishing graphene monolayers from bilayers and thicker films. The heights

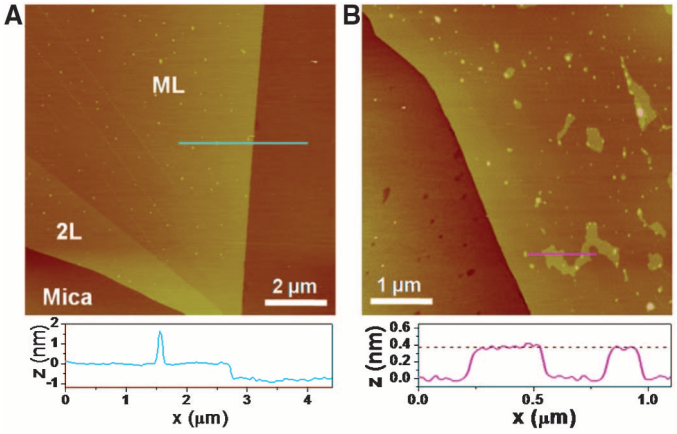

Fig. 2. AFM images of graphene deposited on mica at RH ~ 2%, revealing the influence of surface defects on water adlayer nucleation. (**A**) A representative sample. ML indicates monolayer graphene; 2L, bilayer graphene. A dotlike defect is highlighted in the height profile across the cyan line. (**B**) Image of monolayer graphene deposited on a mica surface with high density of surface defects. A height profile is given for the pink line. The dash line indicates z = 0.37 nm. The same height scale (4 nm) is used for both images.

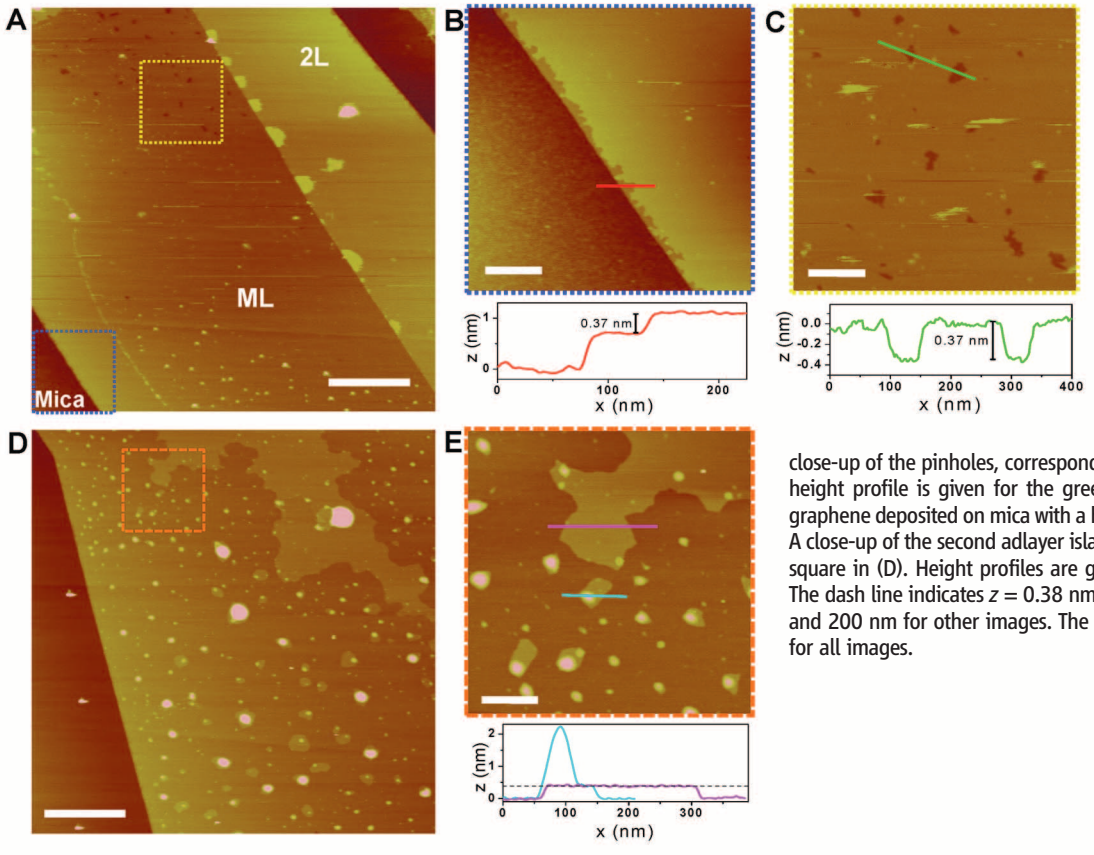

Fig. 3. AFM images of graphene deposited on mica at RH ~ 90%, revealing the structure of the second water adlayer. (**A**) A representative sample. ML, monolayer graphene; 2L, bilayer graphene. (**B**) A close-up of the graphene edge, corresponding to the blue square at the bottom left of (A). A height profile is given for the red line. The first step (~0.7 nm in height) corresponds to monolayer graphene on bare mica surface. The second step (~0.37 nm) corresponds to the first water adlayer on mica, which had been sealed by the graphene. (**C**) A close-up of the pinholes, corresponding to the yellow square in (A). A height profile is given for the green line. (**D**) Image of monolayer graphene deposited on mica with a high density of surface defects. (**E**) A close-up of the second adlayer islands, corresponding to the orange square in (D). Height profiles are given for the pink and cyan lines. The dash line indicates z = 0.38 nm. Scale bars, 1 μm for (A) and (D) and 200 nm for other images. The same height scale (4 nm) is used for all images.

of the water islands in this study, however, can be accurately determined: The AFM tip always interacted with the same material (graphene) that uniformly coats the underlying sample (Fig. 1A); variations in tip-sample interactions were avoided.

Patchy islands were occasionally observed for graphene deposited, at 2% RH, on mica surfaces that were characterized by a high density of surface defects (Fig. 2B). The same height of ~0.37 nm is again measured for those islands, indicating a single adlayer of water. Interestingly, most islands connect nearby defects, suggesting the importance of defects for water adlayer nucleation. The adlayer boundaries appear round near the defect sites but resume the 120° polygonal shape away from the defects, indicating a competition between capillary interactions and the epitaxial interactions with the substrate.

When graphene was deposited on mica at high humidity (RH ~ 90%), the samples typically appear flat over large areas (Fig. 3A). However, a closer look at the edge of the graphene sheets revealed that the graphene rides on top of a near-complete monolayer of water adlayer (Fig. 3B). At about 10 nm from the edge of the graphene-water-mica sandwich structure, water evaporated away and graphene came into direct contact with the mica surface, sealing and preserving the remaining water adlayers. The ~0.37-nm height (Fig. 3B) indicates that the trapped water is a single adlayer. Polygonal pinholes ~10 nm in lateral size and ~0.37 nm in depth were also observed on the overall continuous adlayer (Fig. 3C), indicating that the monolayer is not 100% complete.

Different results were obtained for graphene deposited, at 90% RH, on a mica characterized by a high density of surface defects (Fig. 3D). Besides a completed (no pinholes) first adlayer of water that is missing only at the graphene sheet edge, islands of various lateral sizes were observed on top of the first adlayer, often surrounding or connecting local defect sites. These islands were atomically flat (fig. S6) and were 0.38 ± 0.02 nm in height over the first adlayer (Fig. 3E), again in agreement with the height of a single puckered bilayer of ice (0.369 nm). The observed ~120° polygonal shapes of these islands agree with previous SPFM results on tip-induced second water adlayers (*2*, *11*, *12*). Thus, the islands observed in Fig. 3, D and E, are the second water adlayer, which also has an icelike structure at room temperature and is epitaxial to the first adlayer. Bulgelike features a few nanometers in height were also observed but appeared to be liquidlike (roundish) and have varying heights. No icelike islands or plateaus were observed beyond the second adlayer. Previous optical studies (*3*, *5*, *7*) indicated that statistically only a few adlayers on the mica surface exist at RH ~ 90%, but with large sample-to-sample variations, a result that is consistent with the observations reported here.

Under ambient conditions, water adlayers grow epitaxially on mica in a strictly layer-by-layer fashion: The second adlayer forms only after the first adlayer is fully completed. In the submonolayer regime, two-dimensional islands form because of interactions between adsorbed molecules, possibly akin to the Frank–van der Merwe growth mechanism in heteroepitaxy (*28*). This result is consistent with previous studies that indicated the absence of dangling O-H bonds (*6*) and a minimum in entropy (*7*) at one statistical monolayer coverage. It also explains why water adsorption isotherms cannot be modeled with theories based on continuum models (*5*). Our findings also highlight the role that surface defects play in water adsorption: Defects apparently serve as nucleation centers for the formation of both the first and second adlayers. The importance of surface defects helps explain the large sample-to-sample variations previously reported in isotherm measurements (*3*, *5*). The use of STM (*29*–*31*) to characterize the atomic structures of graphene on water adlayers represents an exciting future challenge.

References and Notes

1. P. A. Thiel, T. E. Madey, *Surf. Sci. Rep.* **7**, 211 (1987).
2. A. Verdaguer, G. M. Sacha, H. Bluhm, M. Salmeron, *Chem. Rev.* **106**, 1478 (2006).
3. G. E. Ewing, *Chem. Rev.* **106**, 1511 (2006).
4. P. J. Feibelman, *Phys. Today* **63**, 34 (2010).
5. D. Beaglehole, E. Z. Radlinska, B. W. Ninham, H. K. Christenson, *Phys. Rev. Lett.* **66**, 2084 (1991).
6. P. B. Miranda, L. Xu, Y. R. Shen, M. Salmeron, *Phys. Rev. Lett.* **81**, 5876 (1998).
7. W. Cantrell, G. E. Ewing, *J. Phys. Chem. B* **105**, 5434 (2001).
8. H. Bluhm, M. Salmeron, *J. Chem. Phys.* **111**, 6947 (1999).
9. K. Ogawa, A. Majumdar, *Microscale Thermophys. Eng.* **3**, 101 (1999).
10. R. D. Piner, C. A. Mirkin, *Langmuir* **13**, 6864 (1997).
11. J. Hu, X.-D. Xiao, D. F. Ogletree, M. Salmeron, *Science* **268**, 267 (1995).
12. L. Xu, M. Salmeron, in *Nano-Surface Chemistry*, M. Rosoff, Ed. (Dekker, New York, 2001), pp. 243–287.
13. K. S. Novoselov *et al.*, *Proc. Natl. Acad. Sci. U.S.A.* **102**, 10451 (2005).
14. C. H. Lui, L. Liu, K. F. Mak, G. W. Flynn, T. F. Heinz, *Nature* **462**, 339 (2009).
15. R. R. Nair *et al.*, *Science* **320**, 1308 (2008); published online 3 April 2008 (10.1126/science.1156965).
16. Materials and methods are available as supporting material on *Science* Online.
17. A. C. Ferrari *et al.*, *Phys. Rev. Lett.* **97**, 187401 (2006).
18. D. Graf *et al.*, *Nano Lett.* **7**, 238 (2007).
19. C. Lee *et al.*, *Science* **328**, 76 (2010).
20. J. S. Bunch *et al.*, *Nano Lett.* **8**, 2458 (2008).
21. E. Stolyarova *et al.*, *Nano Lett.* **9**, 332 (2009).
22. N. H. Fletcher, *The Chemical Physics of Ice* (Cambridge Univ. Press, London, 1970).
23. D. L. Doering, T. E. Madey, *Surf. Sci.* **123**, 305 (1982).
24. O. Leenaerts, B. Partoens, F. M. Peeters, *Phys. Rev. B* **79**, 235440 (2009).
25. Y. J. Shin *et al.*, *Langmuir* **26**, 3798 (2010).
26. A. S. Bolina, A. J. Wolff, W. A. Brown, *J. Phys. Chem. B* **109**, 16836 (2005).
27. K. S. Novoselov *et al.*, *Science* **306**, 666 (2004).
28. M. A. Herman, W. Richter, H. Sitter, *Epitaxy: Physical Principles and Technical Implementation* (Springer, Berlin, 2004).
29. M. Ishigami, J. H. Chen, W. G. Cullen, M. S. Fuhrer, E. D. Williams, *Nano Lett.* **7**, 1643 (2007).
30. E. Stolyarova *et al.*, *Proc. Natl. Acad. Sci. U.S.A.* **104**, 9209 (2007).
31. K. Xu, P. G. Cao, J. R. Heath, *Nano Lett.* **9**, 4446 (2009).

32. We thank G. Rossman for generous assistance in using the micro-Raman spectrometer and L. Qin and W. Li for helpful discussions. This work was supported by the U.S. Department of Energy, Basic Energy Sciences (grant no. DE-FG02-04ER46175).

Supporting Online Material

www.sciencemag.org/cgi/content/full/329/5996/1188/DC1
Materials and Methods
Figs. S1 to S6
References

27 May 2010; accepted 13 July 2010
10.1126/science.1192907

The Shifting Balance of Diversity Among Major Marine Animal Groups

J. Alroy*

The fossil record demonstrates that each major taxonomic group has a consistent net rate of diversification and a limit to its species richness. It has been thought that long-term changes in the dominance of major taxonomic groups can be predicted from these characteristics. However, new analyses show that diversity limits may rise or fall in response to adaptive radiations or extinctions. These changes are idiosyncratic and occur at different times in each taxa. For example, the end-Permian mass extinction permanently reduced the diversity of important, previously dominant groups such as brachiopods and crinoids. The current global crisis may therefore permanently alter the biosphere's taxonomic composition by changing the rules of evolution.

Although most higher taxa are affected by major marine radiations and extinctions, different groups have peaked in diversity at different times (*1*). For example, Paleozoic ocean floors were dominated by trilobites, brachiopods, and crinoids, whereas Cenozoic communities were dominated by scleractinian corals and molluscs. Long-term shifts in composition may be explained in two fundamental ways. First, they could result from persistent differences among groups in their styles of diversification (*2*, *3*). On the basis of this theory, the decline in background extinction rates through the Phanerozoic (*4*) has been attributed to the loss of groups with high intrinsic turnover rates (*5*). Second, shifts could reflect isolated adaptive radiations or differential responses

Paleobiology Database, University of California, 735 State Street, Santa Barbara, CA 93101, USA.

*Present address: Department of Biological Sciences, Faculty of Science, Macquarie University, NSW 2109, Australia.

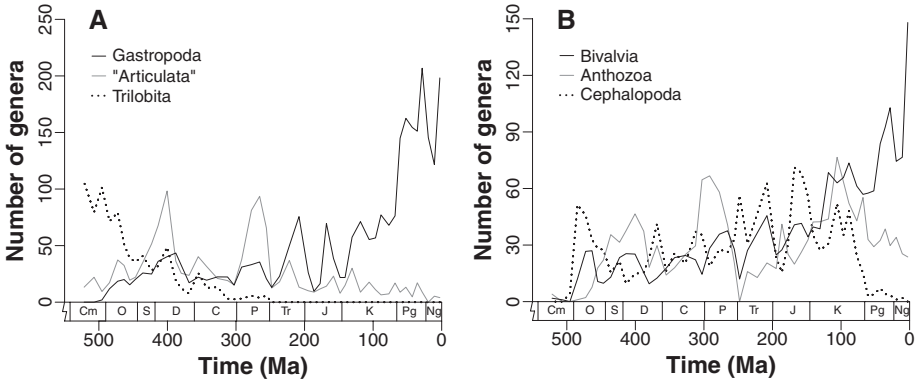

Fig. 1. Diversity trajectories of six marine groups having standardized diversity levels with peaks of at least 100 genera or medians of at least 20 genera. (**A**) Data for the most important groups in each evolutionary fauna: Trilobita (dotted line), articulate Brachiopoda (gray line), and Gastropoda (black line). (**B**) Data for other important groups: Cephalopoda (dotted line), Anthozoa (gray line), and Bivalvia (black line).

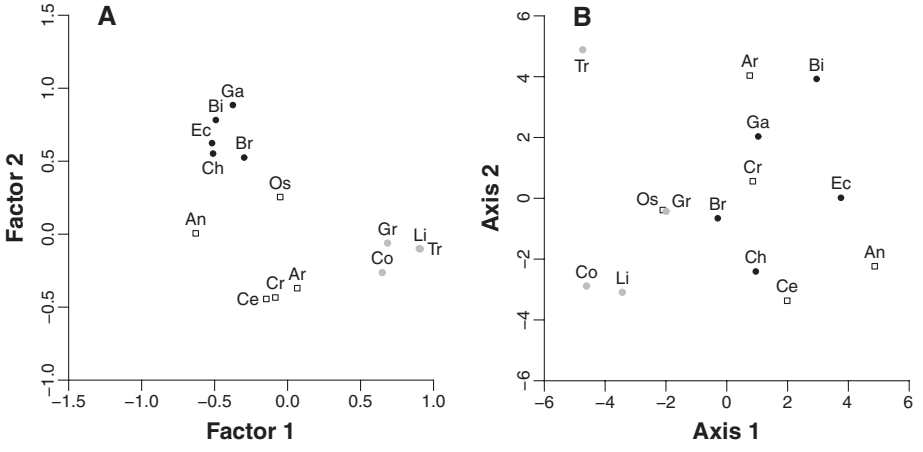

Fig. 2. Multivariate ordinations of diversity estimates for 14 major marine animal higher taxa ranging across 50 time intervals (Fig. 1). Similar results were obtained (*14*) by analyzing Sepkoski's family- and genus-level compendia (*21*). Points are identified by the first two letters of group names. Groups are Trilobita, Linguliformea, Graptolithina, and Conodonta (Cambrian fauna, gray circles); Anthozoa, Ostracoda, nonlinguliform Brachiopoda (articulates, Ar), Cephalopoda, and Crinoidea (Paleozoic fauna, open squares); and Bryozoa, Bivalvia, Gastropoda, Echinoidea, and Chondrichthyes (Modern fauna, solid circles). (**A**) Factor analysis of raw counts with zero values included, as in (*2*). (**B**) Principal coordinates analysis of logged and differenced counts. Similar results are yielded by other methods, such as hierarchical cluster analysis (*14*).

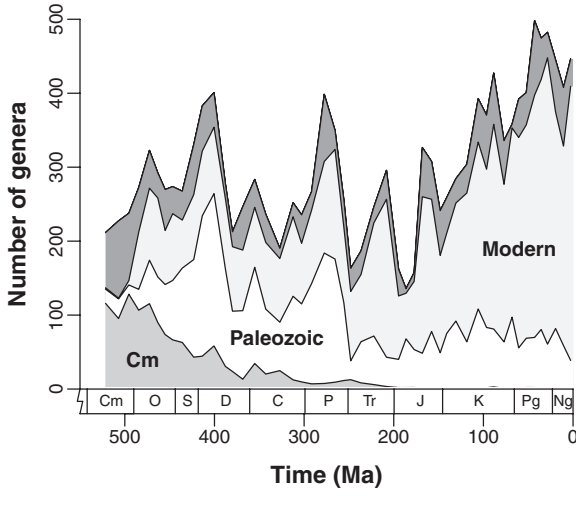

Fig. 3. Sampling-standardized Phanerozoic diversity curve for the three marine evolutionary faunas. Values are summed curves for constituent groups that were generated independently (*14*). Unlabeled area represents groups not assigned to a fauna.

to mass extinctions. Numerical models of Phanerozoic marine diversification have often combined both perspectives (*3*, *6*, *7*).

If diversity trends are determined by group-specific characteristics and these characteristics are invariant, then mass extinctions merely delay the rise of groups that are fated to prosper (*3*). Furthermore, given these assumptions, it is possible to predict which groups will recover most quickly from the mass extinction that is now occurring. Successful groups would be expected to exhibit logistic dynamics [a decline of growth rates as diversity rises (*3*, *8*, *9*)]. Each group's intrinsic rate of increase and equilibrium diversity level must be quantified in order to test this prediction.

Robust estimates of these dynamical parameters cannot be obtained simply by fitting a line to a fossil diversity curve [a kinetic analysis sensu (*3*)] because apparent plateaus can be generated by other processes such as random walks. Modeling net diversification rates (a dynamic analysis) removes this ambiguity. These rates are less likely to be misleading because they generally show weak trends and little autocorrelation. They can be quantified easily by taking log ratios of consecutive values (*9*).

Here, I address these questions using Phanerozoic-scale diversity counts for the 14 most commonly occurring marine animal higher taxa, including six major groups (Fig. 1). The counts were generated from taxonomic occurrences housed in the Paleobiology Database (*10*). Other recent studies have used the same resource (*9*, *11*–*13*). Data for other groups are not sufficient to yield complete and precise time series.

The counts were generated by sampling standardization—randomly drawing a comparable amount of data in each time interval (*9*, *12*). However, the method used in this paper differs from simple standardization because it ensures fair representation of uncommon taxa. It works by tracking coverage of the occurrence-frequency distribution, meaning the sum of frequencies of taxa that have been seen at least once in a given subsample. Sampling continues until coverage (as opposed to sheer sample size) reaches a specified target (*14*). Subsampling and frequency coverage are long-established concepts in the ecological literature, but they have not been bound together methodologically. The algorithm derived here can be used to estimate the relative number of classes in any set of sampling universes regardless of whether the data are biological (*14*).

Most individual groups were found to diversify without any change in underlying dynamics for periods of at least 200 million years. More specifically, almost every group's curve exhibits some kind of logistic growth. This finding is based on a nonparametric maximum likelihood analysis comparing observed and predicted changes in diversity (*14*). Random walk and exponential models can be excluded for eight groups, and multiphase logistic growth models were favored (Akaike weight > 0.75) for Linguliformea, Bryozoa, and Echinoidea.

Similarly, previous studies suggested that subclades of particular marine groups such as bryozoans (*15*), bivalves (*16*), and gastropods (*17*) experienced density-dependence. Although the curves for Anthozoa, Trilobita, Gastropoda, and Bivalvia could be fit to an exponential model, support for other models is as strong or stronger in all of these cases.

These findings refute the idea that diversity trends, including successive replacements of groups, are a function of exponential or random growth interrupted by mass extinctions (*6*, *7*, *18*). Such arguments only ever seemed plausible because biases in older data sets, including the greater quantity and quality of data in the Cenozoic, created the appearance of a steep post-Paleozoic increase (*12*). These biases also obscured large, rapid shifts in diversity such as the Cambrian explosion and the mid-Jurassic radiation.

Sepkoski (*3*) categorized marine animals into so-called Cambrian, Paleozoic, and Modern evolutionary faunas on the basis of shared curve shapes. This categorization has served as a benchmark for macroevolutionary research at the Phanerozoic scale [for example, (*19*)]. Sepkoski (*2*, *3*, *20*) also modeled the rate and timing of taxonomic replacements by assuming that each fauna has diversified logistically and that the underlying logistic parameters have held constant through the Phanerozoic. If so, then recoveries from any mass extinction should be predictable, and extinctions should not alter the fate of the major groups (*3*).

Curve-shape similarities are easily recognized by applying multivariate ordination methods (*20*), and a factor analysis of the 14 diversity curves recovers the three original categories (Fig. 2A). Furthermore, the summed diversity trajectory of each evolutionary fauna is proportionately about the same in either Sepkoski's original family-level compendium (*3*, *20*), his genus-level compendium (*21*), or the data set analyzed here (Figs. 1 and 3). The general resilience of the proportions is noteworthy because the global diversity curve (Fig. 3) differs from all published curves that stem from Sepkoski's compendia (*3*, *21*, *22*). The older curves feature proportionately lower Cambrian and Modern faunal diversity in the Paleozoic. These differences result from methods of sampling and counting taxa (*12*, *14*) and do not reflect important discrepancies in the underlying data (*12*).

Because net diversification rates yield evidence about process instead of pattern, it is necessary to show whether Sepkoski's scheme also summarizes such rates adequately. The best approach is to perform a principal coordinates analysis on a Euclidean distance matrix derived from the rates. Doing so allows ignoring undefined values for extinct groups while using the same similarity metric that underlies factor analysis (*14*). This ordination fails to separate the three faunas cleanly: Although some structure is evident, the Paleozoic groups are widely scattered (Fig. 2B).

Sepkoski himself went into great detail about exceptions to his model (*3*, *20*), and later analyses of his data also called the evolutionary fauna scheme into question (*23*). Furthermore, a three-fauna pattern can be generated by factoring data produced with a simple simulation (*6*), and little correspondence exists between traditional faunal membership and ecological attributes such as mineralogy, motility, physiological buffering, trophic level, or habitat affinity (*13*, *24*). Thus, the three-fauna pattern seems only to summarize coincidental peaks in diversity trajectories (*20*).

A far more important problem with Sepkoski's model is that equilibrium diversity levels have changed once or even twice in most taxonomic groups (table S1). The overall diversity trend (Fig. 3) also suggests offset logistic growth (table S1) (*9*). These changes in equilibrium points are unpredictable in the sense that they come at very different geological times and are equally likely to involve increases or decreases, as shown by the lack of correlation between early Paleozoic and Cenozoic carrying capacities (Spearman's $\rho = 0.264$; $P = 0.435$) (table S2).

Sepkoski's model implies that average diversification rates are a good predictor of long-term success. If so, then dominant groups such as bivalves may be expected to recover quickly from the current mass extinction. However, there is no strong correlation of median net diversification rates and Plio-Pleistocene diversity for living groups ($\rho = 0.437$; $P = 0.179$) (table S2). The result changes if we add zero diversity values to represent the three extinct groups ($\rho = 0.654$; $P = 0.011$), but this observation merely demonstrates that groups with unfavorable diversification rates had already been sifted out (*5*) by the early Mesozoic.

The lack of a relationship between average rates and eventual success is a side effect of the Permo-Triassic mass extinction, which was the worst in the history of life on Earth (*4*, *9*). The groups that might otherwise have been the most diverse today can be identified by starting with the end-Permian diversity estimates, ignoring changes going into the Early Triassic, and using the post-Paleozoic rates to project forward up to the Recent. In contrast, these adjusted diversity estimates are well correlated with median diversification rates ($\rho = 0.664$; $P = 0.031$). Moreover, there is a strong negative correlation between median overall rates and rates for this boundary ($\rho = -0.655$; $P = 0.034$). Examples of otherwise successful groups that suffered include anthozoans, bivalves, gastropods, crinoids, and "articulate" brachiopods. The first three eventually recovered, but the last two stagnated at low diversity levels. Effectively, then, the Permo-Triassic mass extinction reset the clock on diversification and overturned the balance of groups.

These factors together explain why individual diversity curves are so idiosyncratic (Fig. 1). For example, the key "Cambrian fauna" clade Trilobita rose immediately to dominance and then declined swiftly, unlike any other group (Fig. 1A). The curve for nonlinguliform brachiopods (articulates) includes two large, distinctive Paleozoic peaks (Fig. 1A) that relate to radiations in particular subclades (*14*). Anthozoa and Cephalopoda were both important throughout the Paleozoic and Mesozoic (Fig. 1B), but peaks in their curves do not match, and shelled cephalopods were the only large group to suffer a large and irreversible decline at the Cretaceous-Paleogene boundary.

Meanwhile, the two major existing classes—Bivalvia and Gastropoda—achieved their prominence in different ways. The former increased throughout the Phanerozoic (*16*), although the current data depict a shallow trend (Fig. 1B). Meanwhile, gastropods tracked a modest plateau throughout the Paleozoic and Mesozoic before suddenly rising to a new equilibrium level near the end of the Cretaceous (Fig. 1A). This clear offset reflects the adaptive radiation of the carnivorous clade Neogastropoda and corresponds to the Mesozoic marine revolution, which involved an "arms race" between gastropods and shell-crushing predators (*25*).

Global diversity should rebound from today's extinction crisis within roughly the equivalent of a geological period (*9*). However, it is not possible to predict changes in taxonomic composition (table S1), which are more ecologically and evolutionarily important than total counts of taxa. The most severe extinctions also have unexpected impacts on the relative abundance of closely related groups (*26*), the shape of species-abundance distributions (*11*), and patterns of epifaunal and infaunal tiering (*27*). Thus, it would be unwise to assume that any large number of species can be lost today without forever altering the basic biological character of Earth's oceans.

References and Notes

1. N. D. Newell, *J. Paleontol.* **26**, 371 (1952).
2. J. J. Sepkoski Jr., *Paleobiology* **5**, 222 (1979).
3. J. J. Sepkoski Jr., *Paleobiology* **10**, 246 (1984).
4. D. M. Raup, J. J. Sepkoski Jr., *Science* **215**, 1501 (1982).
5. N. L. Gilinsky, *Paleobiology* **20**, 445 (1994).
6. A. Hoffman, E. J. Fenster, *Palaeontology* **29**, 655 (1986).
7. M. J. Benton, *Science* **268**, 52 (1995).
8. J. J. Sepkoski Jr., *Paleobiology* **4**, 223 (1978).
9. J. Alroy, *Proc. Natl. Acad. Sci. U.S.A.* **105** (suppl. 1), 11536 (2008).
10. http://paleodb.org.
11. P. J. Wagner, M. A. Kosnik, S. Lidgard, *Science* **314**, 1289 (2006).
12. J. Alroy *et al.*, *Science* **321**, 97 (2008).
13. W. Kiessling, M. Aberhan, L. Villier, *Nat. Geosci.* **1**, 527 (2008).
14. Materials and methods are available as supporting material on *Science* Online.
15. J. J. Sepkoski Jr., F. K. McKinney, S. Lidgard, *Paleobiology* **26**, 7 (2000).
16. A. I. Miller, J. J. Sepkoski Jr., *Paleobiology* **14**, 364 (1988).
17. P. J. Wagner, *Paleobiology* **21**, 410 (1995).
18. S. M. Stanley, *Paleobiology* **33**, 1 (2007).
19. S. E. Peters, *Nature* **454**, 626 (2008).
20. J. J. Sepkoski Jr., *Paleobiology* **7**, 36 (1981).
21. J. J. Sepkoski Jr., *J. Paleontol.* **71**, 533 (1997).
22. R. K. Bambach, *Geobios* **32**, 131 (1999).
23. J. Alroy, *Evol. Ecol. Res.* **6**, 1 (2004).
24. R. K. Bambach, A. H. Knoll, J. J. Sepkoski Jr., *Proc. Natl. Acad. Sci. U.S.A.* **32**, 6854 (2002).
25. G. Vermeij, *Paleobiology* **3**, 245 (1977).
26. F. K. McKinney, S. Lidgard, J. J. Sepkoski Jr., P. D. Taylor, *Science* **281**, 807 (1998).
27. D. J. Bottjer, W. I. Ausich, *Paleobiology* **12**, 400 (1986).

28. I thank J. Sepkoski and D. Raup for asking the questions I seek to answer. I am grateful to M. Foote, S. Holland,

G. Hunt, A. Miller, T. Olszewski, and P. Wagner for their suggestions; M. Kosnik and A. Miller for reviews; and M. Foote for verifying that my subsampling algorithms were programmed correctly. Numerous contributors to the Paleobiology Database made this study possible, and I am particularly grateful to M. Clapham, A. Hendy, and W. Kiessling for recent contributions. Research described here was funded by donations from anonymous private individuals having no connection to it. This is Paleobiology Database publication 117.

Supporting Online Material
www.sciencemag.org/cgi/content/full/329/5996/1191/DC1
Materials and Methods
Figs. S1 to S9
Tables S1 and S2
References

22 March 2010; accepted 30 June 2010
10.1126/science.1189910

The Spread of Behavior in an Online Social Network Experiment

Damon Centola

How do social networks affect the spread of behavior? A popular hypothesis states that networks with many clustered ties and a high degree of separation will be less effective for behavioral diffusion than networks in which locally redundant ties are rewired to provide shortcuts across the social space. A competing hypothesis argues that when behaviors require social reinforcement, a network with more clustering may be more advantageous, even if the network as a whole has a larger diameter. I investigated the effects of network structure on diffusion by studying the spread of health behavior through artificially structured online communities. Individual adoption was much more likely when participants received social reinforcement from multiple neighbors in the social network. The behavior spread farther and faster across clustered-lattice networks than across corresponding random networks.

Many behaviors spread through social contact (*1*–*3*). As a result, the network structure of who is connected to whom can critically affect the extent to which a behavior diffuses across a population (*2*–*8*). There are two competing hypotheses about how network structure affects diffusion. The "strength of weak ties" hypothesis predicts that networks with many "long ties" (e.g., "small-world" topologies) will spread a social behavior farther and more quickly than a network in which ties are highly clustered (*4*–*6*). This hypothesis treats the spread of behavior as a simple contagion, such as disease or information: A single contact with an "infected" individual is usually sufficient to transmit the behavior (*2*). The power of long ties is that they reduce the redundancy of the diffusion process by connecting people whose friends do not know each other, thereby allowing a behavior to rapidly spread to other areas of the network (*3*–*5*). The ideal case for this lack of redundancy is a "random" network, in which, in expectation for a large population, each of an individual's ties reaches out to different neighborhoods (*4*, *9*). The other hypothesis states that, unlike disease, social behavior is a complex contagion: People usually require contact with multiple sources of "infection" before being convinced to adopt a behavior (*2*). This hypothesis predicts that because clustered networks have more redundant ties, which provide social reinforcement for adoption, they will better promote the diffusion of behaviors across large populations (*2*, *7*). Despite the scientific (*6*, *7*, *10*) and practical (*1*, *2*, *11*) importance of understanding the spread of behavior through social networks, an empirical test of these predictions has not been possible, because it requires the ability to independently vary the topological structure of a social network (*12*).

I tested the effects of network structure on diffusion using a controlled experimental approach. I studied the spread of a health behavior through a network-embedded population by creating an Internet-based health community, containing 1528 participants recruited from health-interest World Wide Web sites (*13*).

Each participant created an anonymous online profile, including an avatar, a user name, and a set of health interests. They were then matched with other participants in the study—referred to as "health buddies"—as members of an online health community. Participants could not contact their health buddies directly, but they could receive emails from the study informing them of their health buddies' activities. To preserve anonymity and to prevent people from trying to identify friends who may have also signed up for the study (or from trying to contact health buddies outside the context of the experiment), I blinded the identifiers that people used. Participants made decisions about whether or not to adopt a health behavior based on the adoption patterns of their health buddies. The health behavior used for this study was the decision to register for an Internet-based health forum, which offered access and rating tools for online health resources (*13*).

The health forum was not known (or accessible) to anyone except participants in the experiment. This ensured that the only sources of encouragement that participants had to join the forum were the signals that they received from their health buddies. The forum was populated with initial ratings to provide content for the early adopters. However, all subsequent content was contributed by the participants who joined the forum.

Participants arriving to the study were randomly assigned to one of two experimental conditions—a clustered-lattice network and a random network—that were distinguished only by the topological structure of the social networks (Fig. 1). In the clustered-lattice–network condition, there was a high level of clustering (*5*, *6*, *13*) created by redundant ties that linked each node's neighbors to one another. The random network condition was created by rewiring the clustered-lattice network via a permutation algorithm based on the small-world–network model (*6*, *13*–*15*). This ensured that each node maintained the exact same number of neighbors as in the clustered network (that is, a homogeneous degree distribution), while simultaneously reducing clustering in the network and eliminating redundant ties within and between neighborhoods (*4*, *6*, *14*).

The network topologies were created before the participants arrived, and the participants could

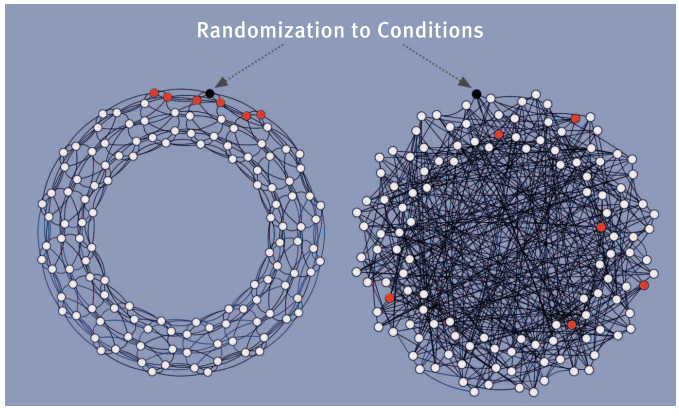

Fig. 1. Randomization of participants to clustered-lattice and random-network conditions in a single trial of this study (N = 128, Z = 6). In each condition, the black node shows the focal node of a neighborhood to which an individual is being assigned, and the red nodes correspond to that individual's neighbors in the network. In the clustered-lattice network, the red nodes share neighbors with each other, whereas in the random network they do not. White nodes indicate individuals who are not connected to the focal node.

Sloan School of Management, Massachusetts Institute of Technology, Cambridge, MA 02142, USA. E-mail: dcentola@mit.edu

not alter the topology in which they were embedded (e.g., by making new ties). In both conditions, each participant was randomly assigned to occupy a single node in one network. The occupants of the immediately adjacent nodes in the network (i.e., the network neighbors) constituted a participant's health buddies (*13*). Each node in a social network had an identical number of neighbors as the other nodes in the network, and participants could only see the immediate neighbors to whom they were connected.

Consequently, the size of each participant's social neighborhood was identical for all participants within a network and across conditions. More generally, every aspect of a participant's experience before the initiation of the diffusion dynamics was equivalent across conditions, and the only difference between the conditions was the pattern of connectedness of the social networks in which the participants were embedded. Thus, any differences in the dynamics of diffusion between the two conditions can be attributed to the effects of network topology.

There are four advantages of this experimental design over observational data. (i) The present study isolates the effects of network topology, independent of frequently co-occurring factors such as homophily (*3*, *16*), geographic proximity (*17*), and interpersonal affect (*4*, *18*), which are easily conflated with the effects of topological structure in observational studies (*2*, *3*, *11*). (ii) I study the spread of a health-related behavior that is unknown to the participants before the study (*13*), thereby eliminating the effects of nonnetwork factors from the diffusion dynamics, such as advertising, availability, and pricing, which can confound the effects of topology on diffusion when, for example, the local structure of a social network correlates with greater resources for learning about or adopting an innovation (*11*, *19*). (iii) This study eliminates the possibility for social ties to change and thereby identifies the effects of network structure on the dynamics of diffusion without the confounding effects of homophilous tie formation (*1*, *20*). (iv) Finally, this design allows the same diffusion process to be observed multiple times, under identical structural conditions, thus allowing the often stochastic process of individual adoption (*21*) to be studied in a way that provides robust evidence for the effects of network topology on the dynamics of diffusion.

I report the results from six independent trials of this experimental design, each consisting of a matched pair of network conditions. In each pair, participants were randomized to either a clustered-lattice network or a corresponding random network (*13*). This yielded 12 independent diffusion processes. Diffusion was initiated by selecting a random "seed node," which sent signals to its network neighbors encouraging them to adopt a health-related behavior—namely, registering for a health forum Web site (*13*). Every time a participant adopted the behavior (i.e., registered for the health forum), messages were sent to her health buddies inviting them to adopt. If a participant had multiple health buddies who adopted the behavior, then she would receive multiple signals, one from each neighbor. The more neighbors who adopted, the more reinforcing signals a participant received. The sequence of adoption decisions made by the

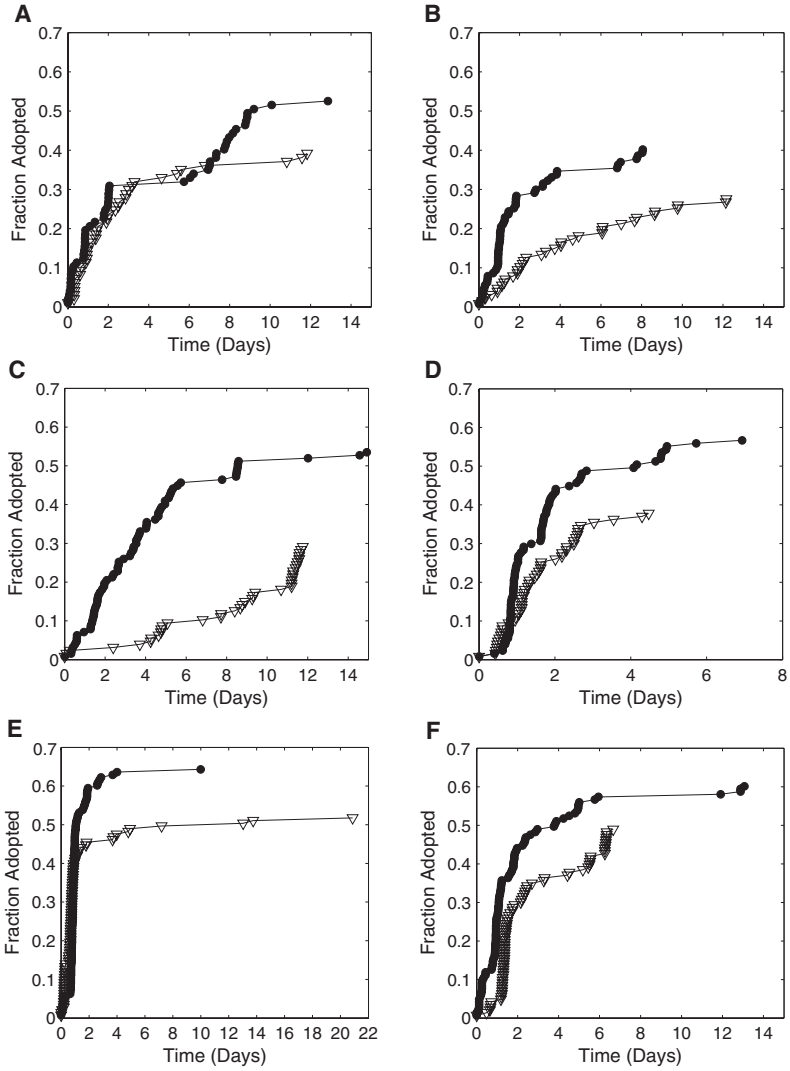

Fig. 2. Time series showing the adoption of a health behavior spreading through clustered-lattice (solid black circles) and random (open triangles) social networks. Six independent trials of the study are shown, including (**A**) $N = 98$, $Z = 6$, (**B** to **D**) $N = 128$, $Z = 6$, and (**E** and **F**) $N = 144$, $Z = 8$. The success of diffusion was measured by the fraction of the total network that adopted the behavior. The speed of the diffusion process was evaluated by comparing the time required for the behavior to spread to the greatest fraction reached by both conditions in each trial.

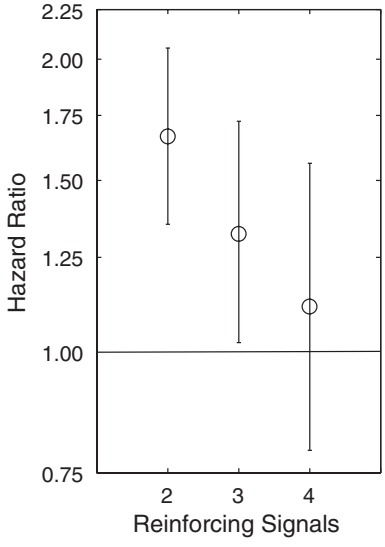

Fig. 3. Hazard ratios for adoption for individuals receiving two, three, and four social signals. The hazard ratio g indicates that the likelihood of adoption increases by a factor of g for each additional signal k, compared to the likelihood of adoption from receiving $k - 1$ signals. The 95% confidence intervals from the Cox proportional hazards model are shown by error bars. The effect of an additional signal on the likelihood of adoption is significant if the 95% confidence interval does not contain $g = 1$ (*13*).

members of each social network provides a precise time series of the spread of the behavior through the population. It also provides an exact record of the number of signals required for individuals to adopt the behavior. The starting time (time = 0) for each diffusion process corresponds to the instant when the seed node was activated and the initial signals were sent. For each trial, the diffusion process was allowed to run for 3 weeks (~1.8 million seconds). To test for the possible effects of population size (N) and degree (Z, the number of health buddies each person had) on the diffusion dynamics, I used three different versions of the experiment: (i) $N = 98$, $Z = 6$; (ii) $N = 128$, $Z = 6$; and (iii) $N = 144$, $Z = 8$ (*13*). The modest range of population sizes tested and the correspondingly narrow range of degrees were due to the challenges of recruiting large numbers of people simultaneously. Among the networks I used, there were no effects of population size (*13*).

The results show that network structure has a significant effect on the dynamics of behavioral diffusion. Surprisingly, the topologies with greater clustering and a larger diameter were much more effective for spreading behavior. Figure 2 shows the time series generated by the six independent trials of the experiment. Adoption typically spread to a greater fraction of the population in the clustered networks (solid black circles) than in the random networks (open triangles). On average, the behavior reached 53.77% of the clustered networks, whereas only 38.26% of the population adopted in the random networks (*13*). I also found that the behavior diffused more quickly in the clustered networks than in the random networks. The average rate of diffusion in the clustered networks (0.2820×10^{-3} nodes/s) was more than four times faster than that of the random condition (0.0643×10^{-3} nodes/s). Differences in both the success and the rate of diffusion between network conditions are statistically significant ($P < 0.01$ using the Wilcoxon rank sum–Mann-Whitney U test) (*13*).

The experimental findings were qualitatively the same across different network and neighborhood sizes. However, networks with a greater degree ($Z = 8$) performed better than those with a lower degree ($Z = 6$). Although this finding is consistent with the hypothesis that more redundant ties between neighborhoods can improve the global spread of behavior, it may also indicate that other topological features, such as degree and density, are relevant factors affecting behavioral diffusion (*2*, *7*). This suggests important avenues for future research.

At the individual level, the results (Fig. 3) show that redundant signals significantly increased the likelihood of adoption; social reinforcement from multiple health buddies made participants much more willing to adopt the behavior. Figure 3 compares the baseline likelihood of adoption after receiving one social signal to the increased likelihood of adoption for nodes receiving second, third, and fourth reinforcing signals. Participants were significantly more likely to adopt after receiving a second signal than after receiving only one signal ($P < 0.001$ using the Cox proportional hazards model). Receiving a third signal also significantly increased the likelihood of adoption, but with a smaller marginal-effect size ($P < 0.05$, Cox proportional hazards model) (*13*). Additional signals had no significant effect. This can be attributed to the attenuation of the sample size as the number of signals increased.

A secondary, but important, issue related to adoption is the level of commitment that individuals have to a behavior once they have adopted it. To investigate the effects of social reinforcement on individuals' level of engagement with the health forum, I compared the number of return visits to the forum after registering, for adopters grouped by the number of social signals that they received (Fig. 4) (participants could not receive additional signals once they had registered). Figure 4 shows pairwise comparisons of the number of return visits for adopters receiving only one signal (solid lines) versus those receiving two to five signals (dashed lines in panels A to D, respectively). Though less than 15% of adopters receiving one signal made a return visit to the forum, more than 30% of participants receiving two signals made return visits, and 40% of participants receiving three signals made at least one return visit. Pairwise statistical comparisons between group one and groups two through five are all significant ($P < 0.01$ for all four comparisons, using the Kolmogorov-Smirnov test) (*13*), indicating that participants who received more than one social signal were significantly more likely to return to the health forum than those who only received a single signal. This suggests that there was a significant effect of social reinforcement on participants' level of engagement with the adopted behavior.

As with all experiments, design choices that aided my control of the study also put constraints on the behaviors that I could test. A key limitation of my design is that, unlike in my experiment, adopting a new health behavior is often extremely difficult in the real world. To adopt behaviors such as getting a vaccination, going on a diet, starting an exercise routine, or getting a screening, people may be required to pay the costs of time, deprivation, or even physical pain. Because of this, I expect that the need for social reinforcement would be greater for adopting these health behaviors than it was for the behavior in my study. Consequently, the diffusion of real-world health behaviors may depend even more on clustered-network structures than did the diffusion dynamics reported in my results.

An additional constraint of my study was that participants did not have any direct commu-

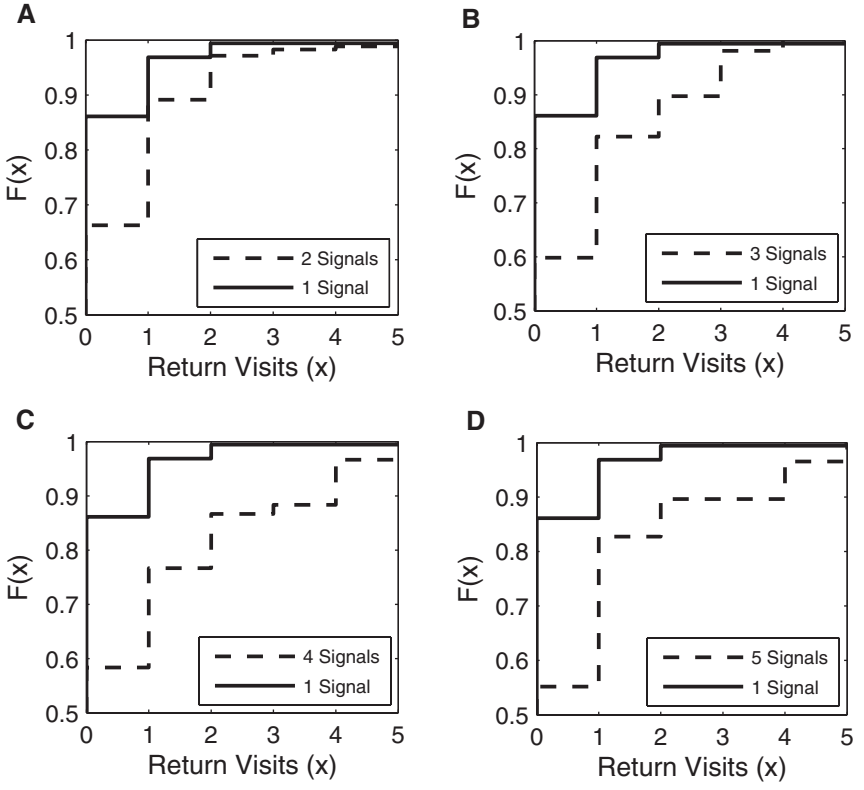

Fig. 4. Cumulative distribution functions of the number of return visits to the health forum (x) for populations of adopters grouped by the number of signals that they received. Comparisons are shown for adopters who received (**A**) one versus two signals, (**B**) one versus three signals, (**C**) one versus four signals, and (**D**) one versus five signals. All pairwise comparisons between groups two through five with each other showed no significant differences ($P > 0.4$ for all six comparisons, using the Kolmogorov-Smirnov test) (*13*).

nication with their health buddies or information about their identities. This allowed me to isolate the effects of network topology on the dynamics of diffusion without the presence of confounding variables. However, it also raises the question of what the strength of the effects of network topology would be when allowed to interact with the effects of interpersonal relationships. An important assumption of this study is that the effects of network topology will not be overwhelmed by individuals' exposure to other social factors. Previous studies have suggested that factors such as homophily and strong interpersonal affect in social ties can improve the diffusion of behaviors through social networks (*3*, *18*). In the real world, these features of social relationships tend to be highly correlated with the formation of clustered social ties (*3*, *22*, *23*). Consequently, I expect that these reinforcing factors would amplify the observed effects of clustered social networks in promoting the diffusion of health behaviors across a large population. However, new experimental designs are required to test the interaction effects of these variables (and other variables such as gender, memory, and frequency of interaction) on the spread of social behaviors.

Evidence in support of the "strength of weak ties" hypothesis has suggested that networks with high levels of local clustering and tightly knit neighborhoods are inefficient for large-scale diffusion processes (*4*, *5*, *9*). My findings show that, not only is individual adoption improved by reinforcing signals that come from clustered social ties (Fig. 3), but this individual-level effect also translates into a system-level phenomenon whereby large-scale diffusion can reach more people and spread more quickly in clustered networks than in random networks (Fig. 2). Whereas locally clustered ties may be redundant for simple contagions, like information or disease (*4*, *6*, *24*), they can be highly efficient for promoting behavioral diffusion. On the basis of these findings, I predict that public health interventions aimed at the spread of new health behaviors (for instance, improved diet, regular exercise, condom use, or needle exchange) may do better to target clustered residential networks rather than the casual contact networks across which disease may spread very quickly (*25*)—particularly if the behaviors to be diffused are highly complex (for instance, because they are costly, difficult, or contravene existing norms).

References and Notes

1. N. A. Christakis, J. H. Fowler, *N. Engl. J. Med.* **357**, 370 (2007).
2. D. Centola, M. Macy, *Am. J. Sociol.* **113**, 702 (2007).
3. E. M. Rogers, *Diffusion of Innovations* (Free Press, New York, 1995).
4. M. Granovetter, *Am. J. Sociol.* **78**, 1360 (1973).
5. D. J. Watts, *Small Worlds: The Dynamics of Networks Between Order and Randomness* (Princeton Univ. Press, Princeton, NJ, 1999).
6. D. J. Watts, S. H. Strogatz, *Nature* **393**, 440 (1998).
7. D. Centola, V. Eguiluz, M. Macy, *Phys. A* **374**, 449 (2007).
8. N. A. Christakis, J. H. Fowler, *N. Engl. J. Med.* **358**, 2249 (2008).
9. M. E. J. Newman, *J. Stat. Phys.* **101**, 819 (2000).
10. S. H. Strogatz, *Nature* **410**, 268 (2001).
11. K. P. Smith, N. A. Christakis, *Annu. Rev. Sociol.* **34**, 405 (2008).
12. M. Kearns, S. Suri, N. Montfort, *Science* **313**, 824 (2006).
13. Materials and methods are available as supporting material on *Science* Online.
14. S. Maslov, K. Sneppen, *Science* **296**, 910 (2002).
15. S. Maslov, K. Sneppen, U. Alon, in *Handbook of Graphs and Networks*, S. Bornholdt, H. G. Schuster, Eds. (Wiley-VCH, Weinheim, Germany, 2003).
16. J. M. McPherson, L. Smith-Lovin, J. M. Cook, *Annu. Rev. Sociol.* **27**, 415 (2001).
17. P. Hedstrom, *Am. J. Sociol.* **99**, 1157 (1994).
18. D. McAdam, R. Paulsen, *Am. J. Sociol.* **99**, 640 (1993).
19. L. F. Berkman, I. Kawachi, *Social Epidemiology* (Oxford Univ. Press, New York, 2000).
20. D. Centola, J. C. Gonzalez-Avella, V. Eguiluz, M. San Miguel, *J. Conf. Resl.* **51**, 905 (2007).
21. M. J. Salganik, P. S. Dodds, D. J. Watts, *Science* **311**, 854 (2006).
22. G. Kossinets, D. J. Watts, *Am. J. Sociol.* **115**, 405 (2009).
23. G. Kossinets, D. J. Watts, *Science* **311**, 88 (2006).
24. M. E. J. Newman, D. J. Watts, *Phys. Rev. E* **60**, 7332 (1999).
25. P. D. Calvert *et al.*, *Nature* **411**, 90 (2001).

26. I thank A. van de Rijt and V. Eguiluz for helpful comments, N. Christakis for useful discussion and guidance, G. Pickard for programming assistance, A. Wagner for developing the Healthy Lifestyle Network Web site, T. Groves for all of the design work, and J. Kreckler and K. Campbell at www.prevention.com and G. Colditz of www.yourdiseaserisk.com for their assistance recruiting participants. This work was supported in part by the James S. McDonnell Foundation and the Robert Wood Johnson Foundation.

Supporting Online Material

www.sciencemag.org/cgi/content/full/329/5996/1194/DC1
Materials and Methods
SOM Text
Figs. S1 to S7
Tables S1 to S3
References

26 November 2009; accepted 19 July 2010
10.1126/science.1185231

Human-Restricted Bacterial Pathogens Block Shedding of Epithelial Cells by Stimulating Integrin Activation

Petra Muenzner,[1] Verena Bachmann,[1] Wolfgang Zimmermann,[2] Jochen Hentschel,[1,3] Christof R. Hauck[1,4]*

Colonization of mucosal surfaces is the key initial step in most bacterial infections. One mechanism protecting the mucosa is the rapid shedding of epithelial cells, also termed exfoliation, but it is unclear how pathogens counteract this process. We found that carcinoembryonic antigen (CEA)–binding bacteria colonized the urogenital tract of CEA transgenic mice, but not of wild-type mice, by suppressing exfoliation of mucosal cells. CEA binding triggered de novo expression of the transforming growth factor receptor CD105, changing focal adhesion composition and activating β_1 integrins. This manipulation of integrin inside-out signaling promotes efficient mucosal colonization and represents a potential target to prevent or cure bacterial infections.

During colonization of mucosal surfaces, incoming microbes must cope with multiple host defenses (*1*). One protective mechanism of the mucosa in stratified and squamous tissues is the accelerated turnover and shedding of superficial epithelial cells, also referred to as exfoliation (*2*–*4*). Although in vitro studies have suggested that microbes modulate cell detachment (*5*, *6*), it is currently unknown how successful mucosal pathogens deal with the exfoliation response in vivo. *Neisseria gonorrhoeae*, a Gram-negative microorganism, causes one of the most common sexually transmitted diseases worldwide (*7*). Even though these bacteria can induce the exfoliation of host cells upon contact (*8*–*11*), they are able to establish themselves on virtually every mucosal surface of the human body.

To investigate how gonococci manage to colonize the urogenital mucosa efficiently, we performed vaginal infection of female mice (*12*). In line with the innate capacity of epithelial cells to respond to this bacterial challenge, *N. gonorrhoeae* triggered detachment of superficial epithelial cells within 20 hours (Fig. 1A) and only small numbers of gonococci could be re-isolated from wild-type mice (Fig. 1B). Gonococci are adapted to humans as their sole natural host. One of the host-specific virulence traits that gonococci share with other specialized mucosal colonizers, including *Haemophilus influenzae*, *Moraxella catarrhalis*, and *N. meningitidis*, is the ability to recognize hu-

[1]Lehrstuhl Zellbiologie, Fachbereich Biologie, Universität Konstanz, 78457 Konstanz, Germany. [2]Tumor Immunology Laboratory, LIFE Center, Ludwig-Maximilians-Universität München, 81377 München, Germany. [3]EM Service, Fachbereich Biologie, Universität Konstanz, 78457 Konstanz, Germany. [4]Konstanz Research School Chemical Biology, Universität Konstanz, 78457 Konstanz, Germany.

*To whom correspondence should be addressed. E-mail: christof.hauck@uni-konstanz.de

man carcinoembryonic antigen–related cell adhesion molecules (CEACAMs) (*13*, *14*). To engage CEACAMs, gonococci use outer membrane adhesins of the colony opacity-associated (Opa) protein family [Opa_{CEA}; for a review see (*15*)]. Bacterial engagement of human CEACAMs can block detachment of infected epithelial cells in vitro, which suggests that gonococci and other CEACAM-binding bacteria might use CEACAMs to modulate exfoliation (*5*).

To test the hypothesis that CEACAM engagement by bacteria attenuates epithelial exfoliation and promotes mucosal colonization, we used a humanized mouse model of gonococcal urogenital tract infection: CEA transgenic (CEAtg) mice harboring the human *CEACAM5* gene (*16*). In CEAtg mice, CEA can be detected on mucosal surfaces including the female urogenital tract (fig. S1A). Wild-type and CEAtg female mice were vaginally infected with 10^8 bacteria, and colonizing bacteria were recovered by urogenital swabs 24 hours later. Consistent with the initial observations, only a few gonococci could be re-isolated from wild-type mice irrespective of the bacterial phenotype, whereas the numbers of gonococci expressing Opa_{CEA} proteins recovered from CEAtg mice were higher by a factor of about 50 to 100 (Fig. 1B). The Opa_{CEA} protein expression by re-isolated bacteria was unaltered (fig. S1B). Some re-isolates expressed additional Opa proteins, further pointing to an in vivo advantage of opaque phenotypes. Isogenic gonococcal strains lacking Opa protein expression (Opa^-), strains expressing type IV pili (Opa^-/P^+), or strains expressing a heparan sulfate proteoglycan-binding Opa protein (Opa_{HSPG}) (*17*, *18*) could not be isolated in increased numbers from CEAtg mice (Fig. 1B). Scanning electron microscopy (SEM) of the upper vaginal tract revealed massive exfoliation of the superficial epithelial layer in wild-type animals infected with Opa_{CEA}-expressing *N. gonorrhoeae* (Ngo Opa_{CEA}) as well as in CEAtg animals infected with non–CEACAM-binding gonococci (Fig. 1C). Vast exfoliation was already evident at low magnification; at higher magnification, the detachment of multiple superficial epithelial cells was apparent (Fig. 1C). In contrast, exfoliation was not elevated in CEAtg mice infected with Ngo Opa_{CEA} (Fig. 1, C and D). Thus, the Opa_{CEA}-CEA interaction suppresses exfoliation and facilitates mucosal colonization.

In the urogenital tract of infected mice, gonococci colocalized with CEA-positive cells on the vaginal surface of CEAtg mice (Fig. 2, A and B). Gonococci lacking Opa protein expression (Ngo Opa^-) were rarely detected on the mucosal surface of CEAtg mice, and gonococci were absent in

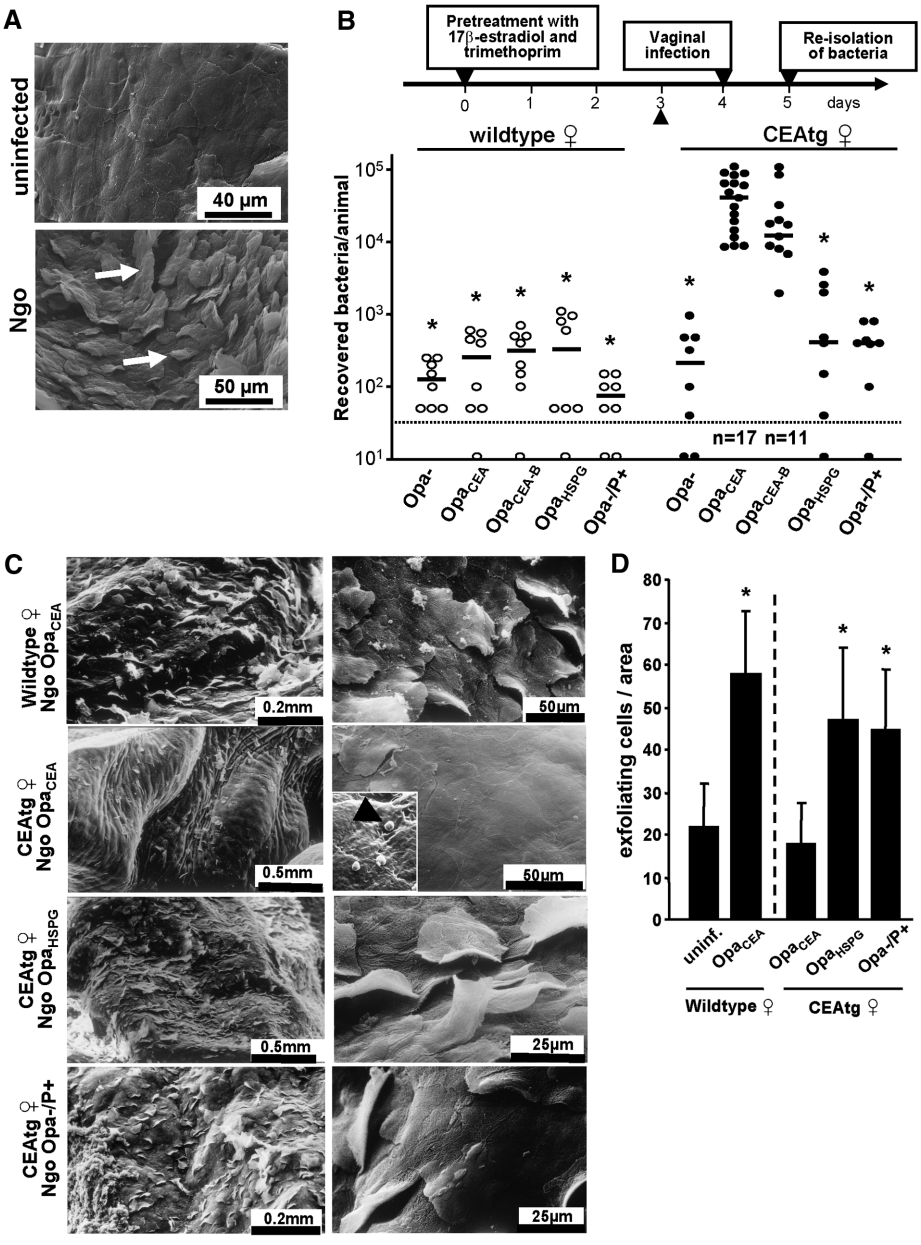

Fig. 1. CEA binding facilitates mucosal colonization and blocks exfoliation of superficial epithelial cells. (**A**) Female wild-type mice were infected for 24 hours with piliated, non-opaque gonococci, or remained uninfected. Genital tracts were excised, fixed, and processed for SEM. Micrographs show the luminal surface of the upper vaginal and cervical region. Exfoliating cells are highlighted by arrows. (**B**) Schematic representation of the infection protocol used with respect to pretreatment of the mice, vaginal infection, and re-isolation of bacteria (▲ indicates the time point of lentiviral transduction). The graph shows colonization of wild-type (○) or CEAtg (●) female mice with the indicated bacterial strains. Each circle reflects the number of bacteria re-isolated from an individual animal ($n = 8$ unless indicated otherwise); data were compiled from six experiments. The dotted line indicates the lower detection limit (40 bacteria per animal). The median for each experimental group of animals is noted; groups were compared against numbers isolated from Ngo Opa_{CEA}-infected CEAtg mice by two-tailed Mann-Whitney U-test (*$P < 0.001$). (**C**) Genital tracts infected as in (B) were excised and processed for SEM. Pictures (at two different magnifications, as indicated by the scale bars) show the luminal surface of the upper vaginal and cervical regions. Inset shows adherent bacteria (black arrowhead). (**D**) Quantification of exfoliating epithelial cells. Bars represent mean ± SD of exfoliating cells in an area of about 0.075 mm^2 ($n = 24$); groups were compared against uninfected mice by one-tailed Mann-Whitney U-test (*$P < 0.01$).

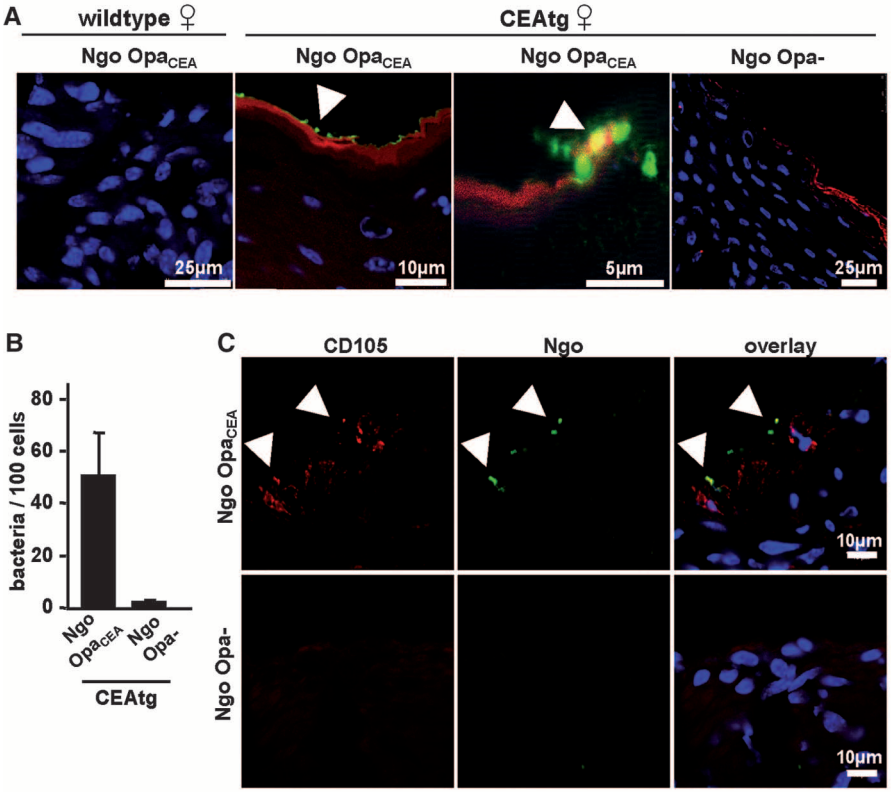

Fig. 2. CEA engagement by bacteria triggers CD105 expression in vivo. (**A**) Genital tracts from wild-type or CEAtg mice infected for 24 hours with Opa$_{CEA}$-expressing (Ngo Opa$_{CEA}$) or non-opaque (Ngo Opa^{-}) gonococci were excised, and cryosections were co-stained with antibodies against *N. gonorrhoeae* (green) and CEA (red). Cell nuclei were visualized by Hoechst (blue). Ngo Opa$_{CEA}$ bound to the CEA-positive mucosal surface of CEAtg mice are indicated by arrowheads. (**B**) Quantification of cell-associated bacteria in CEAtg mice. Bars represent the mean number ± SD of bacteria associated with 100 cells (n = 3). (**C**) Cryosections as in (A) were costained with antibodies against *N. gonorrhoeae* (green), a rat monoclonal antibody against murine CD105 (red), and nuclei (blue). CD105 expression (arrowheads) on the mucosal surface of CEAtg mice is seen in the vicinity of cell-associated Ngo Opa$_{CEA}$.

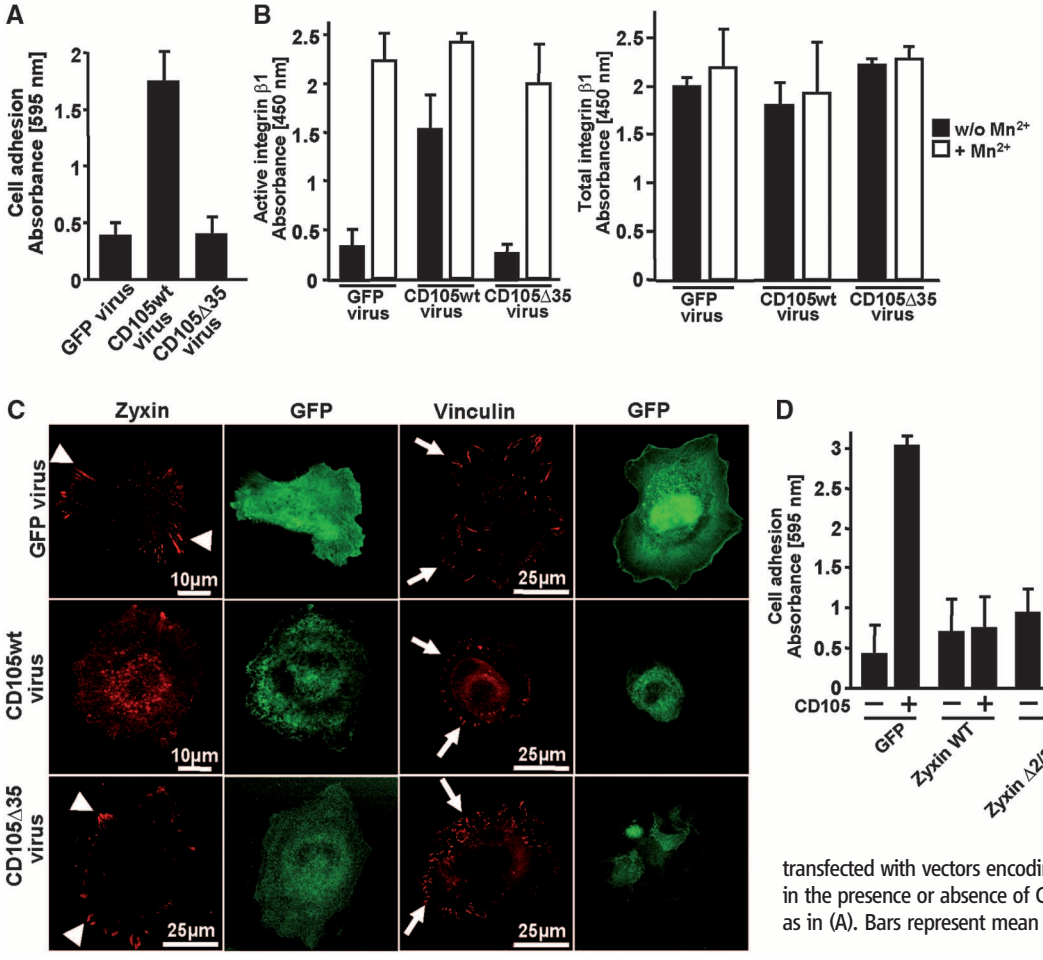

Fig. 3. CD105 enhances integrin activity by delocalization of zyxin. (**A**) Human vaginal epithelial cells (hVECs) were transduced with lentivirus encoding GFP, wild-type CD105 (CD105wt), or CD105Δ35. Cells were used in adhesion assays, and adherent cells were quantified after crystal violet staining. Bars represent mean ± SD of five wells. (**B**) Cells transduced as in (A) were replated onto collagen and stimulated with Mn^{2+} (a global activator of integrin activity), or remained unstimulated, before analysis with an activation-specific integrin β_1 antibody (clone 9EG7; active integrin β_1) or an activation-independent integrin β_1 antibody (clone AIIB2; total integrin β_1). Bars represent the mean ± SD of five wells of a representative experiment repeated twice with similar results. (**C**) hVECs were transduced as in (A), and parallel samples were stained for zyxin or vinculin. Small arrowheads highlight zyxin at focal adhesions, which is missing in CD105wt-expressing cells. Vinculin-positive focal adhesions (arrows) are found in all cells. (**D**) HeLa cells were transfected with vectors encoding GFP, GFP-zyxin, or GFP-zyxin Δ2/3LIM, in the presence or absence of CD105. Cells were used in adhesion assays as in (A). Bars represent mean ± SD of five wells.

wild-type mice, even if infected with Ngo Opa_{CEA} (Fig. 2, A and B). How can the engagement of apically expressed CEA lead to reduced detachment of infected cells? CEACAM-binding by bacteria triggers de novo expression of CD105, a member of the transforming growth factor–β1 receptor (TGFβ1R) family, which promotes cell-matrix adhesion and blocks cell migration (*5*, *19*). Indeed, CEA engagement by Ngo Opa_{CEA} in vitro stimulated the expression of CD105 and increased the adhesiveness of infected cells to several extracellular matrix proteins (fig. S2). Moreover, CEACAM-binding bacteria, but not Opa^- bacteria, triggered de novo expression of CD105 by vaginal epithelial cells of CEAtg mice in vivo (Fig. 2C and fig. S3). CD105, a well-characterized endothelial marker, was present on small blood vessels in the submucosa of wild-type (fig. S4) and CEAtg mice, but was absent from uninfected vaginal epithelial cells (Fig. 2C and fig. S3). Thus, CD105 expression in response to CEA stimulation by gonococci could be responsible for enhanced matrix adhesion of infected epithelial cells and the suppression of exfoliation.

Cell adhesion to the extracellular matrix is mediated by integrins, and TGFβ1Rs influence integrin expression (*20*). However, CD105, a type III nonsignaling member of the TGFβ1R family, does not increase the amount of integrin β_1 or integrin-associated cytoplasmic proteins (*19*, *21*). In HeLa cells and 293 cells, CD105 promoted cell adhesion by stimulating integrin inside-out signaling, leading to enhanced integrin activity (fig. S5). The adhesion-promoting activity of CD105 was located in the cytoplasmic domain of CD105, which was necessary (fig. S6) and sufficient (fig. S7) for this process. In line with these results, transduction with wild-type CD105 (CD105wt), but not with CD105 carrying a 35–amino acid truncation of the cytoplasmic domain (CD105Δ35), enhanced cell-matrix adhesion and increased integrin activity of human vaginal epithelial cells (hVECs) (Fig. 3, A and B). One of the cellular factors that associate with the cytoplasmic part of CD105 is zyxin, a focal adhesion protein that binds CD105 via three LIM (Lin-11 Isl-1 Mec-3) domains (*19*). Zyxin-deficient fibroblasts show enhanced integrin activity and matrix adhesion (*22*), which was not further stimulated by CD105 expression (fig. S8). The dependence of CD105-stimulated integrin activity on zyxin, which by itself acts as a negative regulator of cell adhesion, could be explained by a scenario where de novo expression of CD105 interferes with zyxin's inhibitory function at focal adhesion sites. In hVECs, which express zyxin but not CD105 (fig. S9), zyxin was located at peripheral contact sites (Fig. 3C). However, upon expression of CD105wt, but not CD105Δ35, zyxin was delocalized (Fig. 3C and fig. S9). In contrast, the localization of the focal adhesion protein vinculin was unaltered (Fig. 3C). Increasing the cellular pool of zyxin by overexpression, but not by expression of a zyxin mutant lacking the second and third LIM domains (zyxin Δ2/3LIM), abrogated the increased adhesion of CD105-transfected cells (Fig. 3D). Thus, CD105-mediated delocalization of endogenous zyxin positively influences integrin activity and could be responsible for the enhanced cell adhesion and the suppression of epithelial exfoliation triggered by CEACAM-binding bacteria.

To test a causal relationship among CEACAM-dependent up-regulation of CD105, suppression of epithelial exfoliation, and improved colonization of the urogenital mucosa by pathogenic gonococci, we generated a GFP (green fluorescent protein)– and short hairpin RNA–encoding lentivirus targeting murine CD105 (shCD105) (fig. S10). In vivo, vaginal application of shCD105 or a GFP control virus resulted in strong expression of GFP in the superficial epithelial layer (fig. S10). To investigate the role of CD105 expression for mucosal colonization in vivo, we applied shCD105 or GFP control virus 24 hours before vaginal infection of mice. Application of shCD105 virus suppressed the ability of Ngo Opa_{CEA} to colonize the urogenital tract of CEAtg mice, whereas the GFP control virus had no effect (Fig. 4A). Moreover, SEM of the mucosa revealed that transduction with shCD105 virus reversed the phenotype of the infected epithelial cells and allowed pronounced exfoliation in response to infection with CEACAM-binding bacteria (Fig. 4, B and C). In CEAtg mice treated with the GFP control virus, Ngo Opa_{CEA} were still able to block exfoliation (Fig. 4, B and C). Thus, up-regulation of CD105 on mucosal epithelial cells interferes with exfoliation and promotes gonococcal colonization of the urogenital tract. To further confirm the causal relationship between CD105-initiated molecular processes and the suppression of epithelial exfoliation, we transduced CEAtg mice with lentiviral

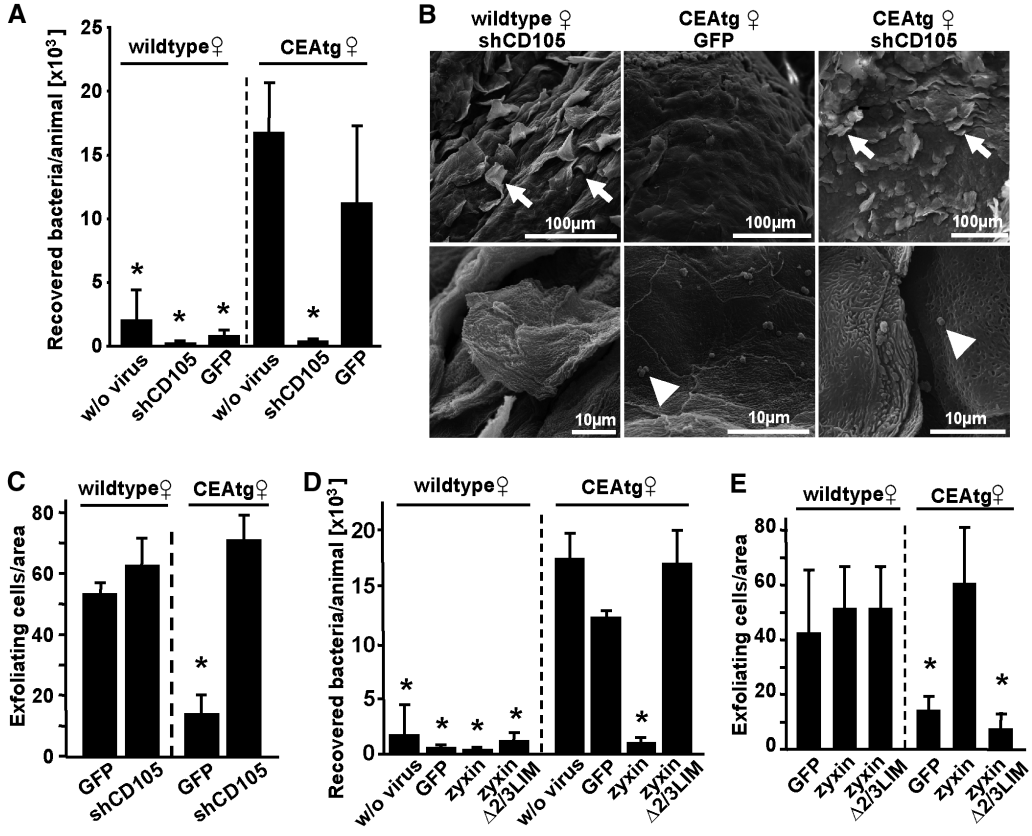

Fig. 4. Bacterial colonization is blocked by inhibition of CD105 expression in vaginal epithelial cells or by mucosal delivery of zyxin. (**A**) Female mice were transduced with GFP, shCD105-encoding virus, or left without virus (w/o virus). Twenty-four hours later, animals were infected with Ngo Opa_{CEA}, and colonizing gonococci were enumerated the next day. Bars represent the mean ± SD of bacteria re-isolated from six individual animals. Groups were compared against numbers isolated from untransduced CEAtg mice by one-tailed Mann-Whitney U-test (*$P < 0.01$). (**B**) SEM of the mucosal epithelium of mice transduced and infected as indicated. Exfoliating epithelial cells are marked by arrows; cell-associated bacteria are indicated by arrowheads. (**C**) Quantification of exfoliating epithelial cells as in Fig. 1D; groups were compared against GFP-transduced wild-type mice by one-tailed Mann-Whitney U-test (*$P < 0.01$). (**D** and **E**) Wild-type or CEAtg mice were transduced with lentiviral particles encoding GFP, GFP-zyxin, or GFP-zyxinΔ2/3LIM, or left without virus (w/o virus) before infection with Ngo Opa_{CEA}. Colonizing gonococci in (D) and exfoliating cells in (E) were enumerated as in (A) and (C), respectively.

particles driving the expression of zyxin-GFP, zyxin-Δ2/3LIM-GFP, or GFP, respectively (fig. S11). Delivery of zyxin to the vaginal epithelium did not result in increased exfoliation of the uninfected mucosa (fig. S11). However, zyxin, but not zyxin-Δ2/3LIM, overexpression blocked the colonization of CEAtg mice by Opa_{CEA}-expressing gonococci (Fig. 4D). The overexpression of zyxin, but not of zyxin-Δ2/3LIM, allowed exfoliation of CEA-positive cells infected with Ngo Opa_{CEA} and reestablished the responsiveness of the vaginal mucosa (Fig. 4E and fig. S11). Thus, CEA-initiated up-regulation of CD105 on superficial epithelial cells and the resulting delocalization of zyxin from integrin-rich focal adhesion sites are the critical molecular events that allow CEACAM-binding microorganisms to counteract the exfoliation response.

Although symptomatic gonococcal infection in humans might be a multistep process orchestrated by additional virulence factors (*13*, *23*), our results establish a specific role of Opa_{CEA} proteins in promoting mucosal colonization. In vivo challenge experiments with male volunteers have revealed that after infection of the urethra with non-opaque gonococci, bacteria re-isolated from these volunteers almost invariably converted to an Opa protein–expressing phenotype (*24*, *25*). In addition to the urogenital tract, members of the CEACAM family are present on all mucosal surfaces including the nasopharynx (*26*). These mucosal habitats are colonized by several Gram-negative bacterial species, which make use of unrelated protein adhesins to engage human CEACAMs (*27*–*31*). The blockage of epithelial exfoliation afforded by CEACAM binding might have driven this convergent evolution that allows specialized bacteria to transform the mucosa into a dependable platform for colonization.

References and Notes

1. J. P. Pearson, I. A. Brownlee, in *Colonization of Mucosal Surfaces*, J. P. Nataro, P. S. Cohen, H. L. T. Mobley, J. N. Weiser, Eds. (ASM Press, Washington, DC, 2005), pp. 3–16.
2. M. A. Mulvey *et al.*, *Science* **282**, 1494 (1998).
3. M. A. Mulvey, J. D. Schilling, J. J. Martinez, S. J. Hultgren, *Proc. Natl. Acad. Sci. U.S.A.* **97**, 8829 (2000).
4. I. U. Mysorekar, M. A. Mulvey, S. J. Hultgren, J. I. Gordon, *J. Biol. Chem.* **277**, 7412 (2002).
5. P. Muenzner, M. Rohde, S. Kneitz, C. R. Hauck, *J. Cell Biol.* **170**, 825 (2005).
6. M. Kim *et al.*, *Nature* **459**, 578 (2009).
7. WHO, *Global Prevalence and Incidence of Selected Curable Sexually Transmitted Infections—Overview and Estimates* (World Health Organization, Geneva, 2001).
8. M. A. Melly, C. R. Gregg, Z. A. McGee, *J. Infect. Dis.* **143**, 423 (1981).
9. Z. A. McGee, A. P. Johnson, D. Taylor-Robinson, *J. Infect. Dis.* **143**, 413 (1981).
10. K. F. Tjia, J. P. van Putten, E. Pels, H. C. Zanen, *Graefes Arch. Clin. Exp. Ophthalmol.* **226**, 341 (1988).
11. I. M. Mosleh, H. J. Boxberger, M. J. Sessler, T. F. Meyer, *Infect. Immun.* **65**, 3391 (1997).
12. See supporting material on *Science* Online.
13. M. Virji, *Nat. Rev. Microbiol.* **7**, 274 (2009).
14. M. Voges, V. Bachmann, R. Kammerer, U. Gophna, C. R. Hauck, *BMC Microbiol.* **10**, 117 (2010).
15. C. R. Hauck, T. F. Meyer, *Curr. Opin. Microbiol.* **6**, 43 (2003).
16. A. M. Eades-Perner *et al.*, *Cancer Res.* **54**, 4169 (1994).
17. J. P. van Putten, S. M. Paul, *EMBO J.* **14**, 2144 (1995).
18. T. Chen, R. J. Belland, J. Wilson, J. Swanson, *J. Exp. Med.* **182**, 511 (1995).
19. B. A. Conley *et al.*, *J. Biol. Chem.* **279**, 27440 (2004).
20. G. Zambruno *et al.*, *J. Cell Biol.* **129**, 853 (1995).
21. M. Guerrero-Esteo *et al.*, *Eur. J. Cell Biol.* **78**, 614 (1999).
22. L. M. Hoffman *et al.*, *J. Cell Biol.* **172**, 771 (2006).
23. A. J. Merz, M. So, *Annu. Rev. Cell Dev. Biol.* **16**, 423 (2000).
24. J. Swanson, O. Barrera, J. Sola, J. Boslego, *J. Exp. Med.* **168**, 2121 (1988).
25. A. E. Jerse *et al.*, *J. Exp. Med.* **179**, 911 (1994).
26. S. Hammarström, *Semin. Cancer Biol.* **9**, 67 (1999).
27. M. Virji, K. Makepeace, D. J. P. Ferguson, S. M. Watt, *Mol. Microbiol.* **22**, 941 (1996).
28. M. Virji *et al.*, *Mol. Microbiol.* **36**, 784 (2000).
29. D. J. Hill, M. Virji, *Mol. Microbiol.* **48**, 117 (2003).
30. C. N. Berger, O. Billker, T. F. Meyer, A. L. Servin, I. Kansau, *Mol. Microbiol.* **52**, 963 (2004).
31. M. Toleman, E. Aho, M. Virji, *Cell. Microbiol.* **3**, 33 (2001).

32. We thank M. C. Beckerle for zyxin-deficient fibroblasts and antibodies; M. Chudakov for the mKate cDNA; J. W. Greiner for sending the CEAtg mice; T. F. Meyer for bacterial strains; D. W. Piston for cDNA of mCerulean; A. J. Schaeffer for hVEC cells; D. Vestweber for providing antibody; C. Hentschel, J. Scharrer, and R. Mak'anyengo for assistance with SEM; and B. Planitz for expert animal care. Supported by Deutsche Forschungsgemeinschaft grant Ha2856/6-1 (C.R.H.).

Supporting Online Material

www.sciencemag.org/cgi/content/full/329/5996/1197/DC1
Materials and Methods
Figs. S1 to S10
References

14 April 2010; accepted 30 June 2010
10.1126/science.1190892

Signaling Kinase AMPK Activates Stress-Promoted Transcription via Histone H2B Phosphorylation

David Bungard,[1] Benjamin J. Fuerth,[2,3] Ping-Yao Zeng,[1,4] Brandon Faubert,[2,3] Nancy L. Maas,[1] Benoit Viollet,[5,6] David Carling,[7] Craig B. Thompson,[8] Russell G. Jones,[2,3,8]* Shelley L. Berger[1,9,10]*

The mammalian adenosine monophosphate–activated protein kinase (AMPK) is a serine-threonine kinase protein complex that is a central regulator of cellular energy homeostasis. However, the mechanisms by which AMPK mediates cellular responses to metabolic stress remain unclear. We found that AMPK activates transcription through direct association with chromatin and phosphorylation of histone H2B at serine 36. AMPK recruitment and H2B Ser^{36} phosphorylation colocalized within genes activated by AMPK-dependent pathways, both in promoters and in transcribed regions. Ectopic expression of H2B in which Ser^{36} was substituted by alanine reduced transcription and RNA polymerase II association to AMPK-dependent genes, and lowered cell survival in response to stress. Our results place AMPK-dependent H2B Ser^{36} phosphorylation in a direct transcriptional and chromatin regulatory pathway leading to cellular adaptation to stress.

Signaling pathways often involve cascades of protein phosphorylation that terminate in regulation of nuclear transcription. However, the central kinases in these pathways are generally not thought to directly modulate transcription. One such signaling kinase, adenosine monophosphate–activated protein kinase (AMPK) (*1*), is activated by high substrate adenosine monophosphate levels under conditions of energetic stress, such as nutrient deprivation or hypoxia. AMPK activation initiates a program of metabolic adaptation to preserve cellular energy (adenosine triphosphate conservation) and maintain cellular viability (*2*).

We investigated possible direct transcriptional mechanisms in the AMPK pathway. First, we examined whether AMPK broadly responds to cellular stress. Mouse embryonic fibroblasts (MEFs) were stressed by ultraviolet (UV) irradiation, γ irradiation, the topoisomerase inhibitor camptothecin, the DNA intercalating agent adriamycin, the alkylating agent *N*-methyl-*N*′-nitro-*N*-nitrosoguanidine, or hydrogen peroxide. AMPK was activated [Thr^{172} phosphorylation in the AMPK activation loop and phosphorylation of substrate ACCα (acetyl coenzyme A–carboxylase-α)] by all agents (Fig. 1A). Liver kinase B1 (LKB1) is one of three mammalian upstream AMPK kinases and activates AMPK upon bioenergetic stress (*3*). LKB1 also activated AMPK in response to either genotoxic (UV irradiation) or metabolic stress [the glycolytic inhibitor 2-deoxyglucose (2-DG)] (fig. S1).

[1]Department of Cellular and Developmental Biology, University of Pennsylvania Medical School, Philadelphia, PA 19104, USA. [2]Rosalind and Morris Goodman Cancer Research Centre, McGill University, Montreal, Quebec H3G 1Y6, Canada. [3]Department of Physiology, McGill University, Montreal, Quebec H3G 1Y6, Canada. [4]Institutes of Biomedical Sciences Epigenetics Program, Mingdao Building, Room 511, Fudan University, Mail Box 281, 138 Yixue Yuan Road, Shanghai 200032, P.R. China. [5]Institut Cochin, Université Paris Descartes, CNRS (UMR 8104), 75014 Paris, France. [6]INSERM U1016, 75014 Paris, France. [7]Cellular Stress Group, MRC Clinical Sciences Centre, Imperial College, Hammersmith Hospital, London W12 0NN, UK. [8]Abramson Cancer Center and Abramson Family Cancer Research Institute, University of Pennsylvania, Philadelphia, PA 19104, USA. [9]Department of Genetics, University of Pennsylvania Medical School, Philadelphia, PA 19104, USA. [10]Department of Biology, School of Arts and Sciences, University of Pennsylvania, Philadelphia, PA 19104, USA.

*To whom correspondence should be addressed. E-mail: russell.jones@mcgill.ca (R.G.J.); bergers@mail.med.upenn.edu (S.L.B.)

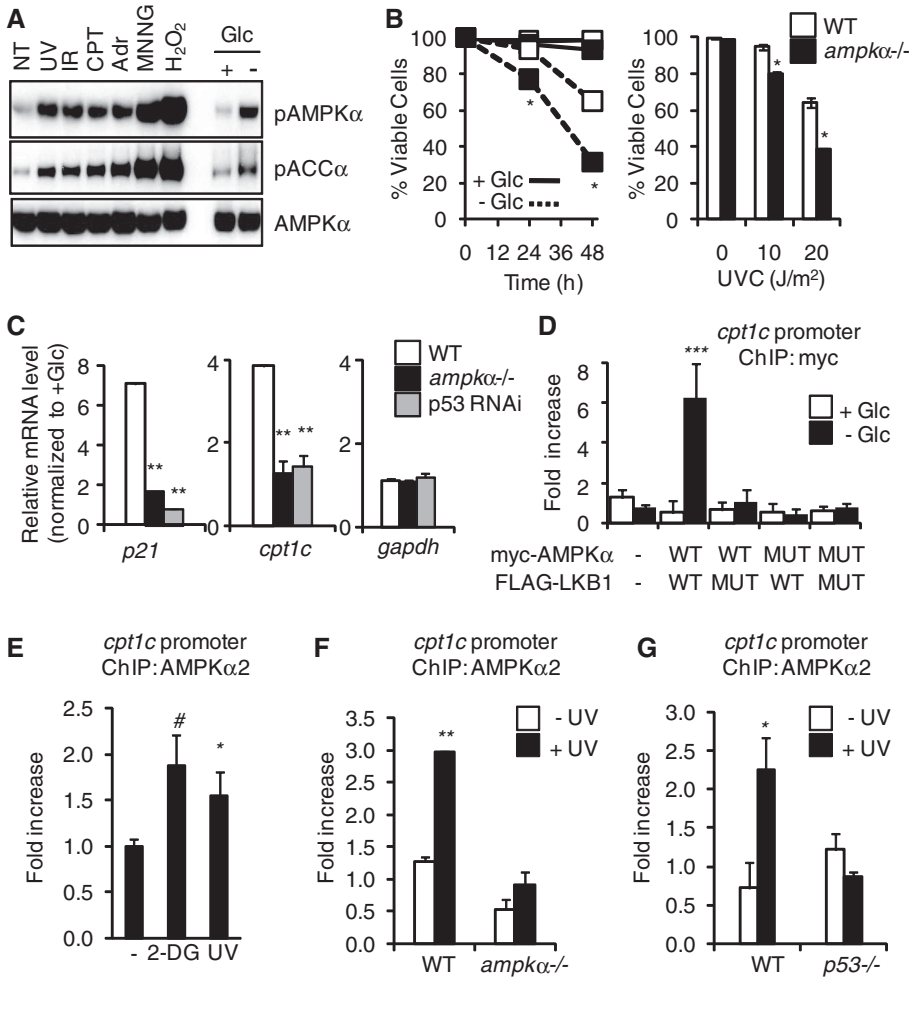

Fig. 1. AMPK is required for stress-dependent transcription and localizes to stress-responsive genes. (**A**) Western blot of AMPK activation (AMPKα pThr^{172}) and ACCα phosphorylation (ACCα pSer^{79}) in MEFs in response to UV light, γ irradiation (IR), camptothecin (CPT), adriamycin (Adr), *N*-methyl-*N*′-nitro-*N*-nitrosoguanidine (MNNG), or hydrogen peroxide (H_2O_2). Exposure times were 6 hours for UV, IR, CPT, and Adr and 30 min for MNNG and H_2O_2. NT, no treatment; Glc, glucose. (**B**) Viability of wild-type (WT) and *ampkα*$^{-/-}$ MEFs in response to indicated stresses. Left panel: glucose (Glc) withdrawal; right panel, UV irradiation (UVC). (**C**) Expression (qPCR) of *p21*, *cpt1c*, and *gapdh* mRNA in wild-type, AMPKα-deficient, or p53 RNAi–expressing MEFs after glucose withdrawal, relative to untreated cells. (**D**) ChIP of WT or dominant negative (MUT) myc-AMPK after glucose withdrawal in *lkb1*$^{-/-}$ MEFs cotransfected with either WT or catalytically inactive (MUT) FLAG-LKB1, both able to be immunoprecipitated [see (A), fig. S7, and (*5*)]. Data represent means ± SEM for $n = 3$. (**E** to **G**) Endogenous AMPKα2 ChIP in untreated MEFs (–), 2-DG (15 min), or UV (6 hours) (E); WT or *ampkα*$^{-/-}$ MEFs (F); and WT or *p53*$^{-/-}$ MEFs (G). Data represent means ± SEM for $n = 3$. #$P < 0.06$, *$P < 0.05$, **$P < 0.01$, ***$P < 0.03$.

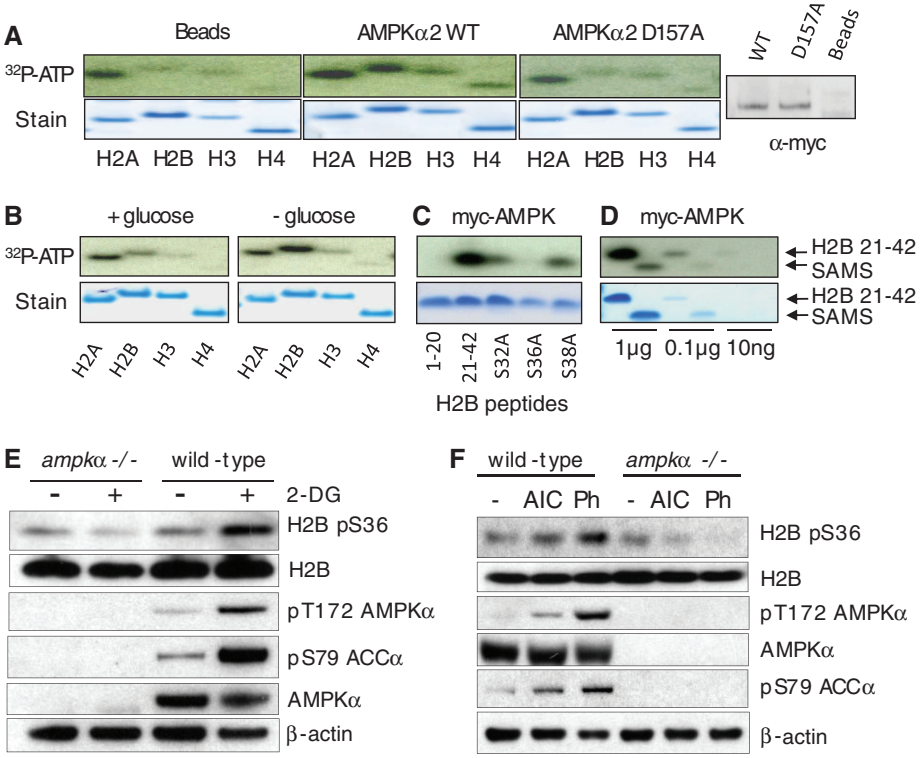

Fig. 2. H2B is an AMPK target. (**A** to **D**) In vitro phosphorylation by myc-AMPK immunoprecipitated from *ampkα*$^{-/-}$ MEFs of recombinant human histones by beads alone, WT myc-AMPK, or catalytic mutant (D157A) myc-AMPK (right: myc Western blot) (A); recombinant human histones using myc-AMPK from glucose-treated cells (+glucose) or untreated cells (–glucose) (B); H2B peptides (C); and H2B 21-42 and SAMS peptide (D). (**E**) Western blots of wild-type or *ampkα*$^{-/-}$ MEFs treated with 2-DG (25 mM for 10 min) or untreated. (**F**) Western blots of MEFs treated for 1 hour with AICAR (AIC, 2 mM) or phenformin (Ph, 3 mM) or untreated.

We next used wild-type or AMPKα1- and AMPKα2-deficient MEFs (*ampkα*$^{-/-}$) to examine whether AMPK influences cellular survival during stress (*4*). The *ampkα*$^{-/-}$ MEFs displayed decreased survival in the presence of metabolic stressors (Fig. 1B and fig. S2), UV irradiation (Fig. 1B), or hydrogen peroxide (fig. S2), indicating that AMPK promotes cell survival in response to various metabolic and genotoxic stresses.

Our previous work implicated AMPK and LKB1 in tumor suppressor p53–dependent metabolic and genotoxic stress responses (*2*, *5*). We examined the involvement of AMPK in transcriptional regulation of p53-responsive genes. *ampkα*$^{-/-}$ MEFs showed decreased induction of *p21*, a well-characterized p53 target gene, in response to both glucose withdrawal and UV irradiation (Fig. 1C and fig. S3). The reduction in glucose-regulated gene expression was similar in magnitude to knockdown of p53 (Fig. 1C). Other p53-dependent genes, including *reprimo*, *cyclinG*, and *cpt1c*, showed reduced expression in *ampkα*$^{-/-}$ cells deprived of glucose, whereas expression of a control gene, *gapdh*, was unaffected (Fig. 1C and fig. S4). A similar defect in stress-dependent transcription was observed in human cancer cells (HCT116 colon carcinoma) (fig. S5). The transcriptional defect observed in UV-treated cells occurred downstream of the DNA-damage checkpoint, as phosphorylation of Chk1, Rad17, and p53 in both *lkb1*$^{-/-}$ and *ampkα*$^{-/-}$ cell lines was similar to that of wild-type controls (fig. S6). Thus, in cell culture, the LKB1-AMPK pathway responds to a wide variety of metabolic and genotoxic stresses and is required for maximal stress-induced transcription of multiple p53-dependent genes that promote survival.

These and previous results (*6*) implicate AMPK in gene activation, although the underlying mechanisms have remained elusive. We used chromatin immunoprecipitation (ChIP) and quantitative polymerase chain reaction (qPCR) to investigate whether AMPK plays a direct role at p53-regulated genes in MEFs. We found that LKB1 coimmunoprecipitated with AMPK in response to UV irradiation, and this interaction was dependent on AMPK kinase activity (fig. S7). ChIP showed ectopic myc-AMPK associated with the *cpt1c* and *p21* gene promoters in response to glucose withdrawal and UV treatment (Fig. 1D and fig. S8). Ectopic kinase-deficient myc-AMPKα or FLAG-tagged LKB1 abrogated the binding of AMPK to chromatin (Fig. 1D and fig. S8). FLAG-LKB1 similarly associated with the *p21* promoter (fig. S9). Binding of AMPK or LKB1 to promoters in unstressed cells was low (Fig. 1D and figs. S8 and S9). AMPK was also detected at the *p21* promoter in human HCT116 cells after UV treatment (fig. S10). This AMPK activation appears to be specific for survival in response to stress, because AMPK was not detected at the PUMA promoter, a p53-dependent, pro-apoptotic gene (fig. S11). The immunoprecipitation and ChIP results suggest a functional, kinase-dependent interaction and promoter association of LKB1 and AMPK.

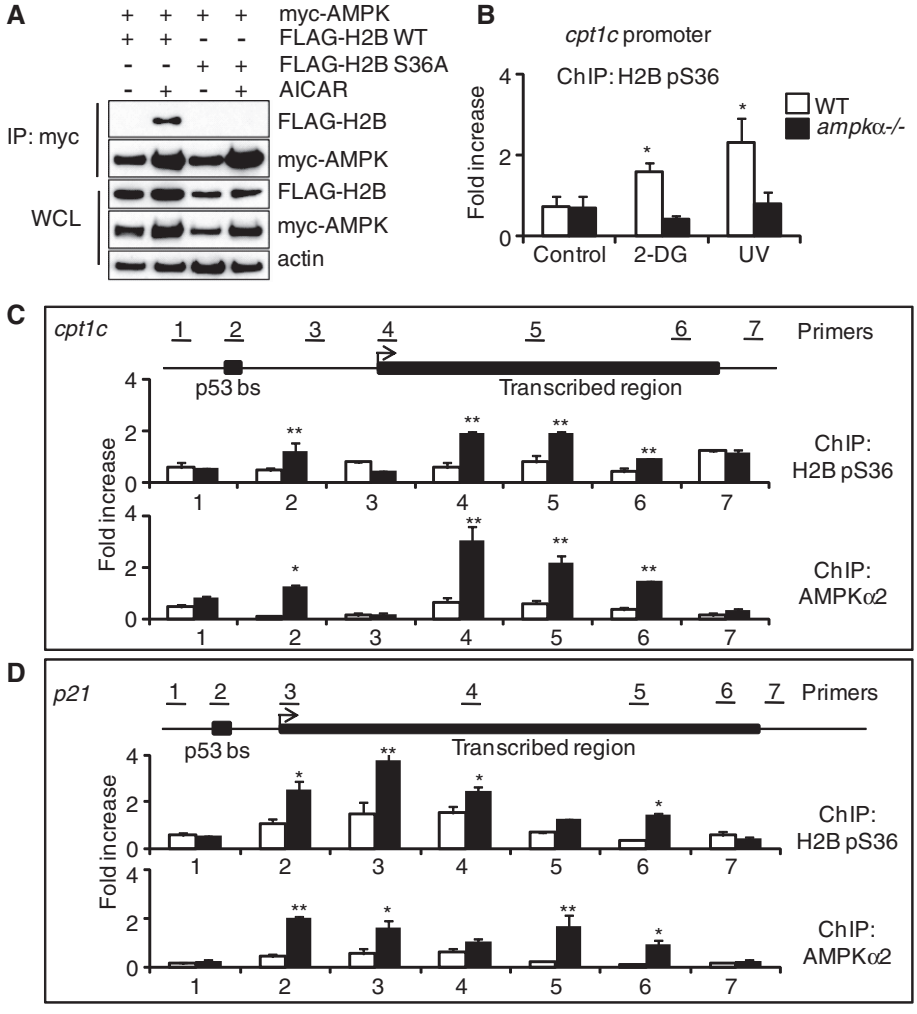

Fig. 3. AMPK and H2B pS36 are localized to chromatin in response to stress. (**A**) Western blots showing myc-AMPK immunoprecipitation from WT H2B– or H2B S36A–expressing cells after AICAR treatment (1 mM, 24 hours). WCL, whole-cell lysate. (**B**) ChIP in WT or *ampkα*$^{-/-}$ MEFs. Data represent means ± SEM for $n = 3$. (**C** and **D**) ChIP along *cpt1c* gene (C) and *p21* gene (D) with glucose (white bars) or without glucose (black bars). Data represent means ± SEM for $n = 3$. *$P < 0.01$, **$P < 0.05$.

Posttranslational modifications of core histones, including phosphorylation, function to regulate transcription (*7*, *8*). To examine histones as substrates of AMPK, we epitope-tagged the predominantly nuclear isoform AMPKα2 (*9*) and immunoprecipitated wild-type AMPKα2 or a catalytic mutant ($Asp^{157} \rightarrow Ala$) from transfected *ampkα*$^{-/-}$ MEFs after low glucose treatment to activate AMPK. The wild-type AMPKα2 complex specifically phosphorylated histone H2B above the nonspecific background activity of all four histones observed in the catalytic mutant and mock immunoprecipitations (Fig. 2A). AMPKα2 from untreated cells exhibited low activity on H2B relative to AMPKα2 from stressed cells (Fig. 2B and fig. S15). H2A was also phosphorylated in these assays; however, phospho-H2A was detected in the mock immunoprecipitation and did not respond to stress, which suggested that the activity is nonspecific. These data indicate that activated AMPKα2 specifically phosphorylates H2B.

Analysis of histone H2B revealed a potential AMPK target motif (*10*, *11*) at Ser^{36} in the N terminus, similar to the AMPK substrates endothelial nitric oxide synthase (eNOS) and phosphofructokinase 2 (PFK2) (H2B, Arg-Ser-Arg-Lys-Glu-Ser; eNOS, Arg-Ile-Arg-Thr-Gln-Ser; PFK2, Arg-Met-Arg-Arg-Asn-Ser), with conserved Arg residues at P–5 and P–3 relative to the phosphoacceptor Ser^{36} (fig. S14) (*12*). We therefore compared peptides corresponding to residues 1 to 20 or 21 to 42 of H2B; only the H2B 21-42 peptide was phosphorylated by immunoprecipitated AMPKα2. Moreover, an H2B 21-42

peptide harboring a Ser^{36} → Ala (S36A) substitution was not phosphorylated, whereas S32A and S38A peptides were phosphorylated (Fig. 2C). In addition, myc-AMPKα2 phosphorylated the H2B 21-42 peptide more efficiently than did SAMS (His-Met-Arg-Ser-Ala-Met-Ser-Gly-Leu-His-Leu-Val-Lys-Arg-Arg) peptide, a canonical AMPK target sequence (Fig. 2D) (*13*). Thus, H2B Ser^{36} is a robust in vitro AMPK substrate.

We next examined whether AMPK is involved in the regulation of H2B Ser^{36} phosphorylation in vivo. We generated an antibody against an H2B pS36 peptide and extensively characterized the affinity-purified antibody in vitro and in vivo (fig. S16). H2B pS36 occurs in cells treated with 2-DG, which induced metabolic stress shown by increased phosphorylation of AMPKα and ACCα (Fig. 2E), whereas other histone marks, including H3, K9me3 H3, and pS10 H3, did not significantly change (fig. S17). In *ampkα*$^{-/-}$ MEFs, H2B pS36 did not increase after 2-DG treatment (Fig. 2E). We detected similar induction of H2B pS36 in cells with two well-characterized AMPK activators, aminoimidazole carboxamide ribonucleotide (AICAR) and phenformin (Fig. 2F). In addition, H2B pS36 was not detected in *lkb1*$^{-/-}$ MEFs but increased after reintroduction of LKB1, and 2-DG stimulated H2B pS36 only when LKB1 was present (fig. S18). These results suggest that H2B Ser^{36} phosphorylation is downstream of the LKB1-AMPK signaling pathway in vivo in response to a broad range of metabolic stresses, and that AMPK is likely the direct kinase in this pathway. This global increase of H2B pS36 may not be limited to p53 target genes (Fig. 1G), because H2B pS36 levels were not reduced in *p53*$^{-/-}$ cells (fig. S19).

We found that transfected myc-AMPK and FLAG-H2B associate in 293T cells in response to the AMPK agonist AICAR (Fig. 3A). This interaction was ablated by an H2B S36A mutation (Fig. 3A), suggesting that Ser^{36} is critical for the interaction of AMPK and H2B. We next performed ChIP experiments in wild type and *ampkα*$^{-/-}$ MEFs to determine whether H2B pS36 is associated with AMPK-dependent genes, specifically at the p53 binding site in the *cpt1c* promoter. The H2B pS36 ChIP signal increased in response to both 2-DG and UV treatment, and the ChIP signal was reduced to background levels in AMPKα-deficient cells (Fig. 3B).

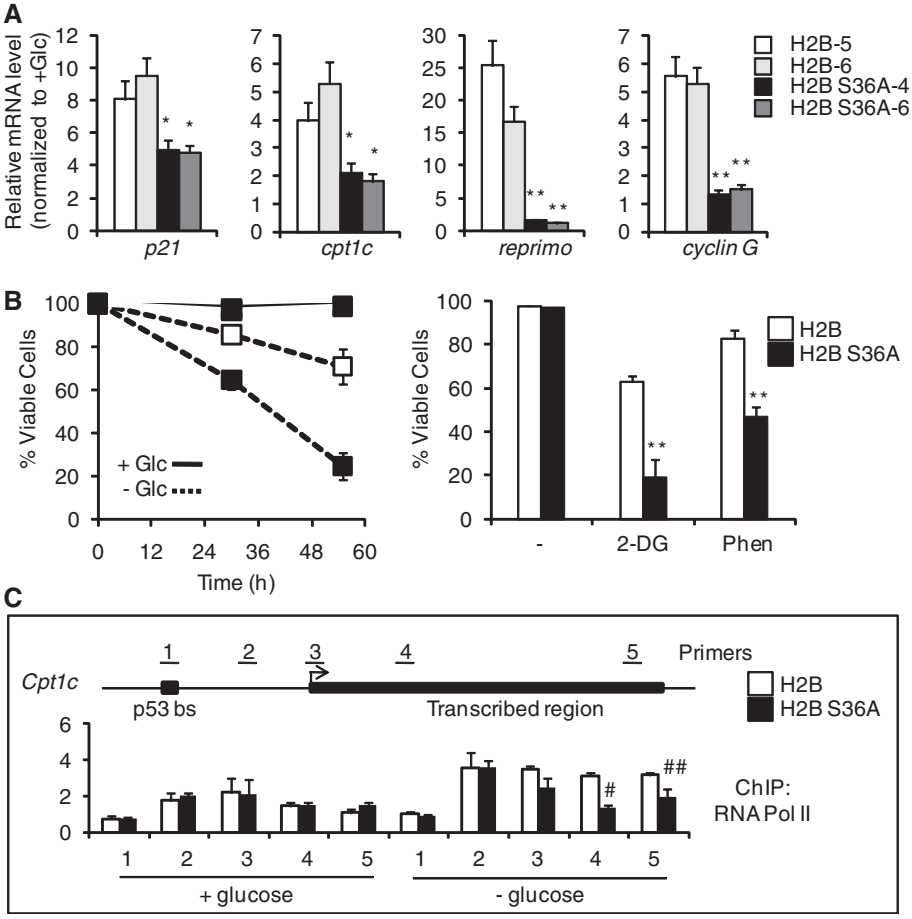

Fig. 4. H2B Ser^{36} is essential for transcription and survival in response to metabolic stress. Data for MEF cell lines expressing wild-type H2B or H2B S36A are shown. (**A**) Relative expression (qPCR) of indicated genes after glucose withdrawal in individual MEF clones (H2B, clones 5 and 6; H2B S36A, clones 4 and 6). (**B**) Viability of H2B (open squares) or H2B S36A (solid squares) MEFs in no glucose, 2-DG (10 mM), or phenformin (3 mM). (**C**) ChIP of RNA Pol II across the *cpt1c* gene. Data represent means ± SEM for $n = 3$. $^{*}P < 0.05$, $^{**}P < 0.01$, $^{\#}P < 0.03$, $^{\#\#}P < 0.08$.

To compare the locations of endogenous AMPK and H2B pS36, we performed ChIP at *cpt1c* under normal and glucose-free conditions, using primers along the promoter, transcribed region, and upstream or downstream nontranscribed regions (Fig. 3C, primer sets 1 to 7). Upon stress, an increase in H2B pS36 occurred at the p53 binding site (p53bs, primer set 2), a larger increase at the transcription start site (TSS, primer set 4), and only background levels upstream (primer set 1) and between (primer set 3) these sites, and downstream of the gene (primer set 7) (Fig. 3C). Notably, H2B pS36 associated throughout the transcribed region of *cpt1c* (primer sets 5 and 6) (Fig. 3C). We then used the AMPKα2 antibody and discovered a positive correlation between locations of endogenous AMPK and H2B pS36, again with localization throughout the transcribed region (Fig. 3C). The *p21* gene showed a similar positive correlation between H2B pS36 and endogenous AMPK localization at the p53 binding sites and along the transcribed region, but not around the gene and only in response to low glucose (Fig. 3D). As a control, we tested the *gapdh* gene, which showed no difference in ChIP signal between the stressed and unstressed cells (fig. S20). Similar results were observed at the *cpt1c* gene in response to UV treatment (fig. S21). Ectopic myc-AMPK also localized along the *p21* transcribed gene in response to low glucose and required AMPK catalytic activity (fig. S22). This correspondence in the location of AMPK and H2B pS36 suggests that the role of AMPK in transcriptional regulation is linked to the phosphorylation of H2B along transcribed regions of target genes.

We generated clonal MEF cell lines with stable ectopic expression of FLAG-H2B or mutant FLAG–H2B S36A, and, as shown above, only FLAG-H2B was detected by the H2B pS36 antibody (fig. S16). The level of FLAG-tagged wild-type or mutant histone H2B was lower than that of endogenous H2B as measured by Western blot (fig. S23); however, both ectopic wild-type and H2B S36A similarly incorporated into chromatin, as determined by ChIP and qPCR at the promoter and transcribed region of the *cpt1c* gene (fig. S24) and by coimmunoprecipitation of endogenous H3 and H2B with FLAG-H2B as shown by Western blot (fig. S25). We isolated several equivalently expressing FLAG-H2B– and FLAG–H2B S36A–expressing clonal lines (fig. S26). The cell lines treated with 2-DG showed comparable levels of AMPK and induction of AMPK Thr^{172} and pACCα Ser^{79} phosphorylation (fig. S27), suggesting that signaling to AMPK is unaffected by the S36A mutation. In response to glucose withdrawal, elevated transcription of the AMPK target genes *p21*, *cpt1c*, *reprimo*, and *cyclinG* was detected in wild-type FLAG-H2B–expressing cells; however, FLAG–H2B S36A–expressing cells showed significantly reduced induction of these genes (Fig. 4A). Expression of the control genes *gapdh* and *hadh* was unaffected by expression of the S36A mutant (fig. S28). Thus, although expression of FLAG-H2B is low relative to endogenous H2B (figs. S23

and S25), we observed a significant and specific transcriptional defect in the cells ectopically expressing S36A mutant H2B.

We next tested the viability of these cells in response to various metabolic stresses including glucose withdrawal, 2-DG, and phenformin. The level of cell death induced by these stresses was significantly greater in the presence of ectopic H2B S36A, relative to cells expressing ectopic wild-type H2B (Fig. 4B).

Finally, we examined whether RNA polymerase II (Pol II) occupancy at genes is altered by ectopic expression of H2B S36A. ChIP analysis showed that Pol II was present through the *cpt1c* gene, and Pol II increased in glucose withdrawal (Fig. 4C). In FLAG–H2B S36A cells, the Pol II ChIP signal was reduced along the transcribed region of the *cpt1c* gene specifically under conditions of glucose withdrawal (Fig. 4C). These data point to AMPK-mediated phosphorylation of H2B at Ser^{36} as a critical transcriptional regulatory step in the cellular adaptation response to stress, to optimize cell survival.

Our results show that AMPK directly associates with chromatin to regulate transcriptional programs required to survive a wide variety of metabolic and environmental stresses. Mammalian AMPK is a histone kinase that preferentially phosphorylates histone H2B at Ser^{36}. Phosphorylation of this site in vivo is acutely dependent on the LKB1-AMPK energy-sensing pathway, and through their direct action at genes.

AMPK and H2B pS36 appear to regulate transcription by direct interaction between the kinase and the H2B substrate. AMPK appears to be recruited to specific promoters by transcription factors such as p53. AMPK may similarly influence other stress-induced transcriptional activators, including Foxo3a, peroxisome proliferator–activated receptor γ coactivator 1α (PGC-1α), and transducer of regulated CREB activity 2 (TORC2) (*2*, *14*–*16*). AMPK colocalizes with and phosphorylates H2B at p53 binding sites and along the transcribed *cpt1c* and *p21* genes. This pattern may be due to activator recruitment of the enzyme, followed by enzyme transit across transcribed regions, as seen for the SAGA-Gcn5-Ubp8 complex and in the acetylation of H3 with deubiquitination of H2B (*17*, *18*). Moreover, histone methylases associate with RNA Pol II to modify H3 across transcribed regions (*19*). Our findings represent evidence for histone phosphorylation across transcribed regions, which suggests that AMPK, via H2B Ser^{36} phosphorylation, may play a role in transcriptional elongation.

Ectopic expression of the H2B S36A mutant, even in the presence of higher levels of endogenous wild-type H2B, significantly reduces transcription of AMPK target genes and stress survival. Hence, the modification may function processively to facilitate transcription elongation. Indeed, H2B Ser^{36} phosphorylation promotes RNA Pol II association to transcribed regions. Ectopic expression of mutant histone genes may be of broad utility to unravel functions of other histone modifications in mammalian cells.

As part of the central energy-sensing pathway in eukaryotes, AMPK functions to maintain cellular energy homeostasis in the face of metabolic perturbations. Our data suggest that modification of H2B by AMPK may be a general stress-response pathway to tune specific transcriptional responses, regulate cellular metabolism, and promote cell survival.

References and Notes

1. D. G. Hardie, *Nat. Rev. Mol. Cell Biol.* **8**, 774 (2007).
2. R. G. Jones *et al.*, *Mol. Cell* **18**, 283 (2005).
3. D. G. Hardie, *Curr. Opin. Cell Biol.* **17**, 167 (2005).
4. K. R. Laderoute *et al.*, *Mol. Cell. Biol.* **26**, 5336 (2006).
5. P. Y. Zeng, S. L. Berger, *Cancer Res.* **66**, 10701 (2006).
6. S. L. McGee, M. Hargreaves, *Front. Biosci.* **13**, 3022 (2008).
7. S. L. Berger, *Nature* **447**, 407 (2007).
8. M. S. Ivaldi, C. S. Karam, V. G. Corces, *Genes Dev.* **21**, 2818 (2007).
9. C. J. Salt *et al.*, *Biochem. J.* **334**, 177 (1998).
10. D. M. Gwinn *et al.*, *Mol. Cell* **30**, 214 (2008).
11. J. Weekes, K. L. Ball, F. B. Caudwell, D. G. Hardie, *FEBS Lett.* **334**, 335 (1993).
12. M. C. Towler, D. G. Hardie, *Circ. Res.* **100**, 328 (2007).
13. D. G. Hardie, I. P. Salt, S. P. Davies, *Methods Mol. Biol.* **99**, 63 (2000).
14. R. J. Shaw *et al.*, *Science* **310**, 1642 (2005).
15. E. L. Greer *et al.*, *J. Biol. Chem.* **282**, 30107 (2007).
16. S. Jäger, C. Handschin, J. St.-Pierre, B. M. Spiegelman, *Proc. Natl. Acad. Sci. U.S.A.* **104**, 12017 (2007).
17. C. K. Govind, F. Zhang, H. Qiu, K. Hofmeyer, A. G. Hinnebusch, *Mol. Cell* **25**, 31 (2007).
18. A. Wyce *et al.*, *Mol. Cell* **27**, 275 (2007).
19. A. Shilatifard, *Annu. Rev. Biochem.* **75**, 243 (2006).

20. Supported by NIH grants CA078831 (S.L.B.) and CA105463 (C.B.T.), NIH Training Program in Basic Cancer Research grant CA09171 (D.B.), Canadian Institutes of Health Research grant MOP-93799 (R.G.J.), the McGill Integrated Cancer Research Training Program (B.F.), and the Leukemia and Lymphoma Society, NIH, National Cancer Institute, and American Association for Cancer Research (AACR)/Stand Up to Cancer (C.B.T.). C.B.T. reports the filing of patent applications exploiting the use of AMPK activators in cancer therapy. He is also a member of the board of directors of Merck, the scientific advisory board of Agios Pharmaceuticals, and the medical advisory board of the Howard Hughes Medical Institute.

Supporting Online Material

www.sciencemag.org/cgi/content/full/science.1191241/DC1
Materials and Methods
Figs. S1 to S28
References

21 April 2010; accepted 23 June 2010
Published online 15 July 2010;
10.1126/science.1191241
Include this information when citing this paper.

The Junctional Adhesion Molecule JAML Is a Costimulatory Receptor for Epithelial γδ T Cell Activation

Deborah A. Witherden,[1] Petra Verdino,[2] Stephanie E. Rieder,[1]* Olivia Garijo,[1] Robyn E. Mills,[1]† Luc Teyton,[1] Wolfgang H. Fischer,[4] Ian A. Wilson,[2,3] Wendy L. Havran[1]‡

γδ T cells present in epithelial tissues provide a crucial first line of defense against environmental insults, including infection, trauma, and malignancy, yet the molecular events surrounding their activation remain poorly defined. Here we identify an epithelial γδ T cell–specific costimulatory molecule, junctional adhesion molecule–like protein (JAML). Binding of JAML to its ligand Coxsackie and adenovirus receptor (CAR) provides costimulation leading to cellular proliferation and cytokine and growth factor production. Inhibition of JAML costimulation leads to diminished γδ T cell activation and delayed wound closure akin to that seen in the absence of γδ T cells. Our results identify JAML as a crucial component of epithelial γδ T cell biology and have broader implications for CAR and JAML in tissue homeostasis and repair.

Key players in cellular immunity, αβ and γδ T cells, fulfill distinct, yet equally important, functions. αβ T cells are primarily involved in foreign antigen recognition, whereas γδ T cells function in tissue homeostasis and recognition of damaged self (*1*–*3*). Epithelial γδ T cells reside at the interface between organism and environment. They provide a rapid response to environmental insults and are crucial to the maintenance of epithelial integrity (*2*, *4*, *5*). γδ T cells in the skin, also known as dendritic epidermal T cells (DETCs), are a prototypic epithelial γδ T cell population. DETCs have cellular projections that are in constant contact with multiple neighboring keratinocytes and Langerhans cells (*6*) and are activated after interaction with damaged or malignant keratinocytes (*2*, *4*). DETC activation likely relies on the interplay of numerous cell surface molecules, as for αβ T cell activation, but the underlying mechanisms of DETC activation are unknown. Furthermore, many of

[1]Department of Immunology and Microbial Science, The Scripps Research Institute, La Jolla, CA 92037, USA. [2]Department of Molecular Biology, The Scripps Research Institute, La Jolla, CA 92037, USA. [3]The Skaggs Institute for Chemical Biology, The Scripps Research Institute, La Jolla, CA 92037, USA. [4]Peptide Biology, The Salk Institute, La Jolla, CA 92037, USA.

*Present address: Abbott Bioresearch Center, Worcester, MA 01605, USA

†Present address: University of California, San Francisco, San Francisco, CA 94143, USA

‡To whom correspondence should be addressed. E-mail: havran@scripps.edu.

the rules that apply to αβ T cell activation do not hold for γδ T cells. Coreceptor engagement and costimulation are integral to effective αβ T cell activation, but DETCs do not express the CD4 or CD8 coreceptors or the costimulatory molecule CD28 (*1*, *7*). Moreover, expression of MHC molecules or the costimulatory ligand B7 on keratinocytes is not required for DETC recognition of antigen (*1*, *7*). Identification of equivalent activation molecules for γδ T cells has remained elusive. Although DETCs do express some costimulatory molecules, such as NKG2D (*4*, *8*), these are not unique to γδ T cells, and their role in γδ T cell activation is not clearly defined.

To shed light on the activation requirements of γδ T cells, we generated monoclonal antibodies (mAbs) to cell surface molecules expressed by DETCs (*9*). Initial screens identified one mAb, HL4E10, as inducing potent proliferation of DETCs. The ligand for HL4E10 was expressed on the cell surface (Fig. 1A), which showed a punctate expression pattern, colocalizing with much of the T cell receptor (TCR) (Fig. 1B) and had a molecular mass of ~55 kD (Fig. 1C). Mass spectrometry identified the ligand as mouse junctional adhesion molecule–like protein (JAML), and the specificity of HL4E10 for mouse JAML was confirmed by flow cytometry and immunoprecipitation (figs. S1 and S2).

JAML is a member of the junctional adhesion molecule (JAM) family (*10*) and in humans is expressed on neutrophils and, to a lesser extent, on memory T cells and monocytes (*10*, *11*). JAM family members are thought to regulate leukocyte-endothelial interactions, to facilitate tight-junction assembly, and to help orchestrate recruitment of leukocytes to sites of inflammation and wound repair (*12*, *13*). As DETCs are primary responders to epidermal insult, JAML may play a crucial role in epidermal wound repair.

Low-level expression of JAML was found on resting γδ T cells isolated from mouse epidermis and intestine, but not spleen (Fig. 1, D and E). When stimulated with a mitogen, 70 to 95% of γδ T cells from each of these tissues up-regulated JAML (Fig. 1D). Increased expression was evident on DETCs within 4 hours and continued to increase for 24 to 48 hours (fig. S3). JAML was not found on B cells, $CD4^+$αβ T cells, or resting $CD8^+$αβ T cells (Fig. 1, F and G). However, about 50% of Concanavalin A (Con A)–activated, splenic $CD8^+$αβ T cells did express JAML (Fig. 1F), as did activated $CD8\alpha\alpha^+$ and $CD8\alpha\beta^+$ αβ T cells in the intestine (fig. S4). In the spleen, the activated $JAML^+CD8^+$ population was indistinguishable from the $JAML^-CD8^+$ T cells on the basis of expression of several activation markers (fig. S5). Analysis of a number of cell lines further supported a restricted expression of mouse JAML (Fig. 1H), and we found no evidence of JAML expression on adult αβ or γδ thymocytes (fig. S6). Thus, the expression pattern, as well as the proliferation results from our initial screen, suggested that JAML plays an important role in γδ T cell activation.

Ligation of JAML with HL4E10 induced costimulation of both short-term cell lines from

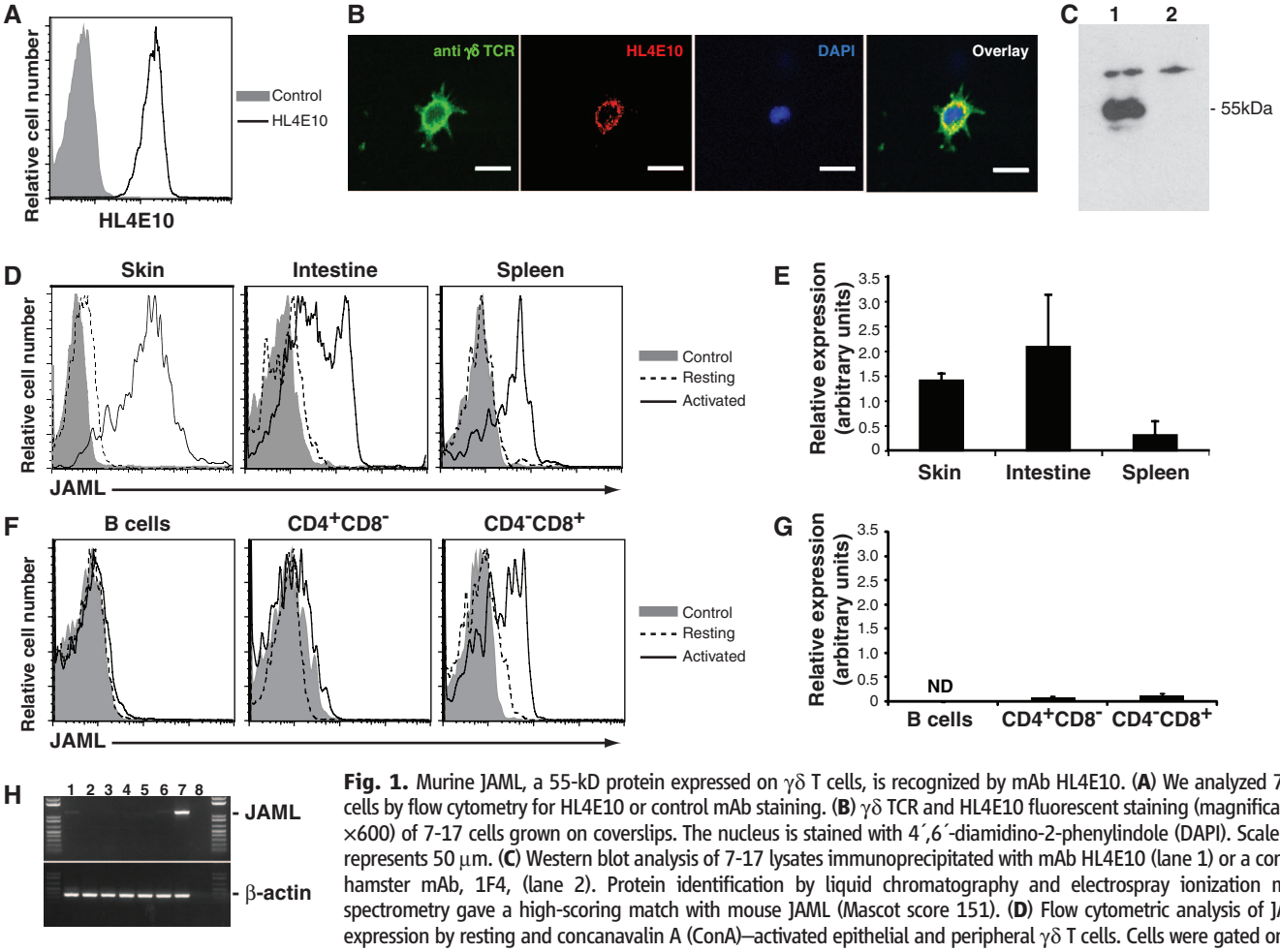

Fig. 1. Murine JAML, a 55-kD protein expressed on γδ T cells, is recognized by mAb HL4E10. (**A**) We analyzed 7-17 cells by flow cytometry for HL4E10 or control mAb staining. (**B**) γδ TCR and HL4E10 fluorescent staining (magnification ×600) of 7-17 cells grown on coverslips. The nucleus is stained with 4′,6′-diamidino-2-phenylindole (DAPI). Scale bar represents 50 μm. (**C**) Western blot analysis of 7-17 lysates immunoprecipitated with mAb HL4E10 (lane 1) or a control hamster mAb, 1F4, (lane 2). Protein identification by liquid chromatography and electrospray ionization mass spectrometry gave a high-scoring match with mouse JAML (Mascot score 151). (**D**) Flow cytometric analysis of JAML expression by resting and concanavalin A (ConA)–activated epithelial and peripheral γδ T cells. Cells were gated on γδ TCR^+. (**E**) Quantitative reverse transcription polymerase chain reaction (RT-PCR) analysis of JAML expression in γδ T cells from epidermis, intestine, and spleen. Relative amounts of JAML mRNA were normalized to β-actin and are shown as arbitrary units. (**F**) Flow cytometric analysis of JAML expression by splenic B cells, $CD4^+$ T cells, and $CD8^+$ T cells. Both resting and activated B cells (lipopolysaccharide-activated) and αβ T cells [phorbol 12-myristate 13-acetate (PMA) and ionomycin] were analyzed. (**G**) Quantitative RT-PCR analysis of JAML expression in $CD4^+CD8^-$ and $CD4^-CD8^+$ splenocytes. Relative amounts of JAML mRNA were normalized to β-actin and are shown as arbitrary units. ND, not determined. (**H**) JAML mRNA isolated from representative epithelial and lymphocyte cell lines: PAM keratinocytes (lane 1); 3T3 fibroblasts (lane 2); double-positive thymocytes (DPK, lane 3); $CD4^+$ T cells (lane 4); $CD8^+$ T cells (lane 5); B cells (lane 6); γδ T cells (7-17, lane 7); and RT control (lane 8). Data in (A) through (H) are representative of at least three experiments.

freshly isolated DETCs (Fig. 2A) and the established 7-17 DETC cell line (fig. S7). Costimulation through JAML induced proliferation (Fig. 2A and fig. S7) and production of the cytokines interleukin-2 (IL-2), tumor necrosis factor-α (TNFα), and interferon-γ (IFN-γ) (Fig. 2B and figs. S7 and S8), which supported a role for JAML in the activation and effector function of epidermal γδ T cells. HL4E10 also induced potent costimulation of intestinal γδ T cells, but not splenic γδ T cells (Fig. 2C), whereas CD28, expressed by γδ T cells in the spleen but not intestine, only costimulated splenic γδ T cells (Fig. 2C). This dichotomy of JAML function between epithelial and lymphoid γδ T cells is perhaps surprising because of the expression of JAML on both γδ T cell populations upon stimulation; however, tissue-resident γδ T cells constitutively express low levels of JAML, whereas lymphoid γδ T cells require activation to produce detectable JAML (Fig. 1, D and E). Indeed, unlike splenic γδ T cells, epithelial-resident γδ T cells were responsive to JAML costimulation directly ex vivo (Fig. 2C and fig. S9). JAML may thus contribute to later stages of lymphoid γδ T cell activation, as suggested for inducible T cell costimulator (ICOS)–mediated costimulation of αβ T cells (*14*).

Although the necessity of costimulation in γδ T cell activation remains an open question, αβ T cells rely on efficient costimulation, most notably through CD28, for their activation and effector function (*15*, *16*). Despite expression of JAML on activated $CD8^+$ αβ T cells (Fig. 1F), it was unable to costimulate either $CD4^+$ or $CD8^+$ αβ T cells (Fig. 2D). Furthermore, intestinal $CD8\alpha\alpha^+$, $CD8\alpha\beta^+$, and $CD4^+$ αβ T cells did not respond to JAML costimulation (Fig. 2, E and F). Thus, the costimulatory function of JAML appears to be specific for epithelial γδ T cells, in contrast to other putative γδ T cell costimulatory molecules (*4*).

Recently, epithelial-expressed Coxsackie and adenovirus receptor (CAR) has been shown to be a ligand for JAML on neutrophils (*17*). We therefore reasoned that the skin JAML ligand might also be CAR. CAR migrates at 46 kD (*18*) and is not expressed by 3T3 fibroblasts (*19*). As expected, soluble JAML (sJAML) bound only to keratinocyte cell lines and not fibroblasts (Fig. 3A) and precipitated a 46-kD protein from keratinocytes (Fig. 3B).

CAR is best characterized as the primary receptor for Coxsackie B virus and adenoviruses (*18*, *20*, *21*). To confirm CAR as the ligand for JAML in the epidermis, we performed competitive binding analysis using a soluble adenovirus fiber protein (Ad5 fiber knob; F5) and JAML (Fig. 3, C to F). Fluorescence-activated cell sorting analysis confirmed that the JAML ligand and CAR are expressed on keratinocytes (Fig. 3C). Addition of F5 to keratinocytes displaced (Fig. 3D) or blocked (Fig. 3E) binding of JAML, whereas fixation of keratinocyte-bound JAML before F5 addition allowed simultaneous binding of some JAML and F5 (Fig. 3F). These data confirmed that CAR is the keratinocyte ligand for JAML and, on the basis of displacement of JAML by F5, appears to represent a lower affinity interaction ($K_d \approx 5$ μM) (*22*) compared with a $K_d \approx 8$ nM for adenovirus serotype 5 (*23*), but comparable to other lymphocyte cell-cell molecular interactions (*24*).

Binding of soluble CAR and HL4E10 to JAML single-domain constructs demonstrated that CAR and HL4E10 recognize different epitopes of JAML. HL4E10 bound the membrane-proximal JAML D2 immunoglobulin domain, whereas CAR-Fc bound the membrane distal JAML D1 immunoglobulin domain (fig. S10). This binding mode was confirmed in the crystal structure of JAML in complex with CAR (*22*), in contrast to previous suggestions (*17*).

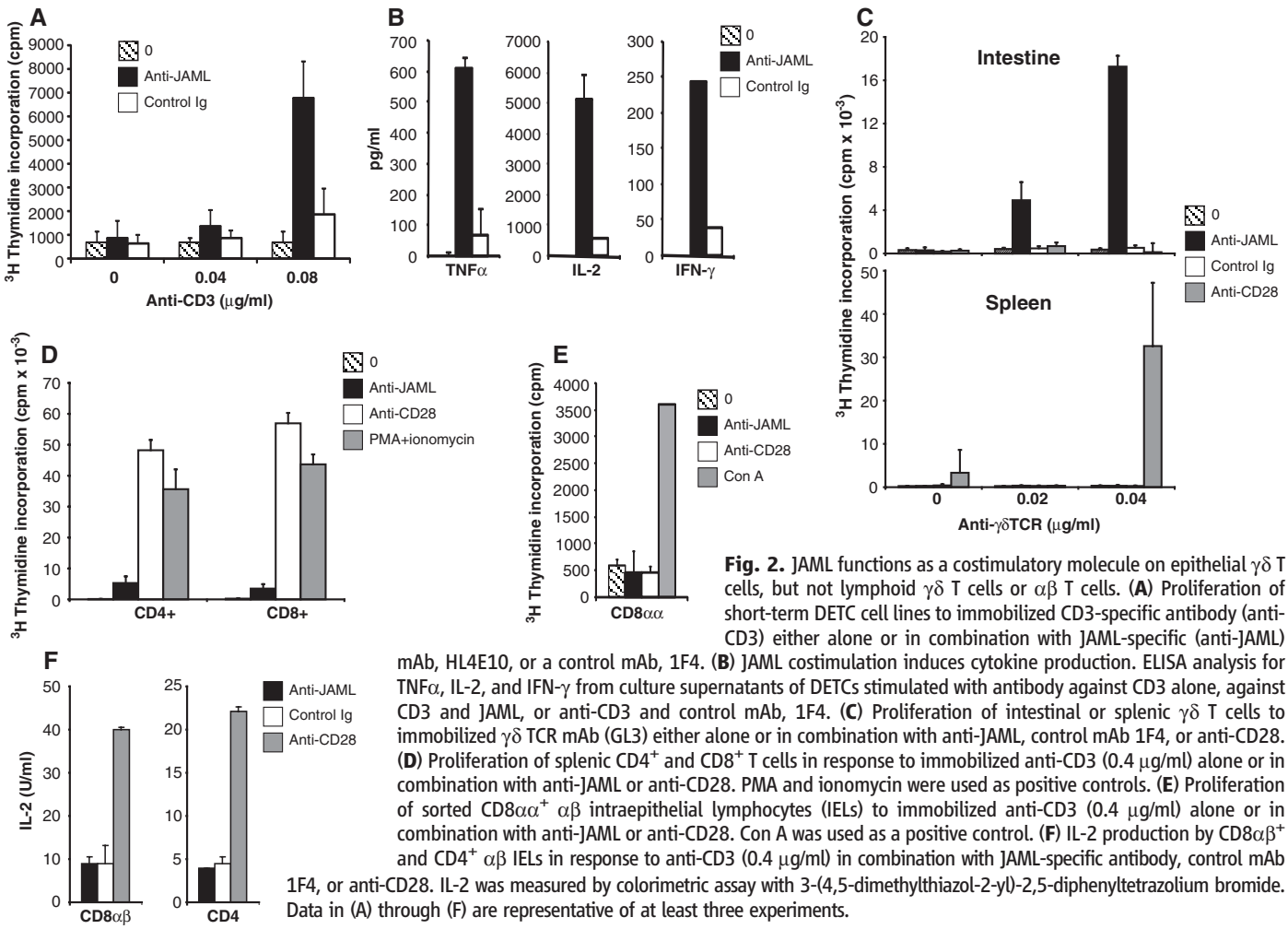

Fig. 2. JAML functions as a costimulatory molecule on epithelial γδ T cells, but not lymphoid γδ T cells or αβ T cells. (**A**) Proliferation of short-term DETC cell lines to immobilized CD3-specific antibody (anti-CD3) either alone or in combination with JAML-specific (anti-JAML) mAb, HL4E10, or a control mAb, 1F4. (**B**) JAML costimulation induces cytokine production. ELISA analysis for TNFα, IL-2, and IFN-γ from culture supernatants of DETCs stimulated with antibody against CD3 alone, against CD3 and JAML, or anti-CD3 and control mAb, 1F4. (**C**) Proliferation of intestinal or splenic γδ T cells to immobilized γδ TCR mAb (GL3) either alone or in combination with anti-JAML, control mAb 1F4, or anti-CD28. (**D**) Proliferation of splenic $CD4^+$ and $CD8^+$ T cells in response to immobilized anti-CD3 (0.4 μg/ml) alone or in combination with anti-JAML or anti-CD28. PMA and ionomycin were used as positive controls. (**E**) Proliferation of sorted $CD8\alpha\alpha^+$ αβ intraepithelial lymphocytes (IELs) to immobilized anti-CD3 (0.4 μg/ml) alone or in combination with anti-JAML or anti-CD28. Con A was used as a positive control. (**F**) IL-2 production by $CD8\alpha\beta^+$ and $CD4^+$ αβ IELs in response to anti-CD3 (0.4 μg/ml) in combination with JAML-specific antibody, control mAb 1F4, or anti-CD28. IL-2 was measured by colorimetric assay with 3-(4,5-dimethylthiazol-2-yl)-2,5-diphenyltetrazolium bromide. Data in (A) through (F) are representative of at least three experiments.

In vitro costimulation assays demonstrated that CAR is a functional ligand for JAML. CAR ligation of JAML induced proliferation (Fig. 3G) and IL-2 production (fig. S11) by DETCs that was comparable to mAb HL4E10. Although CAR has been extensively studied as a virus receptor (*18*, *20*, *21*) and, more recently, as an adhesion molecule (*11*, *17*), these data demonstrate its importance as a signaling molecule in the immune system.

CAR ligation of JAML leads to rapid and sustained phosphoinositide 3-kinase (PI3K) association with a YMxM motif in the JAML intracellular domain (*22*, *25*). In CD28 and ICOS, phosphorylated YMxM is also required for PI3K binding (*26*). CD28 and JAML are the only two molecules that contain a YMxMxPxxP motif in their intracellular domains (*22*), which suggests that they may also share other downstream signals. We therefore examined the effect of JAML ligation on Akt, the key downstream target of PI3K and one of the central molecules for CD28-mediated costimulation. Rapid phosphorylation of Akt at both Ser^{473} and Thr^{308} was induced in DETCs in response to CAR-JAML ligation and was entirely abrogated in the presence of a PI3K inhibitor (Fig. 3H). Thus, CAR-induced PI3K recruitment to JAML is tightly linked to activation of Akt and initiation of downstream signaling events.

Activation of mitogen-activated protein kinase (MAPK) pathways downstream of PI3K association with CD28 is a hallmark feature of αβ T cell activation (*26*). In DETCs, costimulation through JAML led to JNK kinase activity at 5 min of TCR and JAML coligation (Fig. 3I) compared with 20 min for TCR ligation alone (fig. S12), which induced a ninefold increase in JNK activity over TCR stimulation alone and a fivefold increase over HL4E10 alone (Fig. 3J). In contrast, ERK phosphorylation and p38 kinase activity were very similar to TCR ligation alone (Fig. 3, I and J, and fig. S12). The early JNK activation suggests that JAML can enhance signals through the γδ TCR, and it remains to be seen if alternate pathways can also be activated.

To address the role of JAML-CAR interactions in vivo, we first analyzed DETCs directly

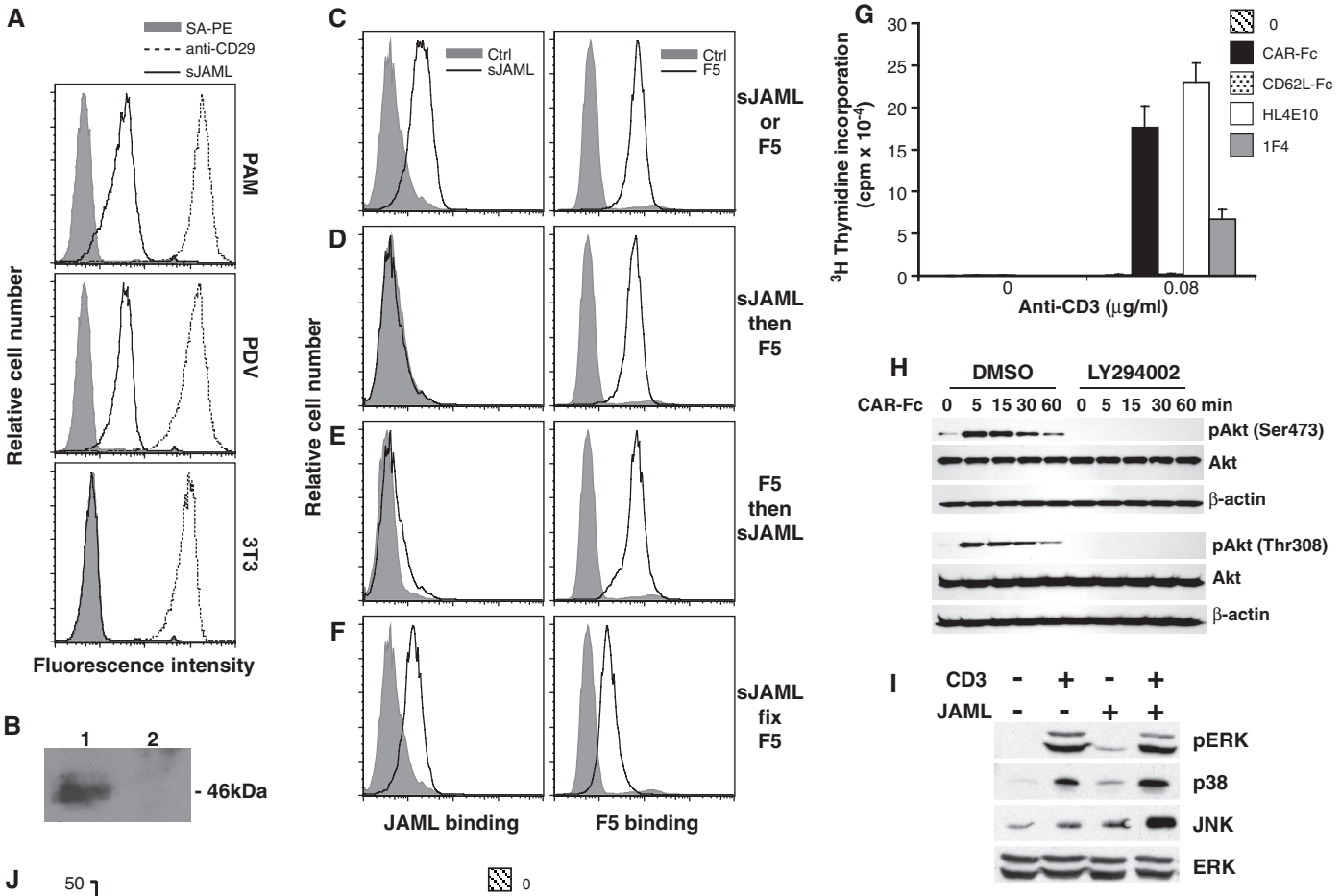

Fig. 3. CAR is a functional ligand for JAML in the epidermis. (**A**) PAM 2-12 and PDV keratinocyte and 3T3 fibroblast cell lines were analyzed by flow cytometry for binding of sJAML, anti-CD29 (positive control), or streptavidin PE (SA-PE) (negative control). (**B**) Western blot analysis of PDV lysates immunoprecipitated with sJAML (lane 1) or empty beads (lane 2). (**C** to **F**) PDV keratinocytes were analyzed by flow cytometry for binding of sJAML and soluble adenovirus fiber protein (F5). Keratinocytes were stained and sometimes fixed as described alongside the graphs. (**G**) Proliferation of the 7-17 γδ T cell line to immobilized anti-CD3 either alone or in combination with CAR-Fc, CD62L-Fc (a negative control Fc fusion protein), HL4E10, or control mAb 1F4. (**H**) Western blot analysis of phosphorylation of Akt Ser^{473} and Thr^{308} and total Akt in 7-17 DETCs after JAML ligation with CAR-Fc, in the presence or absence (dimethyl sulfoxide vehicle control) of the PI3K inhibitor LY294002. β-Actin was used as a loading control. (**I** and **J**) Western blot analysis of extracellular signal–regulated kinase (ERK) 1 and 2 phosphorylation and p38 and JNK kinase activity in 7-17 lysates after 5 min's stimulation with anti-CD3, anti-JAML, or both. Total ERK is shown as a control. Quantification of data in (I) is shown in (J). Data in (A) through (J) are representative of at least three experiments.

isolated from the epidermis, where JAML costimulation resulted in proliferation (Fig. 4A) and cytokine production (fig. S13) comparable to those seen with DETC lines (Fig. 2, A and B, and Fig. 3G). Strikingly, costimulation of DETCs was required for effective cytokine production (Fig. 4B). Proliferation of DETCs in vitro can be achieved with high-dose TCR stimulation (fig. S14), as for αβ T cells (*27*). When we used CD3 alone, at a concentration effective for maximal proliferation of DETCs (fig. S14), only minimal TNFα (Fig. 4B) production was apparent. In contrast, costimulation through JAML resulted in substantially more production of TNFα (Fig. 4B), which suggested that JAML costimulation is necessary for rapid and robust production of the cytokines required for DETC effector function. Consistent with JAML's role as a mediator of γδ T cell function, its use as a costimulator also up-regulated expression of keratinocyte growth factor 1 (KGF-1) in primary DETCs (Fig. 4C), a vital component of the wound repair process (*2*).

A requirement for JAML-CAR costimulation in vivo is further supported by the response of keratinocytes and DETCs to epidermal wounding. Keratinocytes immediately adjacent to the wound site up-regulate CAR expression beginning 4 hours post wounding (Fig. 4D). The neighboring DETCs become activated, as evidenced by an increased production of cytokines and growth factors (*2*, *28*). Blockade of JAML-CAR interactions, immediately after wounding, reduced activation of DETCs isolated from the wound edge (Fig. 4E) and impaired the healing response (Fig. 4F). A significant delay in wound closure followed treatment of wounds with a single dose of soluble adenovirus F5 protein (Fig. 4F) (*29*). Notably, the kinetics of wound closure followed very closely the repair observed in the skin in the absence of γδ T cells (Fig. 4F). No effect was seen after addition of the HL4E10 mAb, presumably because of high levels of constitutive expression of CAR in the epidermis that is available for JAML binding; nevertheless, addition of the HL4E10 to F5-treated wounds restored wound closure kinetics to untreated levels

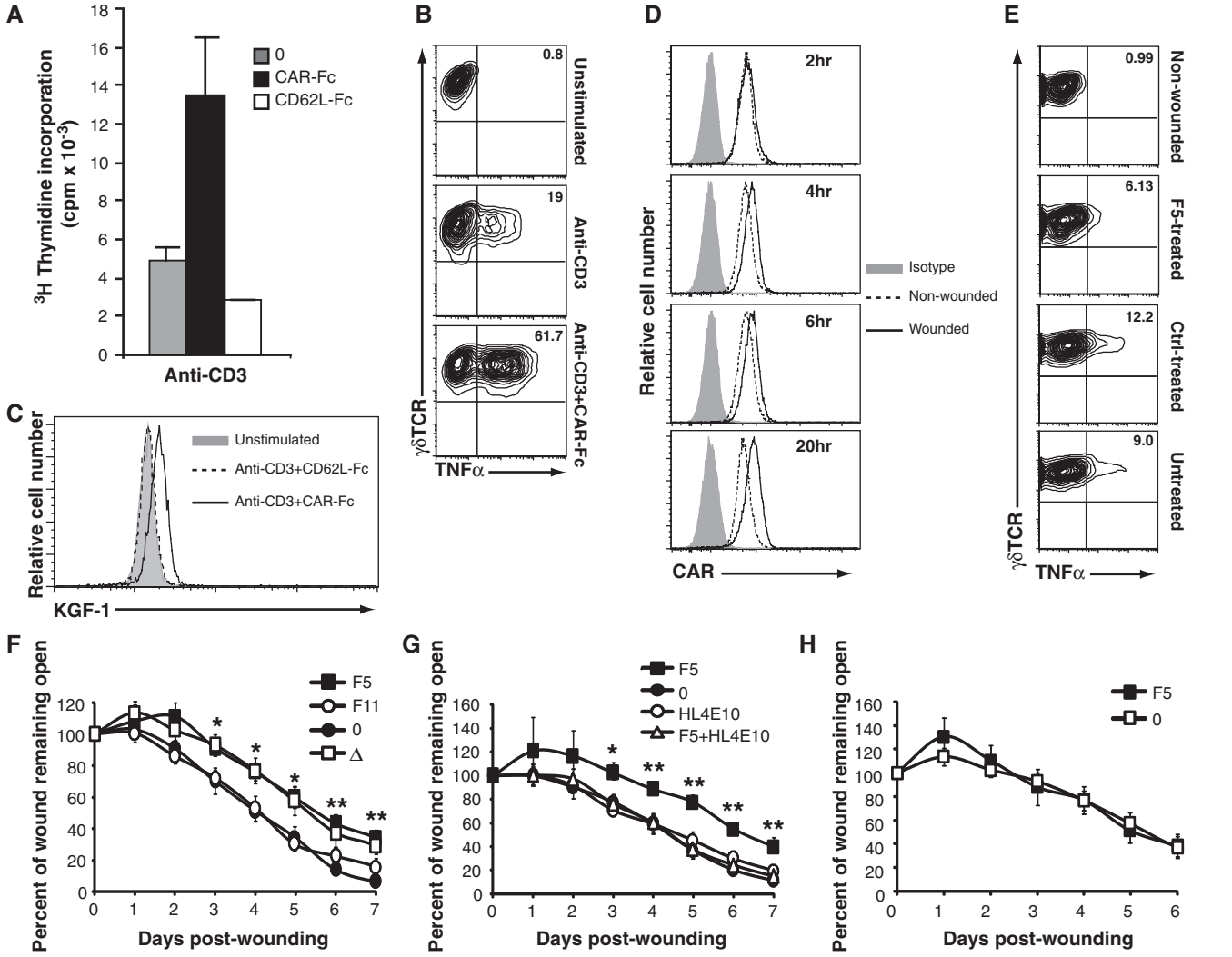

Fig. 4. Costimulation through JAML-CAR interactions mediates epithelial γδ T cell activation and effector function. (**A**) Proliferation of freshly isolated epidermal γδ T cells to immobilized anti-CD3 (1 μg/ml) either alone (0) or in combination with CAR-Fc or a negative control Fc fusion protein, CD62L-Fc. (**B**) Intracellular flow cytometric analysis of TNF-α production by unstimulated, anti-CD3 stimulated (0.5 μg/ml), or anti-CD3 (0.05 μg/ml) and CAR-Fc (10 μg/ml) stimulated 7-17 DETCs. (**C**) Flow cytometric analysis of KGF expression by unstimulated primary DETCs or after stimulation with immobilized anti-CD3 (1 μg/ml) and CAR-Fc or anti-CD3 and control Fc fusion protein, CD62L-Fc. (**D**) Flow cytometric analysis of CAR expression by keratinocytes isolated from epidermis of C57BL/6 mice. Skin was either nonwounded or wounded, and keratinocytes were isolated at the indicated times. (**E**) Flow cytometric analysis of TNFα production by DETCs isolated from epidermis of C57BL/6 mice. Skin was nonwounded, wounded and treated with soluble F5 protein (F5-treated), wounded and treated with control soluble F11 protein (Ctrl-treated), or wounded and not treated. (**F**) Wound closure in vivo in the presence of soluble F5 or a control protein, F11. Untreated C57BL/6 mice (0) and TCRδ$^{-/-}$ mice (Δ) were used as controls. (**G**) Wound closure in the presence of F5, HL4E10, or F5 and HL4E10. Untreated C57BL/6 mice (0) were used as a control for rate of wound closure. (**H**) Wound closure in F5-treated (F5) and untreated (0) TCRδ$^{-/-}$ mice. Data represent means ± SEM of four to eight wounds per condition. Student's *t* test *P* values (**$P < 0.005$ and *$P < 0.05$). Data in (A) through (H) are representative of more than three experiments.

(Fig. 4G). HL4E10 thus appears to be able to substitute for CAR and to restore JAML-mediated costimulation to γδ T cells at the wound site. The specificity of F5 treatment for JAML-CAR blockade on γδ T cells was confirmed by the observation that no further delay in wound closure was found after addition of F5 to TCRδ$^{-/-}$ wounds (Fig. 4H). These data strongly suggest that the JAML-CAR interaction contributes to natural γδ T cell activation and effector function.

Epithelial γδ T cells provide a crucial first line of defense for epithelial barrier tissues. The complete activation of these cells is vital to their responses to epithelial insults, such as infection, trauma, and malignancy. Assessment of the full extent to which epithelial γδ T cells require JAML-CAR interactions in concert with TCR signals cannot be fully addressed until the cognate ligand for these cells is identified. Nevertheless, manipulation of the interaction between JAML and CAR may well increase the effectiveness of the epithelial γδ T cell response in cases of chronic disease, such as nonhealing wounds and epithelial malignancies.

References and Notes

1. W. L. Havran, Y. H. Chien, J. P. Allison, *Science* **252**, 1430 (1991).
2. J. Jameson *et al.*, *Science* **296**, 747 (2002).
3. J. Strid, R. E. Tigelaar, A. C. Hayday, *Semin. Immunol.* **21**, 110 (2009).
4. M. Girardi *et al.*, *Science* **294**, 605 (2001).
5. L. L. Sharp, J. M. Jameson, G. Cauvi, W. L. Havran, *Nat. Immunol.* **6**, 73 (2005).
6. J. Jameson, W. L. Havran, *Immunol. Rev.* **215**, 114 (2007).
7. A. C. Hayday, *Annu. Rev. Immunol.* **18**, 975 (2000).
8. M. I. Whang, N. Guerra, D. H. Raulet, *J. Immunol.* **182**, 4557 (2009).
9. Materials and methods are available as supporting material on *Science* Online.
10. C. Moog-Lutz *et al.*, *Blood* **102**, 3371 (2003).
11. A. C. Luissint, P. G. Lutz, D. A. Calderwood, P. O. Couraud, S. Bourdoulous, *J. Cell Biol.* **183**, 1159 (2008).
12. G. Bazzoni, *Curr. Opin. Cell Biol.* **15**, 525 (2003).
13. K. Ebnet, A. Suzuki, S. Ohno, D. Vestweber, *J. Cell Sci.* **117**, 19 (2004).
14. A. J. Coyle *et al.*, *Immunity* **13**, 95 (2000).
15. M. Croft, C. Dubey, *Crit. Rev. Immunol.* **17**, 89 (1997).
16. K. A. Frauwirth, C. B. Thompson, *J. Clin. Invest.* **109**, 295 (2002).
17. K. Zen *et al.*, *Mol. Biol. Cell* **16**, 2694 (2005).
18. C. B. Coyne, J. M. Bergelson, *Adv. Drug Deliv. Rev.* **57**, 869 (2005).
19. R. P. Tomko, R. Xu, L. Philipson, *Proc. Natl. Acad. Sci. U.S.A.* **94**, 3352 (1997).
20. J. M. Bergelson *et al.*, *J. Virol.* **72**, 415 (1998).
21. J. Howitt, C. W. Anderson, P. Freimuth, *Curr. Top. Microbiol. Immunol.* **272**, 331 (2003).
22. P. Verdino, D. A. Witherden, W. L. Havran, I. A. Wilson, *Science* **329**, 1210 (2010).
23. I. Kirby *et al.*, *J. Virol.* **75**, 7210 (2001).
24. M. M. Davis *et al.*, *Annu. Rev. Biochem.* **72**, 717 (2003).
25. Single-letter abbreviations for the amino acid residues used in this report are as follows: Y, Tyr; M, Met; P, Pro; and X, any amino acid.
26. C. E. Rudd, H. Schneider, *Nat. Rev. Immunol.* **3**, 544 (2003).
27. R. H. Schwartz, *Science* **248**, 1349 (1990).
28. W. L. Havran, J. M. Jameson, *J. Immunol.* **184**, 5423 (2010).
29. F5 and JAML recognize overlapping binding sites on CAR (*22*). As such, F5 is able to block the natural JAML-CAR interaction (Fig. 3, D and E).

30. We thank M. Park and W. Low for MS analysis; G. Nemerow for Fiber 5 and Fiber 11 reagents; J. Kaye for the DPK cell line; and M. Haynes, M. Svoboda, J. Barcas, K. Sendaydiego, D. Yeh, and B. Atteberry for technical assistance. J. Lewis provided advice on culture of short-term DETC lines. M. Kronenberg, R. Boismenu, J. Jameson, K. Mowen, T. Meehan, and K. Komori provided advice and critical reading of the manuscript. This work was supported by NIH grants to W.L.H. (AI52257, AI064811) and I.A.W. (AI42266, CA58896), as well as an Erwin-Schroedinger Fellowship of the Austrian Science Fund (P.V.) and the Leukemia and Lymphoma Society (S.E.R.). MS instrumentation was acquired with an NSF shared equipment grant. The MS Laboratory at the Salk Institute is supported by the Vincent J. Coates Foundation and NIH Blueprint NS057096. This is manuscript number 17711-IMM from The Scripps Research Institute.

Supporting Online Material

www.sciencemag.org/cgi/content/full/329/5996/1205/DC1
Materials and Methods
Figs. S1 to S14
References

24 May 2010; accepted 9 July 2010
10.1126/science.1192698

The Molecular Interaction of CAR and JAML Recruits the Central Cell Signal Transducer PI3K

Petra Verdino,[1] Deborah A. Witherden,[2] Wendy L. Havran,[2] Ian A. Wilson[1,3]*

Coxsackie and adenovirus receptor (CAR) is the primary cellular receptor for group B coxsackieviruses and most adenovirus serotypes and plays a crucial role in adenoviral gene therapy. Recent discovery of the interaction between junctional adhesion molecule–like protein (JAML) and CAR uncovered important functional roles in immunity, inflammation, and tissue homeostasis. Crystal structures of JAML ectodomain (2.2 angstroms) and its complex with CAR (2.8 angstroms) reveal an unusual immunoglobulin-domain assembly for JAML and a charged interface that confers high specificity. Biochemical and mutagenesis studies illustrate how CAR-mediated clustering of JAML recruits phosphoinositide 3-kinase (PI3K) to a JAML intracellular sequence motif as delineated for the αβ T cell costimulatory receptor CD28. Thus, CAR and JAML are cell signaling receptors of the immune system with implications for asthma, cancer, and chronic nonhealing wounds.

The coxsackievirus and adenovirus receptor, CAR (*1*, *2*), plays a crucial role in both virus-related pathology and adenoviral gene therapy (*3*–*5*). The tissue distribution of CAR is broader than the observed virus tropism (*6*), and substantial efforts have been devoted to characterizing and modifying CAR-virus interactions to improve the efficacy and safety of adenoviral gene delivery (*7*). The high conservation of CAR among vertebrates and its low genetic diversity in humans have resulted in its frequent occurrence as a target in the evolution of virus-host interactions (*6*). Such conservation indicates that CAR is physiologically important. However, although roles in embryonic development, cell adhesion, tumor cell growth, inflammation, and tissue regeneration have been reported, the underlying mechanisms remain elusive (*8*, *9*). The junctional adhesion molecule–like protein, JAML (*10*), present on a variety of effector cells of both adaptive and innate immunity (including neutrophils, monocytes, memory T cells, and epithelial γδ T cells) was recently identified as an endogenous ligand of epithelial and endothelial CAR (*11*–*14*). CAR and JAML are both type I transmembrane glycoproteins composed of a globular ectodomain (two immunoglobulin domains), a stalk (CAR: six residues, JAML: 26 residues), a single transmembrane helix, and a cytoplasmic domain. The CAR-JAML interaction is important for leukocyte migration and for activating γδ T cell responses (*11*–*14*), with implications for epithelial challenges, such as wound repair or inflammation (*15*). CAR binding to JAML on epithelial γδ T cells induces cytokine and growth factor production, mitogen-activated protein (MAP) kinase pathway activation, and, ultimately, cell proliferation (*14*), which indicates that JAML and CAR constitute an important cell-signaling complex of the immune system. To elucidate the mechanisms underlying CAR and JAML physiology, we determined the crystal structure of this receptor-ligand pair.

We expressed the mouse JAML ectodomain (residues 1 to 260) in SC2 cells, and purified and crystallized the protein (*16*) (tables S1 and S2). The structure was determined initially by multiwavelength anomalous dispersion phasing at 3.4 Å, by using a heavy atom derivative, and

[1]Department of Molecular Biology, The Scripps Research Institute, 10550 North Torrey Pines Road, La Jolla, CA 92037, USA. [2]Department of Immunology and Microbial Science, The Scripps Research Institute, 10550 North Torrey Pines Road, La Jolla, CA 92037, USA. [3]Skaggs Institute for Chemical Biology, The Scripps Research Institute, 10550 North Torrey Pines Road, La Jolla, CA 92037, USA.

*To whom correspondence should be addressed. E-mail: wilson@scripps.edu

then extended to 2.2 Å by molecular replacement (MR) of the experimental model into a higher-resolution native x-ray data set. In JAML, two V-set immunoglobulin domains (D1 and D2) associate into a compact assembly (Fig. 1A), where their relative orientation is constrained by an interdomain, parallel β-sheet interaction of the D1 B strand and the D2 B′ strand, numerous H bonds, a salt bridge, hydrophobic packing, and a short interdomain linker (Fig. 1, B to D, and fig. S1). The interface between D1 and D2 buries a total molecular surface area of 1050 Å^2 (D1: 540 Å^2, D2: 510 Å^2). The extent of the interface, combined with identical relative orientations of D1 and D2 in four different crystal forms (*17*), indicates that the highly compact JAML globular domain acts as a single rigid unit in contrast with typical, elongated structures of tandem immunoglobulin-domain receptors, such as CAR, CD2, or CD58 (fig. S2) (*18*), where flexibly linked immunoglobulin domains facilitate protein recognition.

Carbohydrate moieties are present at all potential N-linked glycosylation sites (Asn^{59}, Asn^{69}, and Asn^{105}) of JAML (Fig. 1A). However, these sites are not entirely conserved across species, which suggests that N-glycosylation is not directly correlated with JAML function, but might aid protein stabilization and prevent nonspecific interactions on the cell membrane. The stalk, which tethers the extracellular immunoglobulin domains of JAML to the cell membrane, and the C-terminal His tag are disordered in the crystal. This stalk is rich in serine, threonine, proline, and alanine (fig. S3A) and is likely to be O-glycosylated in vivo. The glycosylation would confer some rigidity to the otherwise flexible stalk and would result in a distance of <60 Å between the globular JAML domain and the membrane (Fig. 1A).

JAML can thus be considered an unconventional immunoglobulin-domain receptor where the more compact and rigid assembly of its immunoglobulin domains provides the ligand-binding site, and its extended stalk provides sufficient flexibility to facilitate interaction with CAR on the opposing cell surface. To gain insight into this interaction, we determined the crystal structure of the ectodomain complex of JAML and CAR.

The entire mouse CAR ectodomain (residues 1 to 217) was produced in SF9 cells and crystallized in an equimolar ratio with mouse JAML. The crystal structure was determined at 2.8 Å resolution by MR with unliganded JAML and human CAR D1 [Protein Data Bank accession no. 1EAJ (*19*)] as MR templates. The partially disordered CAR D2 domain was manually built using the nuclear magnetic resonance (NMR) structure of human CAR D2 [2NPL (*20*)] as a model (table S1). CAR and JAML form a 1:1 complex in the crystallographic asymmetric unit and, as expected for interaction of cell surface receptors from opposing cells, their C-terminal stalks protrude in opposite directions (Fig. 2A). Well-defined electron density was observed for JAML and the V-set CAR D1 immunoglobulin domain (*3*, *19*) (including the N-linked glycan at Asn^{87}). The C2-set CAR D2 immunoglobulin domain (*20*) was partially disordered, which indicated flexible linkage of the two CAR immunoglobulin domains and classified CAR as a typical tandem immunoglobulin-domain receptor. At the cell surface, CAR D2 is tethered to the membrane by a short stalk, and its motion may be additionally restricted by an N-glycan (Asn^{182}) in a membrane-proximal loop (fig. S4); thus, the flexibly linked D1 appears to facilitate interaction with JAML and might also aid in attachment of CAR to coxsackie and adenoviruses (*3*, *4*).

The CAR-JAML interface is restricted to the membrane-distal D1 domains of both receptors (Fig. 2A and table S4) in contrast to previous suggestions (*11*). Domain-deletion experiments demonstrate that JAML D1 is sufficient for CAR binding (*14*); however, JAML D2 exhibits indirect effects through enhancing both JAML expression levels and CAR-binding affinity to the JAML D1 domain (fig. S5). The D1 GFCC′C″ sheets of CAR and JAML pack face-to-face, comparable to the variable regions of the light and heavy chain (V_L-V_H) arrangement in antibodies or variable regions Vα-Vβ in T cell receptors. Additionally, the CAR A strand interacts with the JAML CC′-loop. The CAR-JAML interface buries a surface area of 1460 Å^2 (CAR: 740 Å^2, JAML: 720 Å^2), which is in the typical range for protein-protein complexes. Although its shape complementarity (Sc = 0.64) is on the low side for protein-protein interactions, it is consistent with the relatively weak CAR-JAML affinity (K_d ~5 μM) in solution (table S3), as in other cell-cell rec-

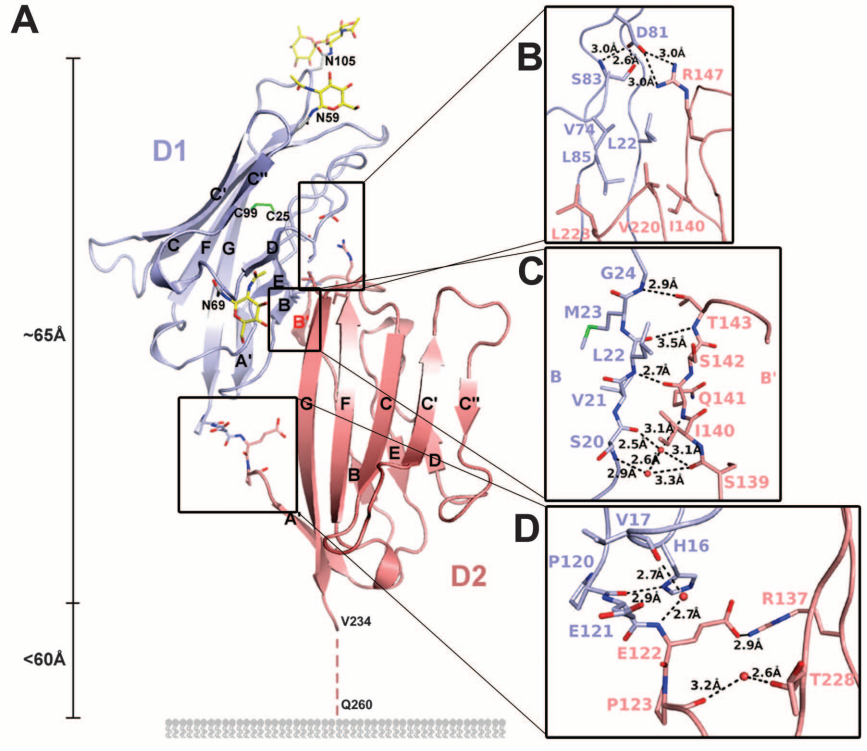

Fig. 1. Crystal structure of the unliganded mouse JAML ectodomain reveals a novel prototype for tandem immunoglobulin-domain receptors. (**A**) Ribbon diagram of JAML D1 (membrane-distal, residues 10 to 121, light blue) and D2 (membrane-proximal, residues 122 to 236, salmon) immunoglobulin V-set domains comprising nine β strands arranged into two antiparallel β sheets (A′GFCC′C″:DEB) linked by canonical disulfide bridges (Cys^{25} to Cys^{99} and Cys^{138} to Cys^{216}, green). D1 tightly packs its BED β sheet against the D2 B′C and FG loops. The D1 A strand (residues 1 to 9) and the C-terminal stalk region (residues 234 to 260, dashes) which tethers the JAML immunoglobulin domains to the cell membrane were disordered. Carbohydrate moieties attached to the three N-linked glycosylation sites (yellow sticks) are labeled. (**B** to **D**) Several interdomain interactions stabilize the relative orientation of D1 and D2 (see inset boxes). (B) A hydrophobic cluster is formed by Leu^{22}, Val^{74}, Leu^{85} of D1, and Ile^{140}, Val^{220}, and Leu^{223} of D2. Arg^{147} forms a salt bridge with Asp^{81}, whose side-chain orientation is restrained by H bonds to Ser^{83}. (C) A short β strand (B′, red) in the BC loop of D2 with the B strand of D1 creates a four-stranded DEBB′ interdomain β sheet. Additional interdomain H bonds (some water-mediated) are not shown: Arg^{14} to Gln^{141}, Glu^{19} to Gln^{141}, Glu^{19} to Ser^{139}, Glu^{19} to Glu^{122}, Ser^{20} to Ser^{225}, Gln^{87} to Glu^{224}, and Gln^{87} to Ser^{225}. (D) A short, rigid linker (residues 120 to 123) directly connects the D1 G strand to the D2 A′ strand, as D2 lacks an A strand. The linker is stabilized by two prolines, an H-bond network, and a salt bridge between Glu^{122} and Arg^{137}.

ognition systems (*21*). However, avidity and concentration effects for cell membrane–tethered receptors likely result in a greater effective molarity on the cell surface (*21*–*23*).

The CAR-JAML interface is unusually hydrophilic (Fig. 2E) and characterized by an array of interdigitated charged residues (Fig. 2C and fig. S6), which are conserved among homologs for both proteins (figs. S3 and S4). Two hydrophobic clusters (Fig. 2D) and an antiparallel β-sheet interaction between the CAR C′ strand and the JAML D1 FG loop (Fig. 2B and fig. S7) provide additional stabilization. A total of 110 protein-protein interactions between CAR and JAML include 13 salt links, 6 H bonds, and 91 van der Waals' contacts (table S4). Of the total buried surface area, 36% (CAR: 270 Å^2, JAML: 260 Å^2) is contributed by charged residues (Asp^{35}, Glu^{37}, Asp^{49}, Lys^{102}, and Lys^{104} of CAR; Asp^{36}, Arg^{37}, Asp^{39}, Glu^{100}, Arg^{102}, and Lys^{111} of JAML) (Fig. 2E and fig. S6). The exceptional number of interdigitating salt bridges contributes binding energy but, more important, imparts high ligand specificity as demonstrated by mutational analysis (figs. S8 and S9). JAML Asp^{39}, Tyr^{52}, Phe^{55}, and Tyr^{57}, and CAR Lys^{104} compose the functional hotspot of the interaction (Fig. 2D). JAML Tyr^{52} orients Asp^{39} such that it binds CAR Lys^{104} in an extended conformation in which its aliphatic portion packs against JAML Phe^{55} and Tyr^{57}. The Tyr^{57} hydroxyl also forms crucial H bonds to the CAR backbone. The charged interface and functional hotspot of the JAML-CAR complex show significant similarities to the CD2-CD58 interaction (*18*) (fig. S10), although low sequence identity (14% for the D1 domains of JAML and CD2, 20% for the D1 domains of CAR and CD58) and different interface topology do not suggest any evolutionary relation between those receptor-ligand pairs.

The JAML-binding site on CAR overlaps with the receptor-binding site for adenoviruses (*3*, *4*) (Fig. 3). Adenoviruses interact with up to 16 of the 18 CAR residues that mediate JAML binding (Fig. 3B and fig. S11) and thus inhibit JAML-CAR interaction (*14*) and induction of γδ T cell signaling (fig. S15). In contrast, only six residues of the Coxsackie B virus–binding site overlap with the functional CAR interface, but notably these include hotspot residue Lys^{104}. The high degree of conservation and the sensitivity of the key residues of the CAR-JAML interface to mutation support the idea that some viruses ensure long-term entry into host cells by interaction with highly conserved receptor-binding sites, as any mutations would compromise receptor function (*9*, *19*).

The CAR-JAML ectodomain interaction induces cell signaling events at the JAML intracellular domain (ICD) (Fig. 4A and fig. S3A) (*14*), but the mechanism of signal transduction across the cell membrane has not been determined previously. Although no significant structural

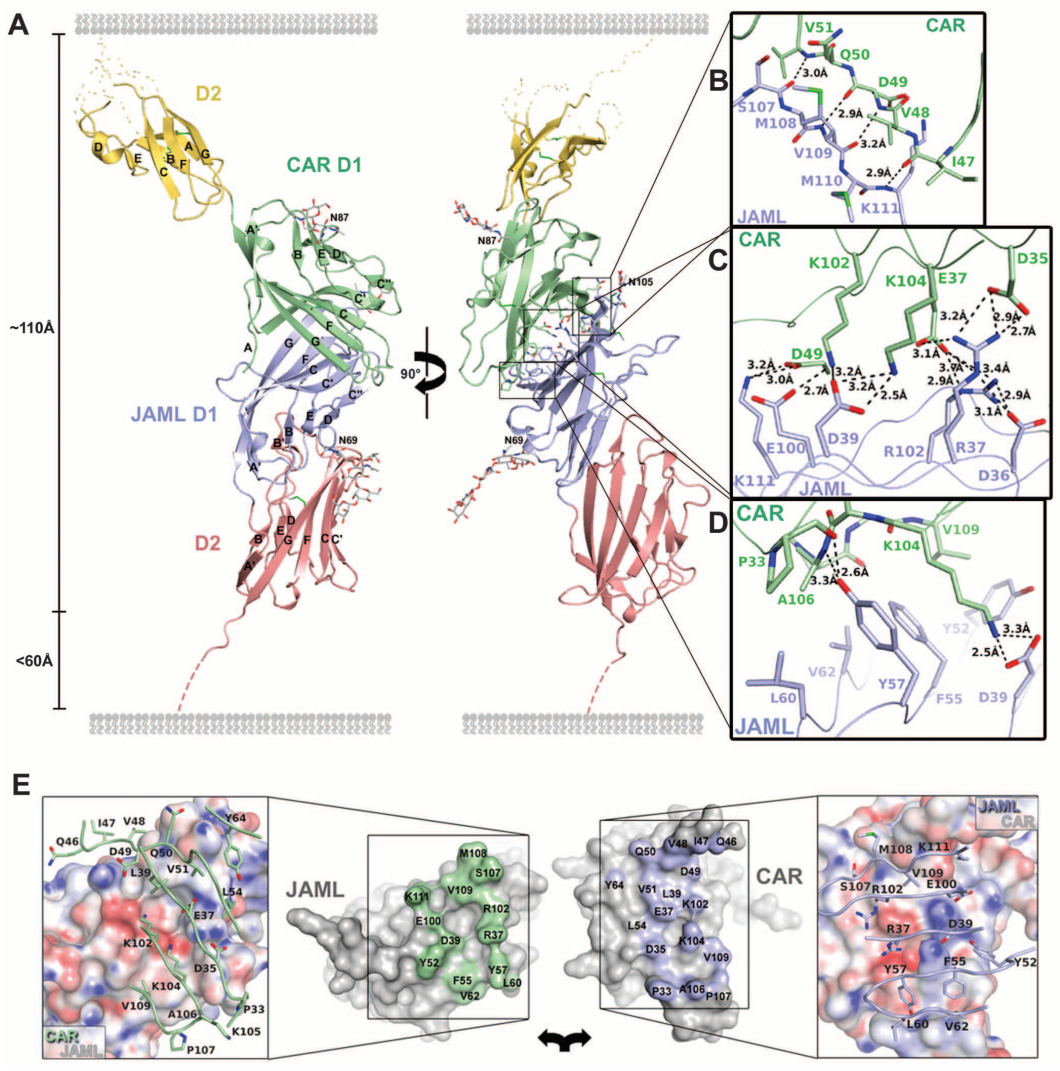

Fig. 2. CAR-JAML ectodomain complex structure. (**A**) Ribbon diagram of the CAR-JAML complex. JAML (D1, residues 11 to 121, light blue; D2, residues 122 to 236, salmon; disordered stalk, dashes), CAR [D1, residues 3 to 120, light green; D2, residues 121 to 216, gold; note that CAR D2 loops that were disordered in the crystal structure were grafted on from the CAR D2 NMR structure (2NPL, dots)], and carbohydrates (gray sticks). CAR and JAML interact with their D1 A′GFCC′C″ β sheets in a face-to-face, hand shake–like fashion. (**B**) An antiparallel β sheet is formed between the G strand (Ser^{107} to Lys^{111}) of JAML and the C′ strand (Ile^{47} to Val^{51}) of CAR, which moves ~6.2 Å as compared with unliganded CAR (fig. S7). (**C**) The interface is characterized by an array of interdigitated charged amino acids. Specifically, JAML Arg^{37} forms salt bridges with CAR Asp^{35} and Glu^{37} and JAML Asp^{36}. CAR Glu^{37} also interacts with JAML Arg^{102}, which forms a salt bridge to JAML Asp^{36}. CAR Lys^{102} interacts with JAML Glu^{100} and Asp^{39}, which in turn forms bidentate interactions with CAR Lys^{104}. (**D**) The functional hotspot of the CAR-JAML interaction: JAML Asp^{39}, Tyr^{52}, Phe^{55}, and Tyr^{57} and CAR Lys^{104}. (**E**) Open-book representation of the CAR-JAML interface. Atoms that form contacts are colored green and blue on the molecular surfaces of JAML and CAR, respectively. Above, the electrostatic potential was mapped onto the molecular surface and contoured at ±35 kT/eV (blue/red). CAR residues contacting JAML are shown as green sticks above the JAML surface. JAML residues contacting CAR are shown as blue sticks above the CAR surface. The surfaces of CAR and JAML are highly complementary, which ensures high ligand specificity. The strong electrostatic component of this interaction accounts for rapid kinetics and likely a high sensitivity to the environment.

rearrangements occur in the JAML ectodomain on CAR ligation, JAML and CAR can apparently exist as both monomers and dimers (*12*, *19*). In the crystal, a dimer of the CAR-JAML complex, with an interface size (~1400 Å^2) and shape complementarity (Sc = 0.73) within the range of typical protein-protein interactions (Sc = 0.70 to 0.76), is assembled on the crystallographic two-fold axis (figs. S12 and S13). Although the biological relevance of this particular assembly remains to be established (*24*), JAML dimerization and/or clustering as a mechanism for signal transduction is strongly supported by the finding that binding of dimeric, but not monomeric, CAR or antibody ligands recruits phosphoinositide 3-kinase (PI3K) to the JAML ICD (Fig. 4, D and E).

How does the interaction between CAR and JAML activate γδ T cell responses during epithelial insults (*14*)? The JAML ICD is highly conserved (which suggests interaction with intracellular proteins) and contains putative serine, threonine, and tyrosine phosphorylation sites (fig. S3A). Notably, it includes a YMxMxPxxP signaling motif (*25*) similar to that in the major costimulatory αβ T cell coreceptor CD28 (fig. S3B). The tyrosine-phosphorylated motif in CD28 binds the universal signal transducer PI3K 1A (*26*–*28*) leading to activation of MAP kinase pathways and interleukin-2 (IL-2) production (*28*, *29*).

As resting and activated epithelial γδ T cells lack the major PI3K-binding αβ costimulatory receptors, CD28 and ICOS, and ligand binding to JAML leads to MAP kinase activation and IL-2 production (*14*), we tested whether JAML mediates costimulation through interaction with PI3K. Indeed, on epithelial γδ T cells, PI3K associates with JAML within 1min of CAR ligation (Fig. 4A). Once PI3K has been recruited, disruption of the CAR-JAML interaction leads to rapid decline of PI3K levels (Fig. 4B), tightly linking extracellular protein-recognition events to intracellular signaling. PI3K binding to JAML also strongly correlates with affinity of the CAR-JAML interaction, as demonstrated by decreased kinase recruitment by CAR mutants that have reduced binding to JAML (Fig. 4C and fig. S9). To further dissect the JAML-PI3K interaction, mutants of the JAML intracellular signaling motifs were generated. In JAML-transfected Chinese hamster ovary (CHO) cells, PI3K binds constitutively to wild-type JAML and a Y314F mutant, but not to a Y336F mutant, of the YMxM motif (Fig. 4F), identifying this region as the PI3K-binding site. In P340A/P343A/P346A JAML mutants, negligible PI3K association occurs, which suggests that, as for CD28 (*26*–*28*), the polyproline motif serves to recruit a primary kinase to phosphorylate YMxM and that PI3K association to JAML critically depends on the phosphorylation state of the PI3K-binding motif. Despite low sequence identity (11% for JAML and CD28, 16% for CAR and B7-1) and the different domain organization of JAML and CD28, these results demonstrate a striking functional similarity

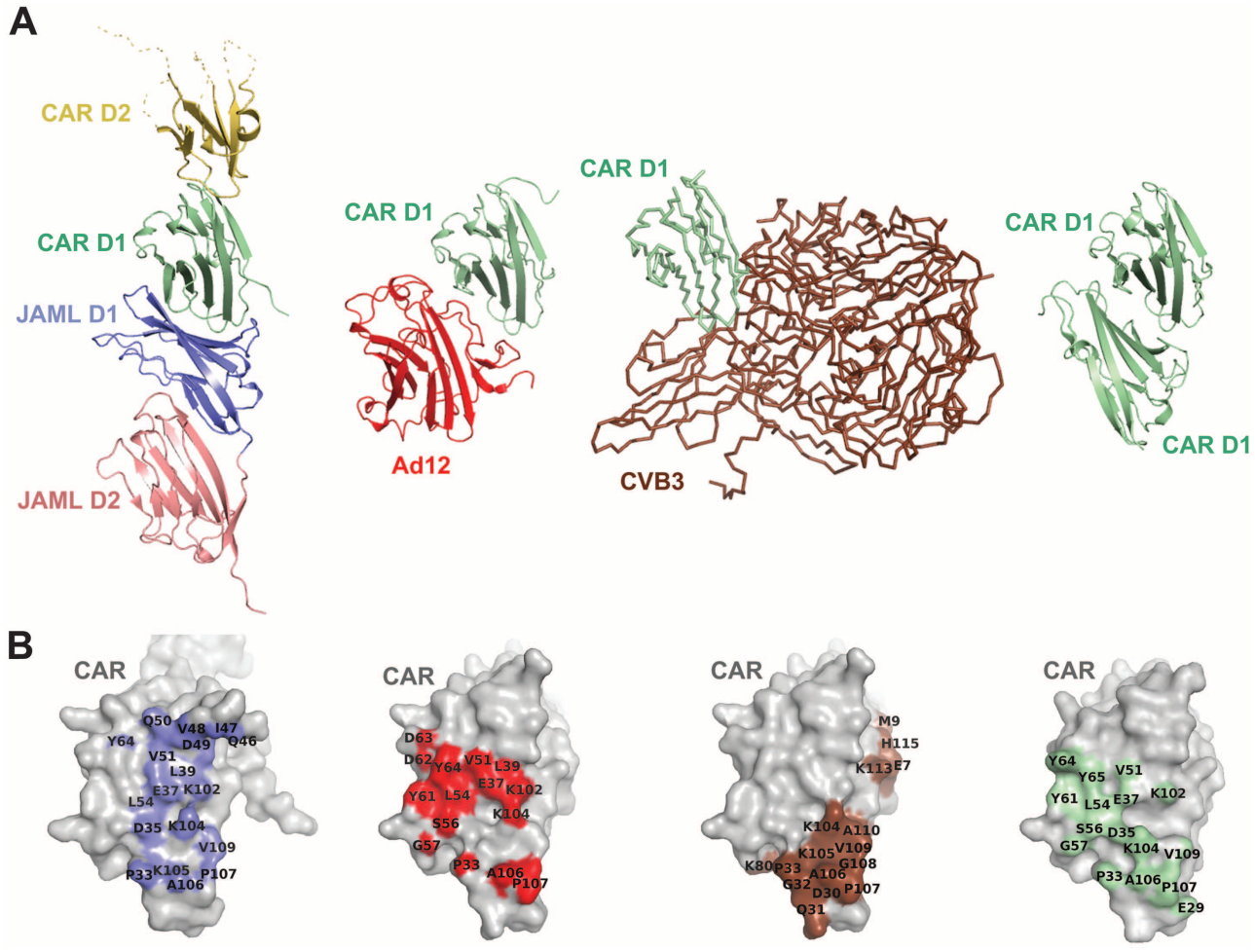

Fig. 3. Comparison of functional and viral epitopes of CAR. (**A**) Schematic representations of CAR complex structures: from left to right: mCAR-mJAML [PDB no. 3MJ7, this work], hCAR-hAd12 [1KAC (*3*)], hCAR-hCVB3 [1JEW (*4*)], and hCAR homodimer [1EA] (*19*)]. (**B**) Molecular surface of the CAR D1 domain in the various CAR complex structures. CAR atoms that are part of the epitope for the respective ligands are colored blue (CAR-JAML), red (CAR-Ad12), brown (CAR-CVB3), and light green (CAR homodimer). The CAR-JAML binding site mostly coincides with both the adenoviral and the homodimerization interface of CAR, whereas the coxsackievirus B–binding site is located at the periphery of the functional CAR interfaces.

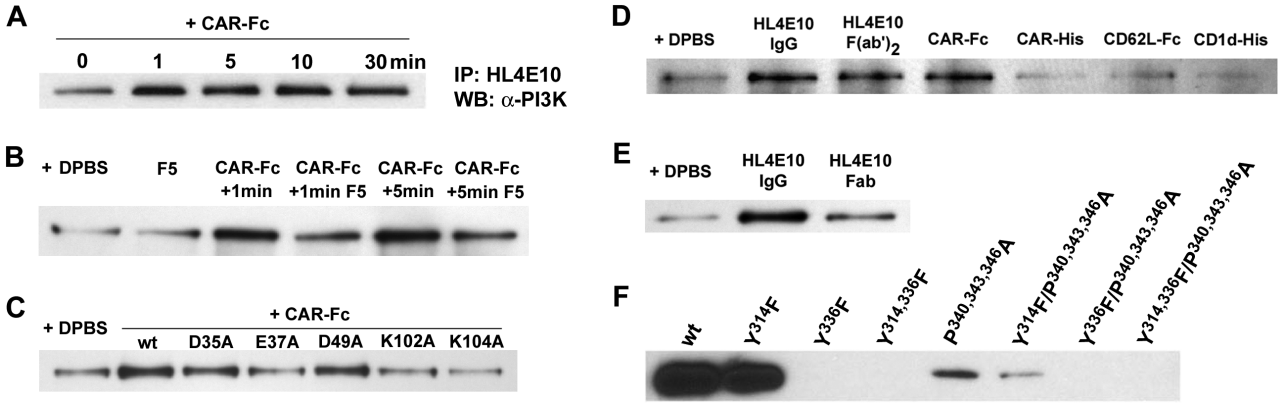

Fig. 4. Ligand-induced PI3K recruitment to the JAML ICD. PI3K-specific antibody Western blots of JAML immunoprecipitated with anti-JAML HL4E10 immunoglobulin G (IgG) from epithelial γδ T cell lysates after stimulation with ligands (A to E) or from JAML mutant-transfected CHO cell lysates (F). (**A**) Time course of stimulation with CAR-Fc. After 1 min, PI3K association to JAML is significantly elevated over the basal level. (**B**) PI3K recruitment is rapidly switched off once CAR is released from the JAML ectodomain. γδ T cells were incubated with buffer (DPBS) or adenovirus F5 protein (F5) or were stimulated with CAR (CAR-Fc) followed by an excess of F5 (which competes with JAML for CAR-binding). F5 alone does not alter basal PI3K levels (DPBS), whereas a 1-min addition of F5 (CAR-Fc+1min F5) significantly decreases PI3K recruitment in CAR-stimulated γδ T cells (CAR-Fc+1min). (**C**) Functional consequences of mutations in the CAR-JAML interface on downstream signaling by JAML. wt CAR-Fc and an N49A mutant induce significant PI3K recruitment, consistent with their comparable JAML-binding characteristics (fig. S9) and location of CAR Asp[49] at the periphery of the JAML-binding site (Fig. 2E), where mutations would be expected to cause smaller effects on binding. Mutation of CAR Asp[35] induces less, but does not entirely abolish, PI3K binding to JAML, consistent with its interaction with JAML Arg[37], for which mutations are well tolerated. In contrast, CAR mutants E37A, K102A, and K104A, all of which interact with JAML hotspot residues (Fig. 2C), do not induce significant PI3K recruitment. (**D** and **E**) Dimeric, but not monomeric, ligands induce PI3K recruitment to JAML. PI3K levels are increased by JAML binding of bivalent HL4E10 IgG, bivalent HL4E10 Fab′$_2$ fragment, and dimeric CAR (CAR-Fc fusion protein), but not by monovalent HL4E10 Fab or monomeric CAR (CAR-His). Fc- or His-tagged control proteins (CD62L-Fc and CD1d-His) do not induce PI3K recruitment. (**F**) Dissection of the role of conserved JAML intracellular signaling motifs in PI3K binding. PI3K constitutively binds to wild-type and Y314F JAML, whereas binding is abolished to any Y336F mutants in the YMxM PI3K-binding motif. PI3K association is greatly reduced in JAML polyproline motif mutants P340A/P343A/P346A and Y314F/P340A/P343A/P346A, even though they still exhibit an intact YMxM motif. Data are representative of at least three independent experiments.

between costimulation and cell signaling through CAR-JAML on epithelial γδ T cells and B7-CD28 on αβ T cells.

Thus, this delineation of the molecular details of the CAR-JAML-PI3K regulatory circuit has now uncovered a physiological role of the major virus receptor CAR and its partner JAML in cell signaling. These insights may serve as a basis for modulating cellular responses during tissue homeostasis and immunity, and have implications for treatment of chronic nonhealing wounds, asthma, and cancer.

References and Notes

1. J. M. Bergelson *et al.*, *Science* **275**, 1320 (1997).
2. R. P. Tomko, R. Xu, L. Philipson, *Proc. Natl. Acad. Sci. U.S.A.* **94**, 3352 (1997).
3. M. C. Bewley, K. Springer, Y. B. Zhang, P. Freimuth, J. M. Flanagan, *Science* **286**, 1579 (1999).
4. Y. He *et al.*, *Nat. Struct. Biol.* **8**, 874 (2001).
5. I. M. Verma, M. D. Weitzman, *Annu. Rev. Biochem.* **74**, 711 (2005).
6. J. Howitt, C. W. Anderson, P. Freimuth, *Curr. Top. Microbiol. Immunol.* **272**, 331 (2003).
7. A. Kanerva, A. Hemminki, *Ann. Med.* **37**, 33 (2005).
8. S. D. Carson, *Rev. Med. Virol.* **11**, 219 (2001).
9. P. Freimuth, L. Philipson, S. D. Carson, *Curr. Top. Microbiol. Immunol.* **323**, 67 (2008).
10. C. Moog-Lutz *et al.*, *Blood* **102**, 3371 (2003).
11. K. Zen *et al.*, *Mol. Biol. Cell* **16**, 2694 (2005).
12. A. C. Luissint, P. G. Lutz, D. A. Calderwood, P. O. Couraud, S. Bourdoulous, *J. Cell Biol.* **183**, 1159 (2008).
13. Y. L. Guo *et al.*, *Arterioscler. Thromb. Vasc. Biol.* **29**, 75 (2009).
14. D. A. Witherden *et al.*, *Science* **329**, XXX (2010).
15. J. Jameson *et al.*, *Science* **296**, 747 (2002).
16. Materials and methods are available as supporting material on *Science* Online.
17. JAML crystallized in space group $P4_3$ in two forms with 1mol/ASU and with 2mol/ASU, in F222 with 1mol/ASU, and in $P3_112$ as the JAML-CAR complex.
18. J. H. Wang *et al.*, *Cell* **97**, 791 (1999).
19. M. J. van Raaij, E. Chouin, H. van der Zandt, J. M. Bergelson, S. Cusack, *Structure* **8**, 1147 (2000).
20. S. Jiang, M. Caffrey, *Protein Sci.* **16**, 539 (2007).
21. S. J. Davis *et al.*, *Nat. Immunol.* **4**, 217 (2003).
22. M. L. Dustin, S. K. Bromley, M. M. Davis, C. Zhu, *Annu. Rev. Cell Dev. Biol.* **17**, 133 (2001).
23. S. K. Bromley *et al.*, *Nat. Immunol.* **2**, 1159 (2001).
24. Although the high protein concentration in the crystal may facilitate CAR-JAML heterotetramer formation analogous to the expected elevation of the effective concentration arising from 2D diffusion of receptors on the cell membrane, the weak affinity constant for oligomerization may explain the difficulty in isolating a CAR-JAML heterotetramer in biochemical experiments. Analytical ultracentrifugation (AUC), coimmunoprecipitation of differentially tagged JAML and CAR, and Bimolecular Fluorescence Complementation (BiFC) assays were used to investigate the formation of CAR-JAML heterotetramers in solution and on the cell surface. Although there was some indication of a CAR-JAML heterotetramer from AUC (table S3) and for JAML dimers from cross-linking experiments and BiFC, providing definitive biochemical evidence for a very low affinity CAR-JAML heterotetramer was intrinsically hampered by experimental constraints (e.g., the limited protein concentrations that could be used in the experiments or that soluble CAR proteins are a poor probe to investigate the heterotypic interactions that naturally occur between the cell-bound JAML and CAR counterreceptors).
25. Single-letter abbreviations for the amino acid residues are as follows: A, Ala; C, Cys; D, Asp; E, Glu; F, Phe; G, Gly; H, His; I, Ile; K, Lys; L, Leu; M, Met; N, Asn; P, Pro; Q, Gln; R, Arg; S, Ser; T, Thr; V, Val; W, Trp; and Y, Tyr; and X, any amino acid.
26. F. Pagès *et al.*, *Nature* **369**, 327 (1994).
27. M. Raab *et al.*, *Proc. Natl. Acad. Sci. U.S.A.* **92**, 8891 (1995).
28. C. E. Rudd, H. Schneider, *Nat. Rev. Immunol.* **3**, 544 (2003).
29. J. A. Deane, D. A. Fruman, *Annu. Rev. Immunol.* **22**, 563 (2004).

30. We thank A. Schiefner for help with the structure solution; S. Ferguson, H. Lindermuth, and J. Vanhasny for technical support; L. Teyton for providing cell lines; J. G. Luz, M. A. Adams-Cioaba, J. Stevens, D. A. Shore, A. L. Corper, R. L. Stanfield, and E. Ollmann Saphire for helpful discussions; and X. Dai and K. Saikatendu for assistance on synchrotron trips. We acknowledge the Advanced Light Source, Stanford Synchrotron Radiation Lightsource, and the Advanced Photon Source for use of their synchrotron facilities. This work was supported by NIH grants AI42266, CA58896 to I.A.W., and AI52257 and AI064811 to W.L.H., an Erwin-Schrödinger Fellowship of the Austrian Science Fund to P.V., and the Skaggs Institute. Atomic coordinates and structure factors for JAML and the CAR-JAML complex have been deposited in the Protein Data Bank with accession numbers 3MJ6 and 3MJ7 respectively. This is manuscript 18641-MB from The Scripps Research Institute.

Supporting Online Material

www.sciencemag.org/cgi/content/full/329/5996/1210/DC1
Materials and Methods
Figs. S1 to S13
Tables S1 to S5
References

5 February 2010; accepted 9 July 2010
10.1126/science.1187996

Glutamine Deamidation and Dysfunction of Ubiquitin/NEDD8 Induced by a Bacterial Effector Family

Jixin Cui,[1,2] Qing Yao,[2] Shan Li,[2] Xiaojun Ding,[2] Qiuhe Lu,[2] Haibin Mao,[3] Liping Liu,[2] Ning Zheng,[3,4] She Chen,[2] Feng Shao[2]*

A family of bacterial effectors including Cif homolog from *Burkholderia pseudomallei* (CHBP) and Cif from Enteropathogenic *Escherichia coli* (EPEC) adopt a functionally important papain-like hydrolytic fold. We show here that CHBP was a potent inhibitor of the eukaryotic ubiquitination pathway. CHBP acted as a deamidase that specifically and efficiently deamidated Gln^{40} in ubiquitin and ubiquitin-like protein NEDD8 both in vitro and during *Burkholderia* infection. Deamidated ubiquitin was impaired in supporting ubiquitin-chain synthesis. Cif selectively deamidated NEDD8, which abolished the activity of neddylated Cullin-RING ubiquitin ligases (CRLs). Ubiquitination and ubiquitin-dependent degradation of multiple CRL substrates were impaired by Cif in EPEC-infected cells. Mutations of substrate-contacting residues in Cif abolished or attenuated EPEC-induced cytopathic phenotypes of cell cycle arrest and actin stress fiber formation.

Gram-negative bacterial pathogens use a type III secretion system (TTSS) to translocate effectors into eukaryotic host cells, serving as a key virulence mechanism (*1*, *2*). Several effectors from different bacteria inhibit host cell cycle progression (*3*–*6*). Cif (cycle inhibiting factor) from Enteropathogenic *E. coli* (EPEC) arrests cell cycle at G2/M or G1/S transition (*7*). Cif homolog in *Burkholderia pseudomallei* (CHBP) also arrests cell cycle when delivered into eukaryotic cells (*8*). Cif and CHBP belong to a growing family of TTSS effectors that adopt a papain-like hydrolytic fold with a Cys-His-Asp/Asn/Glu/Gln catalytic triad (*8*–*10*). The host target and underlying mechanism for cell cycle arrest by the Cif/CHBP family are unknown.

Progression of eukaryotic cell cycle is driven by the ubiquitin-proteasome system (UPS) that mediates timed degradation of key cell cycle regulators. When delivered into HeLa cells that express green fluorescent protein (GFP) reporters of the UPS (*11*), purified CHBP, but not its catalytic mutant (C156S) (*12*), blocked degradation of Ub^{G76V}-GFP and Ub-R-GFP, but not the control Ub-M-GFP reporter (Fig. 1A). TNFα (tumor necrosis factor alpha) induces NF-κB (nuclear factor κB)–regulated gene transcription through UPS-dependent degradation of IκBα (inhibitor of NF-κB), which was also suppressed by CHBP (fig. S1). Ubiquitination is a sequential three-enzyme cascade composed of ubiquitin-activation enzyme E1, ubiquitin-conjugating enzyme E2, and ubiquitin ligase E3. CHBP blocked free ubiquitin-chain synthesis catalyzed by different E3-E2 pairs, including a RING-domain E3 gp78c/Ube2g2 (*13*) (Fig. 1B and fig. S2, A to C). CHBP also blocked ubiquitination of RhoA mediated by a Cullin-based E3 complex (*14*) (Fig. 1C). Blocking ubiquitination required the catalytic cysteine in CHBP. CHBP is not a deubiquitinase, as it failed to disassemble polyubiquitin chains (fig. S2D). CHBP did not affect formation of E1~Ub and E2~Ub thioester intermediates (fig. S3). However, when CHBP-incubated E2~Ub thioester was reacted with E3, chain synthesis was largely inhibited (fig. S4). Thus, CHBP inactivates the E2~Ub thioester and is a potent and general inhibitor of the ubiquitination pathway.

None of E1, E2, ubiquitin, and E2~Ub thioester exhibited any changes when CHBP-incubated E2-charge reaction mixtures were subjected to reducing or nonreducing sodium dodecyl sulfate polyacrylamide gel electrophoresis (SDS-PAGE). When analyzed on a native PAGE gel, the E2~Ub thioester showed a faster migration toward the anode (fig. S5A). E2 recovered from the shifted E2~Ub thioester showed no mobility changes (fig. S5B). When free ubiquitin was treated with purified CHBP, but not its catalytic-triad mutants, a similar faster migration appeared (Fig. 1D). The mobility shift was greater than that of the E2~Ub thioester due to the smaller size of ubiquitin. Mass spectrometry was employed to reveal CHBP-induced modification on ubiquitin. Among the 15 tryptic peptides that cover the entire ubiquitin sequence, three overlapping ones ($_{28}$AKIQDKEGIPPDQQR$_{42}$, $_{30}$IQDKEGIPPDQQR$_{42}$, and $_{30}$IQDKEGIPPDQQRLIFAGK$_{48}$) from CHBP-treated ubiquitin showed a 1-dalton mass increase (fig. S6). Tandem mass spectrometry revealed that the 1-dalton increase occurred on Gln^{40} in ubiquitin (Fig. 2A), indicating a deamidation reaction. Substitution of Gln^{40} with Glu, but not Ala, caused a mobility change indistinguishable from that of CHBP-modified ubiquitin, and further CHBP treatment generated no additional shifts (Fig. 2B). Thus, CHBP specifically deamidates Gln^{40} in ubiquitin.

Similar to the effect of CHBP, ubiquitin Q40E was compromised in supporting in vitro ubiquitin-

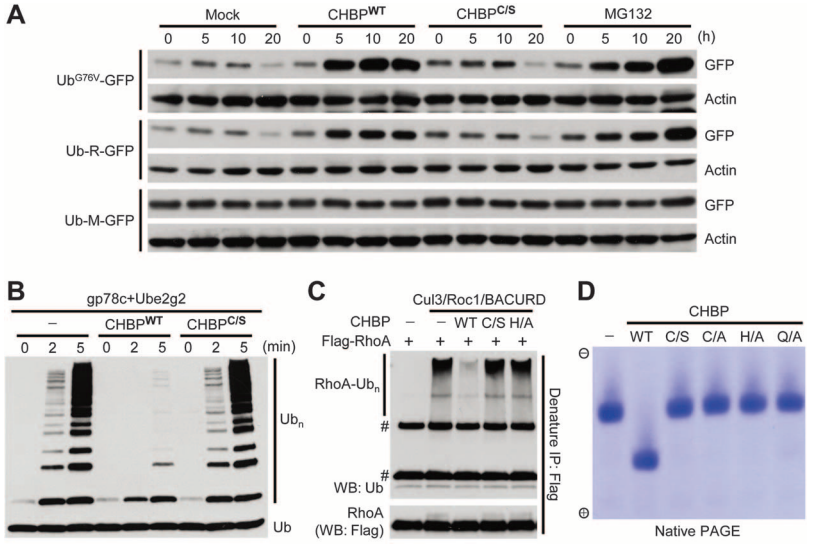

Fig. 1. CHBP blocks ubiquitination by covalently modifying ubiquitin. (**A**) GFP reporter assays of effects of CHBP on the host ubiquitination pathway. Purified CHBP was directly delivered into HeLa cells expressing Ub^{G76V}-GFP, Ub-R-GFP, or Ub-M-GFP reporters. $CHBP^{WT}$, wild-type CHBP; $CHBP^{C/S}$, the catalytic cysteine mutant (C156S). (**B** and **C**) Effects of CHBP on in vitro ubiquitin-chain synthesis. In (B), gp78c and Ube2g2 were used as the E3 and E2, respectively, and reactions were stopped at indicated time points. Ubiquitination of RhoA by the Cul3/Roc1/BACURD complex was examined in (C). Ub_n, ubiquitin chain; #, immunoglobulin G (IgG) heavy and light chains. (**D**) Native PAGE analysis of free ubiquitin treated with purified CHBP. WT, wild-type CHBP; C/S, C/A, H/A, and Q/A are mutations in the catalytic triad of CHBP. Coomassie blue–stained gel is shown.

[1]Graduate Program in Chinese Academy of Medical Sciences and Beijing Union Medical College, Beijing 100730, China. [2]National Institute of Biological Sciences, Beijing, 102206, China. [3]Department of Pharmacology, Box 357280, University of Washington, Seattle, WA, 98195, USA. [4]Department of Pharmacology and Howard Hughes Medical Institute, Box 357280, University of Washington, Seattle, WA, 98195, USA.

*To whom correspondence should be addressed. E-mail: shaofeng@nibs.ac.cn

chain synthesis (Fig. 2C) without affecting E1 and E2 charging (fig. S3). CHBP-inactivated E2~Ub thioester also contained a deamidated Gln^{40} (fig. S7), suggesting that ubiquitin Q40E is defective in being transferred from E2 to the acceptor ubiquitin during chain synthesis. Consistently, Gln^{40} side chain is involved in interactions with E3 in the NEDD4L/E2~Ub oxyester complex (*15*). Ectopic expression of ubiquitin Q40E impaired TNFα-induced NF-κB luciferase reporter activation and led to the accumulation of several UPS substrates (fig. S8). Translocation of CHBP into HeLa cells by the EPEC TTSS also stabilized UPS substrates (fig. S9). Thus, deamidation of Gln^{40} in ubiquitin by CHBP attenuates ubiquitination both in vitro and in cells.

Ubiquitin-like proteins (UBLs) share ubiquitin's three-dimensional fold (*16*). NEDD8 harbors ~80% sequence similarity with ubiquitin, whereas other UBLs are generally not similar to ubiquitin in primary sequence. Gln^{40} is conserved in NEDD8, SUMO2/3, and LC3, but only NEDD8 showed a mobility shift on the native gel upon CHBP treatment (Fig. 2D), resulting from deamidation of Gln^{40} (fig. S10). Thus, NEDD8 is another specific deamidation substrate of CHBP.

B. thailandensis serves as a model to study the virulence-associated TTSS system of *B. pseudomallei* (*17*). *B. thailandensis* harboring a CHBP expression plasmid was used to infect 293T cells that express UbΔGG or NEDD8ΔGG. Nearly 100% of NEDD8ΔGG and about 50% of UbΔGG were deamidated in a CHBP-dependent manner (Fig. 2E). This agrees with the potent in vitro activity of CHBP and its slight preference for NEDD8 over ubiquitin. Thus, CHBP deamidates both NEDD8 and ubiquitin during *Burkholderia* infection.

To compare enzymatic properties of CHBP with its EPEC homolog, 350 pmol of NEDD8 or ubiquitin in a 20-μl reaction (18 μM) was titrated with recombinant CHBP or Cif (fig. S11). After a 20-min reaction, 0.3 pmol and 0.03 pmol of CHBP were sufficient to deamidate nearly all 350 pmol of ubiquitin and NEDD8, respectively (Fig. 3A and fig. S11A). Although the activity of Cif on NEDD8 was comparable to that of CHBP on NEDD8, the activity of Cif on ubiquitin was lower by a factor of about 1000 than that on NEDD8 (Fig. 3A and fig. S11B). Consistently, NEDD8ΔGG was completely deamidated in HeLa cells infected with the Cif-bearing EPEC strain (E22), but not the Cif-deficient strain (E2348/49). In contrast, deamidation of UbΔGG was not detected (Fig. 3B). Complementation of E2348/49 with wild-type Cif, but not the catalytic mutant, restored NEDD8 deamidation (Fig. 3B).

NEDD8 is conjugated to Cullins that mediate the assembly of a large repertoire of Cullin-RING ubiquitin ligases (CRLs), and neddylation stimulates the activity of CRLs (*18*, *19*). In EPEC-infected cells, substrates of CRLs (p27, Nrf2 and HIF-1α) accumulated in a Cif catalytic cysteine-dependent manner (Fig. 3C and fig. S12), whereas their mRNA levels were not affected (fig. S13). Consistently, ubiquitination of Nrf2 and p27 was markedly decreased (Fig. 3D). Non-CRL substrates—including p53, Mcl-1 (*20*), PINK1 (*21*), MOAP1 (*22*), and Ub-R-GFP reporter—were not stabilized (Fig. 3C and fig. S12). Thus, NEDD8 deamidation by Cif inactivates CRLs in infected cells.

Neddylation-stimulated CRL activation was reconstituted using Cul3/Roc1/Keap1 complex-catalyzed Nrf2 ubiquitination (Fig. 3, E and F). Neddylation of Cul3/Roc1 complex resulted in increased Nrf2 ubiquitination, and replacement of NEDD8 with NEDD8 Q40E abolished this stimulation effect (Fig. 3F) without disturbing autoneddylation of the Cul3/Roc1 complex (Fig. 3E and fig. S14). Similarly, deamidated ubiquitin did not affect Cul3 monoubiquitination (fig. S14). NEDD8 Q40E-conjugated Cul3 complex was even less active than the unneddylated counterpart (Fig. 3F), likely due to Glu-40 interfering with conformational changes of the Cullin/Roc1 complex (*23*). Thus, NEDD8 deamidation directly impairs the ubiquitination ligase activity of the neddylated CRL complex.

EPEC infection produces Cif-dependent actin stress fibers (*6*). Mutation of Cif deamidase catalytic residues abolished the development of stress fibers (fig. S15A) without affecting type III–dependent secretion (fig. S16). Actin stress fiber formation is controlled by RhoA, a Rho-family small guanosine triphosphatase (GTPase) and also a specific substrate of the Cul3/BACURD CRL complex (*14*). A panel of Rho GTPases was examined after EPEC infection, and only RhoA was stabilized by the deamidase activity of Cif (fig. S15B). Thus, Cif infection–induced formation of prominent actin stress fibers is probably due to dysfunction of CRLs as a result of NEDD8 deamidation.

Ectopic expression of NEDD8 Q40E resulted in accumulation of CRL substrates such as p27, Nrf2, and HIF-1α, but not non-CRL substrates (Fig. 4A and fig. S17). HeLa cells expressing NEDD8 Q40E showed decreased bromodeoxyuridine (BrdU) incorporation (Fig. 4B), indicating a defect in cell cycle progression. About 35% of transfected HeLa cells became enlarged with strong actin stress fibers, resembling the effect of EPEC infection. Thus, ectopic expression of NEDD8 Q40E partially recapitulates effects of Cif infection on impairing the CRL function.

Several point mutations in Cif were generated according to the crystal structure of CHBP/ubiquitin complex (Protein Data Bank ID code 3NZ5).

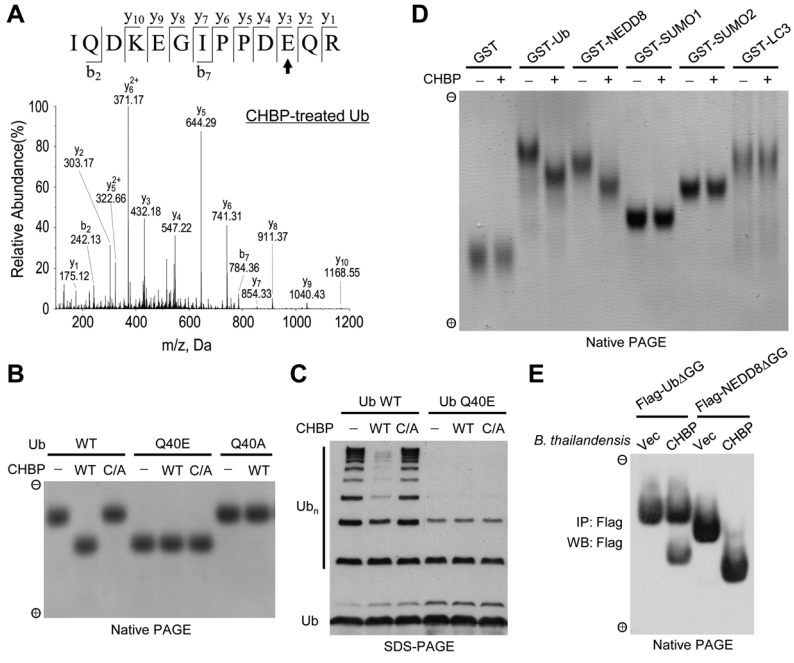

Fig. 2. CHBP deamidates Gln^{40} in ubiquitin and NEDD8 in vitro and during infection. (**A**) Electrospray ionization tandem mass spectrometry (MS/MS) spectrum of a Gln^{40}-containing tryptic peptide from CHBP-treated ubiquitin. b and y ions are marked in the spectrum. The fragmentation patterns that generate the observed b and y ions are illustrated along the peptide sequence shown on top of the spectrum. The arrow marks the residue that shows a 1-dalton mass increase after CHBP treatment and is converted from glutamine into glutamate. (**B**) Native PAGE analysis of ubiquitin Gln^{40} mutants and effects of further CHBP treatment. Coomassie blue–stained gel is shown. (**C**) Chain formation activities of ubiquitin Q40E. Ubiquitination reaction was performed as that in Fig. 1B. (**D**) Native PAGE analysis of glutathione *S*-transferase (GST)–tagged ubiquitin and indicated UBLs after CHBP treatment. Coomassie blue–stained gel is shown. (**E**) Native PAGE assay of ubiquitin and NEDD8 deamidation by type III-secreted CHBP. Flag-UbΔGG and NEDD8ΔGG (deletion of the last two glycine residues) were immunopurified from 293T cells infected with indicated *B. thailandensis* strains and subjected to native gel electrophoresis followed by immunoblotting of antibodies by using Flag.

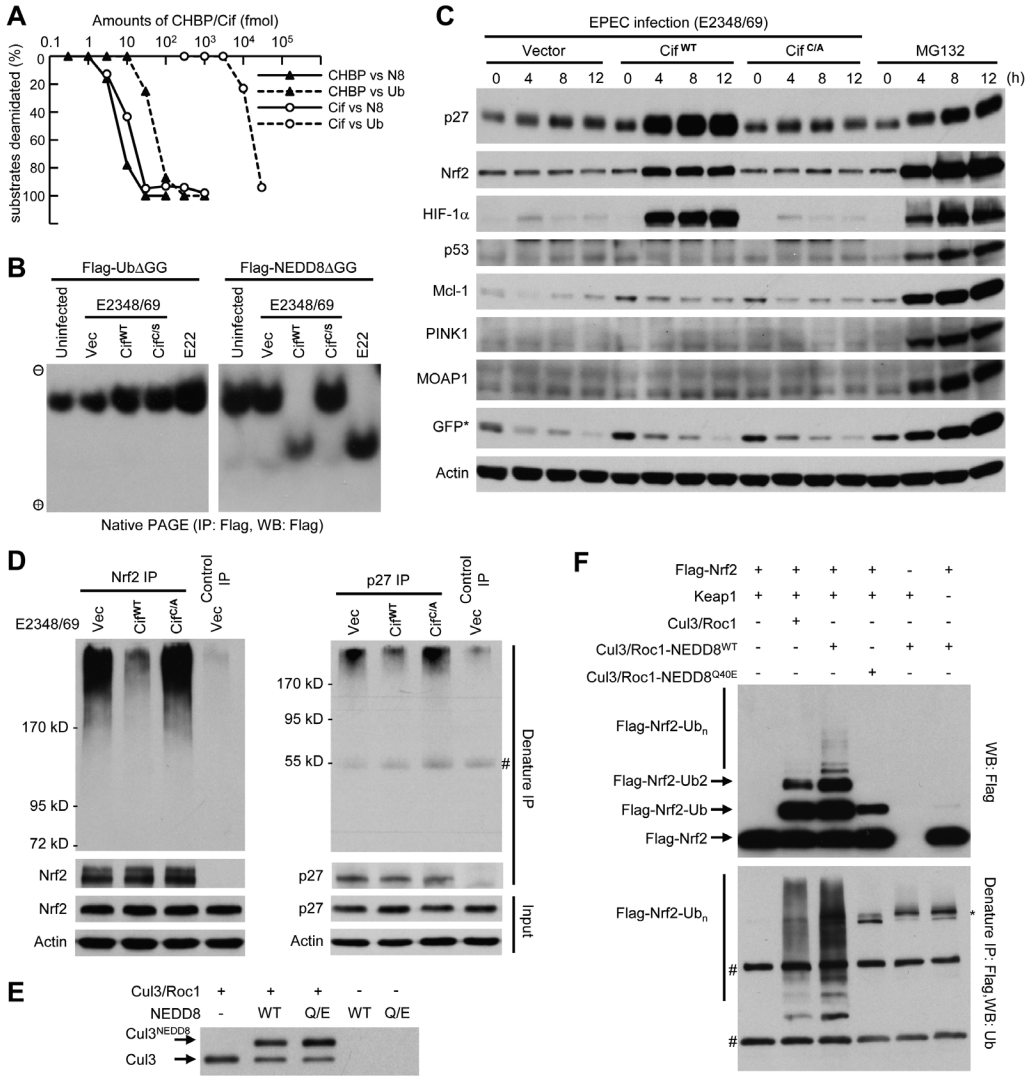

Fig. 3. Cif selectively inactivates CRLs by deamidating NEDD8 in vitro and in vivo. (**A**) Enzyme-titration measurements of the deamidase activity of CHBP/Cif toward ubiquitin and NEDD8. Intensity of native ubiquitin/NEDD8 bands on native gels (fig. S11) was quantified and plotted versus the amount of CHBP/Cif used in each reaction. (**B**) Native PAGE assay of Cif deamidation of NEDD8 during EPEC infection of HeLa cells. EPEC E22 strain bears a functional Cif, whereas EPEC E2348/49 harbors a naturally truncated and nonfunctional Cif. Experiments were performed and data are presented similar to those in Fig. 2E. (**C**) Effects of Cif on steady levels of CRL and non-CRL substrates in EPEC-infected HeLa cells. GFP*, transfected Ub-R-GFP reporter. (**D**) Effects of Cif on ubiquitination of endogenous Nrf2 and p27 in EPEC-infected cells. #, IgG. (**E** and **F**) Effects of NEDD8 deamidation on neddylation-stimulated CRL activity of catalyzing substrate ubiquitination. Neddylation of Cul3 performed with NEDD8 (WT) or NEDD8 Q40E was shown in (E) as an immunoblot by using antibodies to Cul3. The Cul3/GST-Roc1 complex from the left three reactions in (E) was used to ubiquitinate Flag-Nrf2 (1–97) (F). Flag-Nrf2-Ub, Flag-Nrf2-Ub$_2$, and Flag-Nrf2-Ubn denote mono-, di-, and poly-ubiquitinated Nrf2, respectively. #, IgG heavy and light chains; *, a nonspecific band.

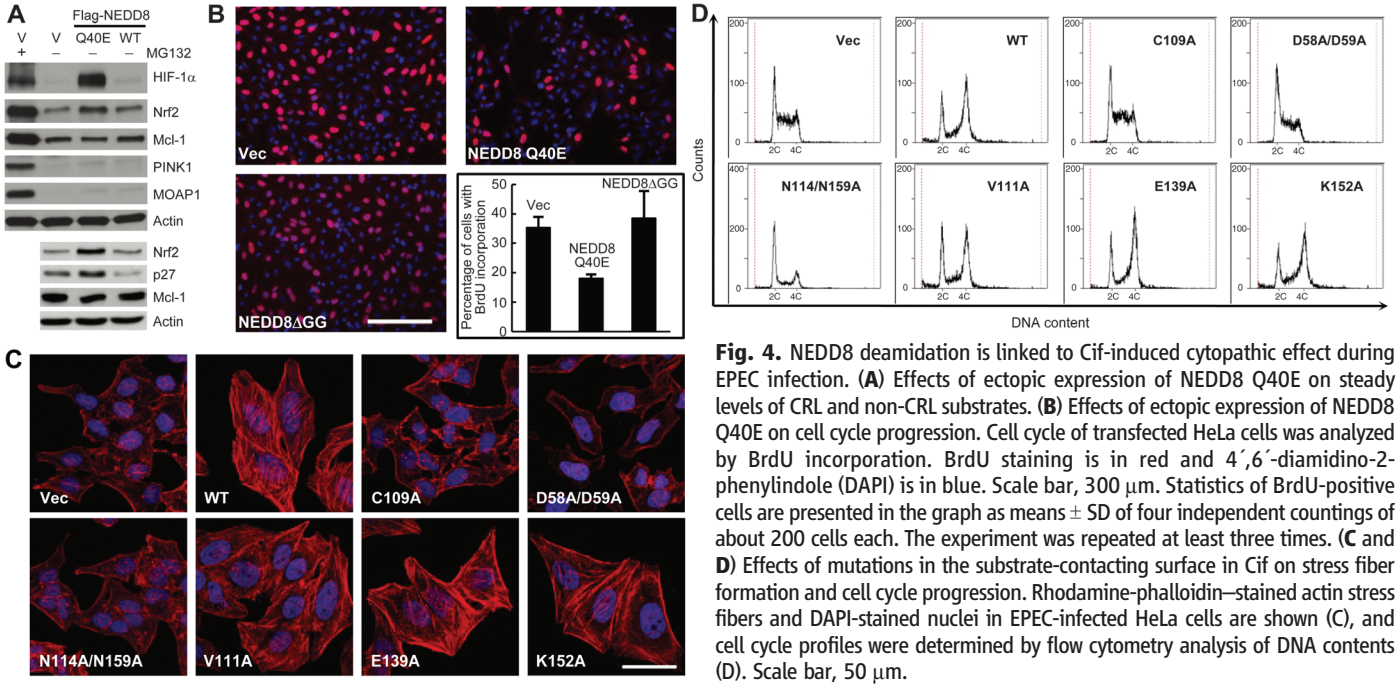

Fig. 4. NEDD8 deamidation is linked to Cif-induced cytopathic effect during EPEC infection. (**A**) Effects of ectopic expression of NEDD8 Q40E on steady levels of CRL and non-CRL substrates. (**B**) Effects of ectopic expression of NEDD8 Q40E on cell cycle progression. Cell cycle of transfected HeLa cells was analyzed by BrdU incorporation. BrdU staining is in red and 4′,6′-diamidino-2-phenylindole (DAPI) is in blue. Scale bar, 300 μm. Statistics of BrdU-positive cells are presented in the graph as means ± SD of four independent countings of about 200 cells each. The experiment was repeated at least three times. (**C** and **D**) Effects of mutations in the substrate-contacting surface in Cif on stress fiber formation and cell cycle progression. Rhodamine-phalloidin–stained actin stress fibers and DAPI-stained nuclei in EPEC-infected HeLa cells are shown (C), and cell cycle profiles were determined by flow cytometry analysis of DNA contents (D). Scale bar, 50 μm.

D58A/D59A and N114A/N159A are mutations at the two enzyme-substrate contact interfaces; the former completely abolished Cif deamidase activity on NEDD8, and activity of the latter mutant is markedly attenuated (fig. S18). Both mutants failed to produce actin stress fibers during EPEC infection (Fig. 4C). The D58A/D59A mutant did not arrest cell cycle and the N114A/N159A mutant only marginally delayed cell cycle progression (Fig. 4D). Mutations of residues not involved in substrate binding (V111A, E139A, and K152A) had little effect on in vitro deamidation of NEDD8 (fig. S18), and these mutants behaved identically as wild-type Cif in producing stress fibers and arresting cell cycle (Fig. 4, C and D). All the mutants were competent for type III–dependent secretion (fig. S16). Thus, NEDD8 deamidation is closely linked to Cif-induced cytopathic effects of actin stress fiber formation and cell cycle arrest.

Here, we have shown that the CHBP/Cif family of TTSS effectors harbor a specific deamidase activity toward Gln^{40} in ubiquitin and NEDD8, rendering them inactive. Deamidated ubiquitin exhibits reduced ubiquitin ligase–catalyzed ubiquitin-chain synthesis, whereas deamidated NEDD8 suppresses the ubiquitin ligase activity of CRLs upon conjugation to Cullins. Selective deamidation of NEDD8 by Cif is linked to EPEC infection–induced cell cycle arrest and actin stress fiber formation. Given the universal role of ubiquitination and Cullin-mediated ubiquitination in many important cellular processes, our discovery further predicts a possible pleiotropic function of the Cif/CHBP family of effectors in bacterial pathogenesis.

References and Notes

1. C. R. Roy, E. S. Mocarski, *Nat. Immunol.* **8**, 1179 (2007).
2. A. P. Bhavsar, J. A. Guttman, B. B. Finlay, *Nature* **449**, 827 (2007).
3. J. Huang, C. F. Lesser, S. Lory, *Nature* **456**, 112 (2008).
4. H. Iwai *et al*., *Cell* **130**, 611 (2007).
5. M. Lara-Tejero, J. E. Galán, *Science* **290**, 354 (2000).
6. O. Marchès *et al*., *Mol. Microbiol.* **50**, 1553 (2003).
7. A. Samba-Louaka *et al*., *Cell. Microbiol.* **10**, 2496 (2008).
8. Q. Yao *et al*., *Proc. Natl. Acad. Sci. U.S.A.* **106**, 3716 (2009).
9. F. Shao, P. M. Merritt, Z. Bao, R. W. Innes, J. E. Dixon, *Cell* **109**, 575 (2002).
10. Y. Hsu *et al*., *J. Mol. Biol.* **384**, 465 (2008).
11. Materials and methods are available as supporting material on *Science* Online.
12. Single-letter abbreviations for the amino acid residues are as follows: A, Cys; D, Asp; E, Glu; F, Phe; G, Gly; H, His; I, Ile; K, Lys; L, Leu; M, Met; N, Asn; P, Pro; Q, Gln; R, Arg; S, Ser; T, Thr; V, Val; W, Trp; X, any amino acid; and Y, Tyr.
13. W. Li, D. Tu, A. T. Brunger, Y. Ye, *Nature* **446**, 333 (2007).
14. Y. Chen *et al*., *Mol. Cell* **35**, 841 (2009).
15. H. B. Kamadurai *et al*., *Mol. Cell* **36**, 1095 (2009).
16. O. Kerscher, R. Felberbaum, M. Hochstrasser, *Annu. Rev. Cell Dev. Biol.* **22**, 159 (2006).
17. A. Haraga, T. E. West, M. J. Brittnacher, S. J. Skerrett, S. I. Miller, *Infect. Immun.* **76**, 5402 (2008).
18. G. Rabut, M. Peter, *EMBO Rep.* **9**, 969 (2008).
19. A. Saha, R. J. Deshaies, *Mol. Cell* **32**, 21 (2008).
20. Q. Zhong, W. Gao, F. Du, X. Wang, *Cell* **121**, 1085 (2005).
21. C. Zhou *et al*., *Proc. Natl. Acad. Sci. U.S.A.* **105**, 12022 (2008).
22. N. Y. Fu, S. K. Sukumaran, V. C. Yu, *Proc. Natl. Acad. Sci. U.S.A.* **104**, 10051 (2007).
23. D. M. Duda *et al*., *Cell* **134**, 995 (2008).

24. We thank Y. Ye, C. Fathman, Z. Pan, D. Haas, V. Yu, E. Boedeker, and Z. Chen for providing reagents. We are grateful to F. Du and X. Wang for their assistance in obtaining reagents. We also thank members of the Shao laboratory for helpful discussions and technical assistance. This work was supported by Chinese Ministry of Science and Technology grant 2008AA022309 and National Basic Research Plan of China 973 grants to F.S. and National Institutes of Health grant R01 CA107134 to N.Z. and H.M. N.Z. is a Howard Hughes Medical Institute investigator.

Supporting Online Material

www.sciencemag.org/cgi/content/full/science.1193844/DC1
Materials and Methods
Figs. S1 to S18
References

16 June 2010; accepted 23 July 2010
Published online 5 August 2010;
10.1126/science.1193844
Include this information when citing this paper.

NEW PRODUCTS

AUTOMATED CHROMATOGRAPHY

The Octave Chromatography System is an automated chromatography platform designed for preparative-scale purification of chemical and biological compounds. The system is able to continuously process racemates, cell lysates, cell culture supernatants, and other crude fractions to yield grams of highly purified antibodies, proteins, sugars, amino acids, fatty acids, and other large and small molecules in just hours. The compact, versatile, and affordable system brings the benefits of simulated moving bed chromatography to the laboratory benchtop. The Octave System carries eight column positions arranged in series and connected through a proprietary pneumatic valve array. The valve and pump configuration provides ultimate flexibility in programming chromatographic protocols via the intuitive software. All flow paths consist of metal-free biocompatible materials that are also compatible with common organic solvents and clean-in-place solutions. The Octave System is available in two configurations with maximum flow rates up to 10 and 100 milliliter/minute.

Dorton Analytical Ltd

For info: +44-(0)-7872-520670 | www.dortonanalytical.co.uk

SOLID PHASE EXTRACTION

Strata-X-A polymeric, high-capacity sorbent delivers maximum retention of anionic compounds, for anion/cation exchange separations. The base polymer of the new Strata-X-A is pH-stable and resists deconditioning, providing more flexibility during method development and reducing the potential for errors. Strata-X-A retains acidic analytes in three different ways: π-π and hydrophobic interactions coupled with a strong anion exchange mechanism. The strong ionic bond allows an aggressive organic wash, leaving the eluent free of interference. This sorbent is ideal for a wide variety of liquid chromatography and gas chromatography applications that involve acid analytes including environmental and forensic toxicology. Strata-X-A is offered in 1 mL, 3 mL, and 6 mL tubes for traditional cleanup, 96-well plates for high throughput extractions, and Giga Tubes (12 mL, 20 mL, and 60 mL) for large-volume applications.

Phenomenex

For info: 310-212-0555 | www.phenomenex.com

CONFOCAL MICROSCOPY

Designed for researchers seeking higher resolution images while working within a tight budget, Leica Microsystems' True Confocal/True Value Program delivers all of the equipment needed to immediately start using confocal imaging for $99,000. The package includes the LeicaTCS SPE II Spectral Confocal with a fully configured upright microscope, objective lens set, three laser lines, and high-performance computer. The Leica TCS SPE II is a high-resolution spectral confocal for daily research. The highly integrated system features durable hardware and the Leica Application Suite Advanced Fluorescence (LAS AF) software platform to ensure smooth, fast operation.

Leica Microsystems, Inc.

For info: 800-248-0123 | www.leica-microsystems.com

SAMPLE TRACKING

The 2D Barcode Reader is specially designed to provide advanced sample tracking functions on Microlab Star automated liquid handling workstation. The new reader has a compact footprint in a standard carrier size to minimize the required deck space. The reader's charge-coupled device camera records barcodes in less than 0.5 seconds from a wide range of sample formats including boxes of SBS tubes and biovials in 96-well format. Five labware positions are available on the device. The 2D barcode reader supports a variety of tubes from many manufacturers, in 24-, 48-, 96-, and 384-well configurations. The new reader is ideal for high throughput screening, sample archival, forensics, and work with single-nucleotide polymorphisms and blood samples.

Hamilton

For info: 800-648-5950 | www.hamiltonrobotics.com

PARP PHARMACODYNAMIC ASSAY

The second generation Poly-ADP-ribose polymerase (PARP) in vivo pharmacodynamic assay accurately measures net poly-ADP-ribose (PAR) levels in cellular extracts and has been used to document differences in PAR levels in human tumor lysates from a variety of tissues, organs, and xenografts. The pharmacodynamic assay uses a validated sample processing regime and a chemiluminescent, sandwich enzyme-linked immunosorbent assay (ELISA) format, with pre-coated 96-stripwell plates. The assay reports PAR levels at high signal-to-noise ratio, with a sensitivity of two picograms/milliliter (pg/ml) and a linear dynamic range to 1000 pg/ml. The new tool provides evidence of drug action on molecular targets and generates baseline values that may be used to stratify patient response to therapy.

AMS Biotechnology

For info: +44-1235-828200 | www.amsbio.com

Electronically submit your new product description or product literature information! Go to **www.sciencemag.org/products/newproducts.dtl** for more information.

Newly offered instrumentation, apparatus, and laboratory materials of interest to researchers in all disciplines in academic, industrial, and governmental organizations are featured in this space. Emphasis is given to purpose, chief characteristics, and availability of products and materials. Endorsement by *Science* or AAAS of any products or materials mentioned is not implied. Additional information may be obtained from the manufacturer or supplier.

POSITIONS OPEN

DIRECTOR
Shanghai Center for Comprehensive Protein Science
Chinese Academy of Sciences
Shanghai Institute
of Biochemistry and Cell Biology
Shanghai Institutes for Biological Sciences
Chinese Academy of Sciences

中国科学院上海蛋白质科学综合研究中心
上海生物化学与细胞生物学研究所
中国科学院上海生命科学研究院

Shanghai Institute of Biochemistry and Cell Biology (SIBCB), Shanghai Institutes for Biological Sciences (SIBS), Chinese Academy of Sciences (CAS) invites applications for the position of Director of Shanghai Center for Comprehensive Protein Science (SCPS), Chinese Academy of Sciences. SIBCB is part of Shanghai Institutes for Biological Sciences, which comprises eight CAS institutes in the area of biological sciences in Shanghai. SIBCB currently has 54 research groups and over 350 scientists with research interests in diverse aspects of molecular and cellular biology, such as gene regulation, epigenetics, protein sciences, signal transduction, cell and stem cell biology, cancer, and other disease models. SCPS will be housed in the National Protein Science Facility (NPSF)-Shanghai, which is the largest Protein Science platform in China and is being constructed and managed by SIBCB and SIBS, CAS. SCPS will conduct research and provide service in many key areas of protein science, including X-ray crystallography, nuclear magnetic resonance, electron microscopy, single molecule technology, functional proteomics, cell imaging, animal imaging, and bioinformatics, as well as synchrotron applications. The Director will be responsible for the overall research and service strategies at SCPS and will also be in charge of administrating NPFS-Shanghai.

Successful candidate for the Director position must be an internationally renowned scientist in protein science with established leadership credentials and must be at the level of tenured Professor. The Director should have a strategic plan for the Center and is responsible for recruiting first-class scientists, researchers, and technical staff. Salary is highly competitive and housing subsidy will be provided. The position offers excellent laboratory facilities, generous start-up funds, and the opportunity to work with outstanding Ph.D. students and postdoctoral fellows. The Director will be expected to work full-time at SCPS and maintain an active research program. Curriculum vitae, a list of publications, a brief summary of previous accomplishment and future research plans, and three letters of references should be sent to: **Mrs. Jinfang Song, CCPS Director Search Committee, SIBCB, SIBS, CAS, 320 Yue-Yang Road, Shanghai 200031, China,** or electronically to **e-mail: songjf@sibs.ac.cn** (**telephone: 086-21-54921022** and **fax: 086-21-54921011**). *SIBCB is an Equal Opportunity Employer.* For more information, please visit **websites: http://www.sibcb.ac.cn** or **http://www.sibs.ac.cn.**

POSTDOCTORAL POSITION. A Postdoctoral Position is available to minority Ph.D. graduates with training in molecular and cell biology or a related discipline to participate in the discovery and mechanistic studies of novel antimetastasis agents. Interested candidates should submit their curriculum vitae to: **Dr. Isaac Donkor, Department of Pharmaceutical Science, University of Tennessee Health Science Center, 847 Monroe Avenue, Memphis, TN 38163. E-mail: idonkor@uthsc.edu.** *UTHSC is an Equal Employment/Affirmative Action/Title VI/IX/Section 504/ADA/ADEA Employer.*

POSITIONS OPEN

UNIVERSITY OF DENVER
START FROM A HIGHER PLACE

EVOLUTIONARY BIOLOGIST

The Department of Biological Sciences, University of Denver (DU), invites applications for a tenure-track position at the **ASSISTANT PROFESSOR** level to begin September 1, 2011. Candidates with expertise in any area of Evolutionary Biology are sought; individuals with expertise in either evolutionary-developmental biology or evolutionary ecology are encouraged to apply. The successful candidate will have a Ph.D. and postdoctoral experience in appropriate fields, will develop an extramurally funded research program, will supervise undergraduate research projects and M.S. and Ph.D. students, and will teach undergraduate and graduate courses in evolutionary biology and specific areas of specialty. All candidates must submit their application through **website: https://www.dujobs.org.** The online application should include: curriculum vitae, statements of teaching philosophy and research interests, and two recent publications. Under separate cover have three letters of recommendation sent to: **Dr. Todd Blankenship, Chair, Evolutionary Biologist Search Committee, Department of Biological Sciences, University of Denver, Denver, CO 80208.** Review of applications will begin October 15, 2010. *The University of Denver is committed to enhancing the diversity of its faculty and staff and encourages applications from women, minorities, people with disabilities and veterans. DU is an Equal Employment Opportunity/Affirmative Action Employer.*

Columbia University's Department of Pathology and Cell Biology, Division of Immunogenetics, invites applications for four **STAFF ASSOCIATE POSITIONS** as follows: (1) Two positions to perform and interpret histocompatibility tests, perform molecular human leukocyte antigen typing and flow cytometry crossmatching, coordinate quality assurance operations, and train new personnel; (2) One position to perform flow cytometric analysis of clinical specimens, report results, and communicate with referring physicians; (3) One position to perform immunologic monitoring of transplant patients, data analysis, and validation.

Minimum requirements are: B.S. degree and four years of experience in cellular immunology and/or molecular genetics. Expertise in flow cytometry and/or histocompatibility testing is essential. The candidate should be certified by the New York State Department of Health as a laboratory technician or technologist. These positions require working evenings and/or weekend hours.

Interested applicants should apply online at **website: academicjobs.columbia.edu/applicants/Central?quickFind=53550.**

Columbia University is an Equal Opportunity/Affirmative Action Employer.

The Department of Ecology and Evolutionary Biology, Tulane University, invites applications for one tenure-track position at the level of **ASSISTANT PROFESSOR.** We encourage applications from **LANDSCAPE** or **ECOSYSTEM ECOLOGISTS** focused on wetland, tropical, and/or plant communities. See **website: http://www.tulane.edu/~ebio/news/new-positions.php** for details about the positions, department, and application process. Send letter of application, curriculum vitae, statements of research and teaching interests, selected publications, and names and addresses of three references to: **EEB Faculty Search, Department of Ecology and Evolutionary Biology, 400 Lindy Boggs Center, Tulane University, New Orleans, LA 70118-5698.** Review of applications will begin October 15, 2010, and the search will remain open until the position is filled. An offer of employment is, however, contingent upon authorization of the position. *Tulane University is an Affirmative Action/Equal Employment Opportunity/ADA Employer. Women and minorities are encouraged to apply.*

Janelia Junior Fellows Program

The Howard Hughes Medical Institute's Janelia Farm Research Campus is a world-class biomedical research center where outstanding scientists from diverse disciplines use emerging and innovative technologies to pursue biology's most challenging problems.

The Janelia Junior Fellows Program is a new initiative that supports enterprising postdoctoral fellows as they develop their own research programs. The junior fellow position is intended for individuals at an early career stage and/or people who have specific research plans but who value the guidance and collaboration of more experienced mentors.

Junior fellows are appointed for a period of up to three years, during which time they are mentored by two or more Janelia Farm lab heads and/or visiting scientists from other institutions. Junior fellows will have responsibility and oversight of a budget, which supports their own salary and benefits, lab supplies, and travel expenses.

We invite applications from early career-stage biochemists, biologists, chemists, computer scientists, engineers, geneticists, mathematicians, neurobiologists, physicists and statisticians who are passionate in their pursuit of important problems in basic scientific and technical research.

For more details about the Janelia Junior Fellows Program, please go to **www.hhmi.org/juniorfellow/sci**

There are three application deadlines per year and the next are: **November 1, 2010, March 1, 2011, and July 1, 2011**

For more information and to submit an application: **www.hhmi.org/juniorfellow/sci**

HHMI
janelia farm
research campus

Scientists at the Janelia Farm Research Campus pursue challenging basic biomedical problems for which future progress requires technological innovation. We focus on two research areas: the identification of general principles that govern how information is processed by neuronal circuits and the development of imaging technologies and computational methods for image analysis.

The Howard Hughes Medical Institute is an equal opportunity employer. Women and members of racial and ethnic groups traditionally underrepresented in the biomedical sciences are encouraged to apply.

Photo by Paul Fetters

MAYO CLINIC

Heal the sick, advance the science, share the knowledge.

Translational Research Investigator Faculty Position in Mayo Clinic HEAL[TH] Program – Diabetes

Mayo Clinic in Arizona seeks outstanding candidates for faculty positions in its HEAL[TH] Program, a new translational research program focused on diabetes mellitus, obesity and vascular disease. This Program is a collaborative partnership with Arizona State University, drawing upon the complementary strengths of both institutions. This position is focused on type 2 diabetes mellitus, but can include investigators with interest in insulin resistance, insulin secretion and diabetic complications.

Candidates would ideally hold an MD or MD/PhD or equivalent degree and have a demonstrated record of relevant research accomplishments, as evidenced by their training, publications and peer-reviewed funding. As multiple faculty positions exist, PhD candidates are also welcomed. Appointment and rank in an appropriate clinical and academic department will be determined based on the applicant's qualifications. Candidates will also have a joint academic appointment at Arizona State University as part of Mayo's collaborative partnership.

The successful applicant will be a member of the Mayo Clinic HEAL[TH] program based in Arizona and the Mayo/Arizona State University Center for Metabolic and Vascular Biology. Mayo resources include ample new laboratory space, a mouse metabolic phenotyping facility, a new clinical research unit designed for state-of-the-art metabolic studies, and access to all Mayo core facilities and shared equipment. Resources at Arizona State University include the Proteomics Laboratory, specializing in proteomics devoted to understanding Metabolic Syndrome conditions, the Genomics and Transcriptomics Laboratory and a clinical research unit specializing in metabolic studies.

Mayo Clinic is an internationally renowned, integrated, multidisciplinary academic medical center with comprehensive programs in medical education and research with campuses in Arizona, Florida and Minnesota. Mayo Clinic supports five schools spanning undergraduate, graduate, medical, postgraduate medical and continuing medical education, and has active biomedical research programs.

In Arizona, Mayo Clinic is a 380-physician, integrated clinical practice, focusing on high-quality, compassionate medical care delivered in a multispecialty academic environment. Mayo Clinic offers a competitive salary, excellent benefits, and has been recognized by *Fortune* magazine as one of the "100 Best Companies to Work For." To learn more about Mayo Clinic, please visit **www.mayo.edu**.

Interested candidates are invited to submit a cover letter, curriculum vitae and brief description of research experience and interests to:

Lawrence J. Mandarino, PhD
HEAL[TH] Program Search Committee
Mayo Clinic
13400 East Shea Boulevard
Scottsdale, AZ 85259
mandarino.lawrence@mayo.edu

Mayo Foundation is an affirmative action and equal opportunity employer and educator. Post-offer/ pre-employment drug screening is required.

Faculty Position Molecular Biology Sloan-Kettering Institute

The Molecular Biology Program of the Sloan-Kettering Institute, Memorial Sloan-Kettering Cancer Center (www.ski.edu), has initiated a faculty search at the Assistant Member level (equivalent to Assistant Professor). We are interested in outstanding individuals who have demonstrated records of significant accomplishment and the potential to make substantial contributions to the biological sciences as independent investigators. Successful applicants will have research interests that move the Program into exciting new areas that complement and expand our existing strengths in the areas of maintenance of genomic integrity, regulation of the cell cycle, and regulation of gene expression. Faculty will be eligible to hold appointments in the Gerstner Sloan-Kettering Graduate School of Biomedical Sciences, the Weill Cornell Graduate School of Medical Sciences, as well as the Tri-Institutional MD/PhD Training Program.

The deadline for applications is **November 1, 2010**. Interested candidates should visit **http://facultysearch.ski.edu** to access the on-line faculty application. Please visit the site as soon as possible, as it contains important information on the required application materials, including deadlines for submission of letters of reference.

Informal inquiries may be sent to **Julie Kwan at kwanj@mskcc.org** or to **Dr. Kenneth Marians, Chair, Molecular Biology Program at kmarians@sloankettering.edu**. MSKCC is an equal opportunity and affirmative action employer committed to diversity and inclusion in all aspects of recruiting and employment. All qualified individuals are encouraged to apply.

Memorial Sloan-Kettering Cancer Center
www.mskcc.org

The Ohio State University

Assistant Professor

Evolution, Ecology and Organismal Biology

The Ohio State University at Lima seeks candidates for a full-time, tenure-track Assistant Professor, with a specialty in Plant Ecology. The appointment will be made in the Department of Evolution, Ecology and Organismal Biology at The Ohio State University and begin in September 2011.

The department seeks a plant ecologist with a strong commitment to the teaching, research and outreach missions of The Ohio State University. The successful candidate will teach undergraduate surveys and major courses in their area of expertise, and serve as an advisor and research mentor within the Biology major. In addition, the position will require the potential for a distinguished record of service and scholarly research. Candidates must have a PhD in hand at the time of appointment; post-graduate teaching experience is preferred. Salary is competitive.

The Ohio State University at Lima is one of five campuses of The Ohio State University. Current enrollment on the Lima campus is 1,500 students and there are approximately 100 full- and part-time faculty in all academic departments. Ohio State Lima offers the first two years of the Ohio State general education curriculum and ten programs leading to baccalaureate degrees, including one in Biology. Ohio State Lima also offers Master's degree programs in Education and Social Work.

THE OHIO STATE UNIVERSITY LIMA

Review of applications will begin on November 7, 2010, and will continue until the position is filled. Please send a cover letter, a current curriculum vita, and three letters of recommendation to:
Dr. Eric Juterbock, Chair, EEOB Search, c/o Office of Human Resources, Public Service Bldg. 122, The Ohio State University at Lima, 4240 Campus Drive, Lima, OH 45804

The Ohio State University is an equal opportunity, affirmative action employer. Qualified women, minorities, veterans and individuals with disabilities are encouraged to apply.

HOWARD HUGHES MEDICAL INSTITUTE

Laboratory Head Positions at Janelia Farm

We invite applications from biochemists, biologists, chemists, computer scientists, engineers, mathematicians, neurobiologists, and physicists at all career stages who are passionate in their pursuit of important problems in basic scientific and technical research.

Appointments may be made at either of two levels:

Fellows

Fellows are independent scientists with labs of up to two additional members.

Appointments are for five years.

Group Leaders

Group leaders are independent scientists, similar to HHMI investigators, with labs of up to six additional members. The initial appointment is for six years. Thereafter, group leaders will be reviewed for reappointment every five years.

There are two application deadlines per year and the next are:

July 15, 2010 and December 15, 2010.

For more information and to submit an application:

www.hhmi.org/ref/janelia/sci

HHMI janelia farm research campus

At Janelia Farm, we pursue challenging basic biomedical problems for which future progress requires technological innovation. We focus on two research areas: the identification of general principles that govern how information is processed by neuronal circuits; and the development of imaging technologies and computational methods for image analysis. This year we have decided to broaden our foci at the Fellow level – we also seek very promising, early career stage scientists with interests beyond these two major foci. We expect that Janelia would be attractive to people with scientific programs that could benefit from collaborators or technologies already at Janelia. We value people with new perspectives who will contribute to our intellectual community.

Examples might include:

- A cell biologist looking to apply super-resolution optical microscopy to their work.
- A computer scientist interested in machine vision.
- A physicist interested in instrument development.
- A biochemist interested in single-molecule imaging.

Janelia Farm is now home to a growing, multidisciplinary community of 35 research groups, comprising postdoctoral associates, graduate students, and technicians. Our scientists are supported by outstanding shared resource facilities within a unique campus less than an hour from Washington, D.C. All laboratories are internally funded, without extramural grants. Lab heads have no formal teaching duties and minimal administrative responsibilities. Janelia Farm offers a supportive working environment with on-site child care, fitness center, and dining facilities.

Individual research groups are limited in size. We value research collaboration between groups as a mechanism to enable long-range innovative science and encourage the self-assembly of interdisciplinary teams of scientists. In addition we support external collaborative science through a scientific visitor program.

The Howard Hughes Medical Institute is an equal opportunity employer. Women and members of racial and ethnic groups traditionally underrepresented in the biomedical sciences are encouraged to apply.

VICTORIA UNIVERSITY OF WELLINGTON

Victoria University delivers internationally-acclaimed results in teaching and research, as well as programmes of national significance and international quality.

As one of Wellington's largest and most established employers, we're committed to providing our staff with opportunities for rewards, recognition and development, all within a dynamic and inclusive culture where innovation and diversity are highly valued.

ASSOCIATE PROFESSOR/PROFESSOR IN FISHERIES BIOLOGY

School of Biological Sciences
Wellington, New Zealand

We seek a Senior Fisheries Biologist with a strong track record in internationally recognised research, significant experience in both securing and leading externally-funded research programs together with experience in teaching and supervision of students.

The successful candidate will be expected to promote Victoria University of Wellington as a leading provider of fisheries research by advancing national and international research networks and leading School activities in outreach programmes in fisheries biology. The successful applicant will be expected to work with government research agencies, and New Zealand or international fishing industry research organisations.

We would welcome applications from specialists in a wide range of fields including stock assessment, population modelling, or resource sustainability. Experience of academic leadership is expected for all professorial candidates.

For further information contact Associate Professor Phil Lester, phil.lester@vuw.ac.nz

Applications close 30 September 2010

Victoria University of Wellington is an EEO employer and actively seeks to meet its obligations under the Treaty of Waitangi.

For more information and to apply online visit **http://vacancies.vuw.ac.nz**

Reference A238-10Q

TE WHARE WĀNANGA O TE ŪPOKO O TE IKA A MĀUI
VICTORIA
UNIVERSITY OF WELLINGTON

UNIVERSITÉ DE GENÈVE

WORKING AT THE UNIVERSITY OF GENEVA

The FACULTY OF SCIENCE invites applications for the position of a

PROFESSOR
in Plant Biology

(Full, Associate or Assistant with Tenure Track)
(**www.unige.ch/sciences/biologie/index.html**)

We seek applicants with a record of excellence in research, who have proven their ability to develop and apply novel concepts in the general area of plant molecular and cellular biology. The position is full time, including teaching at the Bachelor or Master level. The successful candidate is expected to lead a strong, independent research program and attract external funding. He/she will also have the responsibility of overseeing and directing research of undergraduate and graduate students.

ACADEMIC TITLE REQUIRED : Ph.D. degree or equivalent.

STARTING DATE : September 1st 2011 or to be agreed.

Candidates files including a curriculum vitae, a publication list, a summary of current and future research interests, as well as names and addresses of three potential referees must be addressed before **October 31st 2010**, to: Décanat de la Faculté des sciences, 30 Quai Ernest Ansermet, CH-1211 Genève 4 or by e-mail to **gaelle.auge@unige.ch** and from whom additional information can be obtained regarding the responsibilities of the post and other conditions.

The University of Geneva is an equal oppportunity employer and encourages applications from female candidates.

FACULTY POSITIONS IN CANCER BIOLOGY

Applications are invited for tenure-track faculty positions in the Cancer Biology and Genetics Program of the Sloan-Kettering Institute, Memorial Sloan-Kettering Cancer Center (www.ski.edu). Successful candidates will carry out independent research on the genesis, progression, prognosis, prevention and treatment of cancer that synergize with ongoing efforts at the Center. Areas of special interest are, but not limited to: cancer genetics, cancer stem cells, metastasis, tumor microenvironment, inflammation and cancer, and animal models of cancer.

New faculty members will join an interactive, interdisciplinary community of scientists and clinicians at the Center, which offers an outstanding basic and translational research environment within expanded state-of-the-art research facilities. Faculty will be eligible to hold graduate school appointments in the Gerstner Sloan-Kettering Graduate School of Biomedical Sciences, the Weill Cornell Graduate School of Medical Sciences of Cornell University, as well as the Tri-Institutional MD/PhD Training Program.

Cancer Biology & Genetics Faculty
Robert Benezra, PhD - Angiogenesis/Differentiation
Eric Holland, MD/PhD - Glioma Mouse Models
Anna Kenney, PhD - Neural Stem Cells/Brain Tumors
Robert Klein, PhD - Cancer Genetics
Johanna Joyce, PhD - Tumor Microenvironment
Joan Massague, PhD (Chairman) - Cell Regulation/Metastasis
Christine Mayr, MD, PhD - Oncogenic microRNA Target Control
Kenneth Offit, MD - Cancer Genetics
Andrea Ventura, PhD - microRNAs in Development and Cancer
Hans-Guido Wendel, MD - Genetic Basis for Drug Resistance

The deadline for applications is November 1, 2010. Interested candidates should visit http://facultysearch.ski.edu to access the on-line faculty application. Please visit the site as soon as possible, as it contains important information on the required application materials, including deadlines for submission of letters of reference. Inquiries may be sent to **Maria Gordon at gordonm1@mskcc.org or to Dr. Joan Massagué, Chair, Cancer Biology & Genetics Program at massaguj@mskcc.org**. MSKCC is an equal opportunity and affirmative action employer committed to diversity and inclusion in all aspects of recruiting and employment. All qualified individuals are encouraged to apply.

Memorial Sloan-Kettering Cancer Center
www.mskcc.org

ÉCOLE POLYTECHNIQUE
FÉDÉRALE DE LAUSANNE

Faculty Position in Chemical Biology

at the Ecole Polytechnique Fédérale de Lausanne (EPFL)

EPFL anticipates making a faculty appointment at the level of tenure-track assistant professor in its Institute of Chemical Sciences and Engineering (ISIC). The appointment is in the context of the newly established *National Centre of Competence in Research* (NCCR) in Chemical Biology.

The successful applicant is expected to build up an internationally recognized research program in the area of chemical biology and to participate in the NCCR. It is expected that the candidate will be strongly committed to excellence in teaching at both the undergraduate and graduate levels.

We offer internationally competitive salaries, benefits, start-up resources for scientific equipment and annual resources for PhD students, scientific staff and consumables.

The EPFL School of Basic Sciences aims for a strong presence of women amongst its faculty, and qualified female candidates are strongly encouraged to apply.

Applications including a letter of motivation, curriculum vitae, publication list, concise statement of research and teaching interests as well as the names and addresses (including email) of at least five references should be submitted in PDF format via the website **http://sbpositions/applications** by **October 30, 2010**.

For additional information, please contact **Professor Paul Dyson (paul.dyson@epfl.ch)** or consult the following websites: **http://www.epfl.ch/Eplace.html, http://sb.epfl.ch/en** and **http://isic.epfl.ch**

Immunology Faculty Position
Sloan-Kettering Institute

The Immunology Program at the Sloan-Kettering Institute (www.ski.edu) is seeking innovative investigators for tenure-track positions at the Assistant, Associate, and Member levels who wish to address basic problems in immunology with possible relevance to cancer. Applicants should have a doctoral-level degree and the potential to develop a strong independent research program or a proven record of accomplishments, depending on the level of appointment. Qualified applicants with an M.D. degree may be offered a joint appointment in an appropriate department in Memorial Hospital. Candidates will join a faculty with a broad range of research interests, including transplantation, B, T and NK cell development and function, regulation of immune responses, antigen presentation, infectious disease and tumor immunology. The program has recently moved into contiguous space on 3+ floors in a new 23 story laboratory building. Faculty will be eligible to hold graduate school appointments in the Gerstner Sloan-Kettering Graduate School of Biomedical Sciences, the Weill Cornell Graduate School of Medical Sciences, as well as the Tri-Institutional MD/PhD Training Program.

SKI offers a highly interactive, supportive and exciting research environment with programs in Immunology, Cancer Biology & Genetics, Cell Biology, Molecular Pharmacology & Chemistry, Molecular Biology, Developmental Biology, Computational Biology and Structural Biology, as well as unparalleled clinical programs in cancer research, treatment and prevention.

The deadline for applications is **November 1, 2010**. Interested candidates should visit **http://facultysearch.ski.edu** to access the on-line faculty application. Please visit the site as soon as possible, as it contains important information on the required application materials, including deadlines for submission of letters of reference. Inquiries may be sent to **Dwana Agosto at agostod@mskcc.org** or to **Dr. James Allison, Chair, Immunology Program at allisonj@mskcc.org**. MSKCC is an equal opportunity and affirmative action employer committed to diversity and inclusion in all aspects of recruiting and employment. All qualified individuals are encouraged to apply.

Memorial Sloan-Kettering Cancer Center
www.mskcc.org

UMEÅ UNIVERSITET

Umeå Universitet announces...

At Umeå University world-leading research is conducted within several areas. We offer an attractive range of courses and programmes taught in a quality study environment. The Umeå University campus is a creative and exciting place of work and study for our 4,000 employees and 33,000 students.

Three four-year positions as

Group leaders in neurometabolism research

Umeå University in Sweden seek three scientists who will work independently and in collaboration to advance the understanding of neurodegenerative disorders at the cellular and functional level.

Information about Umeå university can be found at www.umu.se and about Umeå community at www.umea.se.

Your complete application, marked with **reference number 316-731-10**, should be sent to jobb@umu.se (state the reference number as subject) or to the registrar, Umeå University, SE-901 87 Umeå, Sweden to arrive **October 1, 2010 at the latest.**

More information: **www.jobb.umu.se**

Department of the Army
U.S. Army Medical Research and Materiel Command
U.S. Army Medical Research Institute of Chemical Defense

Science Director
$123,758 – 155,500

The U.S. Army Medical Research Institute of Chemical Defense (USAMRICD), the Department of Defense's premier research Institute for medical defense against chemical warfare agents and toxins located in the Edgewood Area of the Aberdeen Proving Ground, Maryland, is seeking to fill the new position of Science Director serving as the **DEPUTY COMMANDER FOR RESEARCH, GS-1301-15**. You will serve as the civilian scientific programmatic advisor to the Commander and will assist the Commander in setting the strategic direction and priorities for the Institute. In addition, you will be responsible for integrating the Institute's scientific and consultative activities with the growing interagency medical chemical defense programs for national defense by interfacing with DOD and other external agencies as required. The Deputy Commander for Research will be responsible for ensuring USAMRICD's continued leadership role in the field of chemical defense by facilitating the identification of the scientific staffing, infrastructure, and capital equipment investments required to support the scientific needs of a state-of-the-art, multidisciplinary research organization. Position may require up to 15% national/international travel.

Qualifications: A doctoral degree in Medicine, Veterinary Medicine, or related biomedical sciences, and at least 2 years direct research experience, and at least 10 years relevant experience in leading or developing a world-class research organization is required. Able to obtain and maintain a Secret Clearance. A successful candidate must be a U.S. citizen who is a recognized expert or global leader in one core area of biological research, yet must have a broad understanding of the biomedical sciences. Must have strong process orientation with the ability to understand the strategic and tactical links between basic research and early product development. Must have strong business and scientific perspectives, demonstrated ability to deliver results in a structured organization, and a solid background in the management of a technical organization. Excellent communication skills, both written and oral, strong project management skills, outstanding interpersonal relationship skills, and the ability to work cooperatively in a collaborative, multidisciplinary research environment must be demonstrated.

Interested applicants should apply at: **https://cpolwapp.belvoir.army.mil/public/vabSelfNom/index.jsp** AND send all of the following: a Curriculum Vitae with list of publications; copies of three major publications; a summary of research accomplishments; a statement describing their scientific management philosophy; and three letters of recommendation POSTMARKED BY **30 Sept 2010** to **LTC Deborah Whitmer, c/o DCR Search Committee, USAMRICD – 3100 Ricketts Point Road, Aberdeen Proving Ground, MD 21010-5400**.

Visit us on the web at: **http://usamricd.apgea.army.mil**. Visit APG: **http://www.apg.army.mil/apghome/sites/local**. RECRUITMENT and RELOCATION incentives. PCS is authorized.

Equal Opportunity Employer.

THE UNIVERSITY OF QUEENSLAND
AUSTRALIA

SCHOOL OF BIOMEDICAL SCIENCES, FACULTY OF BIOLOGICAL AND CHEMICAL SCIENCES, THE UNIVERSITY OF QUEENSLAND, BRISBANE, AUSTRALIA

LECTURER / SENIOR LECTURER IN INORGANIC CHEMISTRY

The role Contribute to teaching and research in inorganic chemistry, and work with academic staff in the School's teaching programs to develop contemporary teaching of chemistry.

Remuneration AUD$73,836 – $87,680 p.a. (Level B) or AUD$90,448 – $104,292 p.a. (Level C), plus 17% super. Full-time, continuing appointment at Academic Level B or C.

Applications close 1 October 2010
Reference No. 3021072

To apply: Go to **www.jobsatUQ.net** to obtain a copy of the position description and application process. Applications may be lodged in electronic or hard copy form. UQ is an equal opportunity employer.

CRICOS Provider Number 00025B

東海大学

Tenure Track Positions
TOKAI UNIVERSITY
INSTITUTE OF INNOVATIVE SCIENCE AND TECHNOLOGY
SCHOOL OF MEDICINE

Tokai University is recruiting 3 tenure track researchers for the 2010-11 academic year for a researcher-mentor development program that cultivates researchers who can conduct studies of international stature. Newly employed tenure track researchers at Tokai's TUIIST will be provided with the opportunity to further strengthen their research skills and mentorship capacity in an environment that includes study abroad and the acquisition of invaluable international experience. Tenure track researchers who pass the interim evaluation held in the third year, and the final evaluation in the fifth year, will be appointed as a full-time tenured assistant professor, associate professor, or professor. For more information, visit our website: **http://www.u-tokai.ac.jp/tuiist/english/index.html**.

Requirements: applicants must have obtained a doctoral degree within 10 years and have more than three years of work experience as an assistant professor, a postdoctoral fellow, or an equivalent position. They also must have significant accomplishments in research. **Japanese language ability is not required**, but excellent communication skills and/or ability to train and assist other members are needed.

Term of Employment: January 1, 2011 through March 31, 2015. The contract is renewed annually.
Application materials: C.V. which includes a list of activities in academic conferences and societies, copies of 5 representative papers, a summary of past research activities, a list of external research funding obtained to date, a research plan, comments regarding the future potential, and three letters of recommendation (these should be sent directly to our university). Forms can be downloaded from the web site above.
Deadline: September 30, 2010, 5p.m.(Japan Standard Time)

Applicants may be asked to submit additional documents during the selection process. **Submission of Application Documents:** Please send the application documents as attached files to **iist@tokai-u.jp** and a hard copy via postal mail with delivery confirmation (registered mail, etc.) to the **School of Medicine, TOKAI UNIVERSITY INSTITUTE OF INNOVATIVE SCIENCE AND TECHNOLOGY, Shimokasuya 143, Isehara, Kanagawa 259-1193, Japan**.

STANFORD UNIVERSITY

ASSISTANT PROFESSOR OF STRUCTURAL BIOLOGY

Applications are invited for a tenure-track junior faculty appointment in the Department of Structural Biology, Stanford University School of Medicine. Candidates should have expertise and a commitment to future research in the broad area of structural biology and biophysics. The predominant criterion for appointment in the University Tenure Line is a major commitment to research and teaching.

To be considered for this position, interested individuals should:

1. Fully complete the Structural Biology Faculty Recruitment Form available at: **https://med.stanford.edu/survey/sbio_fclty_recruit**.
2. Prepare the application materials as **one .pdf** file and e-mail the file to **sbio_faculty_recruit@lists.stanford.edu**. PDF file **must contain all** of the following documents: (i) Cover letter, (ii) Curriculum vitae, (iii) Description of research interests (4 page limit), (iv) List of publications, (v) Maximum of 5 representative reprints, (vi) Names and contact information of three referees.
3. Arrange for three reference letters to be e-mailed by each referee directly to: **sbio_fclty_reference@lists.stanford.edu** or send by mail to: **Chair, Faculty Search Committee, Department of Structural Biology, Stanford University School of Medicine, 299 Campus Drive West, D100 Fairchild Bldg., Stanford, CA 94305-5126.**

Candidates must have a PhD and/ or MD degree and a minimum of two years of postdoctoral research experience. Application material and reference letters must be received by **November 1, 2010**.

Stanford University is an Equal Opportunity Employer and is committed to increasing the diversity of its faculty. It welcomes nominations of and applications from women and members of minority groups, as well as others who would bring additional dimensions to the university's research, teaching and clinical missions.

PATENGE ENDOWED PROFESSOR

Michigan State University in East Lansing, Michigan, invites applications and nominations to fill an endowed, tenured, faculty position in cancer biology to be appointed in one or more of the following departments: Biochemistry & Molecular Biology, Microbiology & Molecular Genetics, Pharmacology & Toxicology, or Physiology. The **Walter F. Patenge Health Sciences Professorship** is a laboratory-based research-oriented position. The individual who fills this position will be appointed as an Associate or full Professor. The Patenge Professor will receive: sizeable laboratory space, a substantial setup package, the annual interest from the endowment to further the candidate's research, and an annual salary from the university commensurate with the rank of endowed professor.

MSU has research strengths in a wide array of basic sciences and promotes a highly collegial and interdisciplinary environment with many collaborative opportunities. MSU has established state of the art research support facilities in such areas as genomics, proteomics, and microscopy. The Patenge Professor will have access to graduate students in his/her department(s) as well as graduate students in two interdepartmental programs: Cell & Molecular Biology, and Genetics. The Patenge search is part of a coordinated, well-funded initiative to enhance research on human disease at MSU. The search for the Patenge Professor will run concurrent with a second search for a tenured/tenure stream Assistant, Associate or full Professor also in cancer biology, to be appointed in one or more of the following departments: Biochemistry & Molecular Biology, Microbiology & Molecular Genetics, Pharmacology & Toxicology, or Physiology.

Tenure System, 12-month basis, 100% time.

Salary: $120,000-180,000. Salary and rank commensurate with qualifications, degree and experience.

QUALIFICATIONS: Doctorate or other terminal degree. The Patenge Professor will possess a research and/or medical degree (e.g., Ph.D., Sc.D., D.O., M.D., D.V.M.). Candidates must have a background that demonstrates their ability to work synergistically with both scientific and medical colleagues. An ideal candidate will possess a superior record of peer-reviewed publications and an outstanding record of funded research in topics related to human cancer biology. The Patenge Professor will provide energetic leadership and creative direction in building a world-class cancer research program.

MICHIGAN STATE UNIVERSITY

APPLICATIONS: Due November 1, 2010. Late submissions will be considered if a suitable candidate pool is not identified by the deadline. Applicants who are not U.S. citizens or permanent residents must provide documentation evidencing employment authorization in the United States. Applicants should refer to position 34-862. Send a letter of application, a detailed curriculum vita and a statement of research goals along with pertinent reprints and contact information for three references (address, e-mail, and phone). These materials should be addressed to: **Chairperson, Patenge Search Committee, Carcinogenesis Laboratory, 341 Food Safety & Toxicology Building, Michigan State University, East Lansing, MI 48824**. E-mailed submissions in PDF format are welcomed and encouraged at **patenge.search@hc.msu.edu.**

MSU is committed to achieving excellence through cultural diversity. The university actively encourages applications and/or nominations of women, persons of color, veterans and persons with disabilities.

CANCER BIOLOGY PROFESSOR

Michigan State University in East Lansing, Michigan, invites applications and nominations to fill a tenured/tenure stream faculty position in cancer biology to be appointed in one or more of the following departments: Biochemistry & Molecular Biology, Microbiology & Molecular Genetics, Pharmacology & Toxicology, or Physiology. The position includes competitive salary, startup package, and academic rank (Assistant, Associate or full Professor) commensurate with previous experience.

MSU has research strengths in a wide array of basic and clinical sciences that promote a highly collegial and interdisciplinary environment with many collaborative opportunities. MSU has established state of the art research support facilities in such areas as genomics, proteomics, and microscopy. The candidate who fills this position will have access to graduate students in his/her department(s) as well as graduate students in two interdepartmental programs: Cell & Molecular Biology, and Genetics. This search is part of a coordinated, well-funded initiative to enhance research on human disease at MSU. This search will run concurrent with the search for the Walter F. Patenge Health Sciences Professor in Cancer Biology.

Tenure System, 9-month basis, 100% time.

Salary: $70,000-110,000. Salary and rank commensurate with qualifications, degree and experience.

QUALIFICATIONS: Doctorate or other terminal degree. The candidate will possess a research and/or medical degree (e.g., Ph.D., Sc.D., D.O., M.D., D.V.M.). Candidates must have a background that demonstrates their ability to work synergistically with both scientific and medical colleagues. A strong record of research accomplishment and an independent externally funded research program with national visibility are required. Preference will be given to applicants with a successful track record of sustained, collaborative, peer-reviewed (particularly NIH) funding and high quality publications in topics related to human cancer biology.

MICHIGAN STATE UNIVERSITY

APPLICATIONS: Due November 1, 2010. Late submissions will be considered if a suitable candidate pool is not identified by the deadline. Applicants who are not U.S. citizens or permanent residents must provide documentation evidencing employment authorization in the United States. Applicants should refer to position 34-460. Send a letter of application, a detailed curriculum vita and a statement of research goals along with pertinent reprints and contact information for three references (address, e-mail, and phone). These materials should be addressed to: **Dr. J. Justin McCormick, Associate Dean for Research, College of Osteopathic Medicine, Michigan State University, 341 Food Safety & Toxicology Building, Michigan State University, East Lansing, MI 48824.** E-mailed submissions in PDF format are welcomed and encouraged at **justin.mccormick@hc.msu.edu.**

MSU is committed to achieving excellence through cultural diversity. The university actively encourages applications and/or nominations of women, persons of color, veterans and persons with disabilities.

DIRECTOR
DIVISION OF BIOLOGICAL SCIENCES
University of Missouri-Columbia

The Division of Biological Sciences (**www.biology.missouri.edu**) at the University of Missouri in Columbia, Missouri (**http://www.visitcolumbiamo.com/**) invites applications for a Director with a tenured academic appointment. The new Director of the Division of Biological Sciences should be a strong leader and administrator, with a vision for the Division that recognizes its strengths as a broad, integrated department, but which is also forward-looking with respect to future development. He or she should have a commitment to education and diversity, and have a demonstrated record of scientific success that, together with his or her other qualities, commands respect from colleagues throughout the Division, University, and scientific community. The successful candidate will join a diverse group of biologists in the Division of Biological Sciences with interests in cell and molecular biology, genetics, physiology, neurobiology, behavior, ecology, conservation and evolution. We offer a highly competitive salary and start-up package, an active doctoral program with institutional support for students, and a highly interactive faculty. *We are deeply committed to ethnic, racial and gender diversity in our faculty and strongly encourage applications from women and members of groups underrepresented in science.*

Send application by e-mail to: **DBSDirector@missouri.edu**. Attach a single Adobe Acrobat PDF or Microsoft Word document that includes your vitae, statement of interest in the Director's position, and statement of research and teaching interests. The names and contact information of three references will be requested from the finalists. Review of applications will begin **1 October 2010** and will continue until the position is filled. To request ADA accommodation, please contact **Johnette Blair** at **573-882-6659** or **BlairJo@missouri.edu**.

MU is an Equal Opportunity-Affirmative Action Employer.

UC DAVIS SCHOOL OF MEDICINE

FACULTY POSITION
THE CENTER FOR COMPARATIVE MEDICINE
Schools of Medicine and Veterinary Medicine
University of California, Davis

Candidates are sought for a tenure-track position at the level of **ASSISTANT** or **ASSOCIATE PROFESSOR/ASSISTANT** or **ASSOCIATE PROFESSOR IN RESIDENCE** in the Center for Comparative Medicine, a research center at the University of California, Davis, co-sponsored by the Schools of Medicine and Veterinary Medicine and a relevant Instructional and Research (I&R) academic department. The center is engaged in investigative research involving animal models of human disease. We seek individuals with Ph.D., D.V.M and/or M.D. degrees, postdoctoral experience and a record of publication in high-quality journals. We are soliciting applications from candidates who have enthusiasm for the investigation of human infectious diseases in animal models and the concepts of "One Health". Candidates are expected to have or to establish and maintain a strong extramurally funded research program and to participate in professional and graduate education in their fields. Ample office and laboratory space is available in the Center (including access to BSL2 and BSL3 laboratory space), with state-of-the art facilities, instrumentation, and administrative support. Center research and teaching programs interdigitate with other campus-wide programs and resources in the Schools of Medicine and Veterinary Medicine, the Mouse Biology Program, the California National Primate Research Center, and the Cancer Center. Faculty members will hold an academic appointment in the commensurate department of the School of Veterinary Medicine. The position will provide 0.5 salary support. Review of applications will commence immediately until the position is filled. Priority will be given to applications received by October 1, 2010.

Submit applications with letter of interest, curriculum vitae, concise statement of present and future research plans, summary of teaching experience, up to three representative reprints, and names of four references (including addresses, telephone numbers and e-mail addresses) to: **Recruitment Committee Chair, c/o Center for Comparative Medicine, University of California, Davis, CA 95616**.

The University of California is an Equal Opportunity/Affirmative Action Employer.

Faculty Position
Cell Biology Program
Sloan-Kettering Institute

The Cell Biology Program, Sloan-Kettering Institute (www.ski.edu) has initiated a search for tenure-track faculty members. We are interested in outstanding individuals who have the potential to develop an innovative, independent research program that complements and enhances our existing strengths. Candidates with research interests in exciting areas of eukaryotic cell biology, including aspects of stem cell biology, and using a variety of experimental approaches and systems are encouraged to apply. New faculty will be eligible to hold graduate school appointments in the Gerstner Sloan-Kettering Graduate School of Biomedical Sciences, the Weill Graduate School of Medical Sciences of Cornell University, as well as the Tri-Institutional MD/PhD Training Program. Sloan-Kettering has an outstanding infrastructure as well as state-of-the-art core resources, and we are now significantly expanding our research programs.

The deadline for applications is November 1, 2010. Interested candidates should visit **http://facultysearch.ski.edu** to access the on-line faculty application. Please visit the site as soon as possible, as it contains important information regarding the required application materials, including deadlines for submission of letters of reference. Informal inquiries may be sent to **Tiffany Lennon at lennont@mskcc.org** or **Dr. Alan Hall, Chair, Cell Biology Program at halla@mskcc.org**. Memorial Sloan-Kettering Cancer Center is an equal opportunity and affirmative action employer committed to diversity and inclusion in all aspects of recruiting and employment. All qualified individuals are encouraged to apply.

Memorial Sloan-Kettering Cancer Center
www.mskcc.org

PHYSICAL AND/OR ANALYTICAL CHEMISTRY
COLLEGE OF NATURAL SCIENCES AND MATHEMATICS
Department of Chemistry and Biochemistry
California State University, Fullerton

The Department of Chemistry and Biochemistry at California State University, Fullerton invites applicants for up to two full-time, tenure-track positions at the **ASSISTANT PROFESSOR** level beginning fall 2011. Successful candidates must be committed to excellence in teaching and research. Primary teaching responsibilities will be in analytical and/or physical chemistry lecture and laboratory courses at the undergraduate and graduate levels, as well as general chemistry. Applicants must have a doctorate in chemistry, postdoctoral or equivalent research experience, and have the potential to develop a vigorous research program involving undergraduate and graduate students that attracts external funding and leads to refereed publications. Research interests in all areas of physical and/or analytical chemistry, including those in related and cross-disciplinary areas will be considered. Collaboration with other faculty in chemistry, biochemistry, geology, biology, etc., is encouraged. Additional information is available from **http://chemistry.fullerton.edu** and **http://diversity.fullerton.edu**.

Applicants should send printed copies of a letter explaining how they meet the qualifications outlined above, a *curriculum vitae*, statements of teaching philosophy, research plans and goals, and arrange to have three signed letters of recommendation from individuals familiar with their teaching and research potential sent to: **Chair, Chemistry Search Committee, Department of Chemistry and Biochemistry, California State University, Fullerton, P. O. Box 6866, Fullerton, CA 92834-6866**. Review of applications will begin **October 15, 2010** and will continue until a suitable candidate is appointed. Salary is competitive and commensurate with experience and qualifications.

CSUF is an EEO/Title IX/503/504/VEVRA/ADA Employer. Women and minority candidates are particularly encouraged to apply.

BAYLOR
UNIVERSITY

Baylor University is pleased to accept applications for two new tenure-track strategic hires associated with the Center for Reservoir and Aquatic Systems Research (CRASR).

Positions are available in the areas of aquatic stress or water quality modeling (Department of Environmental Science) and aquatic microbial ecology (Department of Biology). Candidates must have an earned Ph.D. or equivalent degree and have a strong track record in research and scholarship. The successful candidate will develop a vibrant, independent and externally-funded research program with a record of refereed publications in high quality journals. Teaching is expected at both the undergraduate and graduate levels. Baylor offers the Master's in Environmental Science, Ph.D. and Master's in Biology as well as interdisciplinary Ph.D. degrees through The Institute of Ecological, Earth and Environmental Sciences programs (TIE3S) and Institute of Biomedical Studies (BMS). A strong interdisciplinary research focus and developing records in publishing and securing external funds is essential. Additional information regarding CRASR and the Departments of Biology and Environmental Science is available online. Additional information regarding the expectations of the positions and application process is available at **http://www.baylor.edu/hr_services/index.php?id=1342**.

Chartered in 1845 by the Republic of Texas, Baylor University is the oldest university in Texas and the world's largest Baptist University. Baylor's mission is to educate men and women for worldwide leadership and service by integrating academic excellence and Christian commitment within a caring community. Baylor is actively recruiting new faculty with a strong commitment to the classroom and an equally strong commitment to discovering new knowledge as Baylor aspires to become a top tier research university while reaffirming and strengthening its distinctive Christian mission as described in Baylor 2012.

Baylor is a Baptist university affiliated with the Baptist General Convention of Texas. As an Affirmative Action/Equal Employment Opportunity Employer, Baylor encourages minorities, women, veterans, and persons with disabilities to apply.

Burnett School of Biomedical Sciences
College of Medicine

Associate Director

Burnett School of Biomedical Sciences, College of Medicine seeks an Associate Director to provide leadership to its research enterprise. The school is expanding its research programs in Cancer, Cardiovascular and Metabolic, Neurodegenerative and Infectious diseases into the new 198,000 sq.ft. Burnett Biomedical Science Building. The school will be recruiting more than a dozen new faculty within the next few years. The Burnett School has over 2400 majors and over 14,000 students are enrolled in the courses taught by the school faculty. The school offers MS and PhD degrees and MS/MBA and PhD/MBA programs.

The Associate Director is expected to maintain a highly funded research program in any of the four focus areas of the school and provide leadership to the entire research enterprise and graduate programs of the school. The successful candidate must hold an earned doctorate in a discipline appropriate to the school and must have a distinguished record of scholarly accomplishment meriting appointment with tenure at the rank of professor in the school.

A leadership role in recruiting new faculty will be expected. State of the art research facilities including shared core instrumentation and a large transgenic animal facility are available in the Burnett School. UCF the nation's third largest university, ranked third in innovation and patents, is located in the great metropolitan area of Orlando. The Burnett Biomedical Science building is located in the new Health Science campus at Lake Nona that is home also for the new College of Medicine, Sanford-Burnham Medical Research Institute, Nemours Children's Hospital and VA hospital, the beginnings of an exciting major medical city in Central Florida. Further information is available at **http://www.biomed.ucf.edu**

University of Central Florida

Please submit nominations or a CV and a list of at least four references to **pk@mail.ucf.edu**

The University of Central Florida is an equal opportunity, equal access, and affirmative action employer. As a member of the Florida State University System, all application materials and selection procedures are available for public review.

HOWARD HUGHES MEDICAL INSTITUTE

JANELIA CONFERENCES
SPRING 2011

The Janelia Farm Research Campus is pleased to announce its ninth season of conferences. These small, intense conferences are intended to foster rapid scientific advances and collaborative interactions. All participants are expected to contribute to the intellectual content of the meetings. The Howard Hughes Medical Institute fully supports the Janelia Conferences—there are no registration, accommodation, or dining fees for participants. The conference organizers invite all participants, selecting some from an open pool of applicants.

Neural Circuits and Decision Making in Rodents II ▪ March 6–9, 2011
Organizers: Josh Dudman and Alla Karpova (HHMI/Janelia Farm) and Peter Dayan (University College London)

Vision in Flies ▪ March 13–16, 2011
Organizers: Axel Borst (Max Planck Institute), Chi-Hon Lee (National Institutes of Health), and Michael Reiser (HHMI/Janelia Farm)

Producing and Perceiving Complex Acoustic Signals: Songbirds and Mice as Model Systems ▪ March 20–23, 2011
Organizers: Allison Doupe (University of California, San Francisco), Roian Egnor (HHMI/Janelia Farm), and Christine Portfors (Washington State University)

Multiphoton Imaging: The Next $6x10^{23}$ Femtoseconds
April 3–6, 2011
Organizers: Na Ji and Karel Svoboda (HHMI/Janelia Farm) and David Kleinfeld (University of California, San Diego)

The Expanding Roles of Mitochondria in Cell Biology and Disease
May 9–12, 2011
Organizers: David Clayton (HHMI/Janelia Farm), Gerald Shadel (Yale University), and Susan Taylor (HHMI/University of California, San Diego).

Learning and Memory: A Synthesis of Flies and Honeybees
May 15–18, 2011
Organizers: Ron Davis (The Scripps Research Institute), Martin Giurfa (Centre National de la Recherche Scientifique), and Leslie Griffith (Brandeis University).

Computations in Neocortical Circuits: What Does the Cortex Do?
May 22–25, 2011
Organizers: Mitya Chklovskii (HHMI/Janelia Farm), Tony Movshon (New York University), Alex Thomson (University of London), and Rafael Yuste (HHMI/Columbia University).

Janelia Farm offers scholarships to graduate students who would otherwise be unable to participate in the conferences. The scholarships fund students who are from groups that are underrepresented in the sciences or who come from disadvantaged backgrounds.

Information: www.hhmi.org/janelia_conf/sci
Application deadline: November 10, 2010

HHMI janelia farm research campus

Nontraditional Careers:

Opportunities Away From the Bench

Webinar

Want to learn more about exciting and rewarding careers outside of academic/industrial research? View a roundtable discussion that looks at the various career options open to scientists across different sectors and strategies you can use to pursue a nonresearch career.

Now Available
On Demand
www.sciencecareers.org/webinar

Participating Experts:

Dr. Lori Conlan
Director of Postdoc Services,
Office of Intramural Training and Education
National Institutes of Health

Pearl Freier
President
Cambridge BioPartners

Dr. Marion Müller
Director, DFG Office North America
Deutsche Forschungsgemeinschaft
(German Research Foundation)

Richard Weibl
Director, Center for Careers in Science and Technology
American Association for the Advancement of Science

Produced by the
Science/AAAS Business Office.

Science Careers
From the journal *Science* AAAS

FACTS&FICTION

Careers in Industry and Academia

WEBINAR

September 22, 2010 • 12 noon Eastern Time • 9 a.m. Pacific • 4 p.m. GMT

As you near the next stage of your career, you probably have many questions about various career paths. Do industry and academic careers require different skill sets? How can I best prepare for either career option? Do industry jobs have better compensation? Less autonomy? Do academic scientists have less work/life balance? Are there enough academic job openings for everyone who wants one?

Get answers to your questions by viewing our roundtable discussion examining facts and fiction surrounding academia and industry career options for Ph.D.-level scientists.

Questions can be asked live!

Register today for free.
www.sciencecareers.org/webinar

Participating Experts:

Robert Tillman, Ph.D.
Director of Faculty Professional Development
Columbia University Medical Center

Leslie Pond, Ph.D.
Head, Postdoctoral Program Education Office
Novartis Institutes for BioMedical Research

3rd panelist to come

Produced by the
Science/AAAS Business Office.

Science Careers
From the journal *Science* AAAS

Learn how current events are impacting your work.

***Science*Insider, the new policy blog from the journal *Science*,** is your source for breaking news and instant analysis from the nexus of politics and science.

Produced by an international team of science journalists, *Science*Insider offers hard-hitting coverage on a range of issues including climate change, bioterrorism, research funding, and more.

Before research happens at the bench, science policy is formulated in the halls of government. Make sure you understand how current events are impacting your work. Read *Science*Insider today.

www.ScienceInsider.org

*Science*Insider

Breaking news and analysis from the world of science policy

Science

AAAS

BIOLOGIST
BROOKLYN COLLEGE, CUNY

The Department of Biology seeks a broadly trained biologist whose research will add to the breadth and depth of the department. The research should include systematic and molecular approaches in one or more of the following areas: systematics of microbial or other ecology, environmental biology, evolution, or behavior. This work should relate to the College's initiative in the urban environment, including urban marine estuaries. The faculty member will participate in teaching appropriate undergraduate and graduate courses that relate to his/her specialty. Development of a strong, competitive, research program that trains undergraduate and graduate research students and generates external grant funding is essential. Participation in the CUNY biology doctoral program is required.

An appropriate Ph.D. degree in biology or a related field is required. Post-doctoral experience with publications in peer-review biology journals; well-defined plan for developing an independent research program that will generate external funding and provide research training for undergraduate and graduate students; effective communication skills that will enable the candidate to teach at the undergraduate and graduate levels; and some appropriate teaching experience.

This is a tenure-track position, with competitive salary and benefits to begin Fall Semester 2011. Lab space and start-up funds for research will be provided. The successful candidate will join a research-active department of 18 faculties with expertise in microbiology, molecular and cell biology, bioinformatics, and behavioral neurobiology.

For additional information and application instructions, please visit **www.brooklyn.cuny.edu/faculty2011**

Brooklyn College

An AA/EO/IRCA/ADA Employer.

POSITIONS OPEN

UNIVERSITY of WISCONSIN
UWMILWAUKEE

DIRECTOR
Milwaukee Institute of Drug Discovery

The Milwaukee Institute of Drug Discovery (MIDD) is a centerpiece of the University of Wisconsin-Milwaukee's transformation into a top research university with a focus on biomedical and research. The Institute will establish an inter-departmental and inter-institutional program in therapeutics focused on neurological disorders, cancer, and infections. We are seeking a director to manage the institute, interface with pharmaceutical companies and private foundations, and promote collaborative, federally funded projects. This position will either be a senior faculty appointment or a probationary academic staff appointment, depending on the goals and particular qualifications of the candidate. Required qualifications: Ph.D. in a relevant field (biological and chemical sciences or related science, technology, engineering, and mathematics area) with seven or more years of experience in pharmaceutical research and development. Applicants must have extensive experience with preclinical development and investigational new drug filing as well as demonstrated success guiding lead compounds into clinical trials. Preferred qualifications: Special consideration will be given to candidates with experience writing competitive extramural funding applications. Experience overseeing and coordinating multidisciplinary research projects, including supervision of a diverse research team, is also highly desirable. The ideal candidate will have expertise in a broad spectrum of therapeutic areas, including neurological diseases, cancer, and infectious diseases. A detailed understanding of patent law and related legal practice is also desirable. To apply for this position as a faculty appointment, please visit **website: http://jobs.uwm.edu/postings/4787.** To apply for this position as an academic staff appointment, please visit **website: http://jobs.uwm.edu/postings/4795.** Completed application materials include: a cover letter, curriculum vitae with a research history, and the names and contact information of three references. Evaluation of applications will begin October 1, 2010, and will continue until the position is filled. *The University of Wisconsin-Milwaukee is an Affirmative Action/Equal Opportunity Employer.*

FACULTY POSITION in PHARMACOLOGICAL CHEMISTRY
Department of Chemistry and Biochemistry at UC San Diego

The Department of Chemistry and Biochemistry within the Division of Physical Sciences at University of California San Diego (UCSD, **website: http://www-chem.ucsd.edu**) is committed to academic excellence and diversity within the faculty, staff, and student body. We invite applications for a tenure-track position in Pharmacological Chemistry. Candidates must have a Ph.D. in one of the chemical/biological sciences and a demonstrated ability or potential for a recognized program of excellence in both teaching and research in Pharmacological Chemistry, broadly defined. A successful candidate will be judged on teaching and research accomplishments as well as potential for demonstrated leadership in areas contributing to diversity. Salary is commensurate with qualifications and based on University of California pay scale. Candidates should submit online curriculum vitae, list of publications, reprints of up to five representative papers, and a personal statement that includes a summary of research plans as well as their past or potential contributions to diversity at **website: https://apol-recruit.ucsd.edu/.** Please select the following job opening: Chemistry and Biochemistry **ASSISTANT PROFESSOR** in Pharmacological Chemistry (**10-178**). Candidates should also arrange to have three letters of reference addressing research, teaching, and any contributions to diversity submitted at the above mentioned URL. Prompt response is recommended. Review of applications will commence on October 15, 2010 until the position is filled. *UCSD is an Affirmative Action/Equal Opportunity Employer with a strong institutional commitment to excellence through diversity.*

POSITIONS OPEN

IMMUNOLOGIST
Faculty Position
University of Saskatchewan, Saskatoon, Canada

The Department of Microbiology and Immunology, College of Medicine, University of Saskatchewan, invites applications for a tenure-track faculty position as an **ASSISTANT PROFESSOR** in the discipline of immunology. We are interested in an outstanding individual who will pursue a vigorous research program. Applicants must have a Ph.D. or equivalent, postdoctoral research experience, demonstrated research ability and be interested in undergraduate and graduate education. We are seeking an individual with expertise in any field of immunology, either basic or clinical. A description of research by current faculty members can be found on the department online at **website: http://www.medicine.usask.ca/microbio.**

The successful applicant will have a broad range of interactive possibilities on campus with scientists in cognate departments, colleges, including the Saskatchewan Structural Sciences Centre, the Synchrotron facility (Canadian Light Source), and the Vaccine and Infectious Disease Organization, plus a number of national and provincial research institutes. There is an active research park adjacent to campus dedicated to the commercialization of innovation.

The Department is situated in the Health Sciences Building which is currently undergoing extensive renovation and expansion to become the Academic Health Sciences Complex. The Department offers vigorous undergraduate and graduate programs. Its members are involved in basic and translational research and interact with colleagues across campus.

The University of Saskatchewan (**website: http://www.usask.ca**) is situated along a river in the vibrant city of Saskatoon (**website: http://www.tourismsaskatoon.com**), which is a hub of scientific research, the arts, resource development, and agriculture.

Applicants for the position should provide curriculum vitae, a statement of research interests and specific goals, and the names of three references to:

Dr. Peter Bretscher, Head
Department of Microbiology and Immunology
College of Medicine, University of Saskatchewan
107 Wiggins Road
Saskatoon, SK S7N 5E5 Canada

Review of applications will begin October 15, 2010 and continue until a successful candidate is chosen.

Applicants are invited from qualified individuals regardless of their immigration status; however, Canadian or permanent residents will be given priority. The University of Saskatchewan is committed to Employment Equity. Members of Designated Groups (women, aboriginal people, people with disabilities, and visible minorities) are encouraged to apply and identify themselves as belonging to a designated group.

ASSISTANT PROFESSOR of BIOLOGY

The Biology Department at Creighton University invites applications for a tenure-track assistant professorship to begin August 2011. Ph.D. required; postdoctoral experience and prior teaching experience preferred. The successful applicant will teach General Biology as well as courses in one or more of the following areas: microbial biology/ecology, cell biology, plant biology, or endocrinology. Candidates should possess a strong desire to teach in a liberal arts environment. Mentoring of undergraduate research students is expected. Tenure and advancement require effective teaching and development of a research program leading to peer-reviewed publications. Opportunities exist for collaboration with faculty in the Environmental Sciences Program and Creighton's health sciences schools. Please see **website: http://biology.creighton.edu/jobs/** for additional information. Application materials may be submitted at **website: http://www.creighton.edu/hr/careers/index.php.** Application review will begin October 1, 2010, and continue until the position is filled. Creighton is a Catholic Jesuit institution that seeks qualified applicants from all backgrounds who believe they can contribute to the University's outstanding educational traditions. *We are an Equal Opportunity/Affirmative Action Employer. Women and minority candidates are strongly encouraged to apply.*

POSITIONS OPEN

INTEGRATIVE SYSTEMS or CELLULAR BIOLOGIST
Tenure-Track Position

The Department of Biology at Trinity University invites applications for an Integrative Systems or Cellular Biologist whose expertise contributes to the field of neurobiology. The position is tenure-track at the rank of **ASSISTANT PROFESSOR** beginning August 2011. Candidates must possess a Ph.D. and postdoctoral experience is desirable. Successful candidates must demonstrate commitment to excellence in teaching undergraduates and have the potential to develop and sustain a quality research program that involves significant undergraduate participation. Responsibilities include teaching upper division courses in the areas of specialty, participation in the introductory curriculum, and academic advising. Additionally, the candidate will interact with our integrative neuroscience majors program. Applicants should send curriculum vitae, statement of teaching philosophy, summary of research interests, selected publications, and contact information of three references to: **Professor Jonathan King, Chair of Search Committee, Department of Biology, Trinity University, One Trinity Place, San Antonio, TX 78212.** Electronic applications are encouraged and should be sent to **e-mail: jonathan.king@trinity.edu.** For more information on the department see **website: http://www.trinity.edu/departments/biology/.** Application deadline is 22 October 2010. *Women and minority candidates are strongly encouraged to apply. Trinity University is an Equal Opportunity Employer.*

OPEN FACULTY POSITION
Boston College Chemistry Department
http://www.bc.edu/chemistry

The Chemistry Department at Boston College invites applications for the position of **ASSISTANT PROFESSOR** of Organic Chemistry (broadly defined). This is a tenure-track position with a hire date in the fall of 2011. Applicants will be evaluated on their potential to establish a prominent, externally funded research program and to excel in teaching at both the graduate and undergraduate levels. Successful applicants will join a department of approximately 30 postdoctoral fellows, 125 doctoral students, 200 undergraduate chemistry and biochemistry majors, and an internationally recognized faculty. A Ph.D. in Chemistry, Biochemistry, or a related area and postdoctoral experience are required.

Applicants must: Submit a cover letter, curriculum vitae, summary of research plans (maximum of eight pages), and summary of research accomplishments (two pages)—in one transmission using PDF files—to **e-mail: chemsearch@bc.edu.**

Arrange to have three letters of reference in PDF format transmitted to **e-mail: chemsearch@bc.edu.** Original letters may be requested by the department. In your cover letter, please specify the names and contact information of your three references.

Submit all application materials electronically on or before 15 October 2010.

Boston College, a university of eight schools and colleges, is an Equal Opportunity Employer and supports Affirmative Action.

MICROBIOLOGIST

Tenure-track **ASSISTANT PROFESSOR** in Microbiology beginning September 1, 2011. Ph.D. required; postdoctoral and teaching experience desirable. Responsibilities: teach Microbial Physiology as well as Microbial Diversity and Ecology, share in teaching introductory courses, develop research program in microbiology, pursue extramural funding, supervise M.S. theses, and advise majors. Send letter of application, brief statements of teaching philosophy and research interests, curriculum vitae, reprints, three current letters of recommendation, and transcripts (official or photocopy) to: **Chair, Department of Biology and Microbiology, University of Wisconsin Oshkosh, Oshkosh, WI 54901,** by October 22, 2010. At least one letter of recommendation should come from candidate's current institution. For additional information see **website: http://www.uwosh.edu/departments/biology/.** Employment requires criminal background check. *Affirmative Action/Equal Opportunity Employer.*

AAAS is here – increasing diversity in the scientific work force.

AAAS is working to ensure that every student with an aptitude for science, technology, engineering, and mathematics gets an opportunity to pursue a chosen profession, no matter what the challenges. For over 30 years AAAS's ENTRY POINT! program has placed talented, differently abled students in paid internships with leading scientific employers. As a AAAS member your dues support these efforts. If you're not yet a AAAS member, join us. Together we can make a difference.

To learn more, visit **aaas.org/plusyou/entrypoint**

AAAS + U = Δ

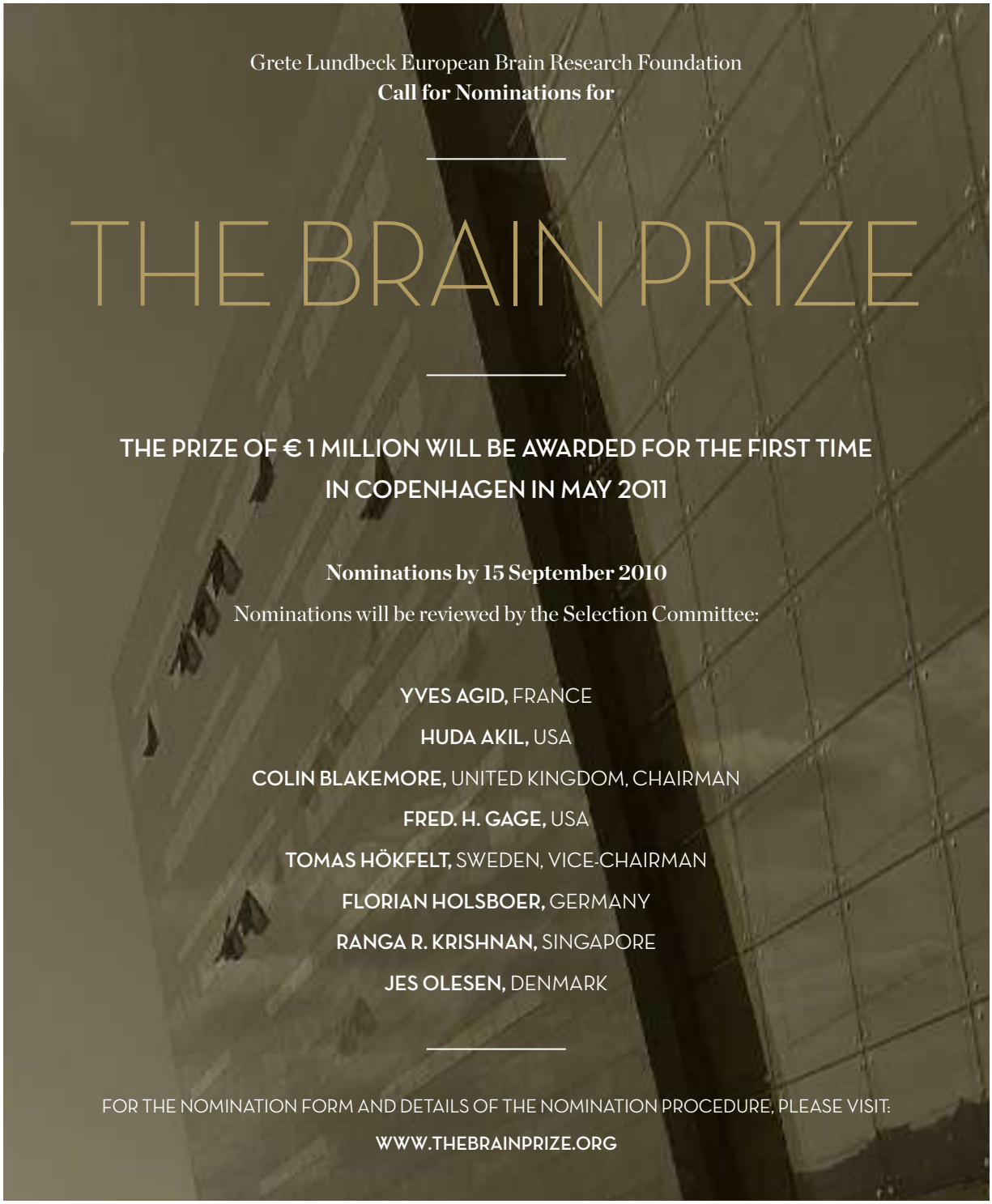
Grete Lundbeck European Brain Research Foundation
Call for Nominations for
THE BRAIN PRIZE
THE PRIZE OF € 1 MILLION WILL BE AWARDED FOR THE FIRST TIME
IN COPENHAGEN IN MAY 2011
Nominations by 15 September 2010
Nominations will be reviewed by the Selection Committee:
YVES AGID, FRANCE
HUDA AKIL, USA
COLIN BLAKEMORE, UNITED KINGDOM, CHAIRMAN
FRED. H. GAGE, USA
TOMAS HÖKFELT, SWEDEN, VICE-CHAIRMAN
FLORIAN HOLSBOER, GERMANY
RANGA R. KRISHNAN, SINGAPORE
JES OLESEN, DENMARK
FOR THE NOMINATION FORM AND DETAILS OF THE NOMINATION PROCEDURE, PLEASE VISIT:
WWW.THEBRAINPRIZE.ORG
GRETE LUNDBECK
EUROPEAN
BRAIN RESEARCH
FOUNDATION
THE BRAIN PRIZE
The Brain Prize recognizes and rewards outstanding contributions to European neuroscience, from basic to clinical

Fonds Fund

InBev-Baillet Latour

NOMINATIONS ARE INVITED

for the prestigious

InBev-BAILLET LATOUR

HEALTH PRIZE

of

€ 250,000

(Two hundred and fifty thousand Euro)

Theme for 2011 :

Infectious Diseases and Immunology

This annual award is intended to recognize outstanding scientific achievements in biomedical research and/or their practical applications for human health and to encourage the laureate in the pursuit of his/her career. Exceptionally, the Prize may be shared between two persons who have collaborated over a long period of time.

The Prize is open to scientists of all nationalities who have not received in their own name an equivalent Prize rewarding the work that is submitted. The themes for the next four years will be in succession : Neurosciences, Cancer, Cardiovascular Diseases, Metabolic Disorders.

Deadline for nominations : September 30th, 2010

Nominations must be submitted in an envelope marked "Confidential" to the Secretary General of the Fund for Scientific Research-FNRS, rue d'Egmont 5, BE - 1000 Brussels, Belgium and postmarked no later than **September 30th, 2010.**

The regulations and the nomination forms are available at the InBev-Baillet Latour website (**www.inbev-baillet-latour.be**) and at the Fund for Scientific Research-FNRS website (**www.frs-fnrs.be**).

POSITIONS OPEN

TENURE-TRACK POSITION in MOLECULAR and CELL BIOLOGY
Joint Science Department
Claremont Mckenna, Pitzer, and Scripps Colleges

The Joint Science Department invites applications for a tenure-track appointment in Molecular and Cell Biology at the **ASSISTANT PROFESSOR** level to begin July 2011. The department, which houses the biology, chemistry, and physics faculty for Claremont McKenna, Pitzer, and Scripps Colleges (three of the five undergraduate Claremont Colleges), offers innovative and interdisciplinary programs in the natural sciences and prides itself on its small class sizes. Many faculty members participate in collaborative research projects, both within the department and with research groups at nearby colleges and universities. We seek a broadly trained biologist who is committed to excellence in teaching and who will develop a vibrant research program that fully engages undergraduate students. Particularly desirable is a focus in the broad areas of functional genomics and/or computational biology to address problems in molecular biology, microbiology, immunology, or neurobiology. The position offers opportunities to teach introductory biology, non-majors courses, advanced undergraduate courses, and a laboratory course in the candidate's field. A Ph.D. degree, postdoctoral experience, and a record of scholarly publication are required.

Please apply online at **website: https://webapps.cmc.edu/jobs/faculty/home.php.** Upload a cover letter, curriculum vitae, statement of teaching philosophy, a description of proposed research with equipment needs, and the names and e-mail addresses of three references. Any inquiries may be addressed to **Professor Jennifer Armstrong** at **e-mail: jarmstrong@jsd.claremont.edu.** Additional information about the department may be found at **website: http://www.jsd.claremont.edu.** Review of applications will begin October 18, 2010, and the position will remain open until filled.

In a continuing effort to enrich its academic environment and provide equal educational and employment opportunities, The Claremont Colleges actively encourage applications from women and members of historically underrepresented social groups in higher education. The Claremont Colleges are an Equal Opportunity Employer.

DEVELOPMENTAL NEUROBIOLOGIST
University of Wyoming

The Department of Zoology and Physiology at the University of Wyoming invites applications for a full-time, nine-month, tenure-track **FACULTY POSITION** at the rank of **ASSISTANT PROFESSOR,** or at a higher rank for an individual with outstanding accomplishments, starting August 2011. We seek applications from individuals working on any fundamental aspect of nervous system development. Individuals whose research compliments the system-level approaches within the department are especially encouraged to apply. The successful candidate must have a Ph.D. or equivalent in neuroscience, zoology or an appropriate field, show strong evidence of research productivity, and a strong commitment to teaching. As a member of the Graduate Neuroscience Program, the NIH funded Neuroscience Center of Biomedical Research Excellence, and the Department of Zoology and Physiology; the candidate will be expected to develop an externally funded research program, and to teach an upper level developmental biology course as well as a course in their area of expertise. A competitive start-up package and access to outstanding microscopy and cellular analytical facilities is available.

Interested applicants should electronically send curriculum vitae, a statement or research and teaching interests, three publications, and three letters of recommendation as PDF files to **e-mail: zprequest@uwyo.edu** for the attention of Developmental Neurobiology Search Committee. **Websites: http://wyo.edu/Zoology; http://uwyo.edu/NeuroScience.** Review of applications will begin October 20, 2010 and continue until the position is filled. *The University of Wyoming is committed to diversity and endorses principles of affirmative action. We welcome applications from individuals of all backgrounds, experiences, and perspectives.*

POSITIONS OPEN

CHAIR OF BIOCHEMISTRY and MOLECULAR BIOLOGY

The College of Medicine of The Pennsylvania State University is seeking applications from, or nominations of, outstanding candidates for the Chair of Biochemistry and Molecular Biology. This individual will play a key role in a large, cross-campus endeavor to build University programs in genetics, genomics, and systems biology with the recruitment of additional faculty members. The new Chair will serve as an important link to the international biochemistry and molecular biology community and advance the position of the department scientifically. In addition to leading an active research program, the new Chair will embrace the education of our medical and graduate students, as well as postdoctoral and resident trainees. The successful candidate will be an internationally recognized scientist with a Ph.D. or equivalent degree who has a record of leadership and experience in the administrative, teaching and research activities of an academic department. The College is part of a large, growing, and fiscally stable academic healthcare center which includes the Penn State Milton S. Hershey Medical Center, Penn State Hershey Cancer Institute, Penn State Hershey Children's Hospital, an outpatient surgery center, and multiple nearby research and clinic facilities. For more information regarding the position, please visit **website: http://med.psu.edu/web/biochemistry/home.** Electronic applications are preferred and should be sent to **e-mail: dsz10@psu.edu** and addressed to: **Dani S. Zander, M.D., Chair of the Department of Pathology, Penn State M.S. Hershey Medical Center - M.C. H083, P.O. Box 850, 500 University Drive, Hershey, PA, 17033.** Resumes accepted until position is filled.

The College of Medicine of the Pennsylvania State University is an Affirmative Action/Equal Opportunity Employer. Women and Minorities are encouraged to apply.

ASSISTANT PROFESSOR
Plant Cell and Molecular Biology
University of British Columbia

The Department of Botany at the University of British Columbia invites applications for a tenure-track Assistant Professor position starting July 1, 2011. We seek outstanding applicants who address fundamental research questions in plant, algal, or fungal biology using cellular, molecular, genetic, genomic, and/or proteomic approaches in areas such as physiology, cell biology, biochemistry, signaling, epigenetics, and development. In addition to pursuing an internationally recognized research program, the successful candidate will be committed to excellence in the teaching of both undergraduate and graduate students. Applicants must have a Ph.D. and preferably postdoctoral experience. Salary will be commensurate with experience.

Responsibilities include establishing and conducting an internationally competitive, externally funded research program, teaching at the undergraduate and graduate levels, supervising graduate students, and performing service duties for the department, university, and academic/scientific community.

View full posting and apply at **website: http://www.hr.ubc.ca/careers/faculty_postings.html,** Job ID **8385.** Screening of applications will begin November 1, 2010.

For information about the Department of Botany please visit **website: http://www.botany.ubc.ca.**

UBC hires on the basis of merit and is committed to employment equity. All qualified persons are encouraged to apply. However, Canadians and permanent residents of Canada will be given priority.

MARKETPLACE